

Journal of ASTM International
Selected Technical Papers



STP 1511

Recent Advancement in Concrete Freezing-Thawing (F-T) Durability

**JAI Guest Editor
Kejin Wang**



Journal of ASTM International
Selected Technical Papers STP1511
**Recent Advancement in Concrete
Freezing-Thawing (F-T) Durability**

JAI Guest Editor
Kejin Wang



ASTM International
100 Barr Harbor Drive
PO Box C700
West Conshohocken, PA 19428-2959

Printed in the U.S.A.

ASTM Stock #: STP1511

Library of Congress Cataloging-in-Publication Data

Recent advancement in concrete freezing-thawing (F-T) durability / JAI guest editor,
Kejin Wang

p. cm.

“ASTM Stock #: STP1511.”

Includes bibliographical references.

ISBN 978-0-8031-3419-5

1. Concrete--Testing. 2. Frost resistant concrete. 3. Concrete construction--Cold weather conditions. I. Wang, Kejin.

TA440.R345 2010

620.1'3616-dc22

2010018681

Copyright © 2010 ASTM INTERNATIONAL, West Conshohocken, PA. All rights reserved. This material may not be reproduced or copied, in whole or in part, in any printed, mechanical, electronic, film, or other distribution and storage media, without the written consent of the publisher.

Journal of ASTM International (JAI) Scope

The JAI is a multi-disciplinary forum to serve the international scientific and engineering community through the timely publication of the results of original research and critical review articles in the physical and life sciences and engineering technologies. These peer-reviewed papers cover diverse topics relevant to the science and research that establish the foundation for standards development within ASTM International.

Photocopy Rights

Authorization to photocopy items for internal, personal, or educational classroom use, or the internal, personal, or educational classroom use of specific clients, is granted by ASTM International provided that the appropriate fee is paid to ASTM International, 100 Barr Harbor Drive, P.O. Box C700, West Conshohocken, PA 19428-2959, Tel: 610-832-9634; online: <http://www.astm.org/copyright>. The Society is not responsible, as a body, for the statements and opinions expressed in this publication. ASTM International does not endorse any products represented in this publication.

Peer Review Policy

Each paper published in this volume was evaluated by two peer reviewers and at least one editor. The authors addressed all of the reviewers' comments to the satisfaction of both the technical editor(s) and the ASTM International Committee on Publications. The quality of the papers in this publication reflects not only the obvious efforts of the authors and the technical editor(s), but also the work of the peer reviewers. In keeping with long-standing publication practices, ASTM International maintains the anonymity of the peer reviewers. The ASTM International Committee on Publications acknowledges with appreciation their dedication and contribution of time and effort on behalf of ASTM International.

Citation of Papers

When citing papers from this publication, the appropriate citation includes the paper authors, “paper title”, J. ASTM Intl., volume and number, Paper doi, ASTM International, West Conshohocken, PA, Paper, year listed in the footnote of the paper. A citation is provided as a footnote on page one of each paper.

Foreword

THIS COMPILATION OF THE *JOURNAL OF ASTM INTERNATIONAL (JAI)*, STP1511, on *Special Issue on Recent Advancement in Concrete Freezing-Thawing (F-T) Durability*, contains papers published in JAI highlighting recent advances in concrete F-T durability. This STP is also associated with ASTM Committee C09 on Concrete and Concrete Aggregates.

The JAI Guest Editor is Dr. Kejin Wang, Iowa State University of Science & Technology, Department of Civil, Construction, and Environmental Engineering, Ames, Iowa.

Contents

Overview	vii
Assessment of Air Entrainment in Fresh Cement Paste Using Ultrasonic Nondestructive Testing	
R. M. Kmack, K. E. Kurtis, L. J. Jacobs, and J.-Y. Kim	1
Evaluation of Two Automated Methods for Air-Void Analysis of Hardened Concrete	
A. M. Ramezaniapour and R. D. Hooton	27
The Practical Application of a Flatbed Scanner for Air-Void Characterization of Hardened Concrete	
K. Peterson, L. Sutter, and M. Radlinski	41
Evaluation of the Critical Air-Void System Parameters for Freeze-Thaw Resistant Ternary Concrete Using the Manual Point-Count and the Flatbed Scanner Methods	
M. Radlinski, J. Olek, Q. Zhang, and K. Peterson	64
Assessing the Durability of Engineered Cementitious Composites Under Freezing and Thawing Cycles	
M. Şahmaran, M. Lachemi, and V. C. Li	85
Experimental Study on Freeze-Thaw Damage Mechanism of Lightweight Aggregate Concrete	
J. Mao, K. Ayuta, H. Qi, and Z. Liu	103
Test Methods for Characterizing Air Void Systems in Portland Cement Pervious Concrete	
J. T. Kevern, K. Wang, and V. R. Schaefer	119
Effects of Strength, Permeability, and Air Void Parameters on Freezing-Thawing Resistance of Concrete with and without Air Entrainment	
G. Lomboy and K. Wang	135
Determining the Air-Entraining Admixture Dosage Response for Concrete with a Single Concrete Mixture	
M. T. Ley	155
Freeze-Thaw Performance of Concrete: Reconciling Laboratory-Based Specifications with Field Experience	
D. J. Janssen	170

Overview

In recent years, concrete technology has advanced dramatically. Various new types of concrete, such as self-consolidating concrete, engineered cementitious composites, and pervious concrete, have been developed. Concretes have served in many difficult environments, including cold climates. A number of new techniques have emerged for characterizing and predicting the performance of concrete subjected to freezing-thawing (F-T) cycles. This special issue highlights recent advances in concrete F-T durability.

This special issue contains ten papers. Four focus on the new technologies and test methods for characterizing air voids in fresh cement paste and hardened concrete. Three provide state-of-the art information on F-T durability of special concrete, such as lightweight concrete, engineered cementitious composites, and pervious concrete. One paper emphasizes the effects of void parameters on concrete F-T resistance. One introduces a new test method for determining air entraining agent demand of a concrete mixture. And one paper offers guidance for interpreting F-T test results of field concrete and for reconciling laboratory-based specifications with field experience.

As a guest editor, I sincerely thank all the authors for their contributions and all the reviewers for their constructive comments and suggestions. I am also indebted to the ASTM and JAI staff members for their timely assistance in organizing and preparing this special issue. I earnestly hope that this special issue will facilitate significant improvements in concrete void characterization, F-T durability evaluation, and test specifications. This special issue should serve as a valuable resource for researchers and engineers to make such improvements.

Kejin Wang
Iowa State University
Ames, Iowa

Richard M. Kmack,¹ Kimberly E. Kurtis,¹ Laurence J. Jacobs,^{1,2}
and Jin-Yeon Kim¹

Assessment of Air Entrainment in Fresh Cement Paste Using Ultrasonic Nondestructive Testing

ABSTRACT: It is understood that the frost protection afforded by entrained air voids in cement-based materials is dependent on their size and distribution or spacing factor. The common practice of adding air-entraining admixtures (AEAs) to concretes and mortars demands economical quality control measures of the air-entrained voids. However, conventional methods for qualifying air content in fresh cement-based materials, such as the pressure, volume, and gravimetric methods, measure only total air volume and cannot assess size (i.e., allow discrimination between entrained and entrapped air voids) or spacing. Ultrasonic monitoring may present an alternative in situ approach for these measurements. In this investigation, using matched pairs of transducers, ultrasonic pulses were transmitted through fresh cement paste specimens (containing 0.0 % up to 0.6 % AEA by weight of cement). The received signals were recorded every 5 min during the first 6 h and then every 15 min thereafter. Analysis of the signals shows strong distinctions between specimens with and those without the AEA. In general, the addition of AEA suppresses the peak-to-peak signal strength, pulse velocity, and peak frequency of the signal transmissions through the specimens. The data also suggest correlations between Vicat setting times, heat of hydration, and autogenous strain and ultrasonic metrics. The findings of this research should be most appropriate as a foundation for an inversion process and improved air-entrainment detection methods.

Manuscript received March 31, 2009; accepted for publication October 12, 2009; published online November 2009.

¹ School of Civil and Environmental Engineering, Georgia Institute of Technology, Atlanta, GA 30332-0355.

² G.W. Woodruff School of Mechanical Engineering, Georgia Institute of Technology, Atlanta, GA 30332-0405.

Cite as: Kmack, R. M., Kurtis, K. E., Jacobs, L. J. and Kim, J.-Y., "Assessment of Air Entrainment in Fresh Cement Paste Using Ultrasonic Nondestructive Testing," *J. ASTM Intl.*, Vol. 7, No. 1. doi:10.1520/JAI102452.

Copyright © 2010 by ASTM International, 100 Barr Harbor Drive, PO Box C700, West Conshohocken, PA 19428-2959.

KEYWORDS: air-entrainment, early age, hydration, ultrasonics

Introduction

Air is commonly entrained in concrete to impart durability to freezing cycles. Both the quantity (i.e., volume) and quality (i.e., size and spacing) of the entrained air are critical to ensuring adequate durability while maintaining the necessary strength. In the field, air content of concrete is typically measured by the “Pressure Method” in ASTM C231-04 [1] or the “Volumetric Method” in ASTM C173-01 [2]. In the laboratory, the “Gravimetric Method” ASTM C138-01a [3] may also be used. With each of these methods, the air content is measured either at the batching facility or on site after the concrete has been discharged but prior to its placement. Construction operations during placement and ongoing (or time-dependent) interactions between the cementitious components, such as fly ash, and the air-entraining chemical admixtures can affect the entrained air system. Thus, the air content measured just after mixing or after discharge may not accurately reflect the entrained air system in the in-place concrete.

Another shortcoming of the existing standard methods is that the *quality* of the air entrainment—or the size of the air voids and their distribution—is not measured. Recently, a new method, the “Air Void Analyzer,” has been introduced. This method measures the size distribution and spacing of the mortar fraction sieved from plastic concrete. Despite the additional information provided by this test, its limitations include that it must be performed on mortar prior to placement, and it is not sufficiently reproducible.

Of course, petrography can be performed in the laboratory on concrete cores to measure both the quantity and quality of air entrainment. But, this method is labor-intensive and is typically used to characterize only small samples, which must be assumed to be representative of the entire section. Also, petrographic analysis may often occur weeks or months after placement. Therefore, information provided by this analysis is generally not useful for altering or improving a mix design.

Thus, improved in situ measurements of entrained air quantity and quality are needed to ensure that the as-placed material meets specifications and performs as expected. While ultrasonic monitoring in concrete practice has been generally reserved for finished structures and hardened material, research efforts in recent years have addressed the application of ultrasonic monitoring to fresh hydrating cement pastes and mortars and could further expand the use of ultrasound in quality control during concrete casting. This new focus emphasizes the time-dependent nature of hydrating paste as opposed to the relatively static condition of hardened paste. Thus, this research examines the potential value ultrasonics may offer as a tool for quality assurance of plastic or early age air-entrained concretes. This investigation serves as a foundation for establishing an inversion process to characterize air-entrainment parameters.

Background

Previous Research

Ultrasonics has had great success in similar applications in the biomedical and aerospace areas. Ultrasonic techniques can provide a direct measure of mechanical properties and enable a quantitative inversion process for critical microstructural components. The use of ultrasonic wave measurements is also an efficient and economical component to structural health monitoring of civil infrastructure. As a nondestructive—and potentially in situ—method, ultrasonic wave measurements of concrete structures provide an effective means of assessing member thicknesses and stiffness as well as cracking and delamination without incurring additional damage to a structure. Recent studies have used ultrasound to quantitatively assess air-entrained voids in hardened cement paste [4].

Interest in the application of ultrasonics to plastic cement paste is relatively recent, however, and investigations into testing mechanisms and the potential for continuous monitoring are limited to a handful of studies. There are currently no standards for the containment system and testing procedures for ultrasonic monitoring of fresh cement paste. Each new study generally utilizes a similar setup to the thru-transmission setup proposed by Reinhardt et al. [5,6]. This involves paste containment between two acrylic sheets separated by an elastomeric spacer. Transducers on the outside surfaces of the assembly transmit and receive signals. Less common is a pulse-echo system, such as that proposed by Oztürk et al. [7], in which a single transducer transmits through a barrier into the paste and records the resulting echoes reflected off of the opposite free surface of the paste.

Sayers and Grenfell [8], using ultrasonic thru-transmission of longitudinal and shear waves, considered the development of mechanical strength and stiffness in cementitious materials through initial and final sets. The tests reveal the critical development of the mechanical properties of cement within the first few hours of curing and emphasize time-dependent distinctions of the ultrasonic waveforms traveling through each slurry.

In further experiments of cement pastes with and without a chemical accelerator (CaCl_2), Sayers and Dahlin [9] found wave propagation during the earliest hours after mixing to be sensitive to air inclusions in the paste. Pastes containing the accelerator transmitted relatively high-frequency wave components in the earliest hours after mixing compared to the lower-frequency spectra of pastes without the accelerator. By further monitoring CaCl_2 that were de-aerated, Sayers and Dahlin proposed that the resonance of air voids resulting as a secondary effect of the addition of CaCl_2 superimposes the higher-frequency wave components.

Aggelis' and Philippidis' [10–12] investigated fresh and hardened cement pastes and mortars of various water-to-cement ratios. Their studies note the distinctions in wave propagation in hardened cement specimens in which solid products provide the means for signal transmission versus fluidous paste in which water provides a means necessary for transmission.

Ultrasonic Waveforms

Ultrasonic testing utilizes mechanical waves being composed of oscillations of particles in the material. Analysis of ultrasonic signals is generally driven by inspection of ultrasonic wave speed, frequency spectra, and attenuation or signal loss. In experimental setups, measured attenuation is the superposition of several attenuation mechanisms. Assuming the geometry is already known, geometric attenuation can be accounted for prior to testing. Generally, interest is mainly on intrinsic attenuation associated with material absorption and scattering effects. A plane stress wave that is attenuated as it propagates through a medium can be expressed in terms of time (t) and distance (x) from the source

$$\sigma(x, t) = \sigma_0 e^{i(\omega t - kx)} \quad (1)$$

where:

ω denotes the angular frequency and

k = wave number.

To make this expression valid for an attenuated wave, the wave number is taken as complex $k = k_1 - i\alpha$. It is understood that the attenuation α causes an exponential decay in pressure amplitude and is not dependent on x . One can then use

$$\sigma(x) = \sigma_0 e^{-\alpha x} \quad (2)$$

to specify the attenuation α . For two different points x_1 and x_2 where $x_1 < x_2$, the difference in expressions at the two points, written in nepers (Np) and decibels (dB), is

$$\alpha = \frac{1}{x_2 - x_1} \log_e \frac{\sigma(x_1)}{\sigma(x_2)} \text{ Np/unit length} \quad (3)$$

$$\alpha = \frac{1}{x_2 - x_1} 20 \log_{10} \frac{\sigma(x_1)}{\sigma(x_2)} \text{ dB/unit length} \quad (4)$$

The cause of total attenuation may be divided into two classes: Those “intrinsic” attenuations that are of physical nature, having to do with physical properties of the material (absorption and scattering), and those apparent or “extrinsic” attenuations arising as a result of the method by which the attenuation measurements are made (geometric).

Material Absorption, α_a —General elasticity theory assumes that a material stores energy without dissipation during deformation. However, many materials (e.g., polymers and composites like cement-based materials) do dissipate part of the stored energy through absorption. Such materials are said to be viscoelastic—combining the properties of an elastic solid and a dissipative viscous liquid. Viscoelasticity occurs if the material stress and strain are not single-valued functions of one another for a complete cycle of oscillatory stress. That is, stress is a function not only of strain but also of the time derivative of strain. The result is the hysteresis effect—the strain cannot keep up with the alternation in stress. If the strain is not homogeneous, temperature gradients will be set up between regions of compression and of rarefaction [13]. This will

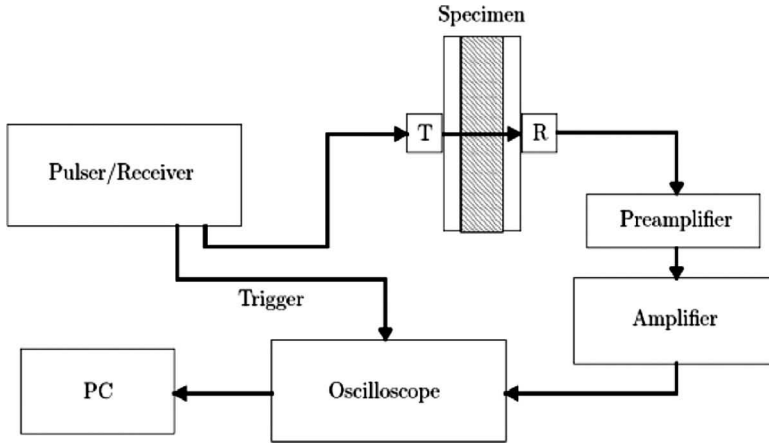


FIG. 1—Schematic diagram of the ultrasonic measurement system for hydrating cement pastes.

lead to a flow of heat, accompanied by a production of entropy, and attenuation of the pressure wave amplitude. This type of attenuation is reportedly proportional to the square of frequency.

Scattering, α_s —Scattering, which is the other part of the intrinsic attenuation, arises at the boundaries between materials, grains, or inclusions with different elastic properties. These differences are associated with the grain structure, multiple phases, precipitates, crystal defects from dislocations, etc. In short, any inhomogeneity can serve as a scatterer.

Geometric Spreading—Spreading of the ultrasonic wave attenuates the initial wave amplitude independent of frequency. Geometric attenuation is dependent on the wave mode and geometry of the elastic body under investigation. Spherical longitudinal wave amplitudes are attenuated at $1/r$, where r is the distance to the (point) source.

Experimental Investigation

Ultrasonic Experimental Setup

Figure 1 illustrates the experimental setup used for conducting ultrasonic measurements. The major components are described as follows.

Pulsar/receiver. A Panametrics 5072PR pulse generator provides the source signals for the ultrasonic experiments. The transmission node on the pulser is connected to a piezoelectric transducer; when the pulser generates an electrical impulse, it excites the crystal within the transducer, which converts the signal to mechanical energy and generates an ultrasonic pulse. The use of impulse signals allows for a broadband performance of the transducer.

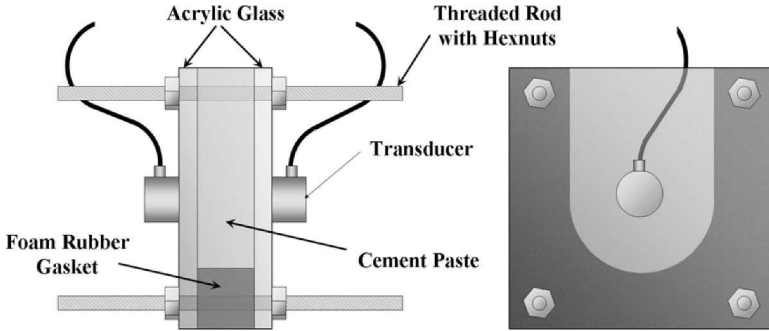


FIG. 2—Specimen containment vessel.

Piezoelectric transducers convert electrical energy into mechanical energy, such as ultrasonic pressure waves, based on the piezoelectric effect. The conversion occurs in the piezoelectric active element of the transducer, in which electrical voltage across the element induces mechanical stress and vice versa. For the experimental setup, a pair of broadband Panametrics V103 1.0/0.5 in. (1 MHz nominal center frequency) transducers was used in a thru-transmission orientation. Ultrasonic longitudinal pulse from the transmitting transducer (T) travels through the specimen to be received and converted to an electrical signal by the receiving transducer (R).

Preamplifier and amplifier. The signal from the receiving transducer is subsequently processed by a Digital Wave PA2040G/A Preamplifier and a Digital Wave FTM4000 amplifier. The preamplifier provides conditioning to the electrical signal by increasing the signal-to-noise ratio. This is essential for monitoring the evolution of ultrasonic waveforms through hydrating paste. As the paste proceeds from a fluid matrix to a solid hardening matrix, the magnitude of signal received can increase by a factor of 100. Without the preamplifier to overcome signal-to-noise issues, the experiment would require much higher pulse energy during the earliest hours of hydration, which could potentially damage the transducers and overwhelm the circuitry of the oscilloscope.

Oscilloscope. Once processed by the preamplifier and amplifier, the signal is displayed and recorded by a Tektronix TDS5034 Digital Oscilloscope. The signal is displayed on the time-domain with amplitude representing the waveform voltage. The oscilloscope allows for the user to specify sampling frequency (resolution), sample size, and signal averaging for the waveform of interest before saving the data.

Specimen Containment

In order to collect ultrasonic waveforms, a thru-transmission technique is used. However, unlike solid specimens, which allow for direct contact between the transducers and specimen surfaces, the fresh paste requires a means of containment that allows for clear measurements while preventing contact between transducer and hydrating paste. Figure 2 illustrates the containment vessel used in the experiments. In this case a closed-cell silicon rubber gasket is sand-

wiched between two 2.0 mm thick acrylic glass sheets, which serve as interfaces for the transducers. The gasket is U-shaped to provide space for the paste. For the sake of holding the transducers in place throughout the measurements, two 20.0 mm acrylic glass sheets drilled with holes fitted to the diameter of the transducers are placed on the outside surfaces of the thinner acrylic glass sheets. With the foam gasket in place, the entire container is compressed by four threaded rods, providing a paste cavity of 12.0 mm in thickness; thicker cavities were found to be too attenuative to early hydration waveforms. The transducers are then coupled to the thinner acrylic surfaces using silicon grease. Signals generated at the transmitting transducer pass through the first 2.0 mm acrylic sheet, into the paste specimen, and finally through the second 2.0 mm acrylic sheet where the receiving transducer collects the signals.

Paste specimens are mixed and immediately placed in the containment vessel through an opening at the top. After consolidation of the paste through vibration or use of a metal rod, a silicon rubber stopper is inserted in the top opening. The gasket and stopper provide an effective moisture barrier, preventing evaporation and ensuring that shrinkage effects in the paste are attributable to autogenous and chemical shrinkage and not drying shrinkage. With this system, ultrasonic measurements can proceed within 20 min of first mixing.

Initially, thicker 25.0 mm acrylic barrier sheets were used for the transducer interfaces with the intent of isolating any echo effects in received waveforms and to prevent elastic deformations of this interface due to dimensional changes in the paste specimen. However, dimensional changes due to plastic shrinkage are practically unavoidable for fresh cement paste, and the paste has a tendency to “pull away” from the acrylic barriers after as little as 5–12 h of hydration. As observed in preliminary tests, this decoupling of paste and acrylic can completely cut off signal transmission to the receiving transducer. Further tests suggested that the highly attenuative nature of fresh cement paste makes echoing effects negligible with any interface.

Surprisingly, previous research into ultrasonic monitoring of fresh cement paste did little to address the issue of interface decoupling due to shrinkage. Several researchers do not address this issue at all despite using thicker and more rigid acrylic interfaces. Among these cases: The use of mortar—cement paste with sand aggregate—may have provided the dimensional stability to make such shrinkage effects negligible [10,11], or monitoring times may be left limited to only those early times not visibly affected by decoupling [7]. Reinhardt and Grosse suggested maintaining a layer of free water at the top of the paste specimen such that it can percolate down to fill gaps formed as the paste separates from the 15.0 mm acrylic interfaces [5,6]. This last solution brings up concerns that the introduction of additional free water will unintentionally increase the w/c ratio and porosity at exposed paste surfaces and possibly alter the original mix design during chemical hydration. Also, any chemical shrinkage that results in dilatation of internal pores will pull additional water into the specimen.

Shrinkage effects in this investigation are unavoidable without altering either the mix design or the container rigidity. In order to maintain a relatively consistent acrylic-paste interface, 2.0 mm acrylic glass sheets were selected such that they can undergo elastic plate deformation with the shrinkage of the

TABLE 1—Cement analysis.

Oxide	Amount (%)	Compound	Amount (%)
SiO ₂	20.06	C ₃ S	64.00
Al ₂ O ₃	4.89	C ₂ S	9.21
Fe ₂ O ₃	3.00	C ₃ A	7.88
CaO	64.22	C ₄ AF	9.13
SO ₃	2.74		

paste while maintaining contact with the specimen. In addition, simply smearing a thin layer of silicon grease—chemically inert to the hydration process—on the interior surfaces of the acrylic glass does improve contact between the hydrating paste and the acrylic—while not completely eliminating the decoupling effect—and offers a practical form-release agent.

Specimens

Specimens were prepared for this investigation from ASTM C150-07 [14] Type I Portland cement produced by Lafarge. Bogue potential composition for this particular cement is provided in Table 1 based on chemical oxide analysis. Specimens vary in the amount of chemical air-entraining agent (Darex air-entraining admixture (AEA) provided by W. R. Grace). Two separate samples were mixed and monitored for each specimen type. All specimens are of w/c equal to 0.35—a relatively low ratio that may be seen in transportation structures. Table 2 summarizes the composition of each specimen. Petrographic analysis (ASTM C457-98 [15]) shows specimens without AEA contain approximately 1.2 % entrained air by volume. The volume fraction of air increases by increments of approximately 1.2 % for each additional 0.2 % of AEA by weight of cement.

Prior to mixing, the ingredients were measured to an accuracy of 0.1 mg. Once all ingredients were combined, they were blended by hand for 30 s to wet the cement and then placed in a planetary (Hobart N-50) mixer set to the lowest speed for 30 s. Then, the sides and bottom of the mixing bowl were scraped before mixing for 60 s at medium speed. The prepared paste was immediately scooped to fill approximately half of the specimen container volume and was then rodded with a metal dowel 25 times. The remaining space in the container was filled with paste and rodded another 25 times. Paste was then removed from the top of the cavity to provide room for a silicon rubber stopper, which was snugly fit in place. This mixing procedure was consistently accomplished such that ultrasonic monitoring could begin at 20 min after the ingredients were combined. For each mixture, ultrasonic measurements were recorded every 5 min for the first 6 h of hydration and then every 15 min thereafter until 12 hours of hydration. In addition to ultrasonic tests, independent tests of Vicat setting time (ASTM C191-04b [16]), heat of hydration (by isothermal calorimetry at 25°C), and autogenous shrinkage (by length change measurements for pastes in sealed corrugated plastic tubes) were conducted for each mix specification.

TABLE 2—Specimen specifications.

Name	w/c	Darex Entrained Agent (% by Cement Mass)	Thickness (mm)	Entrained Air Fraction (% by Volume) ^a
SP01, SP02	0.35	...	12	1.2
SP03, SP04	0.35	0.2	12	2.5
SP05, SP06	0.35	0.4	12	3.7
SP07, SP08	0.35	0.6	12	4.9

^aAs examined by a petrographer at Lafarge for separate specimens (ASTM C457-98).

Waveform Acquisition

Digitization of an analog signal is literally a form of information compression. When processing an analog waveform, such as electrical excitation, through a digital oscilloscope, one must consider appropriate sample parameters in order to preserve meaning and efficiency for future analysis. The sampling rate must be selected such that aliasing effects are avoided. For a periodic signal of period T , if the sampling interval Δt is greater than or equal to $T/2$, then frequency aliasing occurs, and the periodicity of the digitized signal appears deceptively greater than that of the true analog signal. In other words, the sampling frequency ($f_s = 1/\Delta t$) should be greater than or equal to the Nyquist frequency ($f_{ny} = 2/T$) [17].

Another important consideration during digitization is signal averaging. Due to the nature of electronic signal acquisition, noise and unpredictable variations are always inherent in signals. Signal averaging over several waveform records can reduce the interference of these variations and improve the signal-to-noise ratio. Given that the specimens in this investigation are hydrating fresh paste samples and, therefore, undergoing continuous evolution of their viscoelastic structure, any signal averaging distorts the time-dependency of the waveforms. Thus, signal averaging should be substantial enough in number of waveforms averaged such that noise is effectively reduced while also representing a sufficiently short period of time during hydration.

Signal Processing

Ultrasonic waveforms are recorded by the oscilloscope in the time-domain. These measurements can provide immediate comparison of the changes in time duration and relative energy of transmission through the paste. Additional insight into the waveforms can be obtained through analysis in the frequency domain; changes in the frequency response spectra may be more apparent than those in the time-domain.

Conversion of a time-based signal to the frequency domain requires consideration of the waveform as a finite sequence of length N where the signal amplitudes are zero outside of the domain $0 \leq n \leq N-1$. Discretization occurs as a result of digitization of the waveform into individual impulses spaced at regular time intervals Δt . The discrete Fourier transform, or DFT, presumes that this signal representation can be described as a set of complex sinusoidal functions, all harmonics of $(1/N\Delta t)$. The following equations:

$$V(f_n) = \Delta t \sum_{j=0}^{N-1} v(t_j) e^{-i(2\pi/N)jn} \quad (n = 0, 1, \dots, N-1) \quad (5)$$

$$v(t_k) = \frac{1}{N\Delta t} \sum_{n=0}^{N-1} V(f_n) e^{i(2\pi/N)nk} \quad (k = 0, 1, \dots, N-1) \quad (6)$$

represent the discrete values of a time signal and its Fourier transform, respectively, where $\Delta t = t_{k+1} - t_k$ is the sampling time interval and N is the total number of sampled points. It is important to recognize that the DFT presumes that

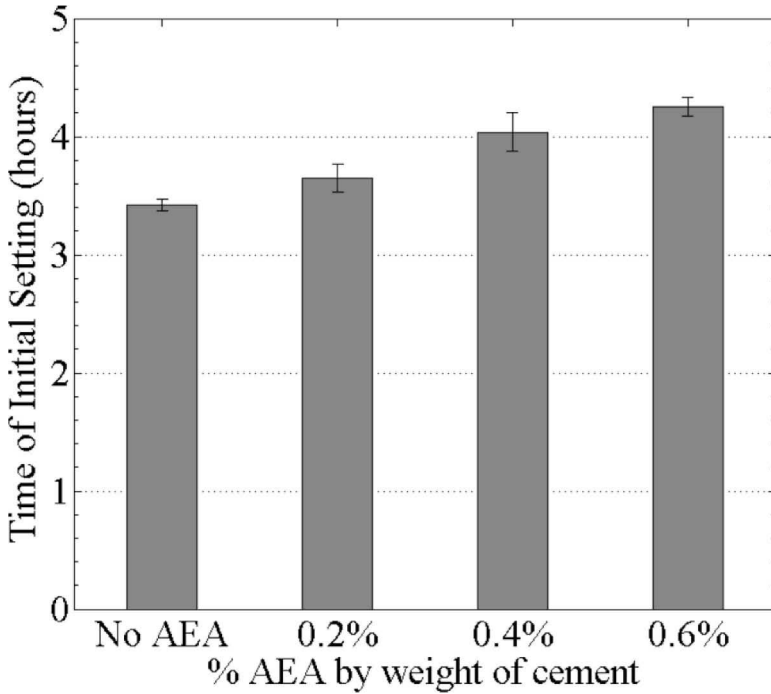


FIG. 3—Vicat time of initial setting for cement specimens.

aperiodic signals of N points are actually periodic with maximum period $T = N\Delta t$. Thus, $v(t_N) = v(N\Delta t)$ is equal to $v(t=0)$, and the N length sample repeats from this point.

Experimental Results and Discussion

Results of the additional tests performed concurrently with the ultrasound tests are described first. Figures 3–5 show test results for initial setting time, heat of hydration during isothermal calorimetry, and autogenous shrinkage. Setting time tests were conducted in accordance with ASTM C191-04b [16] for two separate specimens of each mix type. Figure 3 suggests that the addition of the AEA delays the time of initial set of this cement paste by approximately 15–20 min for each additional 0.2 % addition of the AEA by weight of cement.

Figure 4 shows the results of calorimetry tests for the paste mixes during the first 24 h of hydration. As expected, each has an initial period of rapid heat evolution as the cement components dissolve. The relatively steep positive slope occurring between approximately 2 and 8 h of hydration indicates high C_3S reaction. The Vicat initial set times for each mix occur during this period. The specimens closely correspond to each other in their heat evolution behaviors with the exception of the 0.2 % AEA specimen. The latter leads the other specimens by approximately 45–60 min throughout the first 24 h and has a

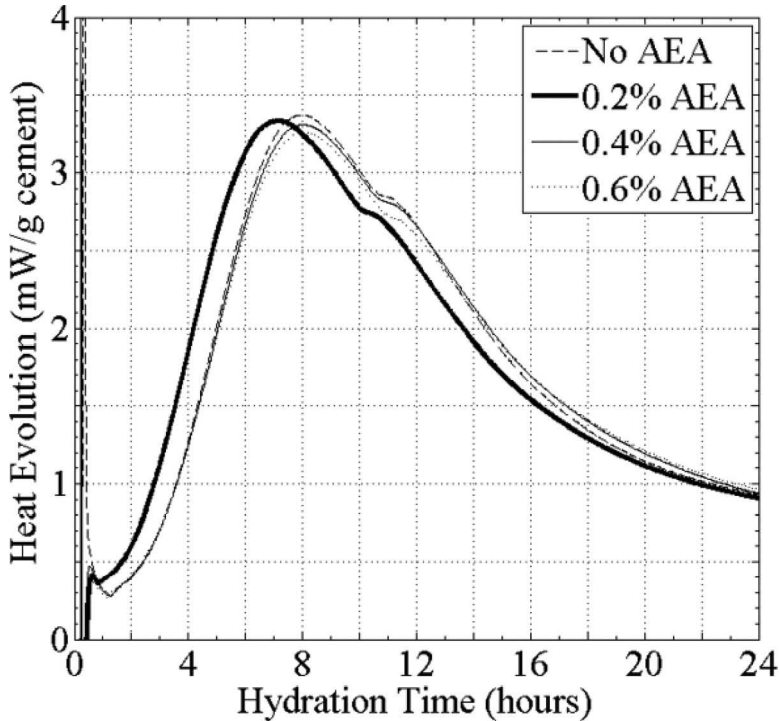


FIG. 4—Heat of hydration for cement specimens.

shorter latent period during the first 2 h of hydration. While the heat evolution peak for the other specimens is at 8 h, the 0.2 % AEA specimen peaks at 7 h. Repeated calorimetry testing confirmed that this phenomenon was genuine and consistent, although the time of set for this mixture was not accelerated, as shown in Fig. 3. This may indicate that flocculation of cement grains otherwise present in cement without AEA is alleviated with the addition of 0.2 % AEA by weight of cement, and any depression of the chemical reaction between water and the cement grains due to the presence of the AEA is offset by an increase in contact between water and cement particle surfaces. However, any further addition of the AEA beyond 0.2 % by weight of cement depresses the hydration reactions. Often, commercial admixtures will contain additional active components designed to offset ancillary effects of the primary component. So, it may be that the AEA used also contains an accelerator to offset any reduction in the reaction rate by the interaction between the cement and AEA. It may be that this effect is noticed when the admixture is used at lower-than-usual dosage rates.

Results of autogenous strain measurements on the fresh pastes are displayed in Fig. 5. All the specimens show a dormant period for the first 30–60 min of hydration during which time measurements of bulk linear deformation are stable at zero. This is followed by a period of considerable shrinkage until roughly 4 h of hydration. During these first 4 h, the pastes maintain plasticity

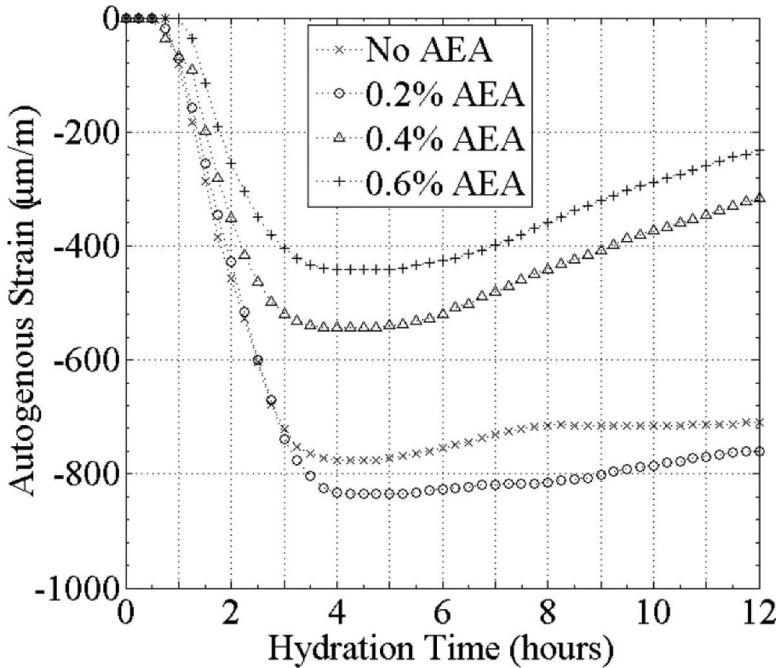


FIG. 5—Autogenous strain for cement specimens.

such that they allow for relatively uninhibited bulk shrinkage. However, the paste matrix undergoes the process of solidification as individual hydration products percolate. Once a sufficient degree of percolation occurs in the solid hydration products, the matrix establishes a rigidity that resists additional autogenous deformations. This resistance is apparent in all of the specimens at 4 h of hydration when the strain measurements stabilize. The pastes then enter a period of expansion starting at 5 h of hydration and proceeding through 12 h of hydration. This last expansion stage is likely due to the formation of calcium aluminate trisulfate hydrate (ettringite). These components will typically destabilize and convert back to monosulfate hydrate as the hydration of C_3A and C_4AF renews. Normally, this expansion effect is more than compensated by plastic shrinkage brought on by environmental evaporation. Since the specimens are sealed, however, no moisture can escape and plastic shrinkage due to evaporation is negligible.

As seen in the heat of hydration tests, the 0.2 % AEA mix appears to be an exception to trends in the other mixes. For the other mixes, the presence of the AEA appears to reduce the autogenous strain at the 4 h peak by approximately 100–120 $\mu\text{m}/\text{m}$ for each additional 0.2 % increase in AEA by weight of cement. As presumed from the discussion of the heat of hydration data, the 0.2 % AEA mix may serve as an ideal case in which cement grain flocculations are dispersed, allowing greater contact between cement particles and water and resulting in greater reactivity than in the non-air-entrained (No AEA) paste.

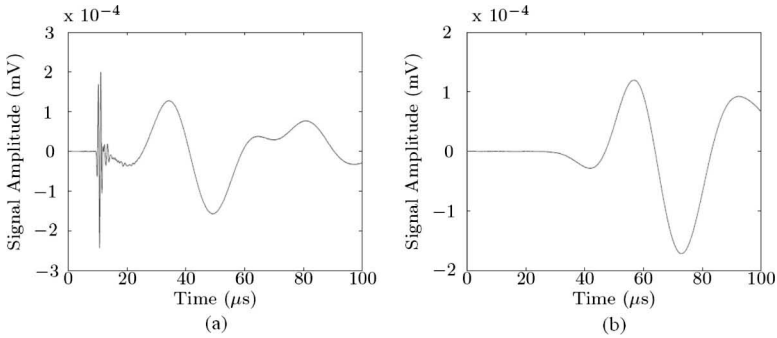


FIG. 6—Comparison of waveforms from (a) a No AEA specimen (SP01) and (b) an air-entrained specimen (SP03) at 90 min of age.

Ultrasonic Tests

Figure 6 shows a comparison of waveforms for a typical No AEA specimen and an air-entrained specimen during the early stages of hydration. The air-entrained specimen (b) has a well-defined wave representing the signal through the paste phase. The No AEA specimen (a) contains a similar waveform with an additional higher-frequency component early in the signal; for the example shown, this higher-frequency component begins at approximately $10 \mu\text{s}$. This effect appears universal and unique to the No AEA specimens tested. Not only does this higher-frequency component arrive sooner than the “bulk” wave, but it also maintains a constant arrival time through the first 90 min. Further, while the bulk wave for both specimens tightens up over time and is clearly dispersive—the wave speed is a function of frequency—the higher-frequency component in the No AEA specimen shows no change to its general shape. This suggests the presence of a transmission path through a stable material—most likely water. This is in sharp contrast to the findings of Sayers and Dahlin [9] who observed the opposite phenomenon in which a higher-frequency wave component occurs only in air-entrained specimens. In the latter case, the higher-frequency components were attributed to resonance of air-entrained voids.

Signal Strength—Figure 7 shows the mean peak-to-peak amplitudes for each specimen mix type over (a) the first 12 h and (b) the first 120 min of hydration, respectively. All specimens show the general trend of increasing peak-to-peak amplitude over the first 12 h of hydration. This observation is consistent with expectations that the increasing stiffness of the hydrating paste improves transmission of compression waves. Indeed, through the described means of specimen containment and signal amplification, the setup is capable of monitoring and discerning the continuous increase in the signal transmission strength over four or five magnitudes.

There is a severe dropoff in peak-to-peak amplitudes for the No AEA and 0.4 % AEA specimens at approximately 4–6 h of hydration. While this dropoff may last for 30 min to 1 h, the signal peak-to-peak readings eventually return to

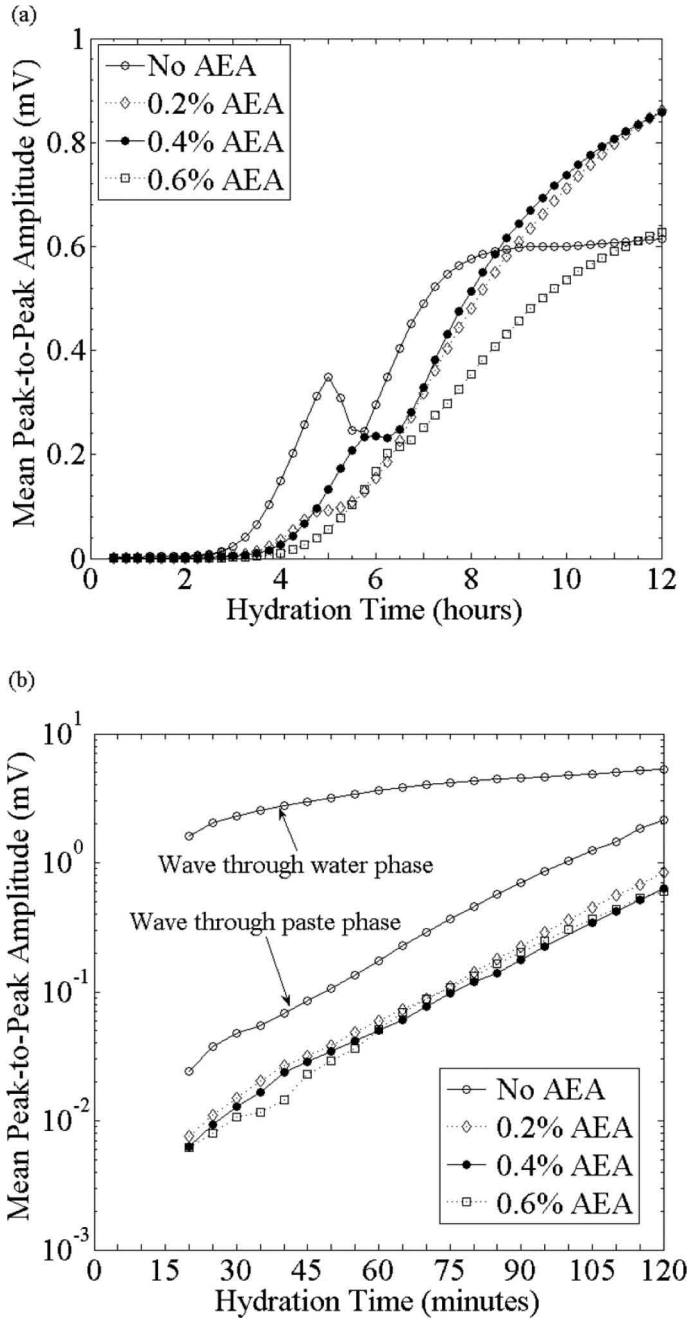


FIG. 7—Peak-to-peak amplitudes during the first (a) 12 h and (b) 120 min of hydration.

their prior rate of increase. The 0.2 % AEA and 0.6 % AEA specimens also show similar but less severe decreases in positive slope. This is analogous to slipping of grips during tensile tests of materials; load displacement curves maintain a consistent or continuous slope due to stiffness with sudden decreases in load due to slipping. In the ultrasonic peak-to-peak case, this “slipping” of amplitude readings suggests a dramatic change to the specimens and/or the bond between the acrylic interface and the surfaces of the specimens. Referring again to Fig. 5, the stabilization of autogenous strain at 4–5 h and the drops in peak-to-peak amplitudes suggest a correlation between the rigidity of the paste matrix and the reliability of the ultrasonic transmission. In other words, despite efforts to account for early age shrinkage and decoupling of the paste from the acrylic interfaces, the solidification of the paste eventually results in a material rigidity sufficient enough to resist plastic bonding to the interface. The use of the silicon coupling grease does appear to maintain a transmission medium between the paste and the acrylic even after slippage of the peak-to-peak curve, thus allowing continuous monitoring through the first 12 h of hydration. Considering the various factors of material solidification, autogenous and chemical shrinkage, interface bond, and plate deformation in the acrylic sheets, the peak-to-peak measurements suggest that signal transmission strength through the material cannot be clearly interpreted with the present setup beyond 2–4 h.

Comparison of Fig. 7(a) with Fig. 3 suggests correlation between the regions of greatest slope in the peak-to-peak plots and the initial setting times as observed through Vicat tests. This rapid increase in peak-to-peak amplitudes through the specimens is indicative of the onset of percolation of hydration solids, which provide less attenuative paths than those of the plastic cement paste.

Figure 7(b) shows the mean peak-to-peak values for each mix type over the first 2 h of hydration. The No AEA specimens are represented by two sets of data: “Wave through water phase” considers the entire signal including the higher-frequency wavelet at initial incidence described in Fig. 6, while “wave through paste phase” neglects this wavelet and focuses instead on the bulk wave. In the case of the wave traveling through water, the plots of the peak-to-peak magnitudes reveal a behavior slightly different from that of the wave traveling through the paste phase. Waves traveling through the No AEA paste phase and the air-entrained specimens increase exponentially in signal transmission strength starting from approximately 0.0001 to 0.001 mV at 20 min. In contrast, the waves traveling through the water phase in the No AEA specimens have initial peak-to-peak signal strengths one to two magnitudes higher than the other specimens but do not increase at as great an exponential rate during the first two hours of hydration. A possible reason for this dramatic difference is that the air-entrainer actually aids in the stabilization of the mix water in the paste. The AEA inhibits cement flocculation, resulting in improved dispersion of cement grains while also reducing the surface tension of the mix water, thus providing a quicker adsorption of the water component into the paste matrix than in the No AEA specimens. Ultrasonic wave transmission through these specimens may be most dependent on the scattering nature of the solid particles and their interconnectivity within the paste. In contrast, the No AEA specimens still provide strict free-water lines of transmission—liquid percola-

tion phases—as the water is not completely adsorbed into the paste, and the signal transmitted is therefore most influenced by the water. Thus, it is reasonable to conclude that the No AEA specimens do indeed contain a water-only travel path—in addition to the bulk paste path—and which is most evident and dominant during the first hours of hydration.

Figure 7(b) shows some decrease in peak-to-peak signal strength with additional AEA during the first 60 min of hydration. For now, the comparisons are qualitative at best, and numerical distinctions carry a high degree of uncertainty given the limited number of specimens.

Velocity—For this investigation, both pulse velocity and phase velocity measurements were attempted. Pulse velocity refers to the time dt_1 at which the receiving transducer registers the initial disturbance brought about by the pulse. Given this time of travel through one specimen thickness x , the measured velocity is x/dt_1 . Phase velocity refers to the time-delay dt_2 between corresponding phase points within the initial received disturbance and the following echo. Since this requires the second disturbance to travel through twice the specimen thickness x , the measured velocity is $2x/dt_2$. However, fresh cement paste is inherently highly attenuative; a considerable amount of amplification is required to merely register the initial pulse disturbance. Unfortunately, using phase velocity methods proved impossible given that there were no detectable echoes received in any of the specimens at any time. A variation in the phase velocity technique [8] might establish the time-of-travel based on two specimen thicknesses: If the difference in specimen thicknesses is $x_2 - x_1$ and the phase point of interest is delayed $t_2 - t_1$ within the thicker specimen compared to the thinner specimen, then the measured velocity is $(x_2 - x_1)/(t_2 - t_1)$. Again, this approach failed to produce reasonable results; often the time-delay appears negative when comparing the travel time through additional thickness for equivalent mixes at the same time of hydration. These discrepancies could be due to geometric spreading as well as high-sensitivity to the state of hydration.

Given the elusiveness of phase velocity measurements, a more exhaustive effort was made in obtaining pulse velocity measurements. Time-of-arrival was determined for each signal through visual inspection of the waveforms. For the signals occurring at the latest hydration times, this was not difficult as signal-to-noise is relatively high. The earliest times of hydration were more difficult though as the lower signal-to-noise ratio often obfuscated the discrete point of the initial pulse arrival, and there existed the possibility of the electronic equipment adding their own static artifacts. This last difficulty was mitigated by overlaying consecutive time signals to highlight any static elements from the electronic systems. Once these time-of-arrival points were established, they were corrected for the travel time through the acrylic sheets. This procedure for extracting pulse velocity data could be made more efficient with automated software. It is also suggested that further studies take measurements for multiple travel distances in each specimen. This would allow for phase velocity measurements.

Figure 8 shows the mean pulse velocity measurements over (a) the first 12 h and (b) the first 240 min of hydration, respectively. As expected, the specimens—with the exception of the No AEA specimens—show a continuous

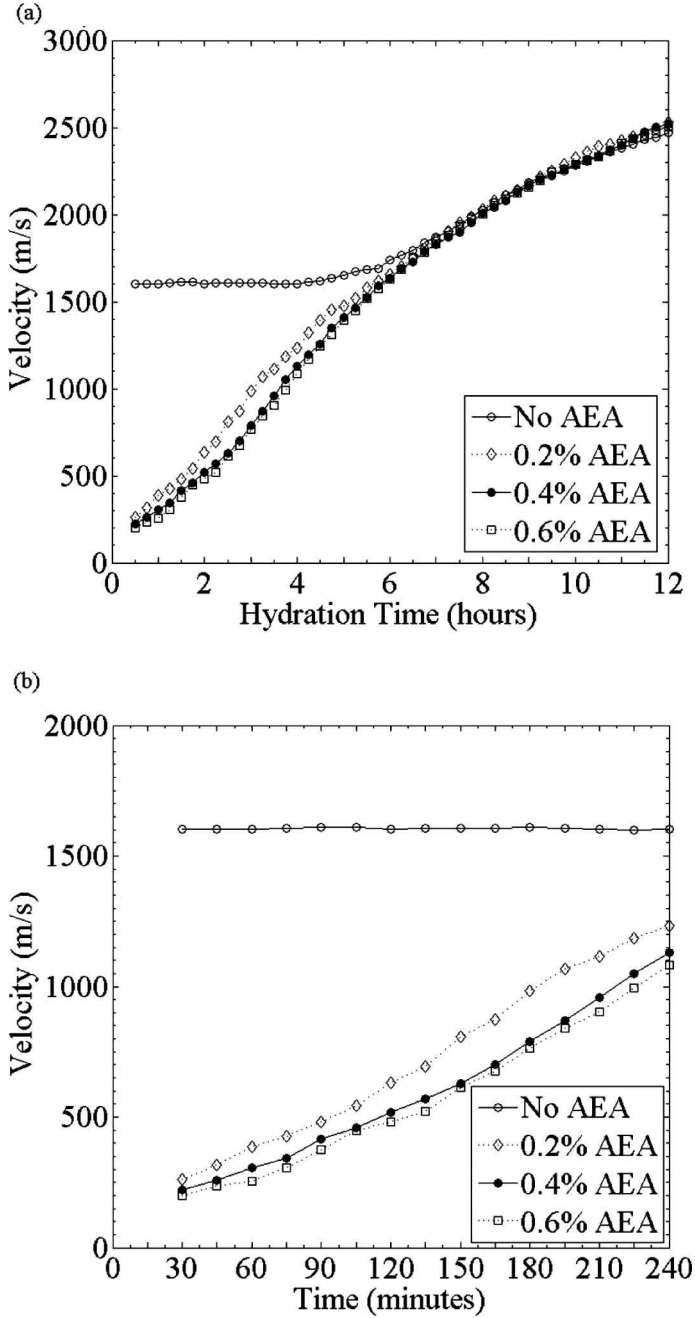


FIG. 8—Mean pulse velocity during the first (a) 12 h and (b) 240 min of hydration.

increase in pulse velocity as hydration proceeds and additional solid percolation paths emerge. The rate of increase in pulse velocity appears greatest during the first 6 h of hydration and is probably related to this being the most active period of hydration of the calcium silicates.

There is a clear distinction between the pulse velocities of the No AEA specimens and the air-entrained specimens during the first 6 h of hydration. Where the air-entrained specimens show a continuous roughly linear increase in pulse velocity starting at approximately 200 m/s at 30 min of hydration, the No AEA specimens show a constant pulse velocity of approximately 1600 m/s through the first 6 h. The latter speed is similar to the speed of sound through liquid water and provides further evidence of a water percolation path unique to the No AEA specimens. Unlike the peak-to-peak magnitude measurements, which allowed for distinction between the early higher-frequency wavelet and the later paste phase wave found in the No AEA specimens, there is no way to objectively determine the pulse velocity of only the paste wave component through the No AEA specimens due to interference by the water phase component.

Despite the water phase dominating the first 6 h of hydration in the No AEA specimens, the mean velocities of each mix type appear to converge by 8 h of hydration. Plots of the first 4 h of hydration suggest hierarchy of pulse velocities based on the amount of AEA in each mix with velocities generally decreasing by 100–200 m/s with each additional 0.2 % AEA by weight of cement at a given time. From another perspective, the hierarchy among the mean pulse velocities for the air-entrained specimens may also be viewed in terms of time-delay of setting. Recalling Fig. 3, the presence of AEA appears to delay the initial set by approximately 15–20 min with each incremental addition of 0.2 % AEA by weight of cement. Figure 8(b) shows the pulse velocities of the air-entrained specimens maintain roughly 5–30 min time-delays for each additional 0.2 % increment of AEA during the first 4 h of hydration.

Frequency—Fast Fourier transform analysis was performed for each signal using a Hanning window about the “main bang” of each waveform. The main bang is the first full time-domain cycle of disturbance detected by the receiving transducer. This initial disturbance is the only portion of the waveforms that can be consistently and objectively defined at every time during hydration. That is, when attempting to extract multiple cycles for each waveform, difficulty occurs in the middle hours (approximately 4–8 h) when the character of the waveform undergoes transition from a fluid-influenced wave to a solid-influenced wave. Visual inspection of the waveforms for each specimen reveals a transition from a waveform with multiple peaks during the early hours of hydration to a waveform with one main disturbance during the later hours. Figure 9 illustrates (a) a typical frequency spectra used in the analysis along with indication of the (b) peak frequency and bandwidth parameters. The frequency spectra as shown in Fig. 9(b) are shown normalized by dividing by the maximum magnitude located at the peak frequency.

Figure 10 shows the evolution of the mean peak (central) frequencies for each mix type through (a) the first 12 h and (b) the first 240 min of hydration, respectively. Compared to the evolution of the peak-to-peak amplitudes, inter-

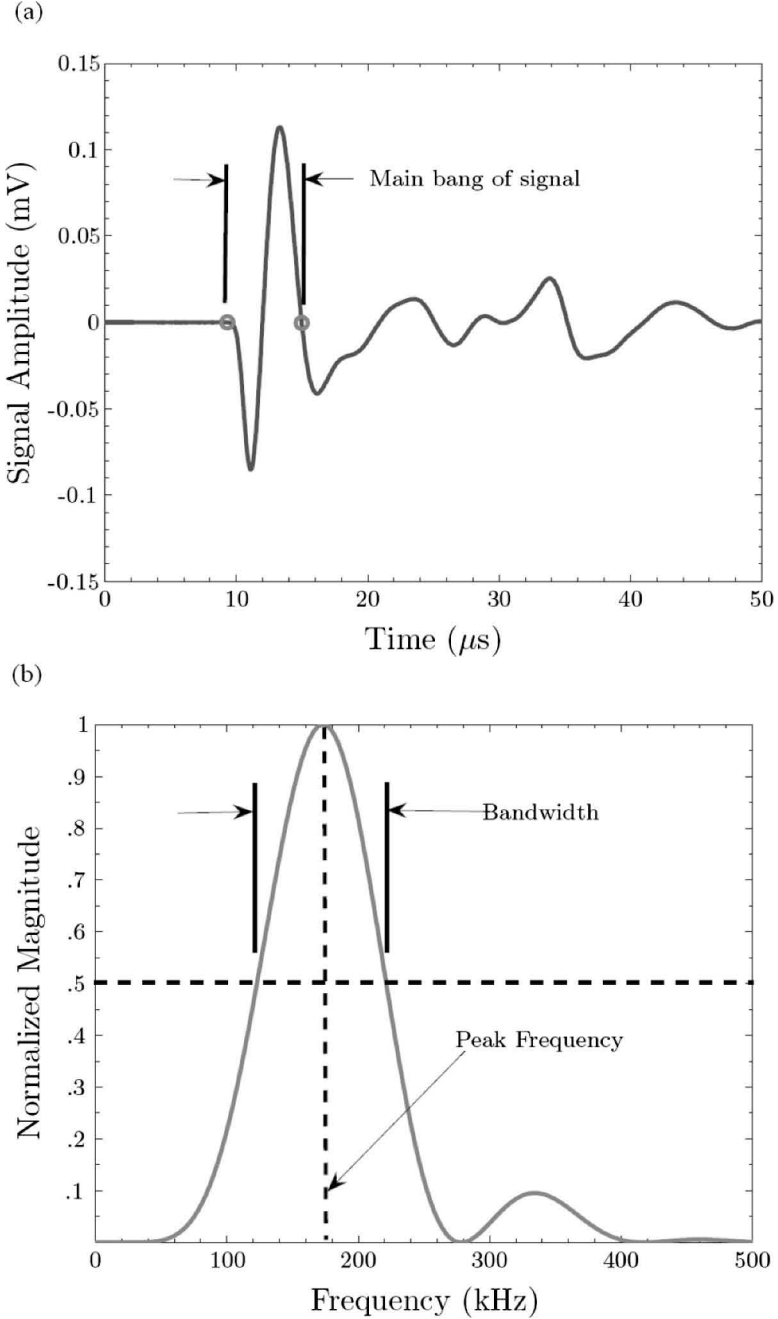


FIG. 9—(a) Typical time-domain signal with main bang indicated between circles. (b) Typical frequency spectra acquired using Hanning window. Bandwidth is taken at 50 % of the maximum magnitude.

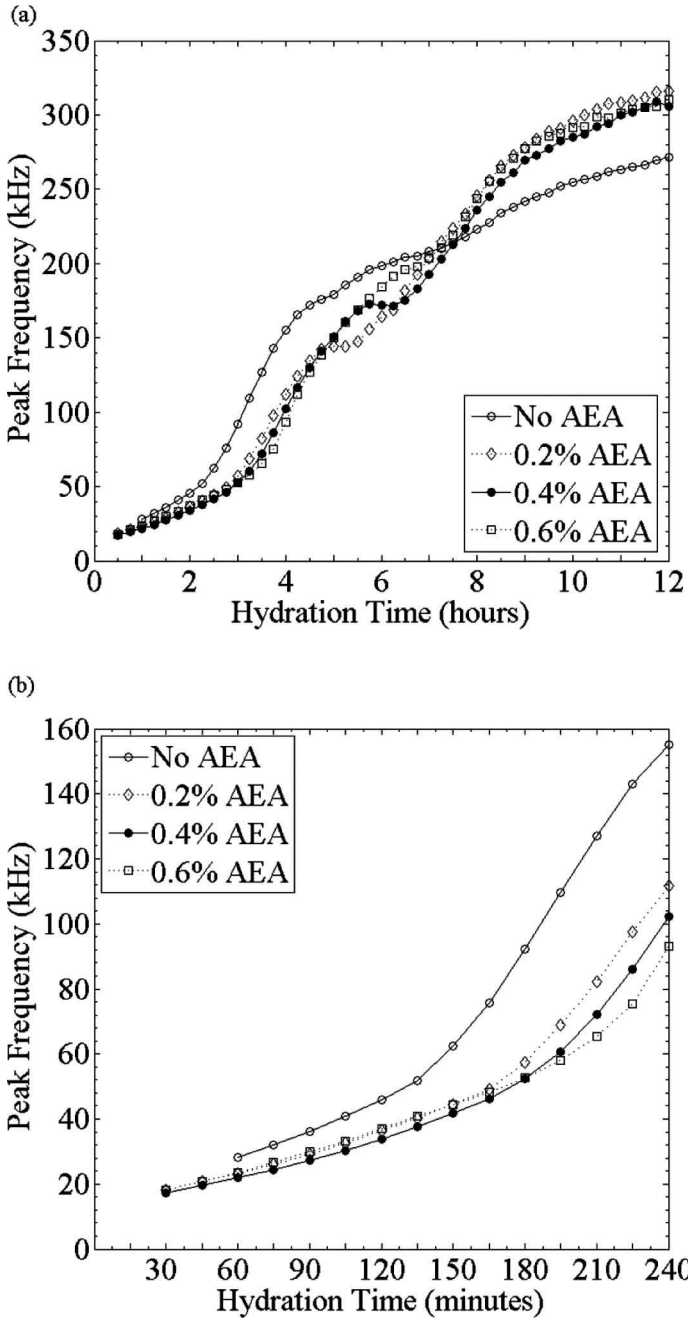


FIG. 10—Mean peak frequency of initial received pulse during the first (a) 12 h and (b) 240 min of hydration.

pretation of these plots appears relatively simple. Each plot can be considered in terms of approximate time periods. During the first 2–3 h of hydration, the paste is dominated by the fluid phase, and the peak frequency response of the system is in the 20–50 kHz range and increasing roughly linearly at 3–4 kHz every 15 min. Also, the peak frequency of the No AEA specimen is offset 10–15 kHz additional to that of the other specimens.

After 2–4 h of hydration, the specimens arrive at a threshold time of hydration—what may be called the “takeoff” points—at which peak frequency response increases sharply by 8–10 kHz every 15 min. At the takeoff point, the paste enters a period during which the peak frequency response transitions from one dominated by a fluid phase to one dominated by the solid phase. This transition is consistent with observations from the autogenous strain tests in Fig. 4. As solid paths emerge through percolation of hydration products, both the stiffness and peak frequency of the bulk paste increase rapidly.

The air-entrained specimens initially show close correlation while the paste is in its initial fluid phase. The sharp increase in the slope of the peak frequency plots, as mentioned previously, is delayed for each additional increment of AEA added to the mix. These mean that takeoff points are probably due to the first instances of solid percolation paths. Although these thresholds lead the Vicat times of setting by 30–40 min, this only means that even with available solid paths, sufficient shear resistance for a specimen—as technically measured in the Vicat tests—may still be developing. From another perspective, this suggests that monitoring the rate of increase in the peak frequency provides better evidence of the solid network and thus a better means of defining initial set.

The transition from the relatively dormant first period to the more active second period occurs approximately 1–2 h later than the similar transition that occurs in heat of hydration measurements (recall Fig. 5) when the cement paste enters its most active period of hydration of the calcium silicates. This 1–2 h time-delay may reflect the necessary degree of hydration of calcium silicates before sufficient solid percolation paths—and thus, higher peak frequency paths—can be established through the paste. In other words, setting and solidification become more apparent during this second period.

Further, the plot of peak frequency response for each specimen displays a distinct pause or dropoff during this transition period. These dropoffs, which occur at times at or within 2 h after the cement matrix has achieved sufficient rigidity to resist further autogenous shrinkage, suggest distortion of the frequency response as the interface decouples slightly from the paste. In the final period, the frequency response converges to that of the final solid phase and is a full magnitude greater than the initial frequency response of the fluid phase.

Note that the peak frequencies for the No AEA specimens are not shown at 30 and 45 min of hydration. These times are dominated by peak frequencies in the 600–800 kHz range due to the previously discussed water percolation phase.

Figure 11 shows the evolution of the 50 % bandwidth for each specimen through (a) the first 12 h and (b) the 240 min of hydration, respectively. This essentially indicates the width of the frequency spectra about the peak frequency as indicated by a cutoff frequency, in this case 50 % of the magnitude at the peak frequency. The observations made for the peak frequency plots in Fig.

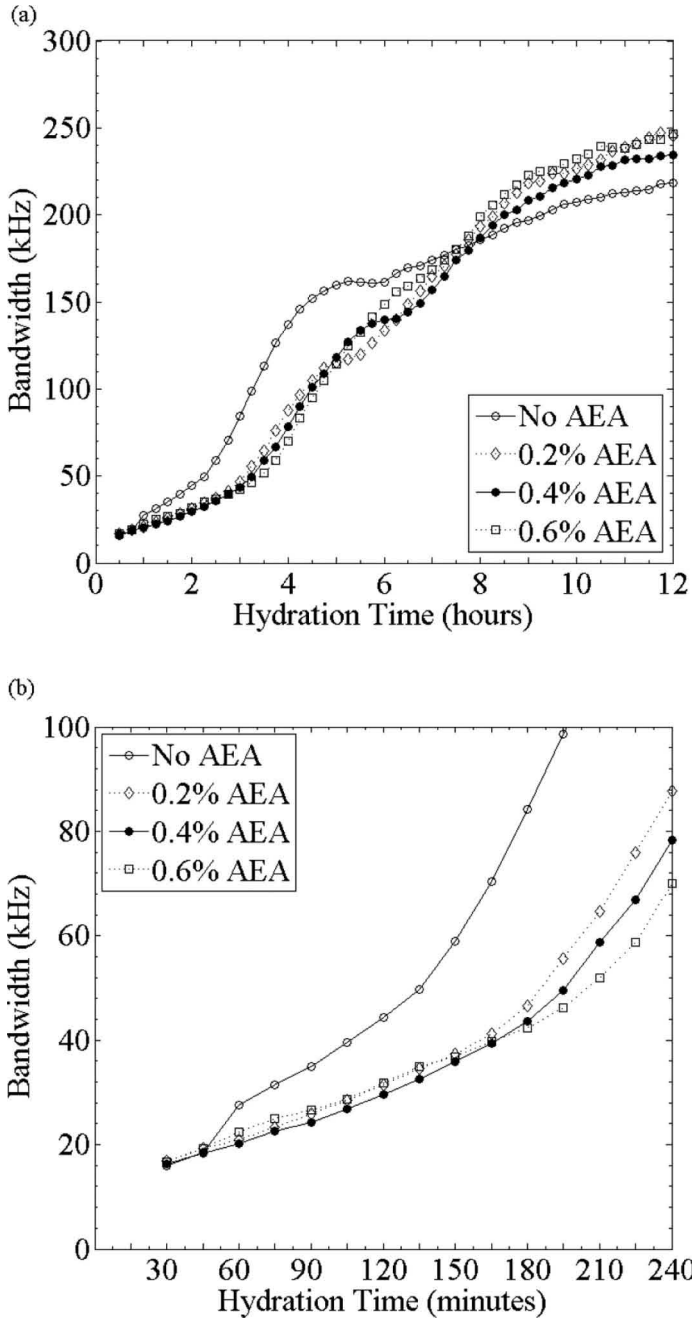


FIG. 11—Typical mean bandwidth of initial received pulse during the first (a) 12 h and (b) 240 min of hydration.

10 are the same for the bandwidth measurements. The peak frequency and bandwidth show close correlation to each other even during instances of decoupling, suggesting that deviations between mix types are strictly material-based. Indeed, there is a stable peak frequency to bandwidth ratio of 1.1–1.3 throughout the 12 h hydration period for each of the specimens. In other words, the bandwidth measurements provide verification of the observations in the peak frequency measurements.

Conclusions

Although specimens were monitored through the first 12 h of hydration, the data acquired with the current methods appear to be most relevant through the first 2–4 h of hydration depending on the metric analyzed. The most obvious result apparent in the data analysis is the clear distinction between those specimens with and without the AEA. As confirmed by the measurements of signal strength (peak-to-peak), pulse velocity, and frequency spectra, the No AEA specimens contain liquid water percolation phases. The No AEA specimens are most distinguishable from the air-entrained specimens through inspection of the peak-to-peak and pulse velocity data. The peak-to-peak strength for the No AEA specimens is significantly higher than that of the air-entrained specimens during the first two hours of hydration. Likewise, the pulse velocities of the No AEA specimens are also substantially higher than those of the air-entrained specimens—and similar to that of water—through the first 4 h of hydration. Inspection of the collected waveforms themselves reveals the unique and universal superposition of a higher-frequency “water phase” wave and a slower lower-frequency “paste wave” in the No AEA specimens.

Tests for time of initial setting, heat of hydration, and autogenous shrinkage provide additional insight into the changes in ultrasonic wave transmission as they relate to paste hydration. Signal strength transmission and peak frequency data reflect solidification in the pastes. Rapid increases in peak frequency responses at approximately 4 h of hydration highlight percolation of hydration solids. This same solidification is likewise confirmed by autogenous strain tests as the pastes develop sufficient rigidity to resist further shrinkage. Further, these indications of solidification in the frequency response tests actually lead the Vicat initial set times by approximately 30–40 min. The addition of the AEA produces a delay in time of initial set as observed by Vicat. This delay is similarly reflected as time-shifts in the development of wave velocity.

The data suggest that in general, the addition of the AEA suppresses the peak-to-peak signal strength, pulse velocity, and peak frequency in the fresh paste. While an inversion process requires further experimentation, the investigation does highlight the practical challenges inherent in ultrasonic monitoring of fresh cement paste. Applying the same experimental methods to slabs thicker than roughly 16 mm requires either sample extraction—not ideal for in situ—or equipment, including transducers, capable of more substantial power capabilities. Further, where hardened cement paste specimens offer the advantage of testing at multiple locations on the specimen thickness and using a variety of signals, fresh paste specimen tests are rather limited—the technician

cannot assume a chemically stable material over a time scope greater than a few minutes and cannot easily test multiple areas of the specimen using one set of transducers. The former disadvantage prevents testing the same specimen using a range of input signals, i.e., multiple discrete input frequencies, without introducing error due to changes in the paste matrix during a time window. The latter disadvantage requires either a relatively high degree of uncertainty when only testing at one specimen location or several transducer pairs on the same specimen to reduce uncertainty.

The long-term goal for this research is the development of a technique, including an inversion process, for characterizing the content, size, and spacing of air voids in fresh cement paste. This particular investigation provides initial observations regarding the effects of air-entrainment on ultrasonic signatures. Further research should allow for ultrasonic measurements at varying thicknesses within the same paste specimen.

Acknowledgments

The writers wish to acknowledge the generous support of the Georgia Department of Transportation GTI Project, "In situ measurement of air content in rigid pavements." In addition, the first writer is grateful for the support of the American Concrete Institute and the ACI Graduate Fellowship Program, the Georgia Tech Foundation, W. R. Grace, Lafarge, and the Ira Hardin Family.

References

- [1] ASTM C231-04, 2004, "Standard Test Method for Air Content of Freshly Mixed Concrete by the Pressure Method," *Annual Book of ASTM Standards*, Vol. 04.02, ASTM International, West Conshohocken, PA.
- [2] ASTM C173-01, 2001, "Standard Test Method for Air Content of Freshly Mixed Concrete by the Volumetric Method," *Annual Book of ASTM Standards*, Vol. 04.02, ASTM International, West Conshohocken, PA.
- [3] ASTM C138-01a, 2001, "Standard Test Method for Density (Unit Weight), Yield, and Air Content (Gravimetric) of Concrete," *Annual Book of ASTM Standards*, Vol. 04.02, ASTM International, West Conshohocken, PA.
- [4] Punurai, W., Jarzynski, J., Qu, J., Kim, J.-Y., Jacobs, L. J., and Kurtis, K., "Characterization of Multi-Scale Porosity in Cement Paste by Advanced Ultrasonic Techniques," *Cem. Concr. Res.*, Vol. 37, 2007, pp. 38–46.
- [5] Reinhardt, H. W. and Grosse, C. U., "Continuous Monitoring of Setting and Hardening of Mortar and Concrete," *Constr. Build. Mater.*, Vol. 18, 2004, pp. 145–154.
- [6] Reinhardt, H. W., Grosse, C. U., and Herb, A. T., "Ultrasonic Monitoring of Setting and Hardening of Cement Mortar—A New Device," *Mater. Struct.*, Vol. 33, 2000, pp. 580–583.
- [7] Oztürk, T., Kroggel, O., Grubl, P., and Popovics, J. S., "Improved Ultrasonic Wave Reflection Technique to Monitor the Setting of Cement-Based Materials," *NDT & E Int.*, Vol. 39, 2006, pp. 258–263.
- [8] Sayers, C. M. and Grenfell, R. L., "Ultrasonic Propagation Through Hydrating Cements," *Ultrasonics*, Vol. 31, 1993, pp. 147–153.

- [9] Sayers, C. M. and Dahlin, A., "Propagation of Ultrasound Through Hydrating Cement Pastes at Early Times," *Adv. Cem. Base. Mater.*, Vol. 1, 1993, pp. 12–21.
- [10] Aggelis, D. G. and Philippidis, T. P., "Ultrasonic Wave Dispersion and Attenuation in Fresh Mortar," *NDT & E Int.*, Vol. 37, 2004, pp. 617–631.
- [11] Aggelis, D. G., Polyzos, D., and Philippidis, T. P., "Wave Dispersion and Attenuation in Fresh Mortar: Theoretical Predictions Versus Experimental Results," *J. Mech. Phys. Solids*, Vol. 53, 2005, pp. 857–883.
- [12] Philippidis, T. P. and Aggelis, D. G., "Experimental Study of Wave Dispersion and Attenuation in Concrete," *Ultrasonics*, Vol. 43, 2005, pp. 584–595.
- [13] Mason, W. P., *Physical Acoustics and Properties of Solids*, Van Nostrand, Princeton, 1958.
- [14] ASTM C150-07, 2004, "Standard Specification for Portland Cement," *Annual Book of ASTM Standards*, Vol. 04.01, ASTM International, West Conshohocken, PA.
- [15] ASTM C457-98, 1998, "Standard Test Method for Microscopical Determination of Parameters of the Air-Void System in Hardened Concrete," *Annual Book of ASTM Standards*, Vol. 04.02, ASTM International, West Conshohocken, PA.
- [16] ASTM C191-04b, 2004, "Standard Tests Methods for Time of Setting of Hydraulic Cements by Vicat Needle," *Annual Book of ASTM Standards*, Vol. 04.01, ASTM International, West Conshohocken, PA.
- [17] Santamarina, J. C. and Fratta, D., *Introduction to Discrete Signals and Inverse Problems in Civil Engineering*, ASCE Press, Reston, VA, 1998.

A. M. Ramezaniapour¹ and R. D. Hooton²

Evaluation of Two Automated Methods for Air-Void Analysis of Hardened Concrete

ABSTRACT: Air-void analysis of hardened concrete is typically performed according to ASTM C457–09 [“Standard Test Method for Microscopical Determination of Parameters of Air-Void System in Hardened Concrete,” *Annual Book of ASTM Standards*, Vol. 4.2, ASTM International, West Conshohocken, PA], which can be tedious to perform and is operator subjective. Several alternative automated methods have been proposed, two of which are the Rapid Air 457 and the scanner method developed at Michigan Technological University. In each of these methods, images are collected from contrast enhanced surfaces of polished concrete, and image analysis is performed to calculate air-void system parameters. In this research, 22 concrete samples were examined using these two methods, the air-void system parameters were compared to those obtained from the ASTM C457 standard, and the precision of the results was compared to the recommendations of ASTM standard. It was concluded that the total air content and the spacing factor of the air voids measured by Rapid Air 457 and the scanner method were comparable to the air content and the spacing factor measured according to the standard manual method. Considering the fact that the automated image systems could detect air voids smaller in diameter than those typically seen by an operator, it was found that if these small air voids are counted, calculated spacing factors are smaller than those calculated by the manual method. If small diameter air voids are removed from the analysis, then spacing factors agree fairly well with those calculated by ASTM C457 from stereo-optical microscopy.

Manuscript received April 18, 2009; accepted for publication October 26, 2009; published online January 2010.

¹ Ph.D. candidate, Dept. of Civil Engineering, Univ. of Toronto, Toronto, ON M5S 1A4, Canada.

² Professor, Dept. of Civil Engineering, Univ. of Toronto, Toronto, ON M5S 1A4, Canada.

Cite as: Ramezaniapour, A. M. and Hooton, R. D., “Evaluation of Two Automated Methods for Air-Void Analysis of Hardened Concrete,” *J. ASTM Intl.*, Vol. 7, No. 2. doi:10.1520/JAI102476.

Copyright © 2010 by ASTM International, 100 Barr Harbor Drive, PO Box C700, West Conshohocken, PA 19428-2959.

KEYWORDS: air-void analysis, hardened concrete, image analysis

Introduction

Determination of air-void system parameters of hardened concrete is usually performed according to ASTM C457 [1] standard. This standard process is tedious, and the results depend on the skill of the operator. Moreover, the results obtained can be influenced by operator bias. Therefore, several attempts have been made to develop automated techniques for conducting the test. The advancements in digital imaging and computer programming have contributed to the automation of the analysis. Various methods have been proposed, which are similar in the sense that a digital image of the concrete specimen is captured, analyzed, and the results for air-void system parameters are calculated with little aid of a human operator. However, the manner in which the images are collected from the surface of the samples is variable.

One of these new methods is the Rapid Air 457 developed by Concrete Experts International in Denmark [2]. This method relies on automated image analysis, and the required images of the concrete surface are collected using a digital microscope. For this purpose, concrete samples are lapped and polished; then the surface of the concrete is colored black, after which surface depressions including the air voids are filled with a white powder or paste to make the contrast. If present, voids in aggregates and cracks are then re-blackened by hand. Next, a microscope and camera moving over an x - y - z stage is used to collect images, and the air-void system parameters are calculated using imaging software. The Rapid Air 457 is used by laboratories in Northern European countries; however, there are several currently used in North America. Compared to the standard ASTM procedure, this method saves a significant amount of time since the analysis and reporting typically take less than 10 min excluding the sample preparation stage. Also, due to the fact that the analysis is done automatically, the results are operator independent, although the skill of the operator can still have an influence in the sample preparation. The paste content needs to be either assumed or calculated by the user from mix proportions. Another new technology for measuring the air-void system parameters of hardened concrete has been developed at Michigan Technological University (MTU) by Carlson et al. [3]. In this method, an ordinary office flat-bed scanner is used to collect images of concrete samples with polished surfaces. In this technique, the surface is contrast enhanced using the blackening substance and white powder, and the surface is then scanned. A computer script was also developed to perform the analysis of the scanned surface. The paste content can either be provided by the user to the program, calculated by the program based on knowledge of the concrete mix proportions entered by the user, or obtained from a point count by the user, which requires an initial scan of the surface before it is contrast enhanced [4].

The objective of this research was to study the Rapid Air 457 and the ordinary scanner method as means of determining the air-void system parameters of hardened concrete according to ASTM C457. For this purpose, a total of 22 hardened concrete samples was tested by these two methods, and the results were compared to those obtained from manual assessment of ASTM C457.

Experiments

The concrete samples examined in this study were obtained from two different sources. Fifteen of the samples were provided by Ministry of Transportation of Ontario, while the remaining seven were provided by a ready-mix concrete supplier in Southern Ontario. They had previously been polished and examined according to ASTM C457 modified point count method in different commercial laboratories. These samples were selected to cover a wide range of air contents and spacing factors, namely, low air content with poor spacing factor, high air content with poor spacing factor, low air content with good spacing factor, and high air content with good spacing factor.

Prior to conducting the automated methods for determination of air-void system parameters, the previously polished samples were contrast enhanced by coloring the surface black using a wide felt-tipped marker, and then the voids were filled with white barium sulfate powder. The purpose of contrast enhancement is to provide a distinction between the air voids and the other phases (paste and aggregates) of concrete. This was achieved through the following steps.

- An initial coat of black ink was applied to the surface of the samples using a 16×8 mm² black permanent marker. The ink was applied in slightly overlapping parallel lines across the sample.
- The first step was repeated, but this time, the lines were perpendicular to the previous lines, providing a second coat of ink.
- Before proceeding, the ink on the surface was allowed to dry. At the end of this step, the surface should be uniformly and completely covered by ink. This was checked under a stereo-optical microscope.
- About 1 teaspoon (5 mL) of white barium sulfate (BaSO_4) powder was sprinkled on the surface. Then, the flat face of a steel spatula was used to trowel the powder into the air voids. The stamping was continued until all the voids appeared filled.
- A razor blade was then dragged along the surface to remove the remaining powder. Dragging was repeated applying a hard pressure but avoiding scratching the black coating.
- Using mineral oil, a slightly oiled fingertip was moved over the surface to remove any excessive powder.
- Under the stereo microscope, the quality of the contrast enhancement was examined. This was to ensure that all the voids were filled with the white powder and that no extra powder remained on the surface. At this point, the air voids appeared in clear contrast to the remaining components.
- Finally, any cracks and voids in the coarse aggregates were manually refilled black using the marker.

Results

Results from Rapid Air 457

Once the voids in the aggregates and cracks were blackened, the samples were prepared for determination of air-void system parameters. The total time re-

quired for measurement of each sample was about 10 min on average. Each sample was tested four times, rotating the sample by 90° each time, and the average of the four results was calculated as the air-void system parameters for that sample. By this means, the variations in the results would be averaged out, and more reliable values would be obtained. As well, provided software was used to remove any voids smaller than 30 μm from the spacing factor calculation (the Rapid Air can image voids as small as 3 μm), as it better simulates the voids seen by an operator in the manual point count method. A paste content of 30 % was assumed for all the samples. Actual paste contents, where mix designs were known, ranged from 30.1 % to 35.1 % (sample 3B1 to sample 4E). Sensitivity analysis was performed, which showed that total air contents were unaffected by the paste content, but that changing the assumed paste content from 30 % to 35 % resulted in a higher calculated spacing factor of ~ 0.01 mm [4].

When the results for the air-void system parameters of the concrete samples were obtained, it was possible to compare the results achieved from the standard method and those of the Rapid Air 457 equipment (Table 1 and Figs. 1 and 2). It can be concluded that the total air content and the spacing factor measured by the Rapid Air 457 system are comparable to the total air content and the spacing factor measured in the standard ASTM C457 method.

As mentioned earlier, the Rapid Air 457 producers have provided an update of the software, which provides the information for air-void system parameters considering only the air voids greater than 30 μm . The samples were retested to study the significance of this issue (Table 2 and Figs. 3 and 4). As expected, if the voids greater than 30 μm are included in the calculation of air-void system parameters, this does not result in a huge difference in the air content; however, the alteration in the spacing factor is considerable. In this case, the new calculated spacing factors are much closer to the values measured by the standard ASTM method.

Results from Flat-Bed Scanner

The air-void system parameters of the previously prepared samples were then determined by the conventional flat-bed scanner method. The samples of the first group were scanned once after being contrast enhanced, while the samples of the second group (sample 3B1 to sample 4E) were scanned before and after contrast enhancement. Using the script developed at MTU, a modified point count analysis was performed for the samples of the second group based on the images captured before the contrast enhancement to estimate the paste content. Approximately 300 points were measured in about 15 min, giving paste contents on average within 0.6 % of those obtained using the ASTM C457 method. This was done to examine whether it could be used as an alternative method for estimating the paste content of the samples. Then, the script was run to automatically perform the point count analysis for the images from the contrast enhanced surfaces. An appropriate threshold value was chosen based on comparison between the grayscale and the binary images for 400×400 pixel portions of the collected images.

The scanned images of the samples were used to determine the air-void

TABLE 1—Air-void system parameters of samples obtained by Manual Point Count and Rapid Air 457.

Sample ID	Manual Point Count		Rapid Air 457	
	Air Content (%)	Spacing Factor (mm)	Air Content (%)	Spacing Factor (mm)
01A0372	9.6	0.130	7.54	0.132
24336	7.4	0.127	7.09	0.071
34413	6.2	0.072	5.37	0.085
9-318-G	6.1	0.121	5.6	0.085
9-318-D	6	0.098	4.6	0.101
24444	5.5	0.119	5.82	0.089
99N1122	7.9	0.202	8.28	0.137
01A0988	7.1	0.216	7.03	0.096
99N1121	7	0.279	6.7	0.132
99N1119	6.4	0.282	6.6	0.161
99N1120	6.3	0.297	6.16	0.208
24537	3.7	0.172	3.77	0.149
99N1125	3.3	0.198	3.82	0.144
99N1123	2.1	0.150	3.52	0.158
44026	1.2	0.399	1.36	0.532
3B1	5.47	0.197	6.47	0.137
3C1	5.19	0.192	5.37	0.122
3C2	6.77	0.186	7.09	0.119
4A	4.96	0.203	5.57	0.124
4B	6.77	0.190	7.68	0.124
4C	6.34	0.163	7.29	0.107
4E	6.69	0.204	6.73	0.110

system parameters of the samples using the available script. The script provides the option to repeat the test while shifting the traverse line by a certain distance. The number of iterations for repeating the test is specified by the operator before the analysis starts. The experiment is repeated for half of the iterations in one direction, and the rest is repeated in the perpendicular direction, i.e., after the image is rotated by 90°. Since the script calculates the standard deviation of each of the parameters, it is recommended that more iterations should be performed to obtain more accurate results. In this study, the iteration number specified for the test was 10. In addition to that, the test was repeated after the image was rotated by 90°. Therefore, each sample was tested 20 times, five in each direction. It should be noted that the total time required for measurement of each sample was about 20 min on average. Also, to be consistent, a paste content of 30 % was assumed for all the samples so that the results could be compared against those from the manual method and Rapid Air 457.

The results obtained for the air-void system parameters of the samples by the flat-bed scanner method are presented in Table 3. Figures 5 and 6 also show

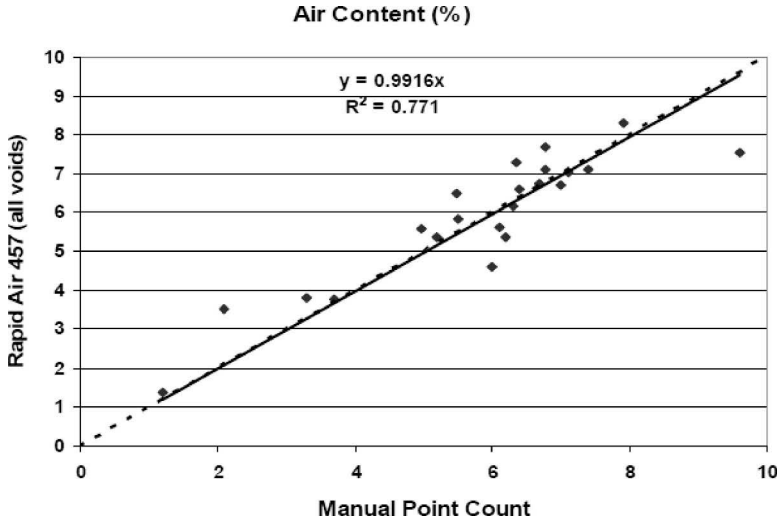


FIG. 1—Air content of samples. Manual point count versus Rapid Air 457.

the relationships between the results of this test and the ASTM C457 manual point count. As the results show, it is clear that the total air content and the spacing factor measured by the scanner method are comparable to the total air content and the spacing factor measured in the standard ASTM C457 method.

Discussion

According to ASTM C457, the allowable difference in the measurement of air content for within laboratory tests is 0.82 % and 1.16 % for between laboratory

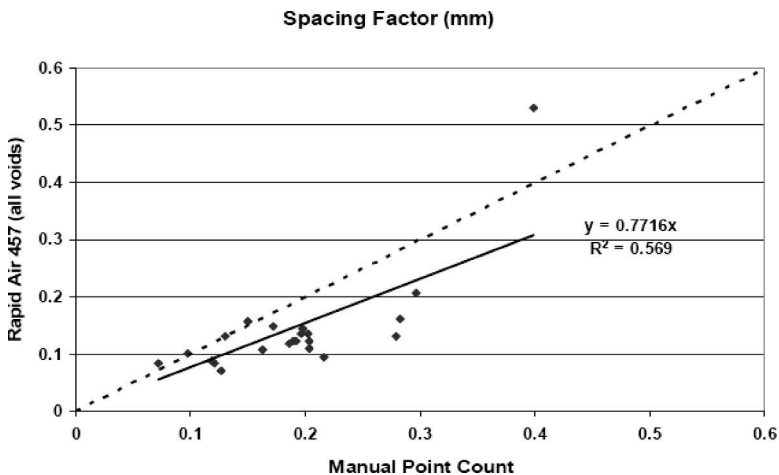


FIG. 2—Spacing factor of samples. Manual point count versus Rapid Air 457.

TABLE 2—Air-void system parameters of samples obtained by Manual Point Count and Rapid Air 457 (voids > 30 μm).

Sample ID	Manual Point Count		Rapid Air 457 (Voids > 30 μm)	
	Air Content (%)	Spacing Factor (mm)	Air Content (%)	Spacing Factor (mm)
01A0372	9.6	0.130	7.47	0.164
24336	7.4	0.127	6.57	0.112
34413	6.2	0.072	4.98	0.137
9-318-G	6.1	0.121	5.13	0.129
9-318-D	6	0.098	4.26	0.141
24444	5.5	0.119	5.79	0.131
99N1122	7.9	0.202	7.86	0.19
01A0988	7.1	0.216	6.46	0.169
99N1121	7	0.279	6.6	0.21
99N1119	6.4	0.282	6.47	0.212
99N1120	6.3	0.297	6.02	0.267
24537	3.7	0.172	3.54	0.211
99N1125	3.3	0.198	3.78	0.212
99N1123	2.1	0.150	3.34	0.199
44026	1.2	0.399	1.17	0.64
3B1	5.47	0.197	6.11	0.209
3C1	5.19	0.192	4.94	0.215
3C2	6.77	0.186	6.64	0.192
4A	4.96	0.203	5.11	0.222
4B	6.77	0.190	7.23	0.198
4C	6.34	0.163	6.76	0.171
4E	6.69	0.204	6.14	0.197

tests. Table 4 presents the difference between the results obtained from the ASTM C457 standard manual count and the Rapid Air 457 test. The average difference in air content measured by the two methods is 0.6 %, and the difference is less than 0.8 % in 95 % of the cases, which is less than the 0.82 % allowable difference for within laboratory tests and 1.16 % for between laboratory tests suggested in the ASTM C457 precision statement. As for the spacing factor, the difference between two methods was calculated to be 29 %, which is higher than the 22.6 % for within laboratory tests but less than the 56.9 % allowed for between laboratory tests. Therefore, it is evident that the results from Rapid Air 457 for the air content and spacing factor are comparable to those obtained from the ASTM standard manual point count method.

Table 5 shows the difference between the results obtained from the ASTM C457 standard manual method and the scanner methods. As the results indicate, the average difference in air content measured by the two methods is 0.5 %, and the difference is less than 0.6 % in 95 % of the cases, which is less than the 0.82 % difference for within laboratory precision and 1.16 % for between

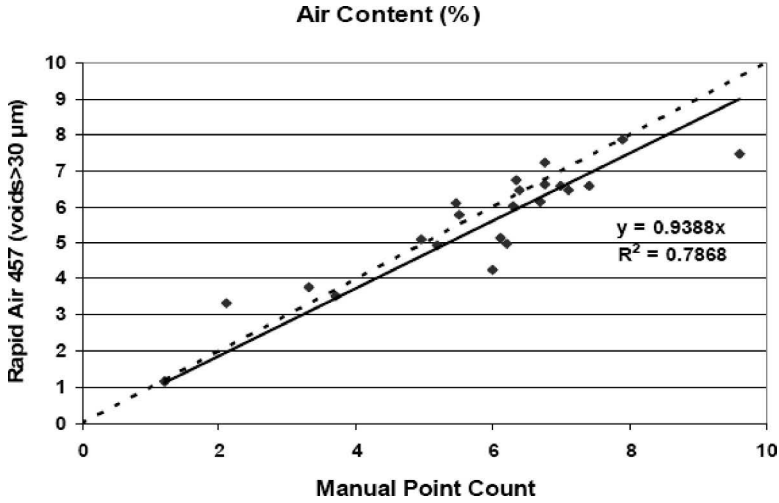


FIG. 3—Air content of samples. Manual point count versus Rapid Air 457 (voids > 30 μm).

laboratory precision stated in ASTM C457. For the spacing factor, the difference between two methods was calculated to be 28.7 %, which is higher than the 22.6 % for within laboratory but less than 56.9 % for different laboratories specified by the standard. Interestingly enough, if the two greatest differences are excluded from the calculations, the corresponding number would be 21.9 %, which is less than the number for within laboratory precision. This clearly

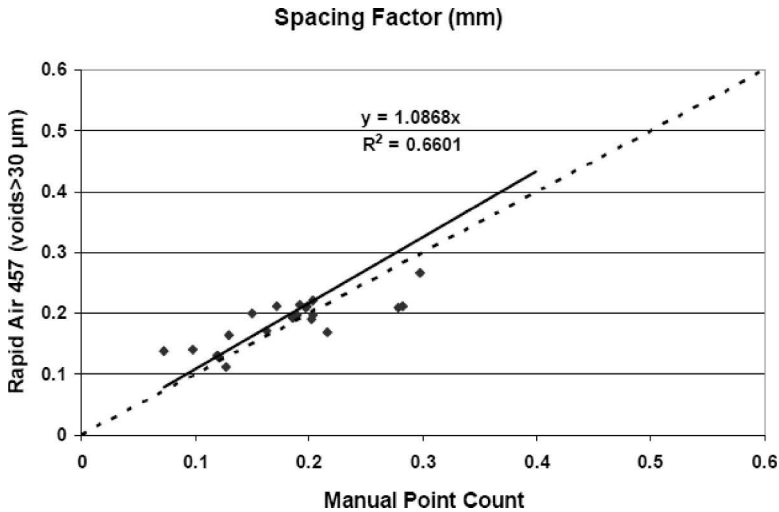


FIG. 4—Air content of samples. Manual point count versus Rapid Air 457 (voids > 30 μm).

TABLE 3—Air-void system parameters of samples obtained from manual point count and the flat-bed scanner method.

Sample ID	Manual Point Count		Scanner	
	Air Content (%)	Spacing Factor (mm)	Air Content (%)	Spacing Factor (mm)
01A0372	9.6	0.130	9.48	0.137
24336	7.4	0.127	7.56	0.092
34413	6.2	0.072	6.49	0.107
9-318-G	6.1	0.121	5.7	0.111
9-318-D	6	0.098	4.79	0.124
24444	5.5	0.119	6.26	0.114
99N1122	7.9	0.202	8.56	0.170
01A0988	7.1	0.216	8.05	0.145
99N1121	7.0	0.279	7.86	0.196
99N1119	6.4	0.282	7.6	0.206
99N1120	6.3	0.297	6.85	0.236
24537	3.7	0.172	3.37	0.174
99N1125	3.3	0.198	3.91	0.175
99N1123	2.1	0.150	3.0	0.243
44026	1.2	0.399	1.38	0.675
3B1	5.47	0.197	5.83	0.181
3C1	5.19	0.192	5.21	0.222
3C2	6.77	0.186	6.76	0.174
4A	4.96	0.203	5.12	0.225
4B	6.77	0.190	6.84	0.183
4C	6.34	0.163	6.46	0.179
4E	6.69	0.204	7.09	0.170

indicates that the results obtained from the flat-bed scanner method are in better agreement with those from the standard manual method with respect to the Rapid Air 457.

Table 6 summarizes the comparison of the results obtained from these two automated methods and the standard method with respect the recommendations of the ASTM C457. As the values clearly indicate, the precision of the results obtained from Rapid Air 457 and the scanner method meets the precision requirements of the ASTM C457 standard if they are considered as tests done by different laboratories. Moreover, the values for 95 % confidence level of difference for both the air content and the spacing factor of the samples measured by the scanner method are less than those of Rapid Air 457. Therefore, it suggests that the results obtained from the scanner method are in better agreement with those from the standard manual method compared to Rapid Air 457.

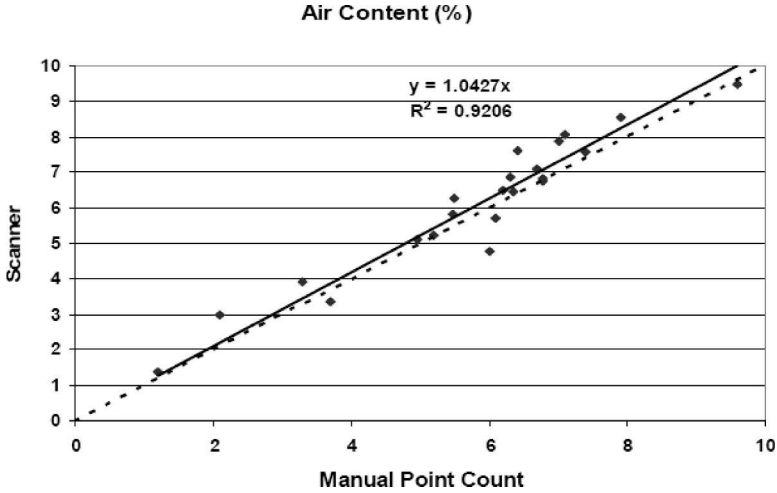


FIG. 5—Air content of the samples. Manual point count versus scanner.

Conclusions

- The measurement, analysis, and reporting time for Rapid Air 457 and the flat-bed scanner method are about 10 and 20 min, respectively. This means they save a significant amount of time compared to the standard ASTM C457, which normally takes about 4–6 h.
- The total air content measured by both the Rapid Air 457 and the scanner method is within the single-laboratory precision of the air content

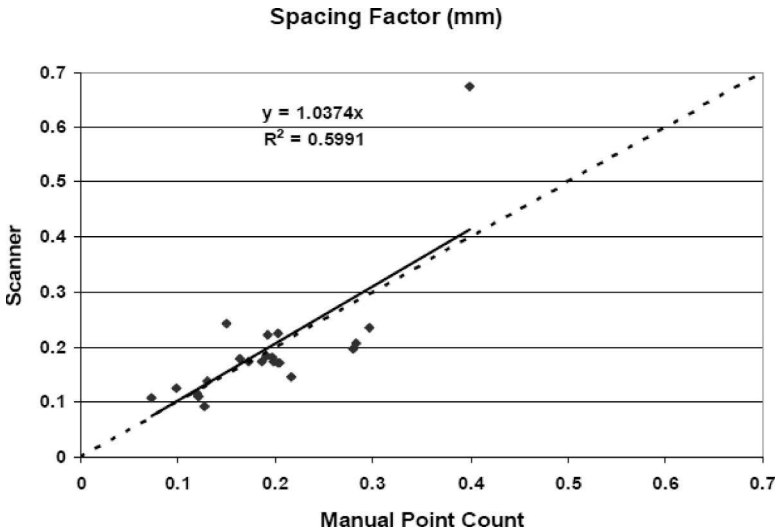


FIG. 6—Spacing factor of the samples. Manual point count versus scanner.

TABLE 4—Difference between the results obtained from the standard manual method and Rapid Air 457 (considering voids > 30 μm).

Sample ID	Absolute Difference Between Manual Point Count and Rapid Air 457 (Considering Voids > 30 μm)		Error (%)	
	Air Content (%)	Spacing Factor (mm)	Air Content	Spacing Factor
01A0372	2.1	0.034	22.2	26.2
24336	0.8	0.015	11.2	11.8
34413	1.2	0.065	19.7	90.3
9-318-G	1.0	0.008	15.9	6.6
9-318-D	1.7	0.043	29.0	43.9
24444	0.3	0.012	5.3	10.1
99N1122	0.0	0.012	0.5	5.9
01A0988	0.6	0.047	9.0	21.8
99N1121	0.4	0.069	5.7	24.7
99N1119	0.1	0.070	1.1	24.8
99N1120	0.3	0.030	4.4	10.1
24537	0.2	0.039	4.3	22.7
99N1125	0.5	0.014	14.5	7.1
99N1123	1.2	0.049	59.0	32.7
44026	0.0	0.241	2.5	60.4
3B1	0.6	0.012	11.7	6.1
3C1	0.3	0.023	4.8	12.0
3C2	0.1	0.006	1.9	3.2
4A	0.2	0.019	3.0	9.4
4B	0.5	0.008	6.8	4.2
4C	0.4	0.008	6.6	4.9
4E	0.6	0.007	8.2	3.4
Average	0.6	0.038	11.3	20.1
Standard deviation	0.6	0.050	13.0	21.4
95 % Confidence	0.8	0.059	16.7	29.0

measured according to the ASTM C457 standard manual method. Also, the spacing factor measured by Rapid Air 457 is comparable to, but is usually less than, that measured according to the standard ASTM C457 method. This is because Rapid Air 457 is better able than the average human operator in detecting very small voids, especially those less than 30 μm . Nonetheless, the precision of the results obtained from either Rapid Air 457 or the scanner method meets the precision recommendations of ASTM C457 if they are considered as tests done by different laboratories.

- The results obtained from the flat-bed scanner method are in better agreement with those from the standard ASTM C457 manual method

TABLE 5—Difference between the results obtained from the standard manual method and the scanner method.

Sample ID	Absolute Difference Between Manual Point Count and Scanner Method		Error (%)	
	Air Content (%)	Spacing Factor (mm)	Air Content	Spacing Factor
01A0372	0.1	0.007	1.2	5.4
24336	0.2	0.035	2.2	27.6
34413	0.3	0.035	4.7	48.6
9-318-G	0.4	0.01	6.6	8.3
9-318-D	1.2	0.026	20.2	26.5
24444	0.8	0.005	13.8	4.2
99N1122	0.7	0.032	8.4	15.8
01A0988	1.0	0.071	13.4	32.9
99N1121	0.9	0.083	12.3	29.7
99N1119	1.2	0.076	18.8	27.0
99N1120	0.6	0.061	8.7	20.5
24537	0.3	0.002	8.9	1.2
99N1125	0.6	0.023	18.5	11.6
99N1123	0.9	0.093	42.9	62.0
44026	0.2	0.276	15.0	69.2
3B1	0.4	0.016	6.6	8.1
3C1	0.0	0.03	0.4	15.6
3C2	0.0	0.012	0.1	6.5
4A	0.2	0.022	3.2	10.8
4B	0.1	0.007	1.0	3.7
4C	0.1	0.016	1.9	9.8
4E	0.4	0.034	6.0	16.7
Average	0.5	0.044	9.8	21.0
Standard deviation	0.4	0.058	9.7	18.6
95 % Confidence	0.6	0.069	13.8	28.7

TABLE 6—Summary of the results obtained from the two automated methods and their comparison against the recommendations of ASTM C457.

	Average Difference Between Rapid Air and Standard (%)	Average Difference Between Scanner and Standard (%)	95 % Confidence Level for Rapid Air (%)	95 % Confidence Level for Scanner (%)	Maximum Allowable According to ASTM C457 (%)	Acceptable (Rapid Air or Scanner)
Air content	0.6	0.5	0.8	0.6	1.16	Both
Spacing factor	20.1	21	29	28.7	56.9	Both

compared to those obtained by the Rapid Air 457. Moreover, as the results from the scanner method are comparable to those from Rapid Air 457 and since the cost of the scanner is significantly lower than Rapid Air 457, the scanner method has the advantage.

- In both rapid methods, if the paste content of the concrete is not known or is not measured independently, less accurate results will occur.

References

- [1] ASTM C457, 2009, "Standard Test Method for Microscopical Determination of Parameters of the Air-Void System in Hardened Concrete," *Annual Book of ASTM Standards*, Vol. 4.2, ASTM International, West Conshohocken, PA.
- [2] Pade, C., Jakobsen, U. H., and Elsen, J., "A New Automatic Analysis System for Analyzing the Air Void System in Hardened Concrete," *Proceedings of the 24th International Conference on Cement Microscopy*, 2002, International Cement Microscopy Association, San Diego, CA, pp. 204–213.
- [3] Carlson, J., Sutter, L., Peterson, K., and Van Dam, T., "An Update on Application of a Flat-Bed Scanner for Performing ASTM C457," *Proceedings of the 27th International Conference on Cement Microscopy*, 2005, International Cement Microscopy Association, Victoria, British Columbia, Canada.
- [4] Ramezani-pour, A. M., 2006, "Evaluation of Two Automated Methods for Determination of the Air-Void System Parameters of Hardened Concrete," M.A.Sc. thesis, University of Toronto.

Karl Peterson,¹ Lawrence Sutter,¹ and Mateusz Radlinski²

The Practical Application of a Flatbed Scanner for Air-Void Characterization of Hardened Concrete

ABSTRACT: Over the past 30 years, with the advent of computers and digital imaging, many automated systems have been introduced for the purpose of air-void characterization. The majority of the systems employs a contrast-enhancement procedure where a polished cross-section of concrete is darkened with paint, and white powder is forced into the depressions left by air-voids. The system described here follows the same approach and uses a flatbed scanner to collect a single digital image of the entire sample. For all of the systems based on contrast enhancement, the first step is to select a threshold level. Image pixels brighter than the threshold level represent air and image pixels darker than the threshold level represent non-air (i.e., paste or aggregate). Further digital processing steps may be employed but the initial selection of threshold level exerts a strong influence on whether a pixel in the final data set is classified as air or non-air. A systematic approach for threshold determination has been proposed based on an iterative procedure that compares automatically determined air-void parameters to manually determined air-void parameters from a set of training specimens. The calibration procedure finds a single optimum threshold level for the automated system that is to be used for all subsequent analyses. The approach was tested on a population of 88 specimens with manually determined air-void parameters, with the goal of determining an appropriate value for the number of training specimens.

KEYWORDS: air-voids, flatbed scanner, contrast enhancement, optimum threshold

Manuscript received March 31, 2009; accepted for publication July 28, 2009; published online September 2009.

¹ Dept. of Civil and Environmental Engineering, Michigan Technological Univ., 1400 Townsend Dr., Houghton, MI 49931.

² Exponent, 149 Commonwealth Dr., Menlo Park, CA 94025.

Cite as: Peterson, K., Sutter, L. and Radlinski, M., "The Practical Application of a Flatbed Scanner for Air-Void Characterization of Hardened Concrete," *J. ASTM Intl.*, Vol. 6, No. 9. doi:10.1520/JAI102446.

Copyright © 2009 by ASTM International, 100 Barr Harbor Drive, PO Box C700, West Conshohocken, PA 19428-2959.

Introduction

Entrained air-voids are an important member of the continuum of pores present in hardened concrete. The interaction between entrained air-voids and the surrounding capillary pore system of the hardened paste is the key to freeze-thaw (FT) durability. Most theories regarding the role of air-entrainment recognize that air-voids are interconnected with the capillary pore system of the hardened paste and that at low temperatures, fluids are likely to migrate to the larger air-voids as opposed to remaining in the capillary pores [1–6]. It is generally accepted that if there is sufficient entrained air to effectively drain the capillary pore system at low temperatures, FT damage can be avoided. Therefore, it is the quantity, size distribution, and spatial distribution of the air-voids relative to the existing capillary pore system that are of importance for concrete durability in FT environments.

Methods of Air-Void Characterization

The task of air-void characterization has traditionally fallen on the microscopist, who, according to ASTM Standard C457-08d, must either record the individual lengths of intercepts through air-voids, aggregates, and hardened paste by a test line (Procedure A Linear Traverse Method) or record the number of intersections between air-voids, aggregates, and hardened paste with a grid of test points; along with the number of intercepts through air-voids by a test line (Procedure B Modified Point-Count Method) [7]. From this data the air-void parameters are computed. Over the years, the spacing factor has been proven to be the most popular parameter for predicting the FT performance of concrete. The spacing factor describes for the bulk of the hardened paste a distance that would in most cases not be exceeded before reaching an air-void [8]. More recently, equations have been developed that utilize linear traverse measurements to determine the probability that a position within the cement paste is within a certain distance of an air-void, as well as the probability that a position within an air-void is within a certain distance of the cement paste [9]. This probability density function, termed the paste-void proximity distribution, is an elegant solution that accounts for most of the complexities of the quantity, size distribution, and spatial distribution of the air-voids in concrete.

Aside from stereologically based characterizations, actual three-dimensional measurements of the quantity, size distribution, and spatial distribution of the air-voids in concrete are possible through X-ray tomography [10]. Equipment is also commercially available for the measurement of the air content and size distribution in fresh concrete. The Air-Void Analyzer³ utilizes a vibrating cage to exclude the coarse aggregate fraction and obtain a mortar specimen from fresh concrete [11]. A known volume of mortar is injected into the base of a column containing a viscous fluid. The mortar is agitated by a magnetic stir-bar, and the air-voids (air bubbles) are released to float up the remainder of the water-filled column. A balance at the top of the column collects the air bubbles, and the change in mass versus time is recorded. Since

³Germann Instruments, Inc., Evanston, IL, USA.

larger air bubbles rise at a faster rate than smaller air bubbles, Stoke's Law is used to transform the recorded data into an air-void size distribution. If mix design information for the fresh concrete is known, estimates for the paste/air volume ratio can be computed, and the measurements converted to ASTM Standard C457-08d parameters.

Automated Stereological Methods

The equipment used to perform ASTM Standard C457-08d has traditionally included a stereomicroscope, a mechanical stage, and a tally counter. Many of the automated systems are based on the same microscope and mechanical stage format. The system used here replaces the microscope and mechanical stage with an ordinary flatbed desktop scanner and replaces the microscopist and tally counter with a personal computer; two pieces of equipment much more readily available than a microscope with a mechanical stage, and certainly easier to find than a person willing to sit for extended periods of time counting air bubbles.

Most of the automated systems in use today are based on the method developed by Chatterji and Gudmundsson, where the polished surface is painted black (or some other dark color) and white powder is forced into the depressions from air-voids [12–21]. The white powder also fills depressions from pores or cracks in the aggregate. The high contrast between regions of white powder and dark paint allows for easy visualization of the air-voids present in the concrete. The first step in the analysis of the digital images is to categorize the pixels that represent the air-voids. Most segmentation procedures based on contrast enhancement begin with a choice of threshold. Pixels in the digital image darker than the threshold level are classified as non-air; pixels brighter than the threshold level are classified as air. The most widely used automated system based on contrast enhancement, the RapidAir 457,³ relies on an operator to set the threshold level for each analysis [18]. Many of the automated systems employ additional digital processing to further refine the distinction between air and non-air pixels, such as dilation or erosion, or the evaluation of shape parameters. For example, cracks and pores in the aggregate, unlike air-voids, tend to be non-circular in cross-section and may be automatically discerned from air-voids on the basis of shape. However, some aggregates contain abundant spherical air-voids and are not well-suited for the application of such shape-based criteria. Automatic systems based on contrast enhancement often recommend the manual darkening of pores in aggregate with a pen prior to the collection of the digital images. This can be time consuming for concrete with abundant porous aggregate material.

In order to compute the spacing factor, the paste/air volume ratio for the specimen must be determined. For most concrete, the paste content is on the order of 25–40 % by volume [22]. Proponents of the RapidAir 457 system have pointed out that minor changes in the estimate of paste volume (on the order of ± 5 %) have a small impact on the calculated spacing factor (on the order of ± 0.02 mm) and thus rationalize the use of mix design information or a quick manual point count to obtain an estimate for paste content [18]. Other contrast-enhancement based methods have explored the application of paint or

chemical stains to preferentially color the hardened paste. By collecting digital color images, paste can then be discerned from aggregate and air-voids through spectral analysis [17,19,21].

Recently, two other automated systems have become commercially available for air-void characterization, both based on shape-recognition of entrained air as exposed on the polished surface under oblique illumination: The Automated Concrete Evaluation System⁴ and the HFMAC01.⁵ These systems collect images from the surfaces as-polished and do not require any contrast-enhancement preparation steps. From the literature, it is not clear how these methods arrive at values for the paste/air volume ratio, but values for spacing factor are determined [23]. Other automated systems have used a scanning electron microscope to collect images [24]. The list of automated systems referenced in this paper is extensive but not exhaustive.

Assessing the Accuracy of Automated Methods

The field of digital image accuracy has been developed primarily by the remote sensing/satellite imaging community [25]. As such, it relies on direct comparisons between information from pixels in a satellite image to information from the corresponding locations on the Earth's surface (ground truth). For example, pixels in a satellite image might be classified to represent either urban or rural areas. Since it is not practical to collect ground truth information from the entire area represented by the digital image, a small subset of pixels is used to perform an accuracy assessment. In this example 200 pixels are selected: 100 from the urban category and 100 from the rural category. The corresponding locations are checked on the Earth's surface. During the collection of ground truth information, it is determined that ten of the pixels categorized as urban are in fact rural, and by default, ten of the pixels categorized as rural are in fact urban. The overall agreement (one of the simplest accuracy assessment parameters) is 180 out of 200, or 90 %. The kappa statistic (\hat{K}) is a more robust accuracy assessment parameter and is a measure of the overall agreement minus the chance agreement. A \hat{K} of one indicates perfect agreement; a \hat{K} of zero indicates that the measured level of agreement is no better than would be expected to occur by chance. In this example, \hat{K} has a value of 0.8. Applied to the problem of air-void analysis, \hat{K} is a much more informative parameter than overall agreement. Suppose a digital image representative of a concrete specimen known to contain 2 % air by volume was analyzed and, perhaps through an inappropriate choice of threshold, was found to contain only 0.1 % air. In this case the image would be classified almost entirely as non-air, and although the overall accuracy near 98 %, \hat{K} would be very low, near 0.09. \hat{K} is the most

⁴Missouri Department of Transportation and the National Nuclear Security Administration Kansas City Plant, Kansas City, MO, USA.

⁵Hachiyo Consultant Co., Ltd., and Fast Corporation, Yamato-shi, Kanagawa Prefecture, Japan.

widely used parameter for digital image accuracy assessment but is rarely used to assess the accuracy of automated air-void analysis systems.

Most laboratories that perform air-void characterization typically have cabinets full of prepared specimens with corresponding results from manual operators. Proponents of automated systems often take advantage of this situation by analyzing the same samples and comparing the results. A similar iterative approach was used here. Scanned images were collected from the specimens, and the threshold automatically stepped between 0 and 255 (the discrete intensity levels of the scanned 8-bit grayscale images). At each threshold level, the images were analyzed, and the air-void parameters were compared to manual test results. An analysis of the absolute values of the residuals was performed to determine the threshold at which the residuals achieved a minimum value. A more rigorous approach would be to determine the threshold at which \hat{K} achieves a maximum. This approach was previously applied to the problem of threshold determination by Fung and LeDrew [26]. Both approaches have been compared and found to yield similar threshold values [27]. The reason the maximum \hat{K} approach is seldom used has to do with the fact that it would require the manual operator (when using Procedure A) to record stage coordinates at the beginning and end of each intercept. If using Procedure B, the manual operator would need to record stage coordinates at each point count stop. No matter which procedure is used, the stage coordinates of fiducial marks would also be required to align the scanned images to the stage coordinate system. Only then could a direct comparison be made between phases identified by the manual operator and the corresponding pixels from the digital images. Since manual operators tend to report only test results and not stage coordinates, it is seldom practical to implement the maximum \hat{K} approach.

Experimental

Materials

The 88 concrete specimens represent 12 different mixes, all with varying slump and air contents. All of the mixes had a water to cementitious ratio of 0.40, a cementitious content of approximately 332 kg/m³, a carbonate coarse aggregate content of approximately 1062 kg/m³ (top size of 19 mm), and a siliceous fine aggregate content of approximately 778 kg/m³. Substitutions of 20 % class C fly ash and 5 % silica fume were made by weight of cement for all mixes. A synthetic air entraining admixture and a high-range water reducing admixture were used, at varying dosages, for all mixes. A mid-range water reducing/set retarding admixture was used at a constant dosage for each mix. 75 mm dia. by 150 mm cylinders were cast after performing initial ASTM Standard C143/C143M-08 slump and ASTM Standard C231-08c fresh air content tests [28,29]. For some mixes, additional cylinders were cast, along with additional slump and air content tests, after either dropping the portion of the mix from a height of 1 m, placing the portion of the mix under vacuum conditions, or allowing the

portion of the mix to rest for a period of 1 h. The fresh air content measurements covered a range of 2–12 %, but the majority (two thirds) was within the range of 6–8 %.

A total of 44 cylinders were cast, and a 28 mm thick slab was cut with a water-cooled diamond saw from the middle of each cylinder. Both faces of each slab were polished for a total of 88 specimens. Each face was lapped using gentle hand pressure applied in a circular manner on a rotating lap charged with soapy water and (successively) 80, 160, 320, 400, and 600 silicon carbide and/or aluminum oxide grit. After the rotating lap, each face was lapped using gentle hand pressure applied in a circular manner on a stationary flat piece of glass charged with soapy water and (successively) 800 and 1000 silicon carbide and/or aluminum oxide grit. The faces and lapping surfaces were cleaned using water and a soft brush after each grit size.

Air-Void Analyses

Manual ASTM Standard C457-08d Procedure B Modified Point Counts were performed on the 88 specimens at a magnification of 60×. After the manual tests were completed, the polished surfaces of the slabs were painted black by drawing slightly overlapping parallel lines with a wide tipped black permanent marker. This was done in six coats, changing the orientation 90° between coats. After the ink dried, a few tablespoons of 2 μm median size white barium sulfate powder were worked into the samples using the flat face of a metal spatula. The spatula was used to scrape away excess powder, leaving behind powder pressed into voids. Residual powder was removed by wiping with a clean and lightly oiled fingertip. Pores and cracks exposed on aggregate particles were darkened with a fine-tipped permanent marker. Six small stickers were placed at intervals around the perimeter of each specimen to prevent the polished surface from resting directly on the glass plate of the flatbed scanner. Each specimen was scanned in 8-bit grayscale at a resolution of 125 dots per min (pixel size of 8 × 8 μm²) and saved in TIFF format using a conventional desktop flatbed scanner controlled by ArcSoftPhotoStudio 5.5 software.⁶ All software automatic filtering and enhancement options were deactivated. Scans were performed in a dark room with the scanner lid open. A flat steel plate with applied black and white vinyl electrical tape was included at the top of each scan. The intensity distribution (histogram) of pixels representative of the black and white tape was recorded for each scan. To compensate for slight differences in brightness and contrast from scan to scan, a linear stretch was performed on each scanned image using the dark and bright histogram peak locations (from the black and white tape) as reference end points [30]. Figure 1 shows an example subset of a scanned and linear-stretched image alongside the same area after the application of a threshold of 79 and after the execution of a watershed digital filter to separate adjacent air-voids [30]. Figure 1, when printed at a width of 17 cm, results in a magnification of approximately 50×, the minimum magnification required by ASTM Standard C457-08d.

⁶ArcSoft, Inc., Fremont, CA, USA.

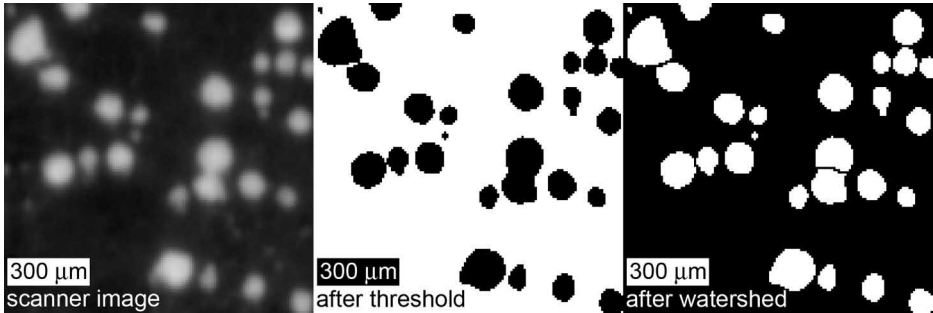


FIG. 1—Example subset of a scanned and linear-stretched image from specimen 20_1 (left), the same area after the application of a threshold of 79 (middle) and after the application of watershed operation (right).

A Visual Basic⁷ script was written to perform the automated analyses of the scanned images [31]. The script utilizes Photoshop CS2⁸ to select the areas on the images to be analyzed, to extract the traverse lines, and to apply the threshold levels. The area analyzed for each specimen was of the order of 75 cm² and the total traverse line length of the order of 5200 mm. Both values exceed the recommended minimum area and traverse length requirements specified by ASTM Standard C457-08d. The script utilizes Excel⁷ and Word⁷ to perform air-void calculations and to generate reports. The script has the option of whether or not to report an air-void chord length distribution. This option was deactivated during the threshold determination process to decrease the amount of time required to perform the analyses. Typically, an analysis with a total traverse length of 5 m and one threshold level takes 2 min to extract the traverse lines and 3 min to perform the calculations when the air-void chord length distribution is included. The same calculations take only 1 min when the air-void chord length distribution is omitted.

The script allows for two different methods for estimating the paste content: Calculation from mix design inputs (using material batch weights and specific gravities) or determination by manual point count on a scanned image of the polished surface collected prior to the contrast-enhancement procedure. To perform the manual point count, the script divides the image into frames, and the operator answers, frame by frame, either “yes” or “no” as to whether or not the cross-hairs falls on an aggregate particle. The paste content is computed by subtracting the sum of the vol % aggregate as determined by the point count and the vol % air as determined by the automated analysis from 100. Equation 1 shows the formula used by the script to calculate paste content from mix design inputs

⁷Microsoft, Inc., Redmond, WA, USA.

⁸Adobe, Inc., San Jose, CA, USA.

$$P = (100 - A) \frac{P_m / \text{Agg}_m}{1 + P_m / \text{Agg}_m} \quad (1)$$

where:

P = vol % paste,

A = vol % air determined from flatbed scanner system,

P_m = paste volume computed from mix design (absolute volume of the sum of cementitious, water, and admixtures), and

Agg_m = aggregate volume computed from mix design (absolute volume of the sum of coarse and fine aggregates).

Alternatively, the script allows the user to simply enter a value for the paste content. Entering mix design information into the script can be tedious, so there is also an option for the user to enter a single value: The hardened paste to aggregate volume ratio (P_m / Agg_m). For the 88 specimens in this study, a constant hardened paste to aggregate volume ratio of 0.355 was used to compute paste content. Although it would be preferable to use the most accurate estimate possible for paste content, the amount of effort required to obtain that estimate must also be taken into consideration. If the mix design is known, it requires little effort to compute the ratio of paste volume to aggregate volume. Similarly, if the mix design is not known, it requires little effort to make a quick visual estimate (guess) of the paste content. Quantifying the paste content through a manual point count requires the most effort, and the accuracy is dependent on the size of the area analyzed and the number of points sampled.

Results

Threshold Determination

During the automated procedure, only two measurements were made: The total number of air-void pixels and the total number of air-void intercepts. From these measurements (and the total linear traverse test line length), air content and void frequency were calculated as outlined in ASTM Standard C457-08d. All the remaining ASTM Standard C457-08d air-void parameters are derived using the values determined for air content, void frequency, and paste content. Therefore, to evaluate the effectiveness of the threshold level, the only parameters considered were air content and void frequency. To assess the influence of threshold on the measured air-void parameters, thresholds were stepped between 0 and 255. Thresholds between 20 and 215 were spaced consecutively. Thresholds from 0 to 20 and from 220 to 250 were spaced at intervals of ten. The script required approximately 3.5 h of computation to complete the full range of thresholds for each specimen for a total of 308 h.

Ideally, plots comparing manual and automated test results should lie on or near the line of unity. Figure 2 plots changes in the average deviation from unity for air content and void frequency versus threshold for the entire set of 88 specimens. To construct the plots, the absolute difference between unity and each automated procedure data point was calculated, and the result was divided by the value of the automated procedure data point. The average devia-

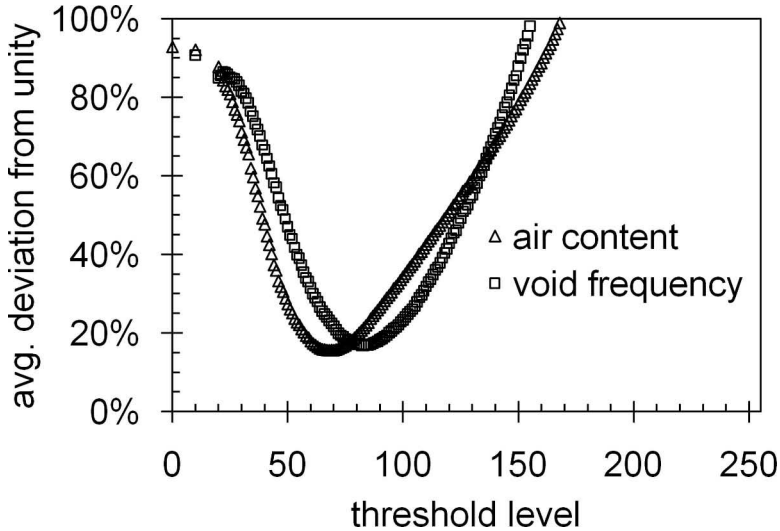


FIG. 2—Average deviation from unity for air content and void frequency versus threshold for the entire set of 88 specimens.

tion from unity was calculated using all of the data points from each specimen for each air-void parameter at each threshold level according to Eq 2 [27]

$$\text{Average deviation from unity} = \frac{1}{n} \sum_{i=1}^n \frac{|x_i - y_i|}{y_i} \quad (2)$$

The pronounced difference in the locations of the minima for air content and void frequency shown in Fig. 2 is due to the conflicting effect threshold has on the two parameters. When the size of an air-void approaches the size of a pixel, but the position of the air-void occurs between neighboring pixels, the intensities of those pixels become an intermediate combination of the bright air-void and the surrounding dark non-air. At a pixel resolution of $8 \times 8 \mu\text{m}^2$, a relatively low threshold is necessary to include these smallest air-voids in the analysis. At the same time, a low threshold will include more of the neighboring non-air pixels around larger air-voids, leading to an overestimation of the air content. For these reasons, the deviation from unity is lowest for void frequency when the threshold level is relatively low, and the deviation from unity is lowest for air content when the threshold level is relatively high.

The midpoint between the values reported for the minimum deviation from unity for air content and void frequency was used as a compromise for the selection of the ideal threshold. Although Fig. 2 is constructed using data from all 88 samples, similar plots were constructed on a specimen by specimen basis, and an individual ideal threshold was determined for each sample. Although an individual ideal threshold can be found for each specimen, the purpose of the exercise is to arrive at a single optimum threshold value to be used for all analyses. The use of a single optimum threshold eliminates the subjectivity

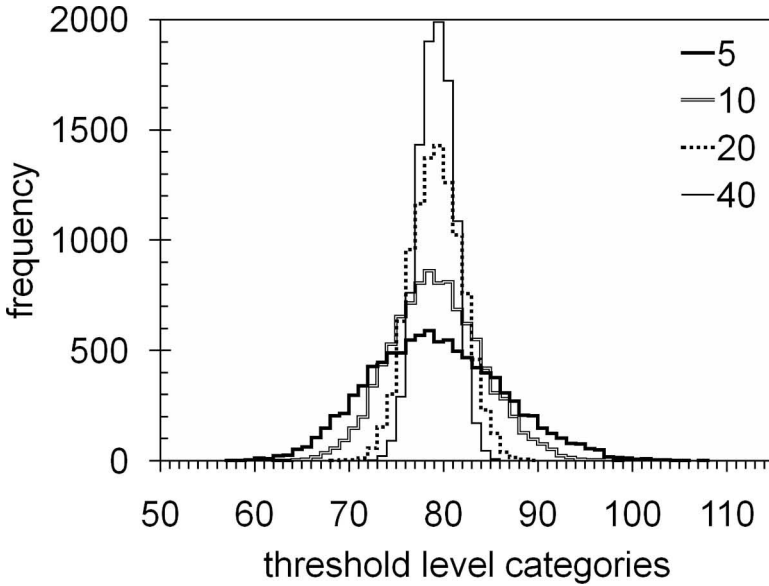


FIG. 3—Distribution of average values computed using random samples of sizes 5, 10, 20, and 40 from the population of 88 ideal threshold values and repeated 10 000 times.

inherent in operator selected thresholds and thereby improves reproducibility. Figure 3 illustrates the result of an experiment where random samples of sizes 5, 10, 20, and 40 were repeatedly taken (10 000 times) from the population of 88 ideal threshold values, and the average was tabulated. From Fig. 3, it appears that an appropriate value for the optimum threshold lies somewhere between 79 and 80. The computed average for the entire population of 88 samples was 79.3, with a standard deviation of 16.1. Threshold levels consist of whole numbers from 0 to 255, so the value of 79.3 must be rounded to the nearest whole number to yield a value for the optimum threshold. Tables 1 and 2 include a list of the individual ideal threshold values for the 88 specimens.

Manually and Automatically Determined Air-Void Parameters

Figure 4 shows the correlation between manual and automatically derived air-void parameters at an optimum threshold value of 79. Tables 1–4 list the manually and automatically derived air-void parameters along with results from the fresh concrete air content tests.

Assuming that the individual ideal thresholds are normally distributed, the sample size necessary to determine a value for the optimum threshold that is within a given confidence interval was computed. At a sample size of 20 and a 95 % confidence level, the confidence interval was ± 7 threshold levels. Even with larger sample sizes (greater than 30), the confidence interval remained on the order of ± 5 threshold levels. From a practical standpoint, considering the labor involved in performing manual air-void analyses, it is important to keep

TABLE 1—Individual ideal threshold values, air content measurements, and paste content measurements from fresh concrete, manual ASTM Standard C457-08d, and flatbed scanner system. All flatbed scanner measurements taken at optimum threshold level of 79.

ID	Ideal Threshold Level (Side 1, Side 2)		Air Content (vol %)				Paste Content (vol %)				
			Fresh Concrete	Manual (Side 1, Side 2)		Flatbed Scanner (Side 1, Side 2)		Manual (Side 1, Side 2)		Flatbed Scanner (Side 1, Side 2)	
20_1	84, 63	12.0	14.5,13.3	14.2,11.9	20.0,20.5	22.5,23.1					
20_4	86, 79	8.0	9.2,8.9	9.0,8.3	17.7,22.3	23.9,24.0					
21_1	72, 68	5.0	7.9,7.6	7.0,6.5	23.3,22.4	24.4,24.5					
21_2	64, 75	4.0	6.8,6.3	4.2,5.1	25.3,23.2	25.1,24.9					
21_4	62, 61	4.3	8.3,7.4	5.8,5.4	22.6,23.1	24.7,24.8					
22_1	78, 54	7.1	8.0,7.4	7.2,5.3	19.3,19.3	24.3,24.8					
22_4	69, 57	5.9	8.4,9.1	7.5,6.6	22.7,19.8	24.2,24.5					
23_1	71, 72	7.1	7.5,8.0	6.5,6.9	22.5,25.2	24.5,24.4					
23_2	75, 55	4.2	5.1,5.8	4.4,3.4	23.2,22.2	25.1,25.3					
23_4	77, 50	5.3	6.8,6.9	6.4,4.8	22.1,20.7	24.5,25.0					
24_1	63, 60	8.5	10.7,13.0	8.6,9.8	19.5,17.9	24.0,23.6					
24_2	68, 74	5.0	5.2,5.7	4.7,5.4	26.7,30.6	25.0,24.8					
24_4	65, 73	6.7	7.8,8.5	6.7,7.9	21.4,21.9	24.4,24.1					
25_1	96, 67	6.7	7.1,7.2	7.1,6.2	20.2,19.1	24.4,24.6					
25_2	74, 70	1.9	4.0,3.1	2.9,2.1	26.1,22.6	25.5,25.7					
25_4	102, 89	5.0	5.5, 5.0	5.6,5.0	25.5,26.6	24.7,24.9					
26_1	93, 60	5.7	6.3,5.5	5.9,4.2	21.8,25.1	24.7,25.1					
26_2	121, 94	3.3	3.2,2.6	3.6,2.8	27.0,25.5	25.3,25.5					
26_3	93, 110	4.7	3.9,4.2	4.0,5.2	25.8,27.4	25.2,24.9					
26_4	131, 89	4.6	4.2,4.6	6.1,4.6	26.9,26.8	24.6,25.0					
27_1	112, 87	11.0	11.9,11.8	13.3,10.9	17.8,18.7	22.7,23.4					
27_2	97, 77	2.2	3.4,3.4	3.3,3.2	20.7,24.7	25.4,25.4					

TABLE 2—Individual ideal threshold values, air content measurements, and paste content measurements from fresh concrete, manual ASTM Standard C457-08d, and flatbed scanner system; continued from Table 1. All flatbed scanner measurements taken at optimum threshold level of 79.

ID	Ideal Threshold Level (Side 1, Side 2)	Air Content (vol %)			Paste Content (vol %)		
		Fresh Concrete	Manual	Flatbed Scanner	Manual	Flatbed Scanner	Manual
			(Side 1, Side 2)	(Side 1, Side 2)			
27_3	103, 91	8.25	7.2,8.3	8.7,8.4	21.3,23.3	23.9,24.0	
27_4	77, 90	8.0	8.6,9.6	8.6,9.3	24.0,21.8	24.0,23.8	
28_1	85, 75	6.5	5.8,5.6	6.0,5.2	30.0,30.2	24.6,24.9	
28_2	108, 89	4.1	3.7,3.5	4.3,3.5	25.4,24.5	25.1,25.3	
28_3	106, 96	4.3	4.5,4.6	5.2,5.0	27.2,25.9	24.8,24.9	
28_4	95, 97	5.3	6.3,5.2	6.0,5.1	32.0,29.2	24.6,24.9	
29_1	95, 77	9.0	11.4,10.5	12.0,10.0	19.1,17.8	23.1,23.6	
29_2	57, 52	2.2	3.8,3.9	1.8,2.0	27.8,24.6	25.7,25.7	
29_3	83, 100	6.8	8.2,6.0	6.7,6.3	22.2,27.0	24.5,24.6	
29_4	69, 81	7.4	9.1,7.7	7.4,7.5	22.6,22.8	24.3,24.2	
30_I_1	78, 78	8.25	9.4,8.5	8.2,7.8	24.5,23.2	24.1,24.2	
30_I_2	95, 69	5.1	5.9,6.7	6.1,5.4	26.5,24.5	24.6,24.8	
30_II_1	59, 57	7.5	7.1,7.9	6.0,5.6	22.1,23.4	24.6,24.8	
30_II_2	77, 61	6.0	6.0,7.4	5.3,5.3	28.7,25.5	24.8,24.8	
30_III_1	74, 74	7.0	8.0,7.2	6.8,6.3	25.7,24.6	24.4,24.6	
30_III_2	76, 85	4.6	5.0,4.4	4.1,3.7	27.3,27.7	25.1,25.2	
31_I_1	75, 71	8.5	9.8,9.1	8.7,8.3	21.1,20.9	23.9,24.0	
31_I_2	70, 77	4.9	5.7,6.5	4.8,8.2	22.0,29.8	25.0,24.1	
31_II_1	100, 84	8.25	6.5,9.0	8.2,8.5	29.8,24.4	24.1,24.0	
31_II_2	91, 82	6.3	5.5,5.3	5.7,5.2	29.6,28.2	24.7,24.8	
31_III_1	79, 62	7.1	7.0,8.2	6.7,5.6	24.2,22.8	24.4,24.8	
31_III_2	65, 79	3.8	5.0,3.9	3.1,3.5	30.2,26.8	25.4,25.3	

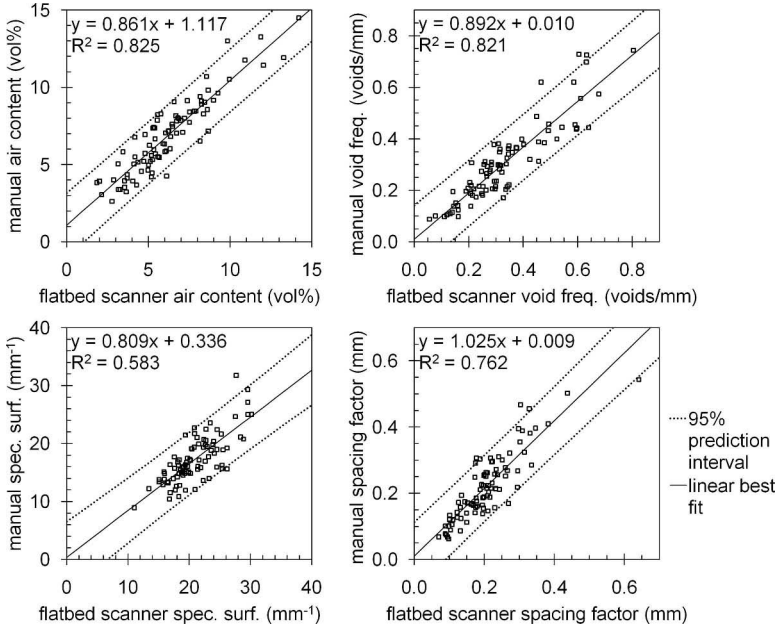


FIG. 4—Manual ASTM Standard C457-08d test results for air-void parameters versus flatbed scanner system at optimum threshold value of 79.

the number of training specimens required for the determination of the optimum threshold as low as possible. However, minimizing the number of training specimens increases the size of confidence interval, which prompts the question of what maximum limits on the size of the confidence interval can be tolerated. Figure 5 plots the effects of a ± 7 change in the optimum threshold value on the locations of the 95 % prediction intervals for the linear best fit with manually derived air-void parameters. Table 5 lists the average and standard deviations for the differences between the air-void parameters obtained at the optimum threshold and the air-void parameters obtained at the ± 7 interval.

Discussion

There is always the chance that the quantities, size distributions, and spatial distributions of the air-voids in the set of training samples are not adequately representative of air-voids in the real world. The choice of a single optimum threshold level may bias results such that the automatically determined air-void parameters are more realistic (i.e., more similar to manually determined air-void parameters) for some concretes than for others. For example, it might be expected that a relatively high choice for the optimum threshold level would yield better results for concretes with low air contents and fewer small entrained air-voids. However, within the population of 88 specimens explored here, no such trend was observed. Figure 6 plots the individual (specimen by

TABLE 3—*Air-void parameters from manual and flatbed scanner system at optimum threshold value of 79.*

ID	Void Frequency (voids/mm)		Specific Surface (mm ⁻¹)		Spacing Factor (mm)	
	Manual (Side 1, Side 2)	Flatbed Scanner (Side 1, Side 2)	Manual (Side 1, Side 2)	Flatbed Scanner (Side 1, Side 2)	Manual (Side 1, Side 2)	Flatbed Scanner (Side 1, Side 2)
	20_1	0.744,0.698	0.805,0.632	20.5,21.0	22.7,21.3	0.067,0.073
20_4	0.574,0.557	0.678,0.610	25.0,25.0	30.2,29.6	0.077,0.100	0.088,0.098
21_1	0.272,0.299	0.278,0.284	13.8,15.7	15.9,17.6	0.214,0.187	0.219,0.216
21_2	0.204,0.180	0.219,0.214	12.1,11.5	20.9,16.9	0.310,0.321	0.241,0.272
21_4	0.264,0.273	0.266,0.247	12.8,14.8	18.4,18.3	0.214,0.211	0.233,0.243
22_1	0.301,0.311	0.338,0.26	15.0,16.8	18.8,19.5	0.160,0.156	0.180,0.230
22_4	0.362,0.360	0.345,0.315	17.2,15.9	18.4,19.1	0.157,0.138	0.176,0.195
23_1	0.299,0.341	0.307,0.346	16.0,17.1	19.0,20.2	0.189,0.185	0.199,0.176
23_2	0.188,0.195	0.207,0.142	14.6,13.4	19.0,16.5	0.277,0.285	0.260,0.335
23_4	0.298,0.307	0.313,0.210	17.5,17.7	19.7,17.6	0.186,0.169	0.196,0.269
24_1	0.726,0.729	0.633,0.604	27.1,22.4	29.6,24.5	0.067,0.061	0.095,0.098
24_2	0.293,0.309	0.268,0.284	22.5,21.7	22.7,20.9	0.193,0.204	0.209,0.213
24_4	0.620,0.620	0.466,0.586	31.8,29.3	27.7,29.6	0.086,0.088	0.131,0.103
25_1	0.235,0.219	0.294,0.209	13.3,12.2	16.6,13.4	0.215,0.218	0.207,0.295
25_2	0.109,0.104	0.131,0.119	10.9,13.6	18.3,22.3	0.456,0.389	0.329,0.309
25_4	0.214,0.214	0.299,0.252	15.5,17.2	21.4,20.1	0.263,0.257	0.205,0.229
26_1	0.201,0.208	0.264,0.198	12.6,15.2	17.9,18.9	0.272,0.268	0.234,0.266
26_2	0.097,0.097	0.161,0.111	120,14.8	17.7,16.0	0.468,0.410	0.303,0.383
26_3	0.187,0.204	0.248,0.297	19.0,19.5	24.5,22.9	0.262,0.254	0.209,0.198
26_4	0.171,0.181	0.327,0.251	16.1,15.8	21.4,21.9	0.303,0.295	0.188,0.220
27_1	0.443,0.445	0.64,0.542	14.9,15.1	19.3,19.9	0.100,0.105	0.089,0.108
27_2	0.137,0.137	0.208,0.144	16.3,16.2	25.3,18.2	0.296,0.324	0.223,0.315

TABLE 4—Air-void parameters from manual and flatbed scanner system at optimum threshold value of 79; continued from Table 3.

ID	Void Frequency (voids/mm)		Specific Surface (mm ⁻¹)		Spacing Factor (mm)	
	Manual (Side 1, Side 2)	Flatbed Scanner (Side 1, Side 2)	Manual (Side 1, Side 2)	Flatbed Scanner (Side 1, Side 2)	Manual (Side 1, Side 2)	Flatbed Scanner (Side 1, Side 2)
27_3	0.442,0.437	0.597,0.595	24.7,21.1	27.5,28.4	0.121,0.133	0.100,0.101
27_4	0.487,0.455	0.450,0.590	22.7,18.9	20.9,25.5	0.123,0.12	0.133,0.101
28_1	0.282,0.279	0.313,0.279	19.4,19.9	20.8,21.5	0.224,0.223	0.197,0.211
28_2	0.123,0.114	0.161,0.139	13.4,12.9	15.1,15.7	0.381,0.397	0.330,0.347
28_3	0.214,0.206	0.342,0.288	19.2,17.7	26.2,23.1	0.248,0.256	0.173,0.200
28_4	0.221,0.203	0.348,0.336	14.0,15.6	23.2,26.2	0.307,0.291	0.177,0.174
29_1	0.399,0.398	0.523,0.395	13.9,15.1	17.4,15.8	0.120,0.112	0.110,0.149
29_2	0.100,0.087	0.077,0.055	10.4,8.9	16.8,11.0	0.503,0.543	0.438,0.642
29_3	0.320,0.313	0.425,0.457	15.7,20.8	25.4,28.9	0.173,0.193	0.144,0.134
29_4	0.347,0.325	0.360,0.340	15.2,16.8	19.5,18.1	0.163,0.176	0.169,0.178
30_I_1	0.431,0.457	0.492,0.493	18.3,21.6	24.1,25.2	0.142,0.127	0.122,0.122
30_I_2	0.236,0.230	0.301,0.204	16.0,13.8	19.7,15.1	0.251,0.267	0.204,0.295
30_II_1	0.378,0.381	0.293,0.310	21.5,19.3	19.4,22.3	0.146,0.154	0.210,0.197
30_II_2	0.295,0.300	0.318,0.256	19.8,16.3	23.9,19.3	0.211,0.212	0.188,0.233
30_III_1	0.378,0.366	0.401,0.375	18.8,20.4	23.6,24.0	0.170,0.168	0.152,0.164
30_III_2	0.187,0.173	0.208,0.227	14.9,15.9	20.2,24.5	0.300,0.306	0.251,0.218
31_I_1	0.379,0.372	0.401,0.347	15.4,16.4	18.5,16.8	0.139,0.14	0.149,0.173
31_I_2	0.215,0.384	0.238,0.478	15.0,23.6	19.9,23.4	0.255,0.172	0.237,0.126
31_II_1	0.384,0.388	0.478,0.456	23.6,17.2	23.4,21.6	0.172,0.157	0.126,0.131
31_II_2	0.270,0.254	0.322,0.267	19.8,19.1	22.6,20.3	0.226,0.231	0.192,0.222
31_III_1	0.363,0.349	0.376,0.314	20.7,17.0	22.3,22.6	0.166,0.164	0.163,0.195
31_III_2	0.151,0.140	0.152,0.160	11.9,14.2	19.4,18.1	0.395,0.355	0.297,0.302

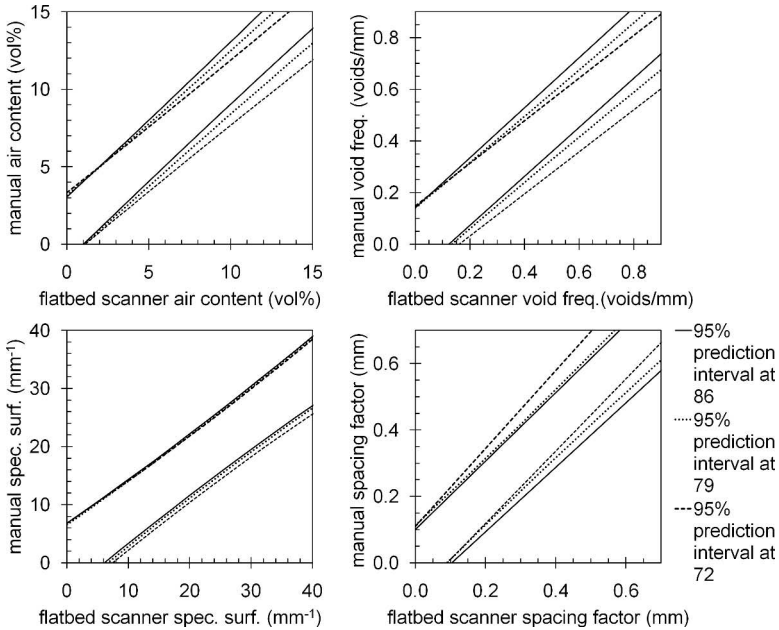


FIG. 5—Change in location of the 95 % prediction intervals for the linear best fit between air-void parameters from manual ASTM Standard C457-08d, and air-void parameters from flatbed scanner system over a ± 7 interval around the optimum threshold value of 79.

specimen) ideal threshold values against the manual results for air content and void frequency. The scatter in these plots is reassuring since it suggests that the individual ideal threshold values are independent of the air-void parameters of the specimens. Therefore, the number of training specimens used for the optimum threshold determination may be more important than a requirement to select training specimens that adequately represent the variety of air-void systems encountered in the real world.

For simplicity and speed, the automated system described here relies solely on threshold level to discern air from non-air. Most other automated systems use filters to some degree. Some are very simple, such as a minimum air-void chord length cut-off limit to remove short intercepts due to surface preparation defects [18]. Others are more sophisticated, using shape analysis to exclude non-circular features [13–16,20,21]. To address the issue of what degree of filtering should be employed, a minimum deviation from unity approach could be implemented. For example, the effectiveness of an air-void chord length cut-off filter could be assessed by varying the cut-off value while monitoring departures from unity with manual test results. Undoubtedly, the performance of the system described here could be improved through the incorporation of digital filters. For example, Fig. 1 shows that a watershed operation is an effective digital filter for the separation of air-voids in close proximity to each other.

TABLE 5—Average and standard deviations for differences between flatbed scanner system air-void parameters obtained at the optimum threshold value of 79 and air-void parameters obtained at the ± 7 threshold interval.

Air-Void Parameters	-7 Threshold (72)		+7 Threshold (86)	
	Avg. Difference	Std. Dev. Difference	Avg. Difference	Std. Dev. Difference
Air content (vol %)	-0.431	0.229	+0.358	0.177
Void frequency (voids/mm)	-0.031	0.017	+0.026	0.013
Specific surface (mm^{-1})	-0.543	0.520	+0.488	0.390
Spacing factor (mm)	+0.016	0.011	-0.014	0.007

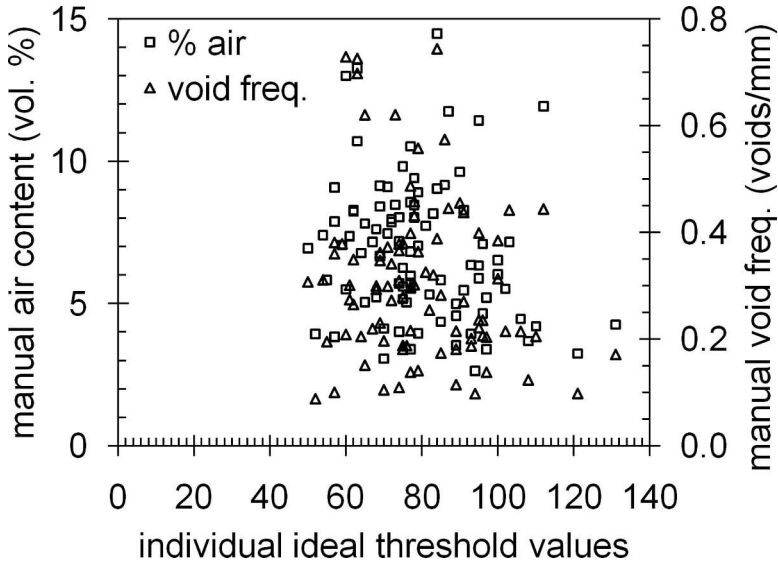


FIG. 6—Individual ideal threshold values versus manual air content and void frequency measurements.

However, it is important to note that the use of digital filters would result in a considerable increase in the time required to run a test.

In the absence of a universal standard, results from a manual operator are consistently used as a basis for comparison for automated systems [12–21,32–34]. Many investigations into the variability of manual test results have been conducted [7,33,35–38]. Some found the level of precision as adequate for “acceptance-rejection quality control,” while others were less sanguine, suggesting that “the wide variation between laboratories strongly supports the development of an automated image analysis system for performing ASTM Standard C457 measurements” [37,38]. Explorations of variation between automated systems have also been conducted [34,39]. The reliance on manual operator results to assess the performance of automated methods raises the question of why no universal standard has been made available. Some researchers have proposed the production of an artificial specimen with “multi-sized black circles superimposed on a white background... appropriate for ensuring that equipment is making accurate measurements” [38]. Even if an automated system is capable of accurately characterizing an artificial specimen, the question remains as to whether or not the automated system can adequately characterize a real concrete specimen. Judging the performance of an automated system based on the analysis of an artificial specimen does not necessarily ensure good results when analyzing the wide variety of concrete encountered in the field. However, ensuring that an automated method can accurately measure circles on an artificial specimen is important, and the production of such a standard should be pursued.

The automated system described here is hardly perfect. A major weakness

is the poor resolution of the scanned images. ASTM Standard C457-08d requires that air-voids of the order of $10\ \mu\text{m}$ in diameter “be clearly distinguishable” [7]. For the images analyzed here, it is doubtful that the appearance of a $10\ \mu\text{m}$ diameter circular intercept would meet that requirement (unless an $8 \times 8\ \mu\text{m}^2$ pixel is considered a clearly distinguishable representation). Although most scanner software packages allow the user to set the pixel size lower than $8 \times 8\ \mu\text{m}^2$, a decrease in pixel size does not necessarily result in an increase in resolution, at least not for ordinary desktop flatbed scanners. Prohibitively expensive high resolution flatbed scanners used by the publishing industry are capable of resolving features of the order of $3\ \mu\text{m}$.

With digital images, researchers are not limited to computing ASTM Standard C457-08d air-void parameters. Images that distinguish between aggregate, air-voids, and paste have been used to compute the distribution of distances between paste pixels and the nearest air-void pixels for the entire cross-section [21,40]. The paste-void proximity distribution, which excludes the presence of aggregate, could also be determined [9].

Conclusions

From Fig. 4 and Tables 1–4, there appears to be a reasonable correlation between the manual and automated test results when using the optimum threshold value of 79. The flatbed scanner method tended to slightly underestimate the manual measurements for air content with predicted values within a range of -3.2 – $+1.9$ vol % of the manual values. The flatbed scanner method tended to slightly overestimate the manual measurements for void frequency with predicted values within a range of -0.15 – $+0.20$ voids/mm of the manual values. The flatbed scanner method tended to overestimate the manual measurements for specific surface with predicted values within a range of -4.0 – $+10.6\ \text{mm}^{-1}$ of the manual values. The flatbed scanner method tended to overestimate the manual measurements for spacing factor with predicted values within a range of -0.16 – $+0.10$ mm of the manual values.

For quality control measurements the spread in scanner results as compared to manual results is problematic, especially in terms of air content, where in the worst-case scenario the flatbed scanner underestimated the manual measurement by 51 %. In spite of this performance, it can be seen from Tables 1–4 that both the flatbed scanner and manual methods performed similarly when compared to fresh concrete test results, with values reported within the ranges of -1.9 – $+2.9$ and -1.8 – $+4.5$ vol % of the fresh concrete air contents, respectively. Regardless of this outcome, the logical choice for quality control testing of air content would not be the labor-intensive ASTM Standard C457-08d based methods but rather the short-duration tests routinely used on fresh concrete: ASTM Standard C231-08c and ASTM Standard C173/C173M-08a [41]. Alternatively, the flatbed scanner method might be appropriate for quality control testing based on spacing factor. Generally, specimens with spacing factors that do not exceed 0.2 mm are expected to be durable in FT environments [7]. From Fig. 4 and Tables 1–4, of the 46 specimens that exceeded the 0.2 mm limit according to the manual test results, eight did not exceed the

0.2 mm limit according to the flatbed scanner results, with an average difference of -0.014 mm and a standard deviation of 0.001 mm (a false-acceptance rate of 17 %). Of the 42 specimens that did not exceed the 0.2 mm limit according to the manual test results, five exceeded the 0.2 mm limit according to the flatbed scanner results, with an average difference of $+0.027$ mm and a standard deviation of 0.025 mm (a false-rejection rate of 12 %). From this perspective, the flatbed scanner might be suitable as a screening method to discern specimens that fall clearly above or below the 0.2 mm limit and reserve the manual ASTM Standard C457-08d testing only for those specimens that fall near the 0.2 mm limit.

From Table 5, it can be seen that a variation of ± 7 on the optimum threshold had a noticeable effect on the measured air-void parameters. However, Fig. 5 suggests that the magnitudes of the changes are subtle when compared to the correlations with manually derived air-void parameters. Although a larger set of training specimens would provide a better estimate of the optimum threshold, a set of 20 specimens may be adequate.

The optimum threshold procedure provides a means of calibration to account for the wide variety of flatbed scanners that might be employed for air-void characterization. The automated system described here offers an easy to implement alternative to the manual ASTM Standard C457-08d procedures but is not a perfect substitute. In situations where large numbers of specimens are in need of air-void system characterization, the flatbed scanner method provides a practical means for consistent process control measurements.

Acknowledgments

This paper would not have been possible without the tireless efforts of Qinghuan Zhang, who provided the manual ASTM C457-08d data presented here.

References

- [1] Powers, T. C., "Freezing Effects in Concrete," *Durability of Concrete, ACI SP-47-1*, American Concrete Institute, Detroit, MI, 1975, pp. 1–12.
- [2] Litvan, G. G., "Freeze-Thaw Durability of Porous Materials," *Durability of Building Materials and Components, ASTM STP 691*, P. J. Sereda and G. G. Litvan, Eds., ASTM International, West Conshohocken, PA, 1978, pp. 455–463.
- [3] Marchand, J., Sellevold, E. J., and Pigeon, M., "The Deicer Salt Scaling Deterioration of Concrete—An Overview," *Durability of Concrete, ACI SP-145*, V. M. Malhotra, Ed., American Concrete Institute, Detroit, MI, 1994, pp. 1–46.
- [4] Pigeon, M. and Pleau, R., *Durability of Concrete in Cold Climates*, E & FN Spon, London, 1995.
- [5] Fagerlund, G., "On the Service Life of Concrete Exposed to Frost Action, Freeze-Thaw Durability of Concrete," *Freeze-Thaw Durability of Concrete, RILEM Proceedings 30*, J. Marchand, M. Pigeon, and M. J. Setzer, Eds., E & FN Spon, London, 1997, pp. 23–39.
- [6] Scherer, G. W. and Valenza, J. J., "Mechanisms of Frost Damage," *Materials Science of Concrete VII*, J. Skalny and F. Young, Eds., American Ceramic Society,

- Westerville, OH, 2005, pp. 209–246.
- [7] ASTM Standard C457-08d, 2008, “Standard Test Method for Microscopical Determination of Parameters of the Air-Void in Hardened Concrete,” *Annual Book of ASTM Standards*, Vol. 04.02, ASTM International, West Conshohocken, PA, pp. 253–256.
 - [8] Powers, T. C., “The Air Requirement of Frost-Resistant Concrete,” *Proceedings of the 29th Annual Meeting of the Highway Research Board*, December 13–16, 1949, Highway Research Board, Washington, D.C., pp. 184–211.
 - [9] Snyder, K., Natesaiyer, K., and Hover, K., “The Stereological and Statistical Properties of Entrained Air-Voids in Concrete: A Mathematical Basis for Air-Void System Characterization,” *Materials Science of Concrete VI*, S. Mindess and J. Skalny, Eds., American Ceramic Society, Westerville, OH, 2001, pp. 129–214.
 - [10] Landis, E. N. and Corr, D. J., “Three-Dimensional Analysis of Air-Voids in Concrete,” *Monitoring and Modeling Concrete Properties*, M. S. Konsta-Gdoutos, Ed., Springer, Dordrecht, 2006, pp. 517–524.
 - [11] Magura, D. D., “Air-Void Analyzer Evaluation,” *Report No. FHWA-SA-96-062*, U.S. Department of Transportation, Federal Highway Administration, Washington, D.C., 1996.
 - [12] Chatterji, S. and Gudmundsson, H., “Characterization of Entrained Air Bubble Systems in Concrete by Means of an Image Analysing Microscope,” *Cem. Concr. Res.*, Vol. 7, No. 4, 1977, pp. 423–428.
 - [13] Roberts, L. R. and Scali, M. J., “Factors Affecting Image Analysis for Measurement of Air Content in Hardened Concrete,” *Proceedings of the Sixth International Conference on Cement Microscopy*, Albuquerque, NM, March 26–29, 1984, International Cement Microscopy Association, pp. 402–419.
 - [14] Dewey, G. R. and Darwin, D., “Image Analysis of Air-Voids in Air-Entrained Concrete, Structural Engineering and Engineering Materials,” *SM Report No. 29*, The University of Kansas Center for Research, Inc., Lawrence, KS, 1991.
 - [15] Laurençot, J. L., Pleau, R., and Pigeon, M., “The Microscopical Determination of Air-Void Characteristics in Hardened Concrete: Development of an Automated System Using Image Analysis Techniques Applied to Micro-Computers,” *Proceedings of the 14th International Conference on Cement Microscopy*, Costa Mesa, CA, April 5–9, 1992, International Cement Microscopy Association, pp. 259–273.
 - [16] Pleau, R., Pigeon, M., and Laurençot, J. L., “Some Findings on the Usefulness of Image Analysis for Determining the Characteristics of the Air-Void System of Hardened Concrete,” *Cem. Concr. Compos.*, Vol. 23, 2001, pp. 237–246.
 - [17] Peterson, K. W., Swartz, R. A., Sutter, L. L., and Van Dam, T. J., “Hardened Concrete Air-Void Analysis with a Flatbed Scanner,” *Transportation Research Record. 1175*, Transportation Research Board, Washington, D.C., 2001, pp. 36–43.
 - [18] Pade, C., Jakobsen, U. H., and Elsen, J., “A New Automatic Analysis System for Analyzing the Air-Void System in Hardened Concrete,” *Proceedings of the 24th International Conference on Cement Microscopy*, San Diego, CA, April 7–11, 2002, International Cement Microscopy Association, pp. 204–213.
 - [19] Peterson, K., Sutter, L., and Van Dam, T., “Air-Void Analysis of Hardened Concrete with a High-Resolution Flatbed Scanner,” *Proceedings of the 24th International Conference on Cement Microscopy*, San Diego, CA, April 7–11, 2002, International Cement Microscopy Association, pp. 304–316.
 - [20] Zhang, Z., Ansari, F., and Vitillo, N., “Automated Determination of Entrained Air-Void Parameters in Hardened Concrete,” *ACI Mater. J.*, Vol. 102, No. 1, 2005, pp. 42–48.
 - [21] Zalocha, D. and Kasperkiewicz, J., “Estimation of the Structure of Air Entrained

- Concrete Using a Flatbed Scanner," *Cem. Concr. Res.*, Vol. 35, No. 10, 2005, pp. 2041–2046.
- [22] Kosmatka, S., Kerkhoff, B., and Panarese, W., *Design and Control of Concrete Mixtures*, 14th ed., Portland Cement Association, Skokie, IL, 2002.
- [23] Baumgart, C. W., Linder, K. D., and Cave, S. P., "An Automated Image Processing System for Concrete Evaluation," *Proceedings of the 23rd International Conference on Cement Microscopy*, Albuquerque, NM, April 29–May 4, 2001, International Cement Microscopy Association, pp. 342–351.
- [24] Schlorholz, S., "Image Analysis for Evaluating Air-Void Parameters of Concrete," *Final Report, Project No. HR-396, ISU-ERI-Ames 98403*, Iowa State University of Science and Technology, Ames, IA, 1998, p. 62.
- [25] Congalton, R. G. and Green, K., *Assessing the Accuracy of Remotely Sensed Data: Principles and Practices*, Lewis Publishers, New York, 1999, p. 137.
- [26] Fung, T. and LeDrew, E., "The Determination of Optimal Threshold Levels for Change Detection Using Various Accuracy Indices," *Photogramm. Eng. Remote Sens.*, Vol. 54, No. 10, 1988, pp. 1449–1454.
- [27] Peterson, K., Carlson, J., Sutter, L., and Van Dam, T., "Methods for Threshold Optimization for Images Collected from Contrast Enhanced Concrete Surfaces for Air-Void System Characterization," *Mater. Charact.*, Vol. 60, No. 7, 2009, pp. 710–715.
- [28] ASTM Standard C143/C143M-08, 2008, "Standard Test Method for Slump of Hydraulic-Cement Concrete," *Annual Book of ASTM Standards*, Vol. 04.02, ASTM International, West Conshohocken, PA, pp. 105–108.
- [29] ASTM Standard C231-08c, 2008, "Standard Test Method for Air Content of Freshly Mixed Concrete by the Pressure Method," *Annual Book of ASTM Standards*, Vol. 04.02, ASTM International, West Conshohocken, PA, pp. 157–165.
- [30] Russ, J. C., *The Image Processing Handbook*, 2nd ed., CRC Press, Inc., Ann Arbor, MI, 1995, p. 674.
- [31] Carlson, J. M., Sutter, L. L., Van Dam, T., and Peterson, K., "Advancement on the Application of a Flat-Bed Scanner for Hardened Portland Cement Concrete Air-Void Analysis," *Proceedings of the 27th International Conference on Cement Microscopy*, Victoria, BC, Canada, April 24–28, 2005, International Cement Microscopy Association.
- [32] Elsen, J., "Automated Air-Void Analysis on Hardened Concrete—Results of a European Intercomparison Testing Program," *Cem. Concr. Res.*, Vol. 31, 2001, pp. 1027–1031.
- [33] Jakobsen, U. H., Pade, C., Thaulow, N., Brown, D., Sahu, S., Magnusson, O., De Buck, S., and De Schutter, G., "Automated Air-Void Analysis of Hardened Concrete—A Round Robin Study," *Cem. Concr. Res.*, Vol. 36, No. 8, 2006, pp. 1444–1452.
- [34] Jana, D., "A Round Robin Test on Measurements of Air-Void Parameters in Hardened Concrete by Various Automated Image Analysis and ASTM C457 Methods," *Proceedings of the 29th International Conference on Cement Microscopy*, Québec, QC, Canada, May 26–28, 2007, International Cement Microscopy Association, pp. 34–69.
- [35] Sommer, H., "The Precision of the Microscopical Determination of the Air-Void in Hardened Concrete," *Cem., Concr., Aggregates*, Vol. 1, No. 2, 1979, pp. 49–55.
- [36] Pleau, R. and Pigeon, M., "Precision Statement for ASTM C457 Practice for Microscopical Determination of Air Content and Other Parameters of the Air-Void System in Hardened Concrete," *Cem., Concr., Aggregates*, Vol. 14, No. 2, 1992, pp. 118–126.

- [37] Saucier, F., Pleau, R., and Vezina, D., "Precision of the Air-Void Characteristics Measurement by ASTM C457: Results of an Interlaboratory Test Program," *Can. J. Civ. Eng.*, Vol. 23, 1996, pp. 1118–1128.
- [38] Simon, M., "An Interlab Evaluation of the Variability in the ASTM C457 Linear Traverse Method," *Final Report No. OR06-009/R198-006B*, Missouri Department of Transportation Organizational Results, Jefferson City, MO, 2005.
- [39] Carlson, J., Sutter, L., Van Dam, T., and Peterson, K., "Comparison of Flatbed Scanner and Rapid Air 457 System for Determining Air-Void Parameters of Hardened Concrete," *Transportation Research Record*. 1979, Transportation Research Board, Washington, D.C., 2006, pp. 54–59.
- [40] Peterson, K., Van Dam, T., and Sutter, L., "Determination of the Paste to Void Proximity Distribution in Two Dimensions from a Cross-Section Through a Concrete Specimen," *Proceedings of the Eighth Euroseminar on Microscopy Applied to Building Materials*, Athens, Greece, September 4–7, 2001, Euroseminar on Microscopy Applied to Building Materials, pp. 611–617.
- [41] ASTM Standard C173/C173M-08a, 2008, "Standard Test Method for Air Content of Freshly Mixed Concrete by the Volumetric Method," *Annual Book of ASTM Standards*, Vol. 04.02, ASTM International, West Conshohocken, PA, pp. 126–133.

Mateusz Radlinski,¹ Jan Olek,² Qinghuan Zhang,³ and Karl Peterson⁴

Evaluation of the Critical Air-Void System Parameters for Freeze-Thaw Resistant Ternary Concrete Using the Manual Point-Count and the Flatbed Scanner Methods

ABSTRACT: This research was conducted to verify whether the semi-automatic method of air-void system characterization (using a flatbed scanner) could be used in lieu of the manual (ASTM C457) method. This research objective was accompanied by evaluating the critical air-void system parameters required to ensure freeze-thaw resistance of ternary concrete containing ordinary portland cement (OPC), 20 % of fly ash (FA), and 5 % of silica fume (SF). It was observed that, due to adverse effect of high superplasticizer dosage on air-void system quality (particularly on specific surface), the majority of high slump ternary mixtures exhibited poor freeze-thaw resistance, even if spacing factor was below the 0.20 mm recommended value. However, when the ternary mixtures were prepared with slump below the

Manuscript received April 1, 2009; accepted for publication March 12, 2010; published online April 2010.

¹ Associate, Exponent Failure Analysis Associates, 149 Commonwealth Dr., Menlo Park, CA 94025. (Corresponding author), e-mail: mradlinski@exponent.com

² Professor, School of Civil Engineering, Purdue Univ., 550 Stadium Mall Dr., West Lafayette, IN 47907, e-mail: olek@purdue.edu

³ Assistant Engineer, China Concrete and Cement Products Association, No. 11 Sanlihe Rd., Haidian Dist., Beijing, 100083, China, e-mail: thu_qhzhang@hotmail.com

⁴ Research Assistant Professor, Dept. of Civil and Environmental Engineering, Michigan Technological Univ., 1400 Townsend Dr., Houghton, MI 49931, e-mail: krpeters@mtu.com

Cite as: Radlinski, M., Olek, J., Zhang, Q. and Peterson, K., "Evaluation of the Critical Air-Void System Parameters for Freeze-Thaw Resistant Ternary Concrete Using the Manual Point-Count and the Flatbed Scanner Methods," *J. ASTM Int'l.*, Vol. 7, No. 4. doi:10.1520/JAI102453.

Copyright © 2010 by ASTM International, 100 Barr Harbor Drive, PO Box C700, West Conshohocken, PA 19428-2959.

limit commonly specified for bridge deck applications (190 mm), the critical air-void system parameters of the OPC/FA/SF concrete were comparable to those typically associated with adequate quality air-void system in conventional concrete. Furthermore, since the critical value of specific surface was independent of slump (i.e., superplasticizer dosage), specific surface appeared to be more objective and reliable predictor of freeze-thaw resistance than spacing factor. When comparing the semi-automatic and manual methods of air-void system characterization, a reasonably strong agreement was obtained for such parameters as air content, void frequency, and spacing factor. Although the results of these methods did not match perfectly, the data suggested that the flatbed scanner technique could be efficiently used for discerning between freeze-thaw durable and non-durable concretes.

KEYWORDS: air-void, flatbed scanner, freeze-thaw, spacing factor, ternary concrete

Introduction

High performance concrete (HPC) has been used in construction applications for several decades now. However, for the last several years there has been an ongoing debate on the critical values of air-void system parameters needed to ensure freeze-thaw (F-T) resistance of HPC [1,2]. It is often argued that HPC may require more stringent air-void system parameters due to different characteristics of portland cement used nowadays, and more importantly, due to substantial amount of supplementary cementitious materials (SCMs), such as slag, fly ash (FA), and silica fume (SF) incorporated in HPC. In fact, several researchers reported relatively low F-T resistance of traditionally air-entrained concrete containing various quantities of SCMs [3,4]. Pigeon et al. [5] concluded that concrete containing SF may require lower spacing factor (and consequently higher air content) than ordinary portland cement (OPC) concrete due to refined system of capillary pores. Those authors hypothesized that such refinement would lead to reduction of the pore size accompanied by an increase in number of pores. Thus, more air-voids would be required to protect these pores.

The focus of the present study was on examining the air-void system in the ternary concrete containing OPC, FA, and SF. Although the ternary (OPC/FA/SF) concrete has proven its potential applicability for transportation structures (particularly for bridge decks [6–12]), virtually no data exist regarding the air-void system characteristics required to ensure adequate F-T resistance in such applications. Several researchers reported good F-T resistance (durability factor (DF) of about 80–100 %) of the OPC/FA/SF concrete with what is usually considered an adequate air-void system for plain (OPC) concrete [8,12,13]. In contrast, a preliminary study conducted by the authors of the present paper [14] revealed that the OPC/FA/SF concrete with fresh air content of 6.5 % (or higher) had substantially lower F-T resistance (DF of about 50–65 %) compared to that of the OPC concrete (DF of 92 %). Since such air content is typically assumed to provide protection against F-T damage, these findings were somewhat unexpected. Upon closer examination, it appeared that the observed reduced F-T durability might be, at least in part, linked to the use of frost-

susceptible aggregate and synthetic air-entraining agent. Nevertheless, the overall conclusion was that OPC/FA/SF concrete may require more stringent air-void system parameters than conventional concrete.

Even though a need for determination of critical air-void system parameters for F-T resistant HPC is well recognized in the concrete community, the cumbersome nature of the microscopical examination of the air-void system in hardened concrete (as per ASTM C457 [15]) creates a significant impediment. Much progress has been made lately to facilitate this process and to minimize the operator's subjectivity often associated with the microscopical determination of the air-void system parameters. As a result, several automated image analysis methods for determination of air-void system parameters have been introduced, including RapidAir 457 system [16], HF-MAC01 system [17], flatbed scanner technique [18], ACE system [19], and automatic image linear traverse method [20]. Of all of those methods, the flatbed scanner technique seems to be most appealing due to its comparatively low cost and readily available equipment (an office scanner).

Several studies have been carried out to assess the accuracy of the data obtained using a flatbed scanner when compared with those obtained from microscopical (ASTM C457) examination [18,21,22]. Although, in general, a good agreement was reported between these two methods, the current authors felt that the automatic method has not been verified on large enough number of specimens to properly address the question of its accuracy. The current research brought about the opportunity to verify the accuracy of the flatbed scanner technique using 88 specimens prepared with air contents (in the fresh state) ranging from about 2 to 12 %.

Objectives

The purpose of the study was twofold. The primary objective was to verify, on an array of concrete mixtures with different air content but having the same composition, whether the automatic method of air-void system analysis could be used in lieu of a time-consuming and operator-subjective manual microscopical determination. The second goal was to evaluate the critical air-void system parameters required to ensure F-T resistance of the ternary (OPC/FA/SF) concrete.

Experimental Program

Materials and Mixture Composition

The study was conducted on 12 batches of ternary concrete of the same nominal composition but with different amounts of superplasticizer and air-entraining admixture (AEA). The nominal water to cementitious materials ratio of all mixtures was 0.40. The mixtures contained 249 kg/m³ of Type I cement, 66 kg/m³ of class C FA (20 % by mass of total binder), 17 kg/m³ of densified SF (5 % by mass of total binder), 133 kg/m³ of water, 778 kg/m³ of fine aggregate (siliceous sand), and 1062 kg/m³ of coarse aggregate (crushed lime-

stone with maximum size of 19 mm). The limestone used in this study contained small amount of deleterious chert inclusions that had previously resulted in concrete with reduced F-T resistance [14]. The dosages of synthetic AEA and polycarboxylate-based high-range water reducing admixture (HRWRA) varied from mixture to mixture and were adjusted to obtain different slumps and air contents (Table 1). In addition, 433 mL/m³ of mid-range water reducing/set retarding admixture was used in each mixture.

Preparation of Test Specimens

All 12 batches were made in a laboratory pan mixer. In order to widen the range of air contents (and thus air-void system quality) beyond that achieved by variation of admixture dosages, samples of concrete from several batches were subjected to additional treatments, as described next. Immediately after completion of mixing, the slump and air content of fresh concrete were measured and one 75 × 150 mm cylindrical specimen (referred to in Table 1 as “Initial”) was cast. Subsequently, for selected batches, a portion of concrete was subjected to either vacuum treatment (using a vacuum pump with parameters prescribed for conditioning of specimens according to ASTM C1202 [23] procedure), dropped from a distance of about 1 m (from upper hopper of compacting factor apparatus [24]) or left undisturbed for 1 h. After each of these treatments, the slump and the air content were determined and one 75 × 150 mm specimen (referred to in Table 1 as, respectively, “Vac,” “Dropped,” and “Final”) was cast. The resulting range of fresh concrete air contents was from 1.9 to 12.0 %, while slump varied from 15 to 255 mm. In total, 44 75 × 150 mm cylindrical specimens were cast from the 12 batches. The summary of fresh concrete properties for all specimens is provided in Table 1. After casting, the specimens were moist cured for approximately 2.5 years prior to testing.

Test Procedures

Manual Air-Void System Analysis—The manual air-void system analysis was conducted using an optical microscope set to magnification of 60× and following the ASTM C457 modified point-count method [15]. This method was adopted from geological sciences and is based on stereological principles of three-dimensional interpretation of planar sections. The original mathematical foundation for the technique laid down by Powers [25,26], Willis [27], and Lord and Willis [28] were later modified by Mielenz et al. [29].

A 70 × 150 mm and 28 mm thick slab was cut from the center of each of 75 × 150 mm cylinders with a water-cooled saw. This size of the slab was selected as a compromise between the need to maximize the area of two sides of the slab for the air-void system determination and to maximize the thickness of the specimen (to minimize the influence of deleterious chert inclusions in coarse aggregate on F-T resistance of concrete determined on the same specimen). To increase the accuracy of determination of air-void system parameters, both of the larger sides of all 44 slabs were polished and tested following the

TABLE 1—*Fresh concrete properties.*

Specimen	AEA Dosage (mL/m ³)	HRWRA Dosage (mL/m ³)	Slump (mm)	Air Content (%)	Density (kg/m ³)	Specimen	AEA Dosage (mL/m ³)	HRWRA Dosage (mL/m ³)	Slump (mm)	Air Content (%)	Density (kg/m ³)
1_Initial	97	2580	190	12.0	2171	8_Dropped			195	8.2	2244
1_Final			65	8.0	2260	8_Final			100	8.1	2244
2_Initial	28	1935	75	5.0	2334	9_Initial	39	2043	110	6.5	2299
2_150 s Vac			35	4.0	2347	9_150 s Vac			70	4.1	2345
2_Final			15	4.3	2360	9_Dropped			50	4.4	2332
3_Initial	43	3118	215	7.1	2275	9_Final			20	5.3	2313
3_Final			70	5.9	2307	10_Initial	65	2903	255	9.1	2196
4_Initial	32	2892	235	7.1	2262	10_150 s Vac			230	2.2	2379
4_150 s Vac			210	4.2	2348	10_Dropped			220	6.8	2267
4_Final			90	5.3	2310	10_Final			150	7.4	2247
5_Initial	86	1720	110	8.5	2228	11_Initial	84	2043	130	8.3	2241
5_150 s Vac			70	5.0	2345	11_30 s Vac			100	5.1	2331
5_Final			20	6.7	2294	11_Initial2			70	7.5	2255
6_Initial	30	2903	230	6.7	2275	11_15 s Vac			70	6.0	2303
6_150 s Vac			200	1.9	2388	11_Initial3			60	7.0	2279
6_Final			70	5.0	2319	11_60 s Vac			50	4.6	2329
7_Initial	32	2043	115	5.7	2311	12_Initial	71	2688	215	8.4	2223
7_150 s Vac			80	3.4	2355	12_30 s Vac			190	4.9	2331
7_Dropped			55	4.7	2327	12_Initial2			150	8.3	2231
7_Final			40	4.6	2355	12_15 s Vac			145	6.3	2289
8_Initial	86	2903	240	11.0	2183	12_Initial3			130	7.1	2265
8_150 s Vac			215	2.3	2390	12_60 s Vac			115	3.8	2335

Note: Each mixture contained 433 mL/m³ of mid-range water reducing/set retarding admixture.

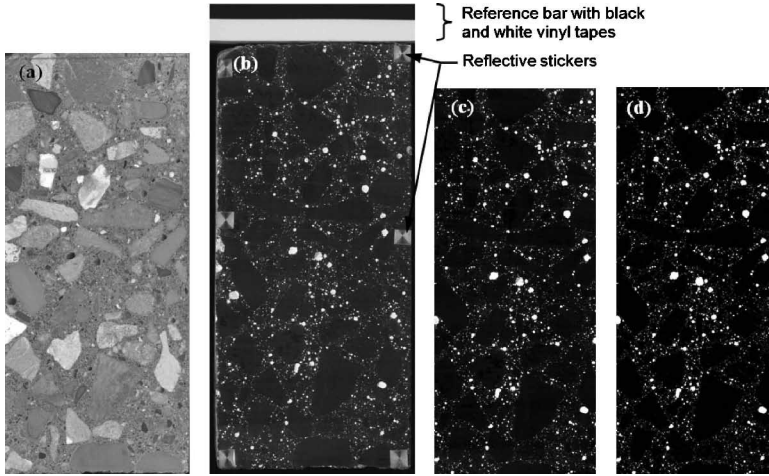


FIG. 1—Illustration of surface of the air-void system analysis specimen: (a) polished (used for manual method); (b) black-colored with filled voids (scanned using flatbed scanner); (c) after histogram stretching and cropping; and (d) after thresholding.

ASTM C457 procedures, which resulted in 88 specimen surfaces available for air-void system analysis. An example of polished specimen surface is shown in Fig. 1(a).

Automatic Air-Void System Analysis—The sample preparation procedure for automatic air-void system analysis was adopted from the previously published studies by Jakobsen et al. [16] and Carlson et al. [30]. A black permanent marker with a 16×4 mm tip was used to paint the concrete surface using a series of parallel, slightly overlapping lines. The painting process was repeated six times in alternately perpendicular directions, after which the ink was allowed to dry. Barium sulfate powder with an average particle size of about $2 \mu\text{m}$ was then uniformly spread on the surface and pressed in the air-voids using a flat metal spatula. The excess powder was removed by first gently passing over the treated surface the edge of a spatula and then a slightly oiled open hand. Next, the barium sulfate in-filled air-voids present in aggregate were over-painted with a narrow-tipped black permanent marker. Following this, six square reflective stickers were applied to the surface (see Fig. 1(b)) to raise the surface of the specimens above the glass panel of the scanner and thus preventing its scratching.

Both sides of each concrete slab were scanned at a resolution of 125 dots per millimeter (dpm) (pixel size $8 \times 8 \mu\text{m}$) in 8-bit grayscale mode using a Canon[®] CanoScan 4400F flatbed scanner controlled by ArcSoft PhotoStudio[®] 5.5 software. All automatic filtering and enhancement options of the software were deactivated and the scanning was performed in a dark room with the cover of the scanner open. To ensure consistency of the automatic air-void system analysis procedure, each of the 88 specimen surfaces was scanned in the presence of a flat metal bar with white and black vinyl tape strips applied to

it, as shown at the top of Fig. 1(b). Analysis of the histogram of the scan for the bar with the vinyl tapes showed it to be essentially bi-modal with a peak corresponding to the black tape centered at a gray level of about 38, rather than 0 (perfectly black), and with a peak corresponding to the white tape centered at about 225, rather than 255 (perfectly white). This analysis was performed for every scan to provide consistent bright and dark reference points, as proposed by Peterson et al. [31]. These reference points were then used to perform linear histogram stretching of the scans of each specimen by ascribing a brightness level equal 0 (black) to the low (~ 38) gray level histogram peak and a value of 255 (white) to the high (~ 225) gray level histogram peak (Fig. 1(c)). The “histogram-stretched” images were subsequently cropped to exclude the stickers while maximizing the area available for the analysis (Fig. 1(c)).

The automatic air-void system analysis was performed using *bubble_counter_v2008.vbs* software developed at Michigan Technological University [21]. The first step of this analysis involved converting the grayscale images into binary (black and white) format. To entirely eliminate the operator's subjectivity while performing this conversion, a constant threshold level of 82 was applied to grayscale images of all 88 specimens. This value represented the optimum threshold level for five randomly selected specimens and was determined using the “minimum deviation from unity” method developed by Peterson et al. [31]. Figure 1(d) shows a binary image of the specimen after thresholding operation. Results of recently conducted sensitivity analysis on the accuracy of the flatbed scanner method with respect to threshold level are published elsewhere [32]. While performing the automatic air-void system analysis, a constant paste-aggregate ratio of 0.355 was assumed for all samples analyzed. This value was based on the volume fractions calculated from the mix design, using batch weights and specific gravities. The number of iterations performed by the software was set at 2. This resulted in total traverse length of approximately 5200 mm, which was well above 2286 mm required by ASTM C457 for the maximum aggregate size used.

Freeze-Thaw Resistance—Once the automatic air-void system analysis was completed, the barium sulfate powder was removed from the air-voids using compressed air. Subsequently, all specimens were placed in lime saturated water for a period of 5 weeks. The mass of the specimens was monitored periodically (every 3 days) and no significant increase was observed for any of the specimens toward the end of the soaking period. After 5 weeks, the specimens were removed from the lime water and subjected to F-T resistance testing as per Procedure A of ASTM C666 [33]. Since the specimen age at the time the F-T test was commenced varied from 2.5 to 3 years, the specimens can be regarded as well cured. As shown in Fig. 2, four slabs were placed in one standard F-T container. The open space surrounding the specimens was reduced to minimum by placing foam insulation between the long sides of the specimens, as well as near the ends of the container, in order to minimize the amount of water surrounding the specimens.

The relative dynamic modulus of elasticity was determined approximately every 36 F-T cycles using the impulse excitation technique (ASTM C1259 [34]). The values of relative dynamic modulus of elasticity after 300 F-T cycles were

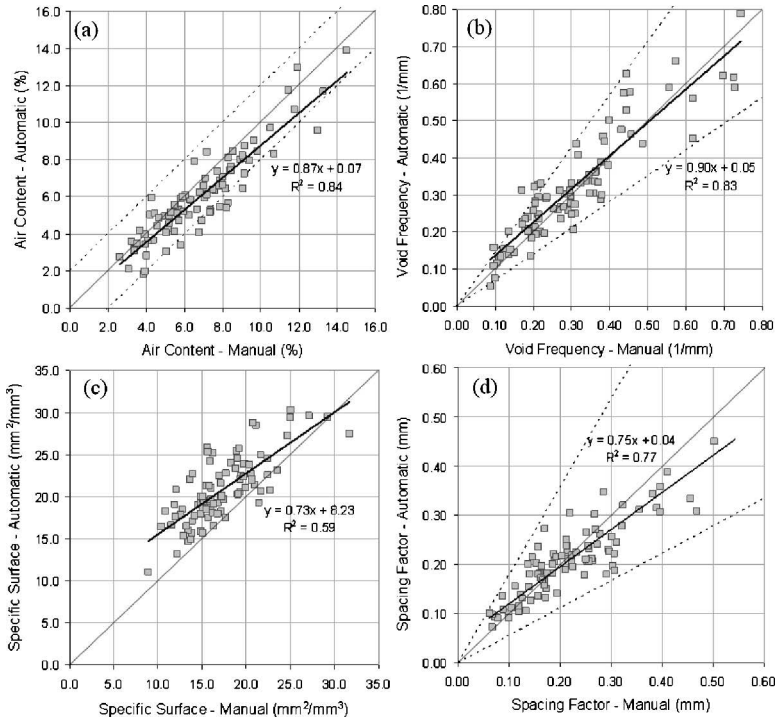


FIG. 3—Comparison of results of air-void system analysis from manual and automatic methods for: (a) air content; (b) void frequency; (c) specific surface; and (d) spacing factor.

differences between two test results for specific surface, it appears that the results obtained from the automatic method are, in almost all cases, higher than those from the manual determination (Fig. 3(c)). This is likely a consequence of lower air contents obtained using the scanner technique as compared to those from the microscopical determination (Fig. 3(a)) at comparable void frequency values (Fig. 3(b)). Finally, the agreement between the two methods for the spacing factor seems acceptable, as none of the data points lay outside of the acceptable range.

In addition, statistical analysis using two-sample t-test with unequal variances (at significance level $\alpha=0.05$) indicated that there was no statistically significant difference ($p\text{-value}\leq 0.05$) between the two methods for the void frequency and spacing factor. Since spacing factor is typically considered the most important parameter describing the ability of air-void system to provide F-T resistance [15,36], it follows that the flatbed scanner technique may be used as a means of recognizing the adequacy of a given air-void system.

It should be noted that the comparison between the manual and automatic method shown in Fig. 3 is relative, i.e., there is no reason as to why one set of data should be viewed as more “correct” than the other. There are several reasons for lack of perfect match of data from the automatic method with those

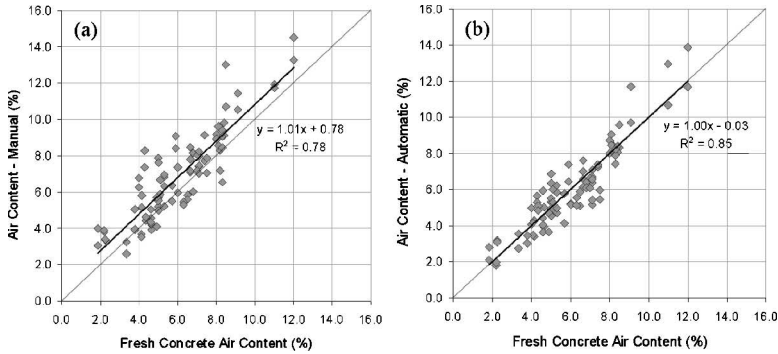


FIG. 4—Relationship between fresh concrete air content and hardened concrete air content from: (a) manual method; (b) automatic method.

from the manual method. To begin with, the automated system incorporated in this study suffers from relatively poor resolution. Since the resolution of the flatbed scanner results in $8 \times 8 \mu\text{m}$ pixel size, there is a possibility that very small air bubbles ($\sim 10 \mu\text{m}$) were not “detected” by the scanner. Furthermore, in an attempt to entirely eliminate the operator’s subjectivity, a single threshold grayscale level (82) was incorporated while processing the images. Sensitivity analysis performed in parallel with the present research [32] showed that each sample has its own “ideal” threshold level, for which the air-void system parameters determined by automatic and manual methods would result in a perfect match for a given specimen. In addition, in the case of the automatic method the paste content was estimated based on mix proportions, whereas it was calculated based on the number of stops in paste during the manual point-count procedure. The aforementioned reasons would suggest that the automatic method inherently produces less correct results compared to the manual method. However, the operator’s subjectivity during the manual air-void system parameters determination has been reported to produce a significant degree of variability [36], whereas the automated method is entirely independent of the operator.

One way to verify which method is more correct would be to perform the air-void system analysis using several other independent methods, such as those mentioned in the “Introduction” part of the paper. In the absence of such data, an attempt to verify the “correctness” of the obtained values was made by comparing the air contents from either the manual point-count or from the automatic method with the air contents measured in fresh concrete (Fig. 4). Interestingly, the hardened concrete air contents from the automatic method appear to correspond better to the fresh concrete air contents from pressure method (note a slope of regression line equal 1.00 and an intercept of 0.03 shown in Fig. 4(b)) than these from the microscopical determination (Fig. 4(a)).

Section 5.6 of ASTM C457 [15] states that for high air content concrete (usually above 7.5 %), the air content determined microscopically may be higher (by 1 % or more) than that of a fresh concrete determined using the ASTM C231 [37] pressure method. This trend has definitely been observed in

the current study, as higher hardened concrete air contents were typically determined for the entire range of fresh concrete air contents tested (1.9–12.0 %) when using the manual method (Fig. 4(a)). On the contrary, for fresh concrete air contents of about 2 to 8.5 %, the estimates from the scanner method are uniformly spread above or below the equality line (Fig. 4(b)), whereas for air contents above about 8.5 % the scanner method tends to show higher air contents than those measured in the fresh state.

One of the common explanations for higher hardened concrete air content (obtained using manual point-count method) compared to fresh concrete air content (obtained using pressure method) is poor surface preparation which tends to erode the void edges [38]. However, the quality of polished surface was carefully examined and was considered excellent. Furthermore, since the same specimens were later tested using automatic method, equally consistent over-estimation of air contents would be expected from the automatic method. Due to the complexity of the problem, this issue has been a topic of discussion for several decades [36,38]. Based on the present study, the most logical explanation for higher air contents from the manual method appears to be subjectivity of the operator conducting the point-count procedure. Specifically, somewhat consistently higher air contents compared to either the scanner technique or the pressure method can be explained by the operator's bias in situations when the cross-hair falls directly on the edge of an air-void.

Determination of Critical Air-Void System Parameters for Ternary Concrete

General—The results presented in the previous section showed that the air-void system parameters obtained using the flatbed scanner technique appear to be comparable to those from the manual point-count method. Since F-T resistance of concrete is ultimately of relevance, it was important to determine whether the flatbed scanner technique is accurate enough to distinguish between F-T durable and non-durable concretes (in the same way as one would expect from the manual method). Comparison of the critical air-void system parameters obtained from the two methods follows.

In the analysis performed in this paper, DF of 60 % was used as a threshold value to distinguish between F-T durable and non-durable concrete, as this threshold value is generally accepted by the industry for these purposes [39–41]. The analysis was performed using the data obtained by averaging the test results for both sides of the specimens. Figure 5 shows the DF as a function of either the air content or the other air-void system parameters determined using the manual point-count method. It can be seen that only two specimens achieved the DF above 80 %. This may be related to the use of synthetic air-entraining agent, which is reportedly less effective in providing F-T resistance than, for instance, Vinsol[®] resin-based admixture [42].

Although the data appear rather scattered with no obvious trends visible, several important features can be derived from these plots. When all data points shown in Fig. 5(a) are taken into consideration, the minimum air content required to ensure the DF higher than 60 % appears to be about 11.5 %. Analogically, the required values of void frequency, specific surface, and spacing factor (Fig. 5(b)–5(d)) appear to be, respectively, 0.42 voids/mm,

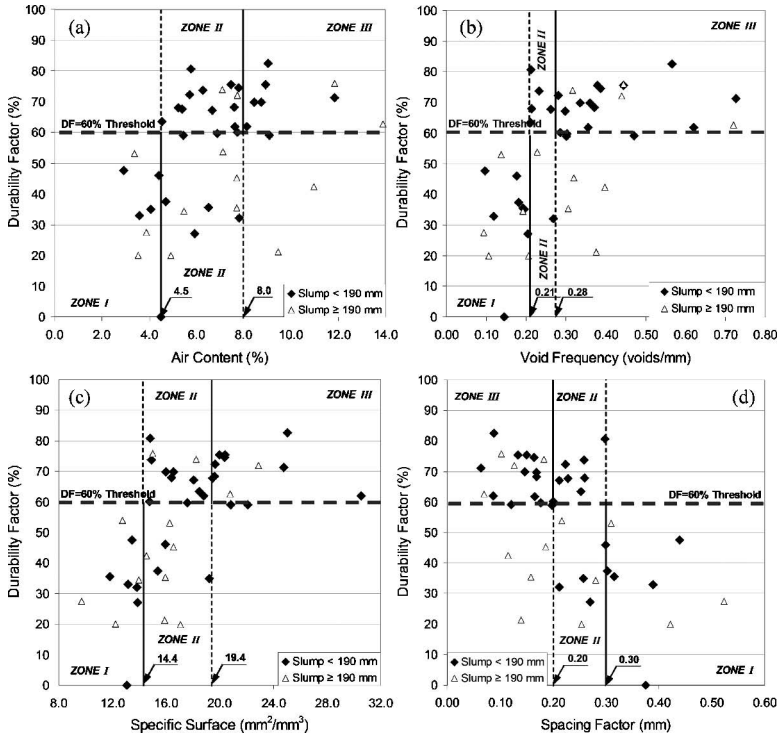


FIG. 5—Relationship between DF and (a) air content; (b) void frequency; (c) specific surface; and (d) spacing factor obtained from manual point-count method.

19.4 mm^2/mm^3 , and 0.10 mm. With the exception of the required specific surface being in agreement with the commonly established criteria for F-T resistant concrete [36], these values seem to be unreasonably rigorous.

Effect of Superplasticizer—A thorough analysis of potential reasons for those rather unexpectedly rigorous values of air content, void frequency and spacing factor revealed that majority (10 out of 14) of the specimens prepared from concrete with excessive (190 mm or higher) slump exhibited poor F-T resistance (Fig. 5). Such outcome could be the result of segregation or bleeding of concrete with excessive slump. However, it was likely not the case in the present study as segregation was observed in one sample only, whereas potential effect of bleeding was minimized by trimming the top sample ends before F-T testing.

While the slump might be slightly affected by the dosage of air-entraining admixture, it was most significantly influenced by the dosage of HRWRA (superplasticizer). This suggests that, as previously reported by others [43–46], the superplasticizer adversely affected the air-void system. Statistical analysis was conducted (at significance level $\alpha=0.05$) to determine the specific effect of the superplasticizer and air-entraining admixture dosages on fresh and hardened

concrete air contents and other air-void system parameters. Such data were available for 12 “Initial” samples (see section “Preparation of Test Specimens”). The results of the analysis (summarized in Table 2) include regression models for each individual parameter with predictor variables being the dosage of air-entraining admixture and, either the dosage of superplasticizer or the product of the two (if statistically significant (p -value ≤ 0.05)). The obtained models indicate that the air content increased with an increase in the superplasticizer dosage. At the same time, the increase in the superplasticizer dosage caused the decrease in the specific surface values. This implies that superplasticizer addition led to creation of air bubbles (as indicated by increased air content) which were coarser than the air bubbles stabilized by air-entraining admixture (as indicated by reduced specific surface values). Interestingly, the R^2 values for all four models developed for the air-void system parameters obtained using the scanner technique were higher than for those from the manual point-count method. Such outcome is likely not coincidental and indirectly suggests a better degree of accuracy of the scanner method.

Critical Air-Void System Parameters for Ternary Concrete with “Acceptable” (<190 mm) Slump—While the previous section discusses detrimental effect of superplasticizer dosage (and hence slump) on the air-void system, the vital question of the critical values of air-void system parameters for ternary concrete with “acceptable” slump remains unanswered. Therefore, the objective of the following section was to determine whether the ternary concrete prepared with slump below the applicable limit requires more stringent (compared to OPC concrete) air-void system parameters to ensure F-T resistance. The threshold slump value of 190 mm was assumed in this study as acceptable as it represents the maximum allowable slump commonly specified for HPC bridge deck concrete [47–49], which is the intended application of the ternary mixture studied in this research.

After sorting all data with respect to slump and excluding all values obtained for specimens with excessive (≥ 190 mm) slump, the analysis of the critical air-void system parameters was repeated, starting with the manual method data. While the selected data still lacks clear trends, it could be reasonably divided into three zones (see Fig. 5). Zone I represents F-T non-durable concrete (DF < 60 %), zone II can be thought of as a transition zone (DF both lower or higher than 60 %), and zone III represents F-T durable concrete (DF > 60%). Such arrangement of data is consistent with that previously proposed by Natesaiyer and Hover [50], who observed that although the present acceptance criteria “can identify concrete that is almost certainly frost-resistant and concrete that is almost certainly non-frost-resistant, there exists a broad, marginal zone or ‘gray area’ in which frost resistance is difficult to judge.” The boundary values selected to separate each of these three cases are shown in Table 3. It seems that (based on the manual method data) the minimum air content required to provide a potential for F-T resistance (zone II) of the ternary concrete studied is about 4.5 %. All concretes with air content of 8.0 % and higher had a DF of at least 60 %. Although this is higher than the typically recommended value of 6.5 %, it should be noted that if it was not for one data point (air content of 7.8 % and DF of 35 %), the boundary between zone II and

TABLE 2—Linear regression model coefficients for air-void system parameters from manual and automatic methods.

Parameter	Method	Constant	Air-Entraining Admixture		R^2
			Admixture Dosage (mL/m ³)	Dosage × Superplasticizer (mL ² /m ⁶)	
Fresh concrete air content (%)	...	+0.0416	+0.0711	...	0.92
Hardened concrete air content (%)	Manual	+4.3949	...	+3.3 × 10 ⁻⁵	0.76
	Automatic	+3.2287	...	+3.4 × 10 ⁻⁵	0.82
Void frequency (voids/mm)	Manual	+0.068	+0.0057	...	0.74
	Automatic	+0.073	+0.0057	...	0.87
Specific surface (mm ² /mm ³)	Manual	+12.99	+0.2530	...	0.74
	Automatic	+15.34	+0.2586	...	0.78
Spacing factor (mm)	Manual	+0.283	-0.0022	...	0.80
	Automatic	+0.292	...	-7.7 × 10 ⁻⁷	0.82

Note: Example of regression equation: Fresh concrete air content = 0.0416 + 0.0711 × air entraining admixture dosage + 0.0015 × superplasticizer dosage.

TABLE 3—Boundary values of air content and air-void system parameters for F-T non-durable concrete (zone I), transition zone (II) and F-T durable concrete (zone III) based on the data from manual and automatic air-void system analyses for specimens with slump lower than 190 mm.

Boundary	Method	Air Content (%)	Void Frequency (voids/mm)	Specific Surface (mm^2/mm^3)	Spacing Factor (mm)
Zone I-II	Manual	4.5	0.21	14.4	0.30
	Automatic	4.7	0.24	15.8	0.28
Zone II-III	Manual	8.0	0.28	19.4	0.20
	Automatic	5.6	0.28	23.6	0.20

III would shift to about 6.5 %.

For the ternary concretes with slump lower than 190 mm, the spacing factor lower than 0.30 mm is needed to provide a potential for F-T resistance (results within zone II). On the other hand, spacing factor of 0.20 mm, which is a commonly recommended value [29,36,50,51], appears to be required to ensure F-T durability. The spacing factor zone II boundaries (0.20–0.30 mm) are in a reasonable agreement with the results previously reported by Ivey and Torrains [52], who concluded that for conventional concrete, “the transition between durable and non-durable concrete seems to be somewhere between an \bar{L} of 0.20–0.25 mm.” Interestingly, of all four air-void system characteristics, the void frequency appears to have the narrowest zone II (Fig. 5(b)). In fact, that zone contains only one data point below the 60 % DF threshold value. Neglecting that single data point, only two zones (of either F-T durable or non-durable concrete) would exist and those would be separated by a boundary at 0.21 voids/mm.

The specific surface data shown in Fig. 5(c) also reveal that the values of zone I-zone II boundary ($14.4 \text{ mm}^2/\text{mm}^3$) and zone III-zone II boundary ($19.4 \text{ mm}^2/\text{mm}^3$) are independent of the concrete slump (no data points below or above the threshold line). This suggests that, due to the earlier discussed interaction of superplasticizer and AEA (and their combined effect on air-void system parameters), the specific surface may be the most objective and reliable predictor of F-T resistance of the ternary mixtures studied.

Comparison of Critical Air-Void System Parameters from Manual and Automatic Methods—Analogical analysis of DF data as that discussed earlier for the manual method was also performed for the set of air-void system parameters from the automatic method. As expected, the plots obtained (see Fig. 6) are generally similar to those for the manual method (Fig. 5). Table 3 provides the comparison of the boundaries between the three different zones obtained using the manual and automatic methods for the specimens with slump lower than 190 mm. It can be seen that, in general, the automatically obtained boundary values were comparable to those from the manual method. The biggest discrepancy was present for zone II-III boundary associated with the air content (5.6 % versus 8.0 %). The agreement for specific surface and spacing factor (which are considered the most reliable indicators of F-T resistance) was satisfactory.

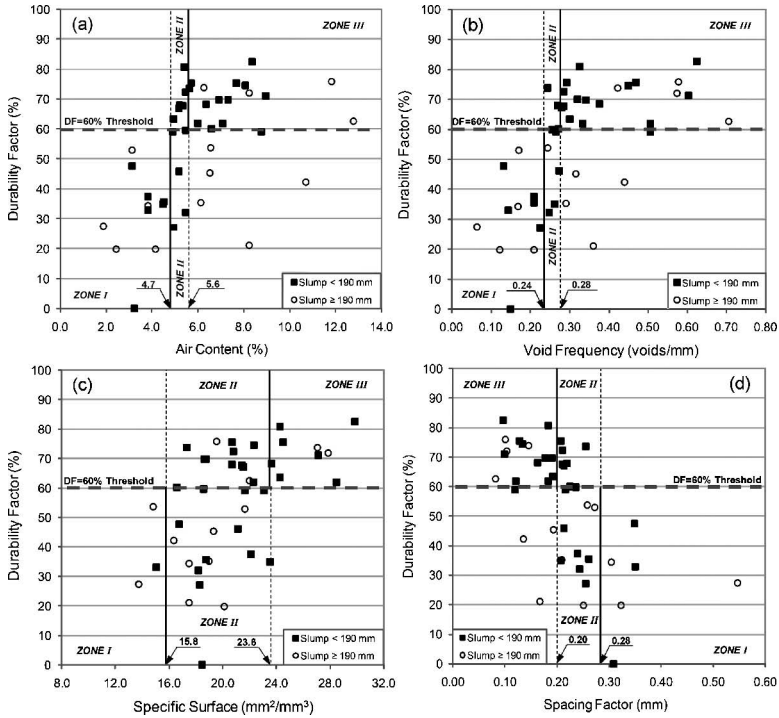


FIG. 6—Relationship between DF and (a) air content; (b) void frequency; (c) specific surface; and (d) spacing factor obtained from automatic (flatbed scanner) method.

Therefore, for the purpose of discerning between F-T durable and non-durable concrete, the agreement between the manual and automatic methods of determination of critical air-void system parameters appears to be sufficient.

Table 4 presents a comparison of critical air-void system parameters required to provide F-T resistance of concrete suggested by different sources. When comparing the different sources for a given parameter, none of the values seems to stand out notably. Therefore, considering the uncertainty associated with determination of each of the air-void system parameters, it appears that the ternary concrete evaluated in the present study does not require more stringent air-void system parameters than the conventional concrete. As such, higher air content is not required for the ternary concrete. However, caution should be used when given mixture design calls for excessive quantities of superplasticizer. Based on the data presented in this paper, it appears that high dosage of superplasticizer may result in compromised quality of the air-void system.

Conclusions

On the basis of the research presented in this paper the following conclusions have been drawn:

TABLE 4—Comparison of critical air-void system parameters required for F-T resistant concrete.

F-T Durable Concrete	Air Content (%)	Void Frequency (voids/mm)	Specific Surface (mm^2/mm^3)	Spacing Factor (mm)
Ternary concrete (current study)—manual point-count method ^a	8.0	0.28	19	0.20
Ternary concrete (current study)—automatic technique using scanner ^a	5.6	0.28	24	0.20
Laboratory tested cores from pavements ^b [53]	...	0.25	15	0.25
Recommended as per Hover [36]	...	(0.04–0.06) × air content	16–24	0.20
Recommended as per ASTM C457 [15]	...	0.32	...	0.20
Recommended as per ACI 201.2R-08 [51]	6.0 ^c	...	25	0.20

^aSpecimens from concrete with slump <190 mm moist cured for ~2.5 years prior to F-T test.

^bConcrete field exposed for several years.

^cFor 19-mm nominal maximum aggregate size.

- A reasonable agreement was established between void frequency and spacing factor values obtained using the manual point-count and the flatbed scanner methods. The air contents from the microscopical determination were consistently higher than those from the flatbed scanner method, whereas the specific surface estimated using a flatbed scanner was (consequently) higher than that from the manual method;
- The air contents measured in hardened concrete using the flatbed scanner technique were closer to those measured in the fresh state (using the pressure method) than the air contents from the manual point-count method;
- The manual and automatic methods gave comparable critical values of the air-void system parameters required to provide F-T resistance. Therefore, the flatbed scanner technique can be efficiently used for the purpose of distinguishing between the F-T durable and non-durable ternary concrete;
- Due to adverse effect of high superplasticizer dosage on air-void system quality (particularly on specific surface), the majority of high slump ternary mixtures exhibited poor F-T resistance, even if spacing factor was below the 0.20 mm recommended value;
- Since the critical value of specific surface was independent of slump (i.e., superplasticizer dosage), specific surface appeared to be a more objective and reliable predictor of F-T resistance than spacing factor; and
- For well cured ternary concrete containing 20 % FA and 5 % SF made with slump below 190 mm, the critical air-void system parameters were comparable to those typically accepted as adequate for conventional concrete. More research is needed to verify this conclusion for wider range of ternary mixture compositions and types of materials used.

References

- [1] Bassuoni, M. T. and Nehdi, M. L., "The Case for Air-Entrainment in High-Performance Concrete," *Proc. ICE—Struct. Build.*, Vol. 158, No. 5, 2005, pp. 311–319.
- [2] Snyder, K. A., "A Numerical Test of Air Void Spacing Equations," *Adv. Cem. Based Mater.*, Vol. 8, No. 1, 1998, pp. 28–44.
- [3] Toutanji, H., Delatte, N., Aggoun, S., Duval, R., and Danson, A., "Effect of Supplementary Cementitious Materials on the Compressive Strength and Durability of Short-Term Cured Concrete," *Cem. Concr. Res.*, Vol. 34, No. 2, 2004, pp. 311–319.
- [4] Chojnacki, T., "Missouri High Performance Concrete Update," *RD&T Quarterly*, Vol. 3, No. 3, Missouri Department of Transportation, Jefferson City, MO, 1999, pp. 1-2.
- [5] Pigeon, M., Pleau, R., and Aïtcin, P.-C., "Freeze-Thaw Durability of Concrete with and Without Silica Fume in ASTM C666 (Procedure A) Test Method: Internal Cracking Versus Scaling," *Cem., Concr., Aggregates*, Vol. 8, No. 2, 1986, pp. 76–85.
- [6] Bajorski, P. and Streeter, D., "Optimization of Amount and Blending of Cementitious Materials in High-Performance Concrete," *Transportation Research Record*. 1698, Transportation Research Board, Washington, D.C., 2000, pp. 30–35.

- [7] Streeter, D., "Developing High-Performance Concrete Mix for New York State Bridge Decks," *Transportation Research Record*. 1532, Transportation Research Board, Washington, D.C., 1996, pp. 60–65.
- [8] Blomberg, J. M., "Laboratory Testing of Bridge Deck Mixes," *Report No. RDT03-004*, Missouri Department of Transportation, Jefferson City, MO, 2003.
- [9] Nassif, H. H. and Suksawang, N., "Effect of Curing Methods on Durability of High-Performance Concrete," *Transportation Research Record*. 1798, Transportation Research Board, Washington, D.C., 2002, pp. 31–38.
- [10] Radlinski, M., Olek, J., Zander, A., and Nantung, T., "Influence of Production Method and Curing Conditions on Chloride Transport, Strength and Drying Shrinkage of Ternary Mix Concrete," *Transport Properties and Concrete Quality, Materials Science of Concrete, Special Volume*, B. Mobasher and J. Skalny, Eds., Wiley & Sons, Hoboken, NJ, 2007, pp. 215–229.
- [11] Xi, Y., Shing, B., and Xie, Z., "Development of Optimal Concrete Mix Designs for Bridge Decks," *Report No. CDOT-DTD-R-2001-11*, Colorado Department of Transportation, Denver, CO, 2001.
- [12] Suksawang, N., Nassif, H., and Capers, H., Jr., "The Development of High-Performance Concrete for Transportation Structures in New Jersey," *Proceedings of the Seventh International Symposium on the Utilization of High-Strength/High-Performance Concrete*, SP 228, H. G. Russell, Ed., Washington, D.C., June 20–24, 2005, American Concrete Institute, Farmington Hills, MI, 2005, pp. 833–849.
- [13] Lawler, J. S., Connolly, J. D., Krauss, P. D., Tracy, S. L., and Ankenman, B. E., "Supplementary Cementitious Materials to Enhance Durability of Concrete Bridge Decks," *NCHRP Report No. 110*, Transportation Research Board, Washington, D.C., 2005.
- [14] Radlinski, M. and Olek, J., "High-Performance Concrete Bridge Decks: A Fast-Track Implementation Study," *Draft Final Report No. FHWA/IN/JTRP-25/11*, Joint Transportation Research Program, Purdue University, West Lafayette, IN, 2008.
- [15] ASTM C457-08, 2008, "Standard Test Method for Microscopical Determination of Parameters of the Air-Void System in Hardened Concrete," *Annual Book of ASTM Standards*, Vol. 04.02, ASTM International, West Conshohocken, PA, pp. 253–266.
- [16] Jakobsen, U. H., Pade, C., Thaulow, N., Brown, D., Sahu, S., Magnusson, O., De Buck, S., and De Schutter, G., "Automated Air Void Analysis of Hardened Concrete—A Round Robin Study," *Cem. Concr. Res.*, Vol. 36, No. 8, 2006, pp. 1444–1452.
- [17] Concrete Structure Inspection Systems 2008, http://www.fast-corp.co.jp/eng/hf_mac01.html (Last accessed 23 July 2008).
- [18] Peterson, K. W., Swartz, R. A., Sutter, L. L., and Van Dam, T. J., "Hardened Concrete Air Void Analysis with a Flatbed Scanner," *Transportation Research Record*. 1775, Transportation Research Board, Washington, D.C., 2001, pp. 36–43.
- [19] Baumgart, C., Blair, R., and Linder, K., "Image Analysis of Hardened Concrete. Performance Enhancement of the Automated Concrete Evaluation System," *Report No. OR07-004*, Missouri Department of Transportation, Jefferson City, MO, 2006.
- [20] Zhang, Z., Ansari, F., and Vitillio, N., "Automated Determination of Entrained Air-Void Parameters in Hardened Concrete," *ACI Mater. J.*, Vol. 17, No. 1, 2005, pp. 42–47.
- [21] Carlson, J., 2005, "Advancement on the Application of a Flat-Bed Scanner for Hardened Portland Cement Concrete Air Void Analysis," M.S. thesis, Michigan Technological University, Houghton, MI.
- [22] Jana, D., "A Round Robin Test on Measurements of Air Void System Parameters in

Hardened Concrete by Various Automated Image Analyses and ASTM C457 Methods," *Proceedings of the 29th Conference on Cement Microscopy*, Quebec City, PQ, Canada, May 20–24, International Cement Microscopy Association, 2007, pp. 34–69.

- [23] ASTM C1202–07, 2008, "Standard Test Method for Electrical Indication of Concrete's Ability to Resist Chloride Ion Penetration," *Annual Book of ASTM Standards*, Vol. 04.02, ASTM International, West Conshohocken, PA, pp. 645-650.
- [24] Neville, A. M., *Properties of Concrete*, 4th ed., Pearson Education Limited, Edinburgh Gate, England, 1995.
- [25] Powers, T. C., "A Working Hypothesis for Further Studies of Frost Resistance of Concrete," *ACI J.*, Vol. 41, No. 4, 1945, pp. 245–272.
- [26] Powers, T. C., "The Air Requirement of Frost-Resistant Concrete," *Highw. Res. Board, Proc. Annu. Meet.*, Vol. 29, 1949, pp. 184–202.
- [27] Willis, T. F., "Discussion of Powers, T. C., 'The Air Requirement of Frost-Resistant Concrete'," *Highw. Res. Board, Proc. Annu. Meet.*, Vol. 29, 1949, pp. 203–211.
- [28] Lord, G. W. and Willis, T. F., "Calculation of Air Bubble Size Distribution from Results of a Rosiwal Traverse of Aerated Concrete," *ASTM Bulletin No. 177*, ASTM International, West Conshohocken, PA, October 1951, pp. 56–61.
- [29] Mielenz, R. C., Wolkodoff, V. E., Backstrom, J. E., and Burrows, R. H., "Origin, Evolution, and Effects of the Air Void System in Concrete. Part 4—The Air Void System and Job Concrete," *ACI J.*, Vol. 55, No. 10, 1958, pp. 507–517.
- [30] Carlson, J., Sutter, L., Van Dam, T., and Peterson, K., 2006, "Comparison of Flatbed Scanner and RapidAir 457 System for Determining Air Void System Parameters of Hardened Concrete," *Transportation Research Record. 1979*, Transportation Research Board, Washington, D.C., pp. 54–59.
- [31] Peterson, K., Carlson, J., Sutter, L., and Van Dam, T., "Methods for Threshold Optimization for Images Collected from Contrast Enhanced Concrete Surfaces for Air-Void System Characterization," *Mater. Charact.*, Vol. 60, No. 7, 2009, pp. 710–715.
- [32] Peterson, K., Sutter, L., and Radlinski, M., "The Practical Application of a Flatbed Scanner for Air-Void Characterization of Hardened Concrete," *J. ASTM Int.*, Vol. 6, No. 9, 2009, paper ID JAI102446.
- [33] ASTM C666/C666M-03, 2008, "Standard Test Method for Resistance of Concrete to Rapid Freezing and Thawing," *Annual Book of ASTM Standards*, Vol. 04.02, ASTM International, West Conshohocken, PA, pp. 348-353.
- [34] ASTM C1259–01, 2003, "Standard Test Method for Dynamic Young's Modulus, Shear Modulus, and Poisson's Ratio for Advanced Ceramics by Impulse Excitation of Vibration," *Annual Book of ASTM Standards*, Vol. 15.01, ASTM International, West Conshohocken, PA, pp. 311-328.
- [35] Sommer, H., "The Precision of the Microscopical Determination of the Air-Void System in Hardened Concrete," *Cem., Concr., Aggregates*, Vol. 1, No. 2, 1979, pp. 49–55.
- [36] Hover, K. C., "Air Content and Unit Weight of Hardened Concrete," *ASTM STP 169D*, ASTM International, West Conshohocken, PA, 2006, pp. 288–308.
- [37] ASTM C231–08b, 2008, "Standard Test Method for Air Content of Freshly Mixed Concrete by the Pressure Method," *Annual Book of ASTM Standards*, Vol. 04.02, ASTM International, West Conshohocken, PA, pp. 157-165.
- [38] Roberts, L. R., "Air Content, Temperature, Density (Unit Weight), and Yield," *ASTM STP 169D*, ASTM International, West Conshohocken, PA, 2006, pp. 73–85.
- [39] Attiogbe, E. K., "Predicting Freeze-Thaw Durability of Concrete—A New Approach," *ACI Mater. J.*, Vol. 93, No. 5, 1996, pp. 1–8.

- [40] Hover, K. C. and Phares, R. J., "Impact of Concrete Placing Method on Air Content, Air-Void System Parameters, and Freeze-Thaw Durability," *Transportation Research Record. 1532*, Transportation Research Board, Washington, D.C., 1996, pp. 1-8.
- [41] Mindess, S. and Young, J. F., *Concrete*, Prentice-Hall, Englewood Cliffs, NJ, 1981, pp. 102-104.
- [42] Tanesi, J. and Meininger, R., "Freeze-Thaw Resistance of Concrete with Marginal Air Content," *Transportation Research Record. 2020*, Transportation Research Board, Washington, D.C., 2007, pp. 61-66.
- [43] Whiting, D. and Nagi, M., "Manual on Control of Air Content in Concrete" *EB116*, Portland Cement Association, Skokie, IL, 1998.
- [44] Van Dam, T. J., Peterson, K. R., Sutter, L. L., Panguluri, A., and Sytsma, J., "Guidelines for Early-Opening-to-Traffic Portland Cement Concrete for Pavement Rehabilitation," *NCHRP Report No. 540*, Transportation Research Board, Washington, D.C., 2005.
- [45] Whiting, D. and Stark, D., "Control of Air Content in Concrete," *National Cooperative Research Program Report No. 258*, Transportation Research Board, Washington, D.C., May 1983.
- [46] American Concrete Institute, 2004, "Guide for the Use of High-Range Water Reducing Admixtures (Superplasticizers) in Concrete," *ACI 212.4R-04*, Farmington Hills, MI.
- [47] Waszczuk, C. M. and Juliano, M. L., "Application of HPC in a New Hampshire Bridge," *Concr. Int.*, Vol. 21, No. 2, 1999, pp. 61-62.
- [48] Beacham, M. W., "HPC Bridge Deck in Nebraska," *Concr. Int.*, Vol. 21, No. 2, 1999, pp. 66-68.
- [49] Indiana Department of Transportation, "Quality Control/Quality Assurance, QC/QA, Superstructure Concrete, Modified," *Indiana Department of Transportation Provisional Specification for SR-23 Bridge*, Indiana Department of Transportation, Indianapolis, IN, 2004.
- [50] Natesaiyer, K. and Hover, K. C., "Protected-Paste Volume of Air-Entrained Cement Paste. Part 1," *J. Mater. Civ. Eng.*, Vol. 4, No. 2, 1992, pp. 166-184.
- [51] American Concrete Institute, 2008, "Guide to Durable Concrete," *ACI 201.2R-08*, Farmington Hills, MI.
- [52] Ivey, D. L. and Torrains, P. H., "Air Void Systems in Ready Mixed Concrete," *J. Mater.*, Vol. 5, No. 2, 1970, pp. 492-522.
- [53] Radlinski, M., Olek, J., Del Mar Arribas, M., Rudy, A., Nantung, T., and Byers, M., "Influence of Air-Void System Parameters on Freeze-Thaw Resistance of Pavement Concrete—Lessons Learned from Field and Laboratory Observation," *Proceedings of the Ninth International Conference on Concrete Pavements*, International Society for Concrete Pavements, San Francisco, CA, August 17-21, 2008, pp. 824-835.

Mustafa Şahmaran,¹ Mohamed Lachemi,² and Victor C. Li³

Assessing the Durability of Engineered Cementitious Composites Under Freezing and Thawing Cycles

ABSTRACT: This paper reports the durability performance of non-air-entrained engineered cementitious composites (ECC) when subjected to freezing and thawing cycles. ECC is a newly developed, high-performance, fiber-reinforced, cementitious composite with substantial benefits both in terms of high ductility under uniaxial tensile loading and improved durability due to intrinsically tight crack width of less than 100 µm. To evaluate the frost durability of ECC, freezing and thawing testing in accordance with ASTM C666 Procedure A was conducted. The mass loss, pulse velocity change, and flexural parameters (ultimate deflection and flexural strength) of specimens subjected to freezing and thawing cycles were determined in the test. In addition, air-void parameters, in accordance with ASTM C457, modified point count method, and pore size distribution obtained by mercury intrusion porosimetry technique were studied. To analyze the influence of micro-fibers and high tensile strain capacity on the freezing and thawing durability of ECC, all of the above-mentioned properties were also investigated for a control ECC matrix (ECC without fibers). After 210 cycles of freezing and thawing, the control ECC matrix specimens were severely deteriorated, requiring removal from the test, but still exhibited better performance than the conventional non-air-entrained concrete, which would fail at much earlier cycles. On the other hand, ECC with fibers without air-entrainment had excellent resistance to cycles of freezing and thawing with minimal reduction in

Manuscript received March 5, 2009; accepted for publication May 26, 2009; published online August 2009.

¹ Dept. of Civil Engineering, Gaziantep Univ., Gaziantep, 27310, Turkey, e-mail: sahmaran@gantep.edu.tr

² Dept. of Civil Engineering, Ryerson Univ., Toronto, M5B 2K3 Canada, e-mail: mlachemi@ryerson.ca

³ Dept. of Civil and Environmental Engineering, The Univ. of Michigan, MI 48109-2125 (Corresponding author), e-mail: vcli@umich.edu

Cite as: Şahmaran, M., Lachemi, M. and Li, V. C., "Assessing the Durability of Engineered Cementitious Composites Under Freezing and Thawing Cycles," *J. ASTM Intl.*, Vol. 6, No. 7. doi:10.1520/JAI102406.

Copyright © 2009 by ASTM International, 100 Barr Harbor Drive, PO Box C700, West Conshohocken, PA 19428-2959.

ultimate tensile strength and ductility. The observed superior frost durability of ECC over control ECC matrix in terms of lower weight loss, pulse velocity change, and higher flexural load and ductility can be attributed to the following reasons: Increase of pore volume larger than approximately $0.30\ \mu\text{m}$ in diameter, intrinsically high tensile ductility and strength due to the presence of micro-poly-vinyl-alcohol fibers.

KEYWORDS: engineered cementitious composites (ECC), ductility, flexural strength, ECC under freezing and thawing cycles

Introduction

Concrete is the world's most widely used construction material. Historically, structural designers have primarily relied on concrete to carry compressive loads. However, in real field conditions, concrete is also subjected to tensile stresses due to loading and environmental effects including shrinkage (if the shrinkage is restrained), chemical attacks, and thermal effects. The tensile strength of concrete is only about 10 % of its compressive strength, and its brittle failure is of particular concern in structures. Durability is vitally important for all concrete structures, and it can be associated with the appearance of cracks when concrete is subjected to tensile stresses.

In recent years, efforts to modify the brittle nature of ordinary concrete have resulted in ultra-high-performance fiber-reinforced cementitious composites, which are characterized by tensile strain-hardening after first cracking. Depending on their composition, their tensile strain capacity can be up to several hundred times that of normal and fiber-reinforced concrete. Engineered cementitious composite (ECC) is a fiber-reinforced cement-based composite material that is micro-mechanically tailored by the addition of short fibers to achieve high ductility and multiple cracking under tensile and shear loading [1–6]. Unlike ordinary concrete materials, ECC strain-hardens after first cracking, similar to a ductile metal, and demonstrates a strain capacity 300–500 times greater than normal concrete. Figure 1 shows a typical uniaxial tensile stress-strain curve of an ECC containing 2 % by volume of poly-vinyl-alcohol

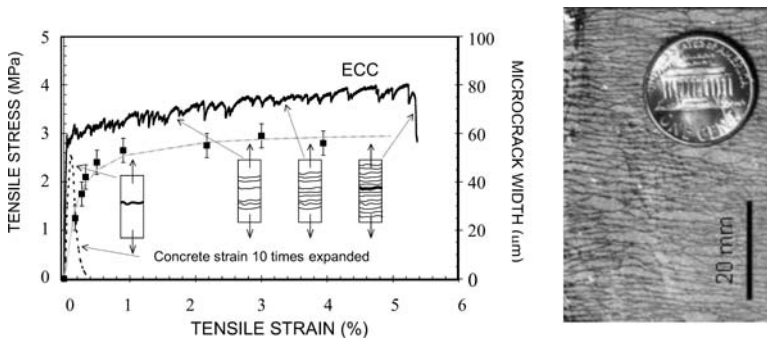


FIG. 1—Typical uniaxial tensile stress-strain curve and crack width development of PVA-ECC.



FIG. 2—Response of ECC beam after 300 freezing and thawing cycles under flexural loading.

fiber (PVA fiber). The characteristic strain-hardening after first cracking is accompanied by sequential development of multiple micro-cracking and a tensile strain capacity 300–500 times that of normal concrete. Crack width development during inelastic straining is also shown in Fig. 1. Even at large imposed deformations, crack widths of ECC remain small; less than $80\ \mu\text{m}$. This tight crack width is self-controlled and, whether the composite is used in combination with conventional reinforcement or not, it is a material characteristic independent of the amount of reinforcing bars. The tight crack width of ECC is important to the durability of ECC structures as the tensile ductility is to the structural safety at ultimate limit state. Under severe bending load, an ECC beam deforms similar to a ductile metal plate through plastic deformation (Fig. 2). In compression, ECC materials exhibit compressive strengths similar to high strength concrete (e.g., greater than 60 MPa) [7]. These properties, along with the relative ease of production including self-consolidation casting [8,9] and shotcreting [10], make ECC materials suitable for various civil engineering applications. ECC is currently emerging in full-scale structural applications [11,12].

Much infrastructures in North America and Turkey are located in regions with severe environmental conditions, where alternate freezing and thawing can seriously affect material/structure integrity. The limited field performance and preliminary freeze-thaw durability study of non-air-entrained ECC indicates that it has a superior freezing and thawing resistance [13–15]. As one of the first field applications of ECC in United States, a concrete bridge deck patch was completed in cooperation with the Michigan Department of Transportation (MDOT) in 2002. A complete summary of this work has been outlined by Li and

Lepech [15]. During this work, one section of a deteriorated bridge deck was repaired with ECC while the remaining portion was repaired with a commercial concrete patching material commonly used by the MDOT. This repair scenario allowed for a unique ECC/concrete comparison subjected to identical environmental and traffic loads. The concrete repair material used was a pre-packaged, commercially available repair mortar. At this writing, the repaired bridge deck has experienced more than eight complete Michigan winter cycles of freezing and thawing, in addition to live loads. While the ECC patch repair has survived in this combined loading environment with minor micro-cracking limited to less than 50 μm , the concrete repair portion has developed localized cracks in excess of 3.5 mm wide and required re-repair in 2005.

A proper air-void system must be maintained in normal concrete to achieve superior freezing and thawing resistance [16]. In the case of ECC, the available information is very limited, but it seems to indicate that in addition to the air-void system, other parameters such as high tensile strain capacity and strain-hardening behavior are important for resisting cycles of freezing and thawing and are affected by the presence of micro-fibers. It is therefore essential to further investigate the reasons behind the excellent frost resistance of ECC. This study was undertaken to comprehensively investigate the freezing and thawing durability of non-air-entrained standard ECC mixture (M45). The resulting data is important in view of the growing use of ECC, especially for highway pavements, airport pavements, and bridge decks in cold climate regions.

To evaluate the freeze-thaw durability of ECC, freezing and thawing testing in accordance with ASTM C666 Procedure A was conducted. The mass loss, pulse velocity change, and flexural parameters (ultimate deflection and flexural strength) of specimens subjected to freezing and thawing cycles were determined. In addition, air-void parameters, in accordance with ASTM C457, modified point count method, and pore size distribution obtained by mercury intrusion porosimetry method were studied. To analyze the influence of micro-fibers and excellent tensile performance (high tensile strain capacity, strain-hardening, and multiple-cracking behaviors) on the freezing and thawing durability of ECC, all of the above-mentioned properties were also investigated for an ECC matrix (ECC without fibers).

Experimental Studies

Materials, Mixture Proportions, and Basic Mechanical Properties

The materials used in the production of standard ECC mixtures were Type-I Portland cement (C), Class-F fly ash (FA) with a lime content of 5.6 %, micro-silica sand with an average and maximum grain size of 110 and 250 μm , respectively, water, PVA fibers, and a polycarboxylic-ether type high-range water reducing (HRWR) admixture. Chemical composition and physical properties of Portland cement and FA are presented in Table 1. The PVA fibers with a diameter of 39 μm and a length of 8 mm are purposely manufactured with a tensile strength of 1620 MPa, elastic modulus of 42.8 GPa, maximum elongation of 6.0

TABLE 1—Chemical composition and physical properties of cement and fly ash.

Chemical Composition, %	Cement	Fly Ash
CaO	61.80	5.57
SiO ₂	19.40	59.50
Al ₂ O ₃	5.30	22.20
Fe ₂ O ₃	2.30	3.90
MgO	0.95	...
SO ₃	3.80	0.19
K ₂ O	1.10	1.11
Na ₂ O	0.20	2.75
Loss on ignition	2.10	0.21
Physical properties		
Specific gravity	3.15	2.18
Retained on 45 μm (0.002 in.), %	12.9	9.6
Water requirement, %	...	93.4

%, and the ability to strain-harden [3]. The PVA fiber tends to rupture instead of pull out in a cementitious matrix, as a result of the strong chemical bonding with cement due to the presence of the hydroxyl group in its molecular chains [3]. This high chemical bonding has a tendency to lead to fiber rupture and limits the tensile strain capacity of the resulting composite. For this reason, the surface of the PVA fibers is coated with a proprietary hydrophobic oiling agent of 1.2 % by mass to tailor the interfacial properties between fiber and matrix for strain-hardening performance.

Standard ECC mixture (M45) with a fly ash-cement ratio (FA/C) of 1.2 by mass was used in this investigation, details of which are given in Table 2. To analyze the influence of micro-fibers and high tensile strain capacity on the

TABLE 2—Mixture properties of ECC.

	ECC (M45) with PVA	ECC Matrix Without PVA
FA/C	1.2	1.2
W/CM ^a	0.27	0.27
Water (W), kg/m ³	326	326
Cement (C), kg/m ³	558	558
Fly ash (FA), kg/m ³	669	669
Sand (S), kg/m ³	446	446
Fiber (PVA), kg/m ³	26	...
HRWR, kg/m ³	2.30	2.30
14 day compressive strength, MPa	39.2	36.1
28 day compressive strength, MPa	62.5	60.3

^aCM denotes cementitious materials (cement+ fly ash).

TABLE 3—Uniaxial tensile properties of ECC specimens at 28 days.

Age	Tensile Strain, %	Tensile Strength, MPa	Residual Crack Width, μm
14 days	2.9 \pm 0.2	4.6 \pm 0.5	~60
28 days	2.7 \pm 0.2	5.1 \pm 0.3	~48

freezing and thawing durability of ECC, ECC matrix (ECC without PVA fibers) was also studied. ECC and ECC matrix were prepared in a standard paddle mixer at a constant amount of cementitious material and constant water to cementitious material ratio (W/CM) of 0.27. All ECC and ECC matrix materials used in this study contain no air-entraining admixture (AEA) and show self-consolidating flow behavior in the fresh state. Previous studies demonstrated that concretes containing HRWR often tend to have air-voids that are larger than those in conventional concrete [17–20]. Such air-void systems tend to be less stable and have larger spacing factors. Since the same dosage of HRWR is used in the production of ECC matrix and ECC, HRWR admixture cannot be a factor responsible for the great differences in the frost durability of ECC and ECC matrix, which will be discussed in the next section.

The compressive strength test results of the ECC and ECC matrix without fibers and the ultimate tensile strain capacity of ECC are listed in Tables 2 and 3, respectively. The compressive strength was computed as an average of three 50 mm cubic specimens. To characterize the direct tensile behavior of the ECC mixtures, 200 \times 75 \times 13 mm³ coupon specimens were used. Direct tensile tests were conducted under displacement control at a loading rate of 0.005 mm/s. The typical tensile stress-strain curves of the ECC mixtures at 14 and 28 days are shown in Fig. 3. As seen from Table 3, the ECC composite exhibited a strain capacity of 2.7 % at 28 days. The strain capacity measured at 28 days of age is slightly lower than the 14 day strain capacity (Fig. 3 and Table 3) but within the

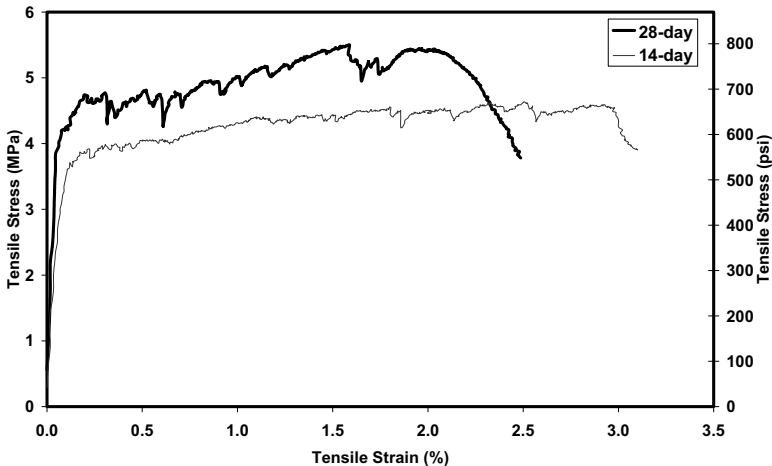


FIG. 3—Typical tensile stress-strain response of standard ECC mixture (M45).

acceptable variability; and the strain capacity exceeding 2.5 % is acceptable. Previous studies demonstrated that the tensile strain capacity seems to stabilize after 28 days. This time dependent stabilization can be ascribed to the increase in fiber/matrix interface properties and matrix toughness associated with the continued cement hydration process [14].

Specimen preparation and testing

From each mixture, eight $400 \times 100 \times 75$ mm³ prisms were prepared for the freezing and thawing test and determination of air-void characteristics. All specimens were cast in one layer without any compaction, demolded at the age of 24 h, and moist cured in lime-saturated water at $23 \pm 2^\circ\text{C}$ for 13 days. Fourteen days after casting, the beam specimens were moved into the freeze-thaw chamber in accordance with ASTM C666 Procedure A and subjected to between five and six freezing and thawing cycles in a 24 h period. The average flexural parameters (ultimate deflection and flexural strength) of the specimens were obtained by testing four companion samples prior to the freezing and thawing cycles. Changes in pulse velocity and mass loss were measured at each interval of nominally 30 cycles of freezing and thawing. The number of cycles to failure for the specimens was also recorded at the time the sample fractured or split into two parts. At the end of 300 freeze-thaw cycles, surviving specimens were tested under four-point bending load with a span length of 355 mm and a height of 75 mm to determine their residual flexural performances, and their load-deflection curves were recorded. Three freeze-thaw specimens were tested for each mixture.

The air-void parameters of hardened ECC and ECC matrix (without fiber) were determined by modified point count method according to ASTM C457. Mercury intrusion porosimetry was also used to characterize the pore size distribution of the ECC and ECC matrix. An instrument capable of producing pressures up to 414 MPa and assuming a contact angle of 130° was used for pore size distribution analysis by the mercury intrusion method. Specimens were dried to constant weight at 50°C prior to testing. All tests included at least two identical specimens tested at the same time.

Results and Discussions

Air-void parameters

The results of the determination of air-void characteristics of the hardened concrete (air content, specific surface and spacing factor), according to ASTM C457, are shown in Table 4, along with the air content measured on the fresh state (as measured by ASTM C231), and total intruded porosity values obtained with the mercury intrusion porosimetry technique. The freeze-thaw durability of concrete has a close relationship with its air-void parameters. The American Concrete Institute (ACI) recommends that frost-resistant concrete should have a calculated spacing factor of less than 0.2 mm and a specific surface greater than 24 mm^{-1} [21].

TABLE 4—Air-void characteristics and porosity.

	ECC (M45) with PVA	ECC matrix without PVA
Fresh air content (%)	7.3	5.9
Hardened air content (%)	8.2	7.3
Specific surface (mm^{-1})	25.6	53.0
Spacing factor (mm)	0.241	0.129
Total intruded porosity (%)	23.7	19.2
Volume of pores $>0.30 \mu\text{m}$ diameter (%)	5.0	0.75

As seen in Table 4, although no AEA was added to the ECC and ECC matrix mixtures, the air contents of these mixtures in the fresh state gave values of 7.3 % and 5.9 %, and in the hardened state, as measured by ASTM C457, gave values of 8.2 % and 7.3 %, respectively. These amounts seemed to be adequate for freeze-thaw durability [21]. The higher air content in these mortar mixtures may be due to the lack of coarse aggregate and the higher viscosity of the mortar matrix during the fresh state [22]; the fine particles and high viscosity tend to prevent some of the air bubbles from rising to the surface during placing operations. Moreover, the air contents measured during the fresh state of the ECC mixture show that this phenomenon is amplified after the addition of PVA fiber to the mixtures (Table 2). When PVA is added to the ECC matrix, it increases the viscosity of the fresh ECC mixture compared to the ECC matrix [23], which further increases the amount of entrapped air-voids inside the matrix.

In the case of hardened ECC, it is interesting to note that the addition of the PVA fiber can result in a significant increase in spacing factor (see Table 4). Moreover, specific surface is significantly higher for ECC matrix, which indirectly implies that the average bubble size is smaller in ECC matrix. This is likely due to the fact that the randomly distributed PVA fibers could possibly form a network that provides a path for the air bubbles to coalesce, thus creating large entrapped air-voids instead of finely distributed air-voids, which can be clearly seen in Fig. 4. It would be necessary to further investigate the reasons behind the increase in spacing factor and reduction in specific surface with the addition of PVA fiber.

Although the spacing factor value (0.241 mm) and specific surface value (25.6 mm^{-1}) of ECC slightly exceed the generally acceptable value of 0.200 mm and 25 mm^{-1} for good freeze-thaw durability, the apparent lack of an ideal air-void characteristic has not adversely affected resistance when ECC is subjected to freezing and thawing cycles, as discussed in the following section.

The total mercury intruded porosities for the various pastes are shown in Table 4. Typical pore size distribution curves are shown in Fig. 5 for the ECC and ECC matrix (without fiber) samples. The ECC exhibited a higher total porosity when compared with the ECC matrix. However, total porosity is not a good indicator of quality (i.e., freeze-thaw durability) since very small gel pores would not negatively influence concrete durability [24]. The radius and size distribution of pores determine the freezing point of pore solution and the

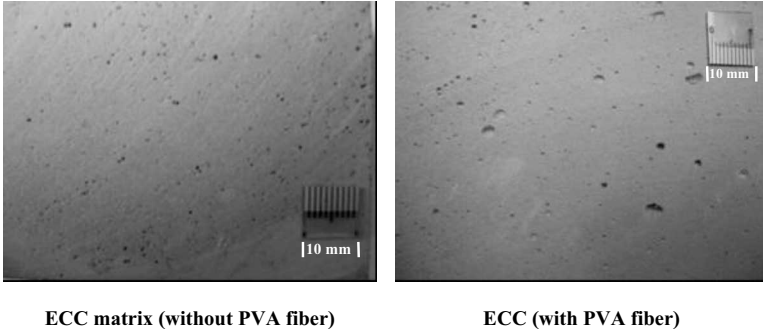


FIG. 4—Typical air-voids in a non-air-entrained ECC specimens (without and with fiber).

amount of ice formed in pores [25]. According to current literature, while a uniform relationship between freeze-thaw resistance and pore size distribution obtained by mercury intrusion technique has not been found, in general, a larger volume of coarse pores (greater than approximately $0.30 \mu\text{m}$ diameter [26–31]) results in higher freeze-thaw resistance. The volumes of pores larger than $0.30 \mu\text{m}$ diameter are also given in Table 4, which shows that due to PVA fiber incorporation, there is a significant difference in pore size distribution, mainly in sizes larger than $0.30 \mu\text{m}$ diameter. The addition of PVA fiber to the matrix significantly increased the volume of these large-size pores and the total porosity, which is favorable to improved frost resistance.

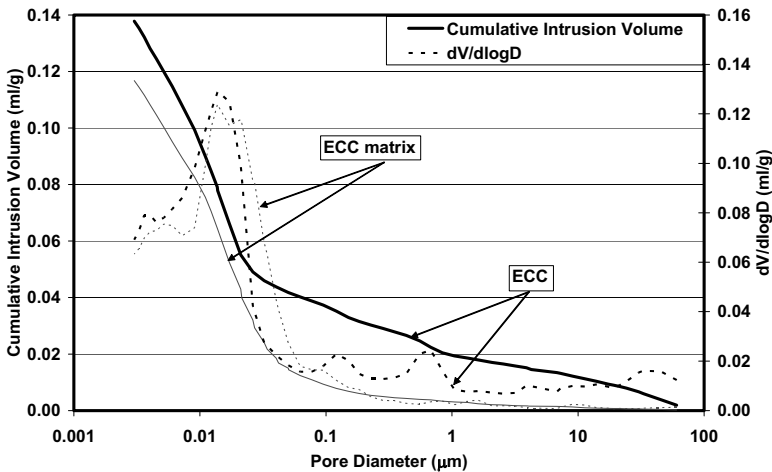


FIG. 5—Cumulative pore size distributions of non-air-entrained ECC specimens (without and with fiber).

TABLE 5—Freezing and thawing resistance of ECC and ECC matrix.

	ECC matrix without PVA	ECC (M45) with PVA
Number of cycles completed	210	300
Change in mass (%)	-7.3	-1.3
Pulse velocity change (%)	-30.9	-2.2

Freezing and Thawing Resistance

The deterioration of specimens during the freezing and thawing cycles was assessed by the computation of mass loss. To measure the internal damage caused by freezing and thawing cycles, the changes in pulse velocity through a prism were also measured. Normally, ASTM C666 specifies the use of the resonant frequency method, not the pulse velocity method. However, previous studies have shown that pulse velocity test method can also be used to measure the deterioration of specimens during freezing and thawing cycles [32].

The freeze-thaw durability test results are summarized in Table 5. Figure 6 shows the data for the relative pulse velocity change (V_i/V_0) and relative mass change (M_i/M_0) with the number of freezing and thawing cycles. V_i and M_i are the pulse velocity and mass, respectively, after a specific number of freezing and thawing cycles, and V_0 and M_0 are initial pulse velocity and mass, respectively, prior to any freezing and thawing cycles. As seen in Fig. 6, the mass and pulse velocity losses of ECC matrix increase with the number of freeze-thaw cycles. After 210 cycles, the ECC matrix specimens had severely deteriorated [Fig. 7(a)], requiring removal from the freeze-thaw machine, as mandated by the testing standard. However, as seen in Table 5, the ECC prisms showed excellent performance when exposed to freezing and thawing cycles, even after 300 cycles. A maximum of only 1.3 % and 2.2 % mass and pulse velocity losses, respectively, were measured for the ECC specimens. This can also be observed in Fig. 6, where the relationship between relative pulse velocity/relative mass loss and number of freezing and thawing cycles is shown for ECC specimens that were subjected to 300 cycles. At the end of 300 cycles, very little scaling was observed on the ECC prism surface [Fig. 7(b)].

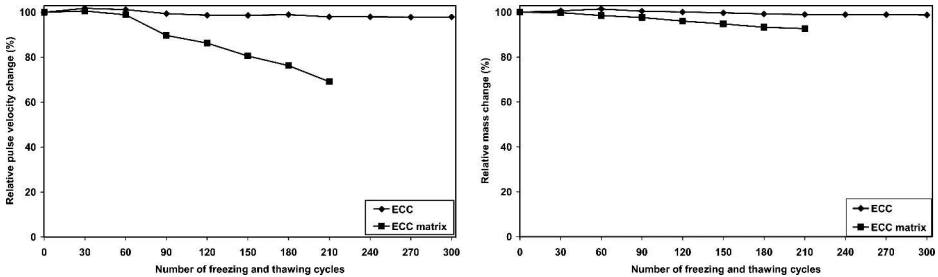
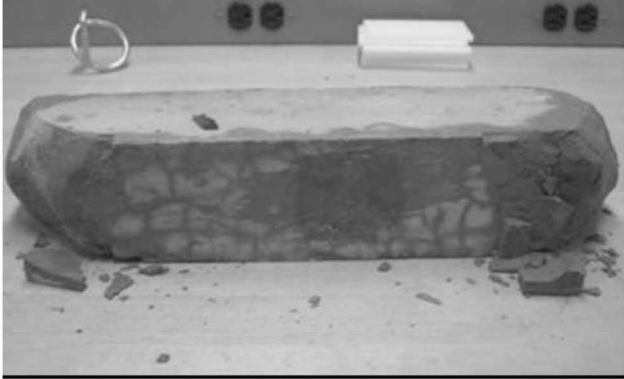


FIG. 6—Relative pulse velocity and mass loss changes as a function of number of freezing and thawing cycles.



(a) ECC matrix (ECC without fiber) after 210 freezing and thawing cycles



(b) ECC (with fiber) after 300 freezing and thawing cycles

FIG. 7—ECC specimen surface appearance after freeze-thaw cycles.

There are a number of possible explanations for the excellent performance of these non-air-entrained ECC samples. A proper air-void system is needed in normal concrete to avoid internal cracking due to freezing and thawing cycles. As discussed in the preceding section, the pore size distributions of ECC matrix are much finer (i.e., fewer coarse pores) than ECC. To make a general conclusion regarding the influence of pore size distribution on frost resistance, large pores (generally larger than $0.3 \mu\text{m}$ in diameter) are beneficial to frost resistance of concrete, whereas small and intermediate pores are detrimental (see “Air-Void Parameters” section).

Another possible reason for the ECC’s excellent frost resistance, which is favored by the authors, can be attributed to its superior tensile properties (see “Flexural Performance” section). It is well known that upon freezing, water in capillary pores expands. If the required volume is greater than the space available, the pressure build-up could reach the tensile strength of the material, resulting in local micro-crack formation, brittle rupture and scaling. Therefore,

the high tensile strength—and particularly fracture resistance in ECC—could lead to its higher frost resistant characteristic. The influence of micro-fiber addition on frost resistance of conventional concrete has also been examined by other researchers [33,34] and is in agreement with what is found in this study. When PVA fiber is incorporated into ECC matrix, both the pressure-releasing effect [due to larger pore size (see “Air-Void Parameters” above)] and the crack-resisting effect contribute to the ability to resist deterioration during freezing and thawing cycles. Further experimental studies are needed to clearly understand the relative contributions of each factor discussed above on the frost resistance of ECC.

Flexural Performance

Table 6 provides the test results in terms of flexural strength (modulus of rupture) and ultimate mid-span beam deflection at peak stress before and after freezing and thawing deterioration. Typical flexural stress-mid-span deflection curves of ECC and ECC matrix (without fiber) specimens before and after freezing and thawing deterioration are shown in Fig. 8. Each result in Table 6 is an average of three to four specimens.

As seen in Table 6, the average flexural strengths were 4.42 and 11.44 MPa for ECC and ECC matrix, respectively, prior to freezing and thawing cycles. The ECC shows a substantially higher ultimate flexural strength than the ECC matrix. This may be attributed to the fact that micro-fibers inhibit the localization of micro-cracks into macro-cracks and consequently, the tensile strength of the ECC matrix increases with the formation of multiple micro-cracks during inelastic deformation. In all of the ECC specimens with/without freezing and thawing deterioration, prismatic specimens showed multiple cracking behaviors with small crack spacing and tight crack widths (<0.1 mm). The first crack started inside the mid-span at the tensile face. The flexural stress increased at a slower rate, along with the development of multiple cracks with small crack spacing and tight crack widths. Micro-cracks developed from the first cracking point and spread out in the mid-span of the flexural beam, as shown in Fig. 9. Bending failure in the ECC occurred when the fiber-bridging strength at one of the micro-cracks was reached, resulting in localized deformation (Fig. 9) once the modulus of rupture was approached. On the other hand, because of their low tensile properties and brittle nature, the ECC matrix beams failed catastrophically with a single crack under the four-point bending test.

Flexural stress-mid-span deflection curves obtained for the ECC prism specimens exposed to 300 freezing and thawing cycles are shown in Fig. 8. The typical flexural stress-deflection curves of ECC specimens after frost deterioration show that the influence of 300 freezing and thawing cycles on the flexural stress-mid-span deflection curves is fairly minor. This result is consistent with the earlier results of mass and pulse velocity losses of ECC specimens after 300 freezing and thawing cycles (Fig. 6). As seen in Fig. 8, the first-cracking strength of the ECC specimens after cyclic exposure falls below the first-cracking strength of the virgin ECC specimens (control specimens prior to freezing and thawing cycles). The slope of the load-deflection curve represents the stiffness

TABLE 6—Flexural properties of ECC (M45) prisms before and after 300 freeze-thaw cycles.

Specimen type	Ultimate Deflection, mm	Flexural Strength, MPa	Residual Crack Width, μm
Cured 21 days moist curing	0.68	4.42	...
	[0.24]	[0.79]	
Subjected to 300 freezing and thawing cycles	5.23	11.44	~61
	[0.16]	[0.54]	[~13]
	4.91	9.70	~70
	[0.40]	[0.19]	[~28]

Note: Numbers in brackets are standard deviations.

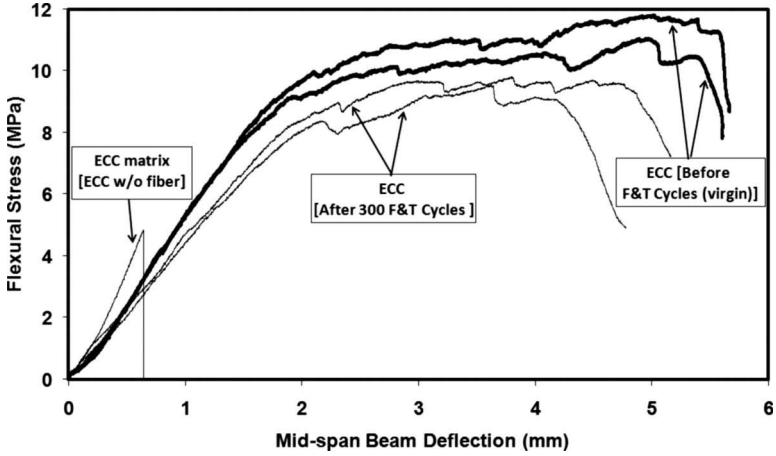


FIG. 8—Effect of freezing and thawing cycles on flexural behavior of ECC.

of the beams; Fig. 8 shows that the slope decreases with frost deterioration, thereby indicating a slight reduction in the stiffness of the ECC beams. Nevertheless, no significant reduction in the flexural strength and deflection capacities of the ECC specimens exposed to 300 freezing and thawing cycles was detected.

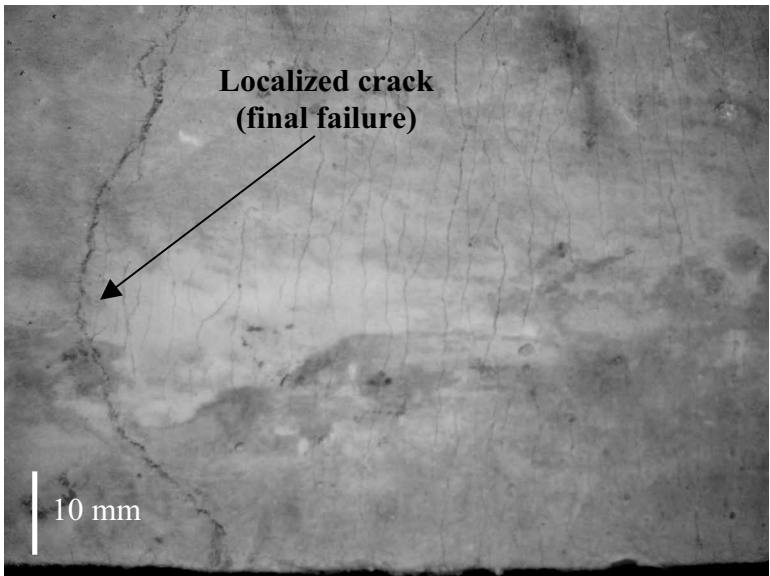


FIG. 9—Typical multiple crack pattern on the bottom tensile surface of ECC beam specimen after flexure load applications.

It should be noted that the residual ultimate flexural load-deflection curves of frost deteriorated ECC beams (Fig. 8) obtained following induced accelerated freeze-thaw cycling (up to six freezing and thawing cycles were achieved in a 24 h period) provide a conservative estimate of their residual flexural properties in actual structures. These accelerated deterioration periods are equivalent to a time span of many years in real structures, even those located in regions with harsh winters. This difference in accelerated and normal frost deterioration periods should have a significant influence on the residual flexural properties of ECC because in the long term, deterioration in ECC as a result of freezing and thawing cycles can easily be closed due to a self-healing process [31]. Thus the flexural performances of ECC summarized in Table 6 are underestimated.

Table 6 summarizes the flexural strength (modulus of rupture) and total mid-span deflection at the peak stress of ECC specimens exposed to 300 freezing and thawing cycles. The total deflection of the ECC beam, which reflects material ductility, exposed to 300 freezing and thawing cycles is 4.91 mm, which is slightly lower than that of ECC mixture prior to undergoing freezing and thawing cycles. Compared to control ECC specimens cured in laboratory air, the test results (Table 6) indicate that the ECC specimens exposed to freezing and thawing cycles showed reductions of nearly 15 % in flexural strength at the end of 300 cycles; this may be attributed to the effects of damage on the fiber/matrix interface and matrix micro-cracking.

Table 6 also shows the residual crack width of ECC mixtures at different ages. The term “residual crack width” indicates that crack width was measured from the unloaded specimen after the four-point flexural test by using a portable microscope with an accuracy of 5 μm . Both frost-deteriorated and virgin ECC specimens reveal saturated multiple cracking (Fig. 9) with crack width at ultimate flexural load limited to below 100 μm . Crack width control is of primary importance for many reinforced concrete applications since it is believed that there is a close relationship between mean or maximum crack widths and the durability of the structure. Moreover, the lower magnitude of the crack width is expected to promote self-healing behavior, and thus the transport properties in cracked composites [35–38]. In terms of permeability and diffusion, crack width less than 100 μm generally behaves like sound concrete [35,39]. Based on experimental results, Şahmaran et al. [35], Evardsen [40], and Reinhardt and Jooss [41] proposed that cracks with a width below 100 μm can be easily closed by a self-healing process. Consequently, in the serviceability limit state, a mean or maximum crack width less than about 0.1 mm is usually prescribed [39,40].

Conclusion

In this study, the frost resistance of ECC assessed by alternate freezing and thawing cycles in accordance with ASTM C666 Procedure A, air-void parameters determined by the modified point count method (ASTM C457), and the pore size distribution obtained by mercury intrusion porosimetry technique were compared with ECC matrix (ECC without PVA fiber). While the control

ECC matrix specimens rapidly failed in freezing and thawing (ASTM C666 Procedure A), ECC easily survived 300 cycles. Apart from the slight reduction in ultimate flexural strength and ductility, the test results presented in this study confirm that ECC provides excellent frost protection compared to ECC matrix. Despite a slight reduction in ductility and flexural strength, after 300 freezing and thawing cycles, ECC samples are found to retain tensile ductility more than a few hundred times, with residual crack width less than 100 μm on reloading, which is that of normal concrete and fiber-reinforced concrete with no environmental exposure. Further, it is important to note that this superior durability performance of ECC under freezing and thawing cycles was achieved without deliberate air-entrainment. For this reason, it is expected that the ECC investigated is suitable for long-term application under severe environmental conditions of alternate freezing and thawing cycles, if the structure is designed based on long-term mechanical properties.

Experimental evidence indicates that the excellent frost durability of ECC was due to the increase of pore volume larger than approximately 0.30 μm diameter, and intrinsically high tensile ductility and strength attained as a result of micro-mechanically based design principles. The presence of micro-PVA fibers critically contributes to the higher crack resistance and larger pore volume, and resulting pressure-releasing effects under freeze-thaw conditions.

Acknowledgments

The authors gratefully acknowledge the Scientific and Technical Research Council (TUBITAK) of Turkey provided under Project No. MAG-108M495 and the financial assistance of the Natural Sciences and Engineering Research Council (NSERC) of Canada, the Canada Research Chair Program. This international research collaboration was enhanced by a CI-Team grant (Grant No. OCI 0636300) from the United States National Science Foundation (NSF).

References

- [1] Li, V. C., "Engineered Cementitious Composites—Tailored Composites Through Micromechanical Modeling," *Fiber Reinforced Concrete: Present and the Future*, N. Banthia, A. Bentur, and A. Mufti, Eds., Canadian Society for Civil Engineering, Montreal, 1997, pp. 64–97.
- [2] Li, V. C., "On Engineered Cementitious Composites (ECC) – A Review of the Material and Its Applications," *J. Adv. Concr. Technol.*, Vol. 1, 2003, pp. 215–230.
- [3] Li, V. C., Wang, S., and Wu, C., "Tensile Strain-Hardening Behavior of PVA-ECC," *ACI Mater. J.*, Vol. 98, 2001, pp. 483–492.
- [4] Li, V. C., Mishra, D. K., and Wu, H. C., "Matrix Design for Pseudo Strain-Hardening Fiber Reinforced Cementitious Composites," *RILEM J. Mater. Struct.*, Vol. 28, 1995, pp. 586–595.
- [5] Maalej, M., Li, V. C., and Hashida, T., "Effect of Fiber Rupture on Tensile Properties of Short Fiber Composites," *J. Eng. Mech.*, Vol. 121, 1995, pp. 903–913.
- [6] Li, V. C., Wu, C., Wang, S., Ogawa, A., and Saito, T., "Interface Tailoring for Strain-Hardening PVA-ECC," *ACI Mater. J.*, Vol. 99, 2002, pp. 463–472.

- [7] Lepech, M. and Li, V. C., "Large Scale Processing of Engineered Cementitious Composites," *ACI Mater. J.*, Vol. 105, 2008, pp. 358–366.
- [8] Kong, H. J., Bike, S., and Li, V. C., "Development of a Self-Consolidating Engineered Cementitious Composite Employing Electrosteric Dispersion/Stabilization," *Cem. Concr. Compos.*, Vol. 25, 2003, pp. 301–309.
- [9] Kong, H. J., Bike, S., and Li, V. C., "Constitutive Rheological Control to Develop A Self-Consolidating Engineered Cementitious Composite Reinforced with Hydrophilic Poly(Vinyl Alcohol) Fibers," *Cem. Concr. Compos.*, Vol. 25, 2003, pp. 333–341.
- [10] Kim, Y. Y., Kong, H. J., and Li, V. C., "Design of Engineered Cementitious Composite (ECC) suitable for wet-mix shotcreting," *ACI Mater. J.*, Vol. 100, 2003, pp. 511–518.
- [11] Kunieda, M. and Rokugo, K., "Recent Progress on HPFRCC in Japan," *J. Adv. Concr. Technol.*, Vol. 4, 2006, pp. 19–33.
- [12] Li, V. C., Lepech, M., and Li, M., "Field Demonstration of Durable Link Slabs for Jointless Bridge Decks Based on Strain-Hardening Cementitious Composites," *Report No. RC-1438*, Michigan Department of Transportation (DOT), 2005.
- [13] Li, V. C., Fischer, G., Kim, Y. Y., Lepech, M., Qian, S., Weimann, M., and Wang, S., "Durable Link Slabs for Jointless Bridge Decks Based on Strain-Hardening Cementitious Composites," *Report No. RC-1438*, Michigan Department of Transportation (DOT), 2003.
- [14] Lepech, M. D. and Li, V. C., "Long Term Durability Performance of Engineered Cementitious Composites," *Int. J. Restor. Build. Monuments*, Vol. 12, 2006, pp. 119–132.
- [15] Li, V. C. and Lepech, M. "Crack Resistant Concrete Material for Transportation Construction," *TRB 83rd Annual Meeting, Washington, D.C., Compendium of Papers (CD ROM)*, Transportation Research Board, Washington, D.C., <, 2004, Paper No. 04-4680.
- [16] Pigeon, M. and Pleau, R., *Durability of Concrete in Cold Climates*, Chapman & Hall, London, 1995.
- [17] Siebel, E., "Air-Void Characteristics and Freezing and Thawing Resistance of Superplasticized Air-Entrained Concrete with High Workability," *Superplasticizers and Other Chemical Admixtures in Concrete, SP-119*, American Concrete Institute, Farmington Hills, MI, 1989, pp. 297–319.
- [18] Saucier, F., Pigeon, M., and Plante, P., "Air-Void Stability, Part III: Field Tests of Superplasticized Concretes," *ACI Mater. J.*, Vol. 87, 1990, pp. 3–11.
- [19] Pigeon, M., Plante, P., and Plante, M., "Air-Void Stability, Part I: Influence of Silica Fume and Other Parameters," *ACI Mater. J.*, Vol. 86, 1989, pp. 482–490.
- [20] Pigeon, M., Saucier, F., and Plante, P., "Air-Void Stability, Part IV: Retempering," *ACI Mater. J.*, Vol. 87, 1990, pp. 252–259.
- [21] ACI Committee 345, "Proposed Revision of ACI 345-74: Standard Practice for Concrete Highway Bridge Deck Construction," *Concr. Int.*, Vol. 3, 1981, pp. 19–53.
- [22] Powers, T. C., "Frost Resistant Concrete," *J. PCA Res. Dev. Lab*, Vol. 6, 1964, pp. 19.
- [23] Yang, E., Şahmaran, M., Yang, Y., and Li, V. C., "Rheological Control in the Production of Engineered Cementitious Composites," *ACI Mater. J.* Vol. 106, 2009 (in press).
- [24] Hooton, R. D., "Influence of Silica Fume Replacement of Cement on Physical Properties and Resistance to Sulfate Attack, Freezing, and Thawing, and Alkali-Silica Reactivity," *ACI Mater. J.*, Vol. 90, 1993, pp. 143–151.
- [25] Cai, H. and Liu, X., "Freeze-Thaw Durability of concrete: Ice Formation Process in Pores," *Cem. Concr. Res.*, Vol. 28, 1998, pp. 1281–1287.

- [26] Litvan, G. G., "Air Entrainment in the Presence of Superplasticizers," *ACI Mater. J.*, Vol. 80, 1983, pp. 326–331.
- [27] Koh, Y. and Kamada, E., "The Influence of Pore Structure of Concrete Made with Absorptive Aggregates on the Frost Durability of Concrete," *Proceedings RILEM/IUPAC International Symposium on Pore Structure and Properties of Materials*, Vol. 11, Artia, Prague, 1973, pp. F45–F62.
- [28] Cebeci, O. Z., "Pore Structure of Air-Entrained Hardened Cement Paste," *Cem. Concr. Res.*, Vol. 11, 1981, pp. 257–265.
- [29] Litvan, G. G. and Sereda, P. J., "Particulate admixture for Enhanced Freeze–Thaw Resistance of Concrete," *Cem. Concr. Res.*, Vol. 8, 1978, pp. 53–60.
- [30] Lange, H. and Modry, S., "Determination of the Frost Resistance of Limestone Aggregates in The Light of Porosity Investigation," *Proceedings of the RILEM Symposium on Durability of Concrete*, Building Research Institute, Prague, 1969, pp. B129–B168.
- [31] Şahmaran, M. and Li, V. C., "De-Icing Salt Scaling Resistance of Mechanically Loaded Engineered Cementitious Composites," *Cem. Concr. Res.*, Vol. 37, 2007, pp. 1035–1046.
- [32] Cohen, M. D., Zhou, Y., and Dolch, W. L., "Non-Air-Entrained High Strength Concrete—Is It Frost Resistant?," *ACI Mater. J.*, Vol. 89, 1992, pp. 406–415.
- [33] Pigeon, M., Azzabi, M., and Pleau, R., "Can Microfibers Prevent Frost Damage?," *Cem. Concr. Res.*, Vol. 26, 1996, pp. 1163–1170.
- [34] Deja, J., "Freezing and De-Icing Salt Resistance of Blast Furnace Slag Concretes," *Cem. Concr. Compos.*, Vol. 25, 2003, pp. 357–361.
- [35] Şahmaran, M., Li, V. C., and Li, M., "Transport Properties of Engineered Cementitious Composites Under Chloride Exposure," *ACI Mater. J.*, Vol. 104, 2007, pp. 604–611.
- [36] Şahmaran, M. and Li, V. C., "Influence of Microcracking on Water Absorption and Sorptivity of ECC," *Mater. Struct.* Vol. 42, 2009, pp. 593–603.
- [37] Lepech, M. D. and Li, V. C., "Water Permeability of Cracked Cementitious Composites," *Paper 4539 of Compendium of Papers* (CD ROM), ICF 11, Turin, Italy, 2005.
- [38] Yang, Y., M. D. Lepech, E. H. Yang, and V.C. Li, "Autogenous Healing of Engineering Cementitious Composites Under Wet-Dry Cycles," *Cem. Concr. Res.* Vol. 39, 2009, pp. 382–390.
- [39] Wang, K., Jansen, D., Shah, S., and Karr, A., "Permeability Study of Cracked Concrete," *Cem. Concr. Res.*, Vol. 27, 1997, pp. 381–393.
- [40] Evarnson, C., "Water Permeability and Autogenous Healing of Cracks in Concrete," *ACI Mater. J.*, Vol. 96, 1999, pp. 448–454.
- [41] Reinhardt, H. W., and Jooss, M., "Permeability and Self-Healing of Cracked Concrete as a Function of Temperature and Crack Width," *Cem. Concr. Res.*, Vol. 33, 2003, pp. 981–985.

Jize Mao,¹ Koichi Ayuta,² Hui Qi,³ and Zongmin Liu⁴

Experimental Study on Freeze-Thaw Damage Mechanism of Lightweight Aggregate Concrete

ABSTRACT: In order to clarify the deterioration process and damage mechanism of lightweight aggregate concrete when subjected to freezing and thawing, it is necessary to investigate the effects of lightweight aggregate on the concrete performance and analyze the relationship of freeze-thaw resistance between them. In this study, rapid freezing and thawing tests were conducted on lightweight concrete and lightweight coarse aggregate, respectively. The results of the concrete tests showed that the freeze-thaw resistance of lightweight concrete was mainly controlled by the water content of the lightweight aggregate. The tests of lightweight aggregate produced similar results: The higher the water content of the aggregate, the higher the weight loss and grain ratio passing 10 mm sieve; the lower the crushing strength, the larger the pore volume after freezing and thawing. When the lightweight aggregate with high water content was subjected to freezing and thawing, the pore volume grew larger since the aggregate structure suffered damage from frost expansion inside the structure. Micro-cracks began to form in the lightweight aggregate, then enlarged and spread to the adjacent mortar, and finally caused expansion and damage of lightweight concrete.

KEYWORDS: lightweight aggregate concrete, damage mechanism, freeze-thaw resistance, water content

Manuscript received March 31, 2009; accepted for publication September 22, 2009; published online November 2009.

¹ Associate Professor, College of Aerospace and Civil Engineering, Harbin Engineering Univ., 145 Nantong St., Nangang District, Harbin 150001, China.

² Professor, Dept. of Civil Engineering, Kitami Institute of Technology, 165 Koen-cho, Kitami 090-8507, Japan.

³ Professor, College of Aerospace and Civil Engineering, Harbin Engineering Univ., 145 Nantong St., Nangang District, Harbin 150001, China.

⁴ Lecturer, College of Aerospace and Civil Engineering, Harbin Engineering Univ., 145 Nantong St., Nangang District, Harbin 150001, China.

Cite as: Mao, J., Ayuta, K., Qi, H. and Liu, Z., "Experimental Study on Freeze-Thaw Damage Mechanism of Lightweight Aggregate Concrete," *J. ASTM Intl.*, Vol. 7, No. 1. doi:10.1520/JAI102450.

Copyright © 2010 by ASTM International, 100 Barr Harbor Drive, PO Box C700, West Conshohocken, PA 19428-2959.

Introduction

Lightweight concrete is a very versatile material for construction, which offers a range of technical, economic, and environment-preserving advantages and is destined to become a dominant material for construction in the new millennium [1]. Lightweight concrete can be manufactured usually by replacing normal aggregate with artificial lightweight aggregate. Lightweight aggregate concrete (LWC) has strengths comparable to normal weight concrete (NWC), yet it is typically 25–35 % lighter. LWC offers design flexibility and substantial cost savings by providing less dead load, improved seismic structural response, longer spans, better fire rating, decreased story height, smaller size structural members, less reinforcing steel, and lower foundation costs. However, lightweight aggregate is still faced with some problems, such as the high cost of aggregate due to high incineration temperature and the resistance to freezing and thawing [2,3]. As for freeze-thaw durability, numerous accelerated freezing and thawing testing programs and comprehensive investigations into the long-term weathering performance of lightweight concrete have arrived at similar conclusions: Properly proportioned and placed lightweight concrete performs equal to or better than NWC [2,4]. But in practical on-site construction, good pumpability of LWC is required to minimize the mixing water being absorbed by lightweight aggregate and ensure pumping operation. It is important to adequately condition the lightweight aggregate by fully prewetting before batching and pumping the concrete. Since lightweight aggregate containing water is easy to suffer greater damage due to freezing and thawing action [5–8], this additional moisture not only increases the density of the aggregate but also increases the risk of freeze-thaw durability. Therefore, the frost damage mechanism and the improvement on the quality of LWC have attracted much attention from researchers [9–13].

Since lightweight aggregate usually accounts for a higher percentage of the concrete by volume, the properties of lightweight aggregate can have a considerable influence on the properties of the resulting concrete. The aggregates with high water content are expected to play a key role in the freeze-thaw damage mechanism of LWC. In order to clarify the deterioration process of lightweight concrete when subjected to freezing and thawing, it is necessary to investigate the effect of lightweight aggregate on the concrete performance and analyze the relationship of freeze-thaw resistance between them. In this study, rapid freezing and thawing tests (6 cycles/day) were conducted on LWC and lightweight coarse aggregate (LWA), respectively, in order to investigate the freeze-thaw resistance of them. The two freezing and thawing tests were carried out on the LWAs with five levels of water content: 0 %, 10 %, 15 %, 20 %, and 30 %. Then the effects of the water content of LWA on the freeze-thaw resistance of both LWC and LWA, together with the change in the LWA pore structure and the process by which cracking is initiated in LWC when subjected to freezing and thawing, were discussed. For comparison, freezing and thawing tests of NWC specimens, which were produced by crushed stone (CS), were also conducted.

TABLE 1—Physical properties of LWA and CS.

Type	Density in Oven-Dried Condition (g/cm ³)	24 h Water Absorption (%)	Maximum Size (mm)
LWA	1.26	9.3	15
CS	2.66	0.78	20

Outline of Experiment

Materials and Mix Proportion of the Concrete

LWA was made from expanded shale. Table 1 shows the physical properties of the LWA and CS. Figure 1 shows the appearance and cross-section of LWA. Figure 2 shows the appearance of CS. Other materials used to make the testing concretes were ordinary Portland cement (density: 3.16 g/cm³ and fineness: 3330 cm²/g), sand (density in saturated surface-dry condition: 2.63 g/cm³, absorption: 1.78 %, and fineness modulus: 2.65), and admixtures (superplasticizer and air-entraining agent). Table 2 shows the mix proportions of the concretes. The water-cement ratios (*W/C*) for lightweight concrete were 30 %, 40 %, and 50 %. The *W/C* value of NWC was set to 40 %. The sand percentages (*S/A* by volume) of LWC were 44.1 %, 46.8 %, and 48.1 %. The water contents of LWAs were adjusted to five levels: 0 %, 10 %, 15 %, 20 %, and 30 %. Since the mass of LWA will change with the different water contents, the unit volume of 350 L/m³ is used in all mix proportions. The unit mass values of LWA are given in Table 2 in each case. The aggregates of CS and sand were in saturated surface-dry condition when the concretes were placed. The quantities of the admixtures in the concretes were adjusted in order to produce the target characteristics of fresh concrete (slump of both LWC and NWC: 8.0 ± 1.0 cm; air content of LWC: 5.5 ± 0.5 %; and air content of NWC: 4.5 ± 0.5 %).

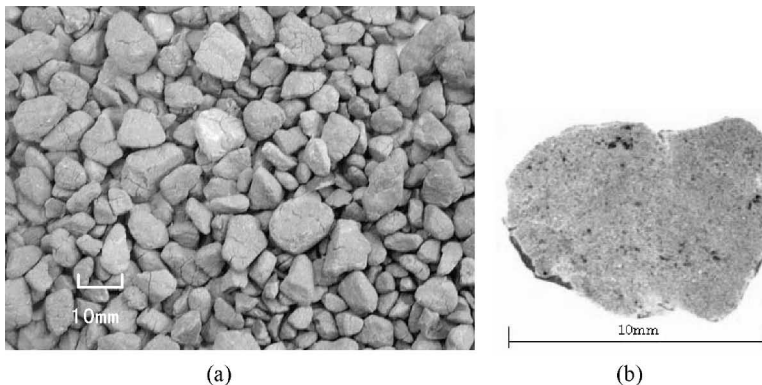


FIG. 1—LWA (a) appearance and (b) cross-section.



FIG. 2—Appearance of CS.

Water Absorption of Lightweight Course Aggregate

The water contents of LWAs were adjusted to five levels: 0 %, 10 %, 15 %, 20 %, and 30 %. The surface water was removed from the aggregate using a water-absorbent cloth before testing. The LWA with 0 % water content was in an oven-dried condition. The LWA with 30 % water content was produced by pre-soaking at high temperature in the aggregate production process. The water content of the other LWAs was adjusted by water immersion testing. Starting from an oven-dried condition, LWAs were immersed in water at atmospheric pressure for a certain period. The water contents of LWAs were measured at various ages of water immersion.

Mixing and Curing of the Concrete

The concrete was mixed in a forced-mixing type pan mixer. Slump and air content were measured according to the Japanese Industrial Standard (JIS) A 1101 (Method of Test for Slump of Concrete) [14] and A 1116 (Method of Test for Unit Mass and Air Content Mass Type of Fresh Concrete) [15], respectively. After placement, the specimens were cured for 24 h in a room maintained at 20°C with over 90 % humidity and then demolded. All testing specimens were cured in water at 20°C up to the age of 28 days (W28) to secure the initial hydration process of cement before being subjected to the freezing and thawing tests.

TABLE 2—*Mix proportions of concretes.*

W/C (%)	S/A (%)	Quantities (kg/m ³)						Measured Water Content Values of LWA (%)
		W	C	S	LWA	SP	AE	
30	44.1	155	517	726	441	6.669	4.136	0
					482	5.532	3.205	9.3
					508	4.653	2.275	15.1
40					520	4.808	1.603	18.0
					579	4.860	1.448	31.2
	46.8	160	400	811	441	3.680	1.120	0
40					482	1.920	1.000	9.3
					506	1.680	0.440	14.8
					524	1.520	0.440	18.9
40					579	1.400	0.320	31.2
	46.8	160	400	811	938 (CS)	1.440	0.880	...
	48.1	166	332	852	441	2.656	0.033	0
50					482	0.896	0.166	9.3
					506	0.564	0.398	14.7
					523	0.398	0.498	18.5
					579	0.100	1.992	31.2

Methods of Freezing and Thawing Test

Testing of Lightweight Aggregate Concrete and Normal Weight Concrete—All test specimens were $100 \times 100 \times 400$ mm³ prisms. They were subjected to freezing and thawing after curing for 28 days in water according to the requirements of ASTM C666-03el Procedure A. Freezing and thawing tests were carried out in water at 6 cycles/day up to 300 cycles.

The performance of the LWC and NWC specimens was measured primarily by the changes in their transverse frequency, which is proportional to the dynamic modulus of elasticity. The transverse frequency was measured prior to the test and at selected intervals during the test period and was reported as the relative dynamic modulus of elasticity, which is the ratio of the square of the frequency at a given cycle to the square of the initial frequency before the freeze and thaw cycling was begun [16]. Then durability factors (DF) of the LWC and NWC specimens were calculated. Length changes of the LWC and NWC specimens were also measured prior to testing and at selected freeze-thaw cycles during the tests. Three specimens were used to determine the testing values of DF and length change in each mix proportion.

Lightweight Coarse Aggregate Testing—The LWA grains used in the tests were 10–15 mm in size. The water contents of the LWA were adjusted to five levels: 0 %, 10 %, 15 %, 20 %, and 30 %. Any free water present on the surface of the LWA was tower-dried prior to testing. Then each of the specimens was put into a polyethylene bottle (volume: 1 L) in surface-dry condition. Freezing and thawing tests were conducted at 6 cycles/day up to 300 cycles by following the requirements of the LWC test.

Weight Loss After every 100 freeze-thaw cycles in each test, the LWA specimens were removed from the freeze-thaw test machine. Then they were passed through a sieve with 10 mm openings. The portions that passed through the sieves were treated as weight loss parts. Then each part was placed in an oven (temperature: 105°C) to dry for 24 h and weighted. The percentage of the weight loss was calculated using the following equation:

$$W_n = W_{nl}/W_0 \quad (1)$$

where:

W_n = weight loss rate at n cycles, %,

W_{nl} = weight of LWA passing through a sieve with 10 mm openings after n cycles, g, and

W_0 = weight of LWA at 0 cycle, g.

Grain Ratio Passing 10 mm Sieve Before the freezing and thawing tests, the initial LWA grain numbers were counted carefully. After every 100 freeze-thaw cycles, the residue grains left in the 10 mm sieve were counted again. The grain ratio passing 10 mm sieve was calculated using the following equation:

$$P_n = (N_0 - N_n)/N_0 \quad (2)$$

where:

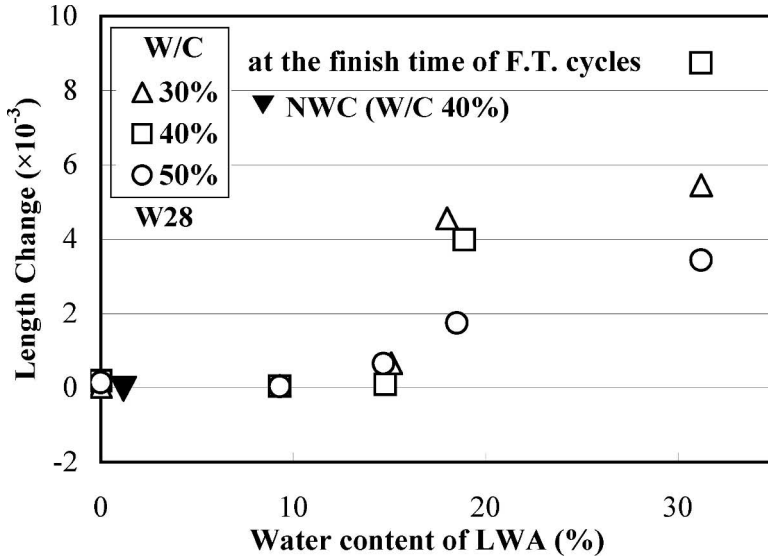


FIG. 3—Relationship between water content of LWA and length change of LWC.

P_n = grain ratio at n cycles, %,

N_0 = LWA grain numbers at 0 cycle, and

N_n = numbers of the residue grains left in the 10 mm sieve after n cycles.

Crushing Strength After the sieve analysis and drying process at every 100 freeze-thaw cycles, the residue left in the sieve was weighed out to 300 g and packed into a cylindrical vessel (ϕ : 81 \times 162 mm). The aggregates were then compressed with a plunger at a fixed rate (0.2–0.3 N/mm² per second). An indicating gauge was used to measure displacement. When the displacement reached 25 mm, the load was recorded immediately and the crushing strength was calculated.

Pore Structure After crushing tests at 0, 100, 200, and 300 freeze-thaw cycles, the crushed aggregate fragments were sieved again to obtain 2.5–5.0 mm particles. The pore structure (pore radius: 3.75–56 200 nm) was then examined by means of a mercury-intrusion porosity metre.

Results and Discussion

Testing results of LWC and NWC are shown in Figs. 3–5.

Figure 3 shows the relationship between the water content of LWA and the changes in length of LWC at the finish time of freezing and thawing cycles. The length change of NWC (W/C of 40%) was also shown in the figure. LWC that contained LWAs with the lower water content (0 %, 10 %, and 15 %) showed almost no noticeable changes in length as well as NWC. However, LWC produced with the higher content LWAs (20 % and 30 %) exhibited particularly

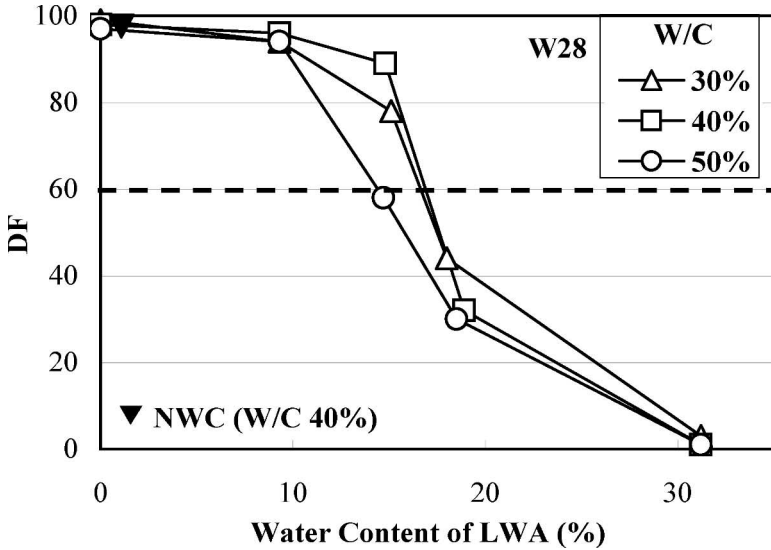


FIG. 4—Relationship between water content of LWA and DF of LWC.

large length increase as the result of the freezing and thawing action. It indicated that cracks occurred in the LWC that contained LWAs with the 20 % and 30 % water content and then to make LWC expand.

Figure 4 shows the relationship between the water content of LWA and the DF of LWC. The DF value of NWC (W/C of 40 %) was also shown in the figure. It is well known that the degree of saturation is a key parameter for the frost durability of concrete [17]. As for LWC, all kinds of water in the concrete can be thought to have influences on the freeze-thaw durability, including water in aggregates (different water contents) and water in concrete (due to W/C, submerge curing, and freeze-thaw test in water). However, in this study it was proven that the freeze-thaw resistance of LWC was mainly controlled by the

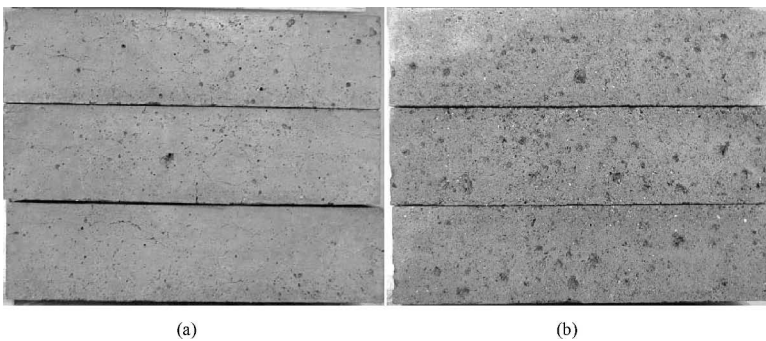


FIG. 5—Appearance of concrete specimens at the finish time of freezing and thawing tests: (a) LWC (W/C: 40 %; water content of LWA: 30 %) and (b) NWC (W/C: 40 %).

water content of the LWA that was used. It was not much related to W/C values; LWC that contained LWAs with the higher water content showed the lower DF values. Furthermore, cracks can be seen on the surface of the LWC made with LWAs with 30 % water content after freezing and thawing (Fig. 5). Just like Fig. 3 shown above, cracks occurred in the LWC containing LWAs with higher water content to cause concrete damage and failure with freeze-thaw action. Figure 5 also showed that there was almost no cement-paste scaling on the surface of LWC. NWC specimens showed superior freeze-thaw resistance with high DF value and quite slight surface scaling. It indicates that the absorbed water from submerge curing and freeze-thaw test has no significant effects on the freeze-thaw resistance of concrete, except it may cause slight scaling of cement paste sometimes. In these testing conditions, especially with 5.5 % air content, when the water content of LWA is below about 17 %, the DF of LWC is above 60, which is an admitted value to meet the freeze-thaw resistance for a common concrete structure.

Testing results of LWA are shown in Figs. 6–11.

Figure 6 shows the relationship between the water immersion time and the water content of LWA. Although the LWA has a dense surface texture, some open voids and fissures are also visible (see Fig. 1). The water content of LWA increased very fast at the beginning period of the water immersion [18]. When the LWA was immersed in the water, much water was absorbed by the voids and fissures. More than half of the 24 h water absorption occurred within the first 30 min. In the whole immersion time (13 weeks), the water absorption rate became slower and slower and the water absorption of LWA tended to be stable.

Figure 7 shows the relationship between the water content and the weight loss of LWA after 300 freeze-thaw cycles. LWAs with the lower water content (0 %, 10 %, 15 %, and 20 %) showed almost no noticeable deterioration when subjected to freezing and thawing action. Even after 300 freeze-thaw cycles, the weight losses remained below 2 % for all of them. However, in the case of the 30 % water content, the weight loss of LWA reached about 7 % and many grains fractured. It is thought to be due to freezing and thawing. Even an individual LWA grain, no cement paste around, the water included in the 30 % water content LWA was able to freeze, and then expansion pressure occurred in LWAs to cause grains damage. Moreover, since the tension strength of LWA decreases with the increase in water content [19], the LWA with 30 % water content is most vulnerable to frost damage and has the highest weight loss value.

Figure 8 shows the relationship between the water content and the grain ratio passing 10 mm sieve after 300 freeze-thaw cycles. In the case of the LWA with the 0 % water content, the grain ratio passing the 10 mm sieve is below 2 %. There is almost no deterioration of LWA due to freezing and thawing action. In the case of LWAs with the 10 %, 15 %, and 20 % water content, the grain ratio passing the 10 mm sieve is almost about 4 %. However, when the water content is 30 %, the grain ratio reached about 10 %, and many grains fractured to pass through the sieve.

Figure 9 shows the relationship between the water content and the crushing strength of LWA after 300 freeze-thaw cycles. With the increase in the water content, the crushing strength of LWAs decreased. In the case of the 30 % water content, the crushing strength is about 10 N/mm^2 , which decreased by about

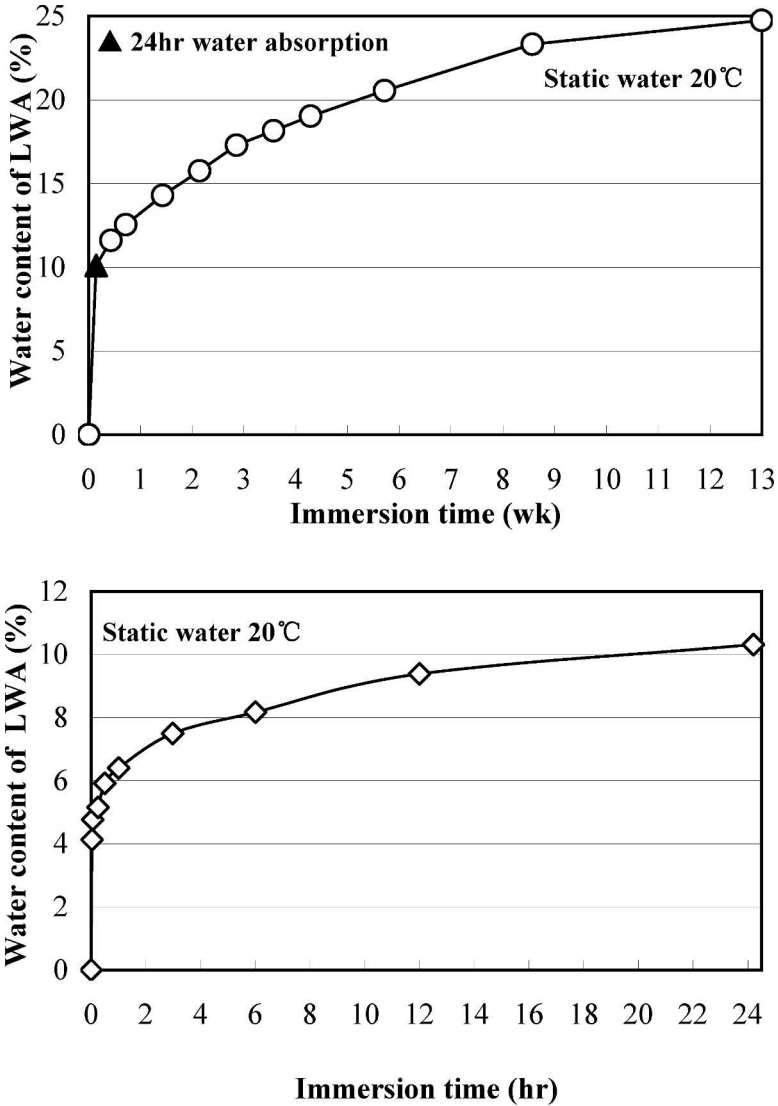


FIG. 6—Relationship between the water immersion time and the water content of LWA.

a third of its initial value. It is because the LWA with higher water content became easier to damage when subjected to freezing and thawing cycles.

Figure 10 shows changes in the total pore volume of LWAs with the freeze-thaw action at different water contents. As the number of freeze-thaw cycles increased, the total pore volume of LWA increased except for the case of the 0% water content. The interior structure of LWA that contained water turned more porous because of water freezing expansion. It can be thought to explain the above phenomena that the LWA grains with higher water content exhibited

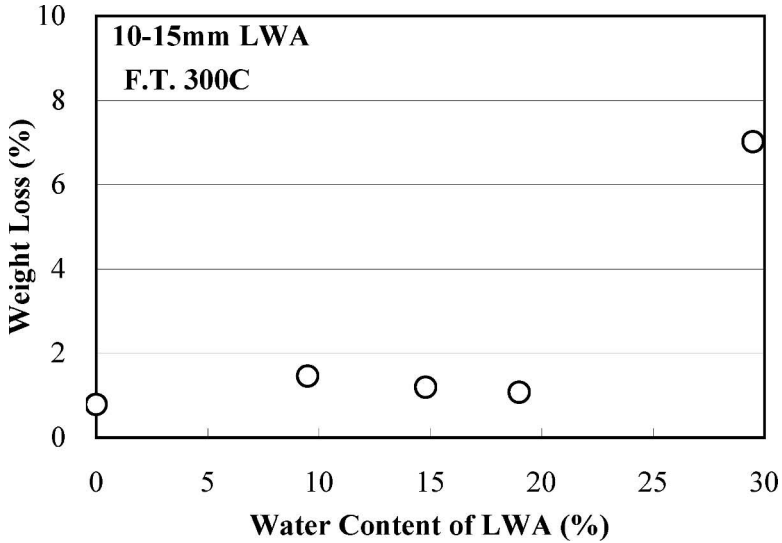


FIG. 7—Relationship between water content and weight loss of LWA.

higher weight loss, higher grain ratio passing 10 mm sieve, and lower crushing strength values after freezing and thawing.

Figure 11 shows the relationship between the water content and the total pore volume of LWAs of different pore radii at 300 freeze-thaw cycles. The total pore volume (pore radius: 3.75–56 200 nm), small pore volume (pore radius:

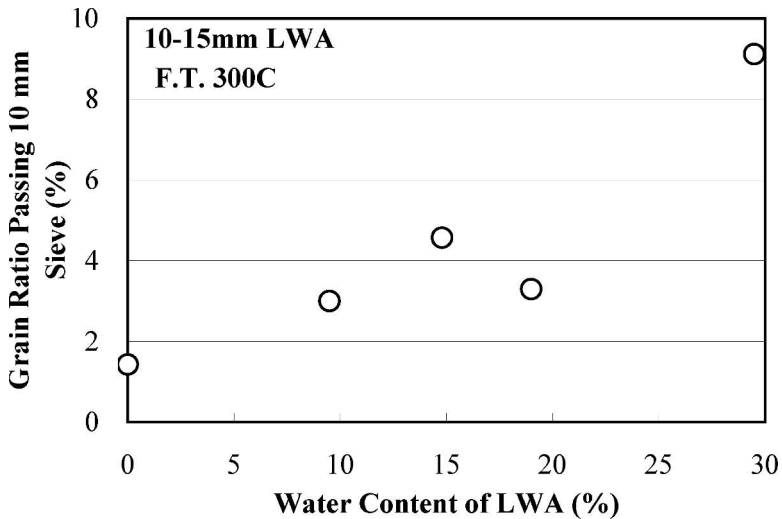


FIG. 8—Relationship between water content and grain ratio passing 10 mm sieve of LWA.

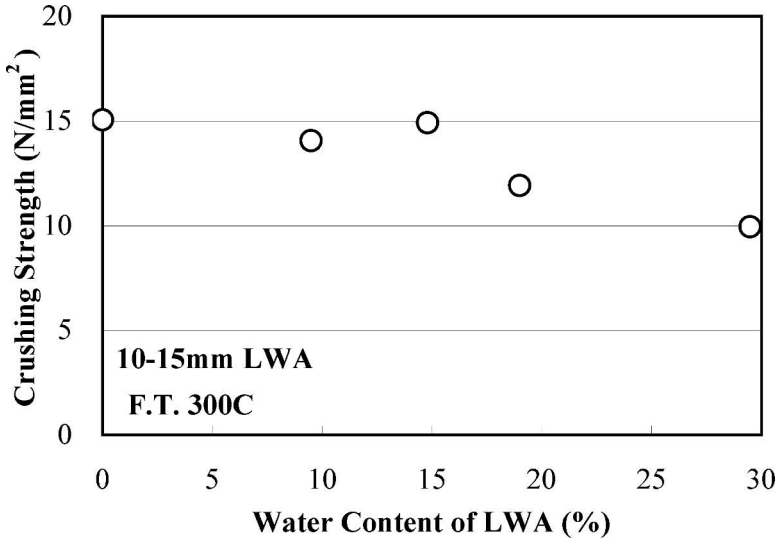


FIG. 9—Relationship between water content and crushing strength of LWA.

3.75–1000 nm), and large pore volume (pore radius: 1000–56 200 nm) are shown together in this figure. The higher the water content of LWA, the higher the total pore volume (pore radius: 3.75–56 200 nm). In the case of the small pore volume (pore radius: 3.75–1000 nm), there was almost no change with the water content of LWA after 300 freeze-thaw cycles. However, for the large pore volume (pore radius: 1000–56 200 nm), it increased with the water content due

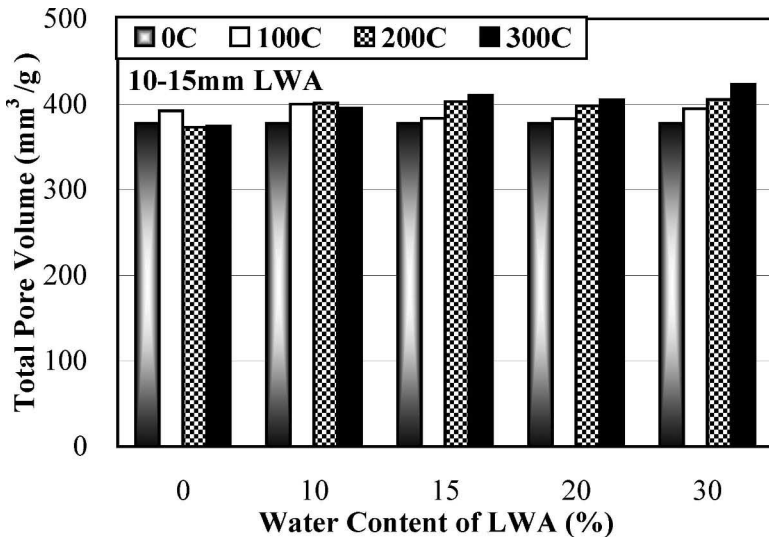


FIG. 10—Changes in the total pore volume of LWA with the freeze-thaw action.

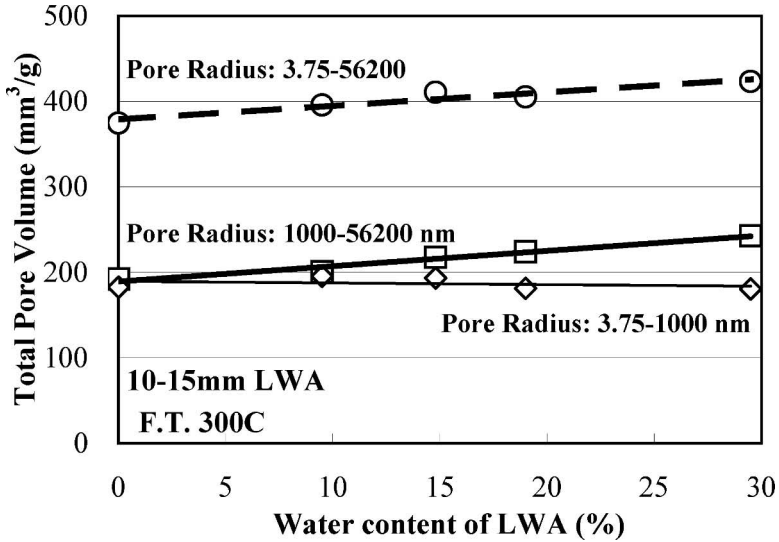


FIG. 11—Relationship between water content and total pore volume of LWA.

to freezing and thawing action. It showed that the large pore volume (pore radius: 1000–56 200 nm) had an important influence on the frost damage process for LWAs with higher water content.

Figure 12 shows the relationship between the total pore volume (pore radius: 1000–56 200 nm) of LWA and the length change of LWC at the finish time

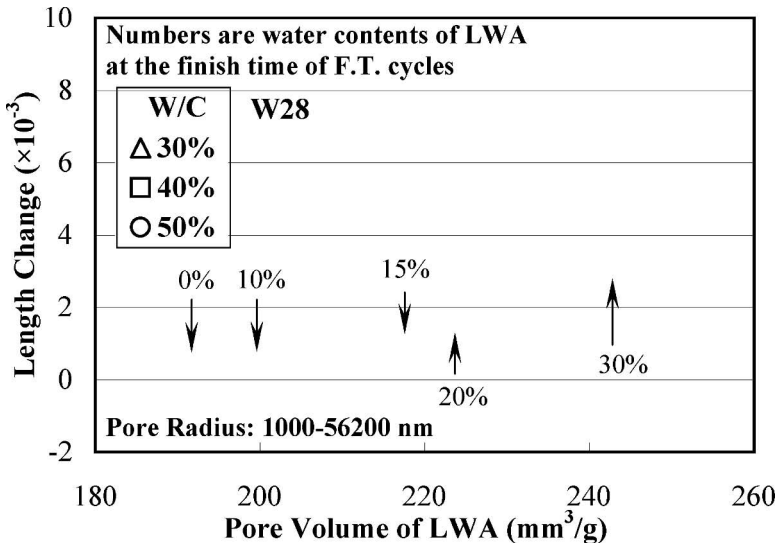


FIG. 12—Relationship between total pore volume of LWA and length change of LWC.

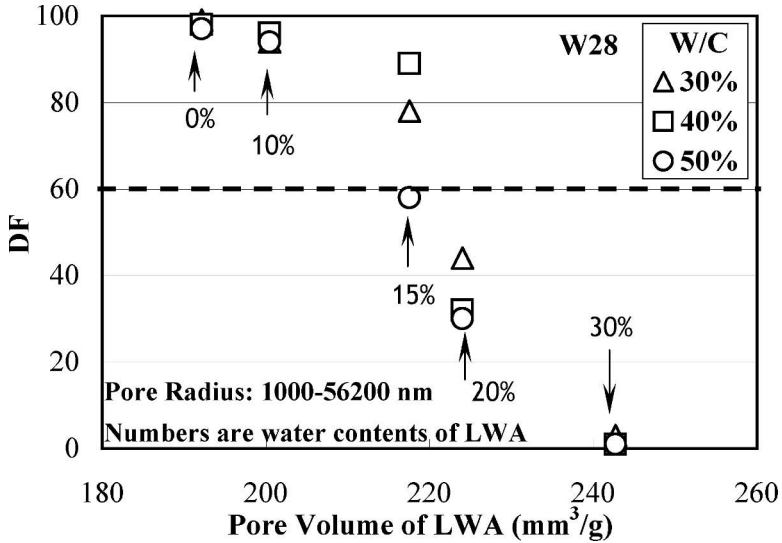


FIG. 13—Relationship between total pore volume of LWA and DF of LWC.

of freezing and thawing cycles. Figure 13 shows the relationship between the total pore volume (pore radius: 1000–56 200 nm) of LWA and the DF values of LWC. In the case of LWAs with large pore volume (20 % and 30 % water content), the length of LWC increased noticeably, and the DF declined when subjected to freezing and thawing. It showed weak freeze-thaw resistance of LWC with large pore volume. However, for the LWAs with small pore volume (0 %, 10 % and 15 % water content), the length of LWC showed almost no changes, the DF values were above 60, and the freeze-thaw resistances were secured.

Figure 14 shows the cross-section of a broken LWC (W/C: 40 %; water content of LWA: 30 %) due to freezing and thawing action. All LWAs fractured and cracks penetrated deeply into LWAs in the LWC. When subjected to freez-

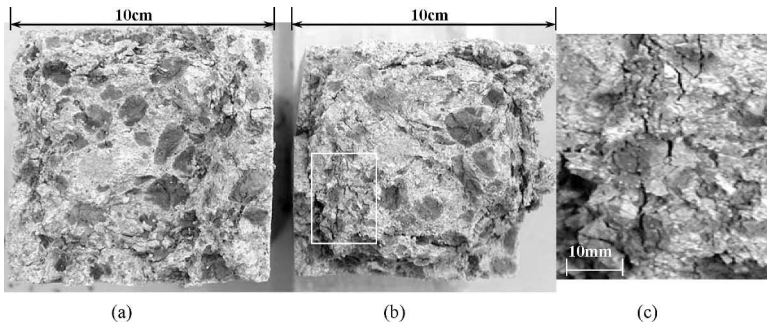


FIG. 14—Cross-section of a broken LWC (W/C: 40 %; water content of LWA: 30 %) due to freezing and thawing action: [(a) and (b)] Broken sections and (c) enlarged picture in white rectangular areas.

ing and thawing, expansion pressure occurred in the LWAs containing water, micro-cracks formed in the aggregates that have large pore volume and low strength, and then enlarged and spread to the mortar as the number of freeze-thaw cycles increased. This process eventually caused LWC expansion and damage.

Conclusions

In this study, rapid freezing and thawing tests (6 cycles/day) were conducted on LWC and LWA, respectively. The results of the LWC tests showed that the freeze-thaw resistance of LWC was mainly controlled by the water content of the LWA that was used. The higher the water content of the LWA, the lower the freeze-thaw resistance of the LWC. When the water content of LWA is below about 17 %, the freeze-thaw resistance of LWC with 5.5 % air content can be secured. The LWA tests produced similar results: The higher the water content of the LWA, the higher the weight loss and grain ratio passing 10 mm sieve; the lower the crushing strength, the larger the pore volume after freezing and thawing. When the LWA with high water content was subjected to freezing and thawing, the pore volume grew larger since the aggregate structure suffered damage from frost expansion inside the structure. Micro-cracks formed in the LWA and then enlarged and spread to the mortar as the number of freeze-thaw cycles increased. This process eventually caused LWC expansion and damage.

Acknowledgments

The project was supported by National Natural Science Foundation of China (Grant No. 50908059) and the Scientific Research Foundation for the Returned Overseas Chinese Scholars, State Education Ministry.

References

- [1] Owens, P. L., "Structural Lightweight Aggregate Concrete—The Future?," *Concrete*, Vol. 33(10), 1999, pp. 45–47.
- [2] ACI Committee 213, *Guide for Structural Lightweight-Aggregate Concrete*, American Concrete Institute, Farmington Hills, MI, 2003.
- [3] Han, S. M., Choi, S. G., and Kim, S. B., "Experimental Study on the Freeze-Thaw Resistance of High Strength Lightweight Aggregate Concrete," *Magazine of the Korea Concrete Institute*, Vol. 10(1), 1998, pp. 125–132.
- [4] Holm, T. A., "Lightweight Concrete and Aggregates," *Tests and Properties of Concrete and Concrete-Making Materials*, ASTM STP 169C, ASTM International, West Conshohocken, PA, 1994, pp. 522–532.
- [5] Mao, J. Z., Ayuta, K., Hanei, T., and Matsui, T., "Effects of Lightweight Coarse Aggregate Properties on Freeze-Thaw Resistance," *Fourth International Conference on Concrete Under Severe Conditions—Environment and Loading*, Seoul, South Korea, 2004, Seoul National University, Seoul, pp. 530–537.
- [6] Mao, J. Z. and Ayuta, K., "Freeze-Thaw Resistance of Lightweight Concrete and Aggregate at Different Freezing Rates," *J. Mater. Civ. Eng.*, Vol. 20(1), 2008, pp.

78–84.

- [7] Hoff, G. C., “Freezing and Thawing of Lightweight Concrete,” *First International Conference on Concrete Under Severe Conditions—Environment and Loading*, Sapporo, Japan, 1995, Hokkaido Development Bureau, Sapporo, pp. 129–138.
- [8] Roberts, J. M., “Freeze-Thaw Durability of Concretes Using Lightweight Aggregate of Differing Absorption Characteristics,” *First International Conference on Concrete Under Severe Conditions—Environment and Loading*, Sapporo, Japan, 1995, Hokkaido Development Bureau, Sapporo, pp. 139–146.
- [9] Gao, X. F., Lo, Y. T., and Tam, C. M., “Investigation of Micro-Cracks and Micro-structure of High Performance Lightweight Aggregate Concrete,” *Build. Environ.*, Vol. 37, 2002, pp. 485–489.
- [10] Choi, Y. W., Moon, D. J., Chung, J. S., and Cho, S. K., “Effects of Waste PET Bottles Aggregates on the Properties of Concrete,” *Cem. Concr. Res.*, Vol. 35, 2005, pp. 776–781.
- [11] Rossignolo, J. A. and Agnesini, M. V. C., “Mechanical Properties of Polymer-Modified Lightweight Aggregate Concrete,” *Cem. Concr. Res.*, Vol. 32, 2002, pp. 329–334.
- [12] Blanco, F., Garcia, P., Mateos, P., and Ayala, J., “Characteristics and Properties of Lightweight Concrete Manufactured with Cenospheres,” *Cem. Concr. Res.*, Vol. 30, 2000, pp. 1715–1722.
- [13] Basri, H. B., Mannan, M. A., and Zain, M. F. M., “Concrete Using Waste Oil Palm Shells as Aggregate,” *Cem. Concr. Res.*, Vol. 29, 1999, pp. 619–622.
- [14] JIS A 1101, 2005, “Method of Test for Slump of Concrete,” Japanese Industrial Standard (JIS), Tokyo.
- [15] JIS A 1116, 2005, “Method of Test for Unit Mass and Air Content Mass Type of Fresh Concrete,” Japanese Industrial Standard (JIS), Tokyo.
- [16] ASTM C666-03e1, 2003, “Standard Test Method for Resistance of Concrete to Rapid Freezing and Thawing,” *Annual Book of ASTM Standards*, Vol. 04.02, ASTM International, West Conshohocken, PA, pp. 337–342.
- [17] Jacobsen, S., Hammer, T. A., and Sellevold, E. J., “Frost Testing High Strength Lightweight Aggregate Concrete Internal Cracking vs. Scaling,” *Proceedings of International Symposium on Structural Lightweight Aggregate Concrete*, Sandefjord, Norway, 1995, Norwegian Concrete Association, Oslo, pp. 541–554.
- [18] Zhang M. H. and GjØrv, O. E., “Characteristics of Lightweight Aggregates for High-Strength Concrete,” *ACI Mater. J.*, Vol. 88(2), 1991, pp. 150–158.
- [19] Tamura, K., Tagaya, K., Yonekura, A., and Tazawa, E., “A Study on Mechanism of Frost Damage of High-Strength Light-Weight Concrete,” *Concrete Research and Technology*, Vol. 6(2), 1995, pp. 77–84 (in Japanese).

John T. Kevern,¹ Kejin Wang,² and Vernon R. Schaefer³

Test Methods for Characterizing Air Void Systems in Portland Cement Pervious Concrete

ABSTRACT: Portland cement pervious concrete is becoming a common tool for stormwater management across the United States. The air void system in pervious concrete is particularly important because of its effect on stormwater infiltration, concrete strength, and long-term durability. However, currently the concrete industry lacks standardized testing techniques for characterizing air void systems in pervious concrete. In this paper a series of air system characterization tests performed during a field placement of pervious concrete is detailed, and the test results are compared. Fresh pervious concrete samples from two delivered mixtures were evaluated using pressure, volumetric, Chace, and air void analyzer air test methods. The hardened concrete samples were tested for water-permeable void content, water permeability, air voids (using ASTM Standard C457 method), and freeze-thaw durability (using ASTM Standard C666A method). Based on the results of the study, determination of air systems for the freeze-thaw protection of pervious concrete is proposed.

KEYWORDS: pervious concrete, freeze-thaw durability, freeze-thaw resistance, air entrainment, air content testing

Manuscript received March 31, 2009; accepted for publication August 17, 2009; published online September 2009.

¹ Assistant Professor of Civil Engineering, Univ. of Missouri–Kansas City, Kansas City, MO 64110, e-mail: kevernj@umkc.edu

² Associate Professor of Civil Engineering, Dept. of Civil, Construction, and Environmental Engineering, Iowa State Univ., Ames, IA 50011, e-mail: kejinw@iastate.edu

³ Professor of Civil Engineering, Dept. of Civil, Construction, and Environmental Engineering, Iowa State Univ., Ames, IA 50011, e-mail: vern@iastate.edu

Cite as: Kevern, J. T., Wang, K. and Schaefer, V. R., "Test Methods for Characterizing Air Void Systems in Portland Cement Pervious Concrete," *J. ASTM Intl.*, Vol. 6, No. 9. doi:10.1520/JAI102451.

Copyright © 2009 by ASTM International, 100 Barr Harbor Drive, PO Box C700, West Conshohocken, PA 19428-2959.

Introduction

It is well-known that air entrainment in concrete improves freeze-thaw durability and workability [1]. Along with unit weight and slump, air content is a commonly tested parameter for fresh concrete to ensure consistency and durability. As Portland cement pervious concrete (PCPC) becomes a commonly utilized best management practice, methods will be required to verify mixture proportions and consistent production. The standard concrete quality control principles (such as slump, air, and unit weight) when applied to pervious concrete either are not appropriate or do not behave in a similar fashion to that of traditional concrete. The new ASTM Standard C1688, "Standard Test Method for Density and Void Content of Freshly Mixed Pervious Concrete," has been developed for determining density of fresh pervious concrete [2]. While ASTM Standard C1688 does predict the density or performance of in-place pervious concrete, it also provides a useful tool for verifying consistency of mixture production and to the submitted mixture design. The durability of pervious concrete is important for the continued installation in cold weather portions of the United States. Previous research at Iowa State University (ISU) shows that air entrainment does occur in "workable" pervious concrete and that increased levels of air entrainment improve freeze-thaw durability in the ASTM Standard C666A, "Standard Test Method for Resistance of Concrete to Rapid Freezing and Thawing," test method [3]. The hardened air entrainment levels were determined using a RapidAir 457 device and the ASTM Standard C457, "Standard Test Method for Microscopical Determination of Parameters of the Air-Void System in Hardened Concrete," procedure A. While the RapidAir device was able to quantify the level of air entrainment, hardened sample preparation means that installations with inadequate air systems are not discovered until at least several days after placement. If entrained air content is to be considered an important characteristic of pervious concrete, methods to determine both fresh and hardened contents need to be verified.

This paper describes a comparison of a majority of common methods to determine entrained air content in traditional concrete applied to an actual pervious concrete field placement at ISU. The fresh methods to determine air entrainment included volumetric air content, Chace air indicator (CAI), pressure method, and use of the air void analyzer (AVA), all on two different mixtures. Hardened air entrainment was evaluated using the RapidAir device. Core samples were taken to evaluate variability in the porosity or water-permeable voids and determine if workability added by air entrainment corresponded to consistency in the in situ material. Samples were also evaluated for freeze-thaw durability using both mass loss and transverse fundamental frequency.

The concrete materials and mixtures studied in the present paper were from an actual field application at a parking lot of ISU (ISU Lot 122). Some of test samples were directly cored from the parking lot. The ISU Lot 122 project was constructed as the Iowa Pervious Concrete Water Quality Project, with the objective to quantify the behavior of a pervious concrete system in cold weather climates and to compare various aspects of the stormwater effluent versus a control parking area. Half of the parking area is PCPC and half is traditional Portland cement concrete pavement. The traditional pavement was sloped to

TABLE 1—Concrete mixture proportions.

Component	Mix		
	Small RG	Large RG	
Cement	298 (503)	298 (503)	kg/m ³ (pcy)
Fly ash	45 (75)	45 (75)	kg/m ³ (pcy)
Coarse agg.	1525 (2570)	1498 (2525)	kg/m ³ (pcy)
Fine agg.	77 (130)	104 (175)	kg/m ³ (pcy)
Fibers	0.9 (1.5)	0.9 (1.5)	kg/m ³ (pcy)
Water	93 (156)	93 (156)	kg/m ³ (pcy)
Mid-range water reducer	4 (6)	4 (6)	mL/kg (oz/cwt)
Hydration stabilizer	4 (6)	4 (6)	mL/kg (oz/cwt)

collect all of the stormwater, and the two sections of pervious concrete was installed to evaluate the effect of different mixture designs and aggregate base configurations.

Material Properties

Two gradations of rounded river gravel (RG) coarse aggregate were used. The small-sized RG had 100 % of the material passing the 12.5 mm (1/2 in.) sieve, 97 % passing the 9.5 mm sieve (3/8 in.), and 19 % passing the 4.75 mm sieve (No. 4). The dry rodded unit weight was 1640 kg/m³ (102 pcf) of the smaller aggregate, porosity of 37.4 %. The large-sized RG had 100 % of the material passing the 12.5 mm (1/2 in.) sieve, 66 % passing the 9.5 mm sieve (3/8 in.), and 4 % passing the 4.75 mm sieve (No. 4). The dry rodded unit weight was 1630 kg/m³ (102 pcf) of the larger aggregate, porosity of 37.8 %. Both aggregates were supplied from the same source and had specific gravities of 2.62, absorption of 1.7 %, and the abrasion obtained using a Micro Deval device was 14.4 %.

River sand was used to replace up to 7 % of the coarse aggregate (by either mass or volume since specific gravity was equal). The sand had a fineness modulus of 2.90, with 90 % passing a 2.36 mm sieve (No. 8). Fine aggregate had a specific gravity of 2.62 and absorption of 1.1 %. Polypropylene fibers were incorporated into the pervious concrete proportions and had a specific gravity of 0.91. An air entraining agent (AEA) and mid-range water reducer were used in all of the pervious concrete mixtures along with a hydration stabilizer. AEA was dosed to produce 6 % air in a standard low slump paving mixture.

Mixture proportions for the two concrete mixtures are shown in Table 1. The mixture containing the small-sized RG is labeled (small RG) and the large-sized RG (large RG).

Sample Preparation

All specimens in the following study were created using concrete delivered during the ISU Lot 122 construction. All samples were placed in the field by lightly

rodding 25 times in three layers to ensure uniform compaction in each lift without consolidation. The samples were demolded after 24 h, placed in a fog room at 98 % relative humidity, and cured according to ASTM Standard C192, "Standard Practice for Making and Curing Concrete Test Specimens in the Laboratory," [4]. Before compression testing, the cylinders were capped using a sulfur capping compound following ASTM Standard C617, "Standard Practice for Capping Cylindrical Concrete Specimens"[5].

Cylinders of 100 mm (4 in.) in diameter and 200 mm (8 in.) in length were used for both compression and tensile strength tests. Cylinders of 75 mm (3 in.) \times 150 mm (6 in.) were used to perform the porosity analysis, and cylinders of 75 mm (3 in.) in diameter and length were used to measure the permeability. Beams with a cross section of 75 mm (3 in.) \times 100 mm (4 in.) and a length of 400 mm (16 in.) were used for freeze-thaw testing placed in two layers.

Cylinder specimens 100 mm (4 in.) in diameter and 200 mm (8 in.) in length were used for RapidAir testing. The top and bottom 50 mm (2 in.) of the hardened concrete cylinders were removed using a concrete slab saw. Two more cuts were then made vertically to produce a specimen with dimensions of 100 mm (4 in.) \times 100 mm (4 in.) \times 19 mm (0.75 in.). The specimen represents a vertical section taken from the center of the cylinder. The samples were then wet-sanded with progressively finer grit paper, finishing with 6 μ m grit.

Samples were treated according to the RapidAir manufacturer's recommendations [6]. The polished samples were coated with a broad-tipped black marker. After the ink had completely dried, the samples were placed into an 80°C oven for 2 h. Then, the samples were removed and coated with a white paste comprised of petroleum jelly and zinc oxide and allowed to cool. The extra paste was removed by dragging an angled razor blade across the surface until all of the paste was removed from the aggregate and cement mortar areas. If porous areas of the aggregates contained any white paste, they were individually colored with a fine-tip black marker [6].

Once a specimen was prepared, the RapidAir device was used to scan across the sample using a video frame width of 748 pixels. Up to ten probe lines per frame can be used to distinguish between the black and white sections. A white-level threshold adjustment further refines the image before air void determination.

Test Methods

Standard material property testing included compressive strength development with time according to ASTM Standard C39, "Standard Test Method for Compressive Strength of Cylindrical Concrete Specimens," [7] on sulfur capped samples. Splitting tensile tests were performed according to ASTM Standard C496, "Standard Test Method for Splitting Tensile Strength of Cylindrical Concrete Specimens," [8]. Modulus of Rupture (MOR) was determined according to ASTM Standard C78 "Standard Test Method for Flexural Strength of Concrete (using simple beam with third point loading)" [9].

The void ratio (porosity) of the pervious concrete was determined by taking

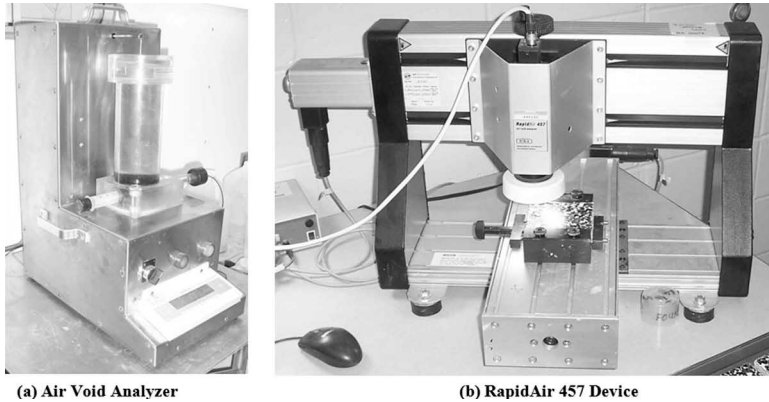


FIG. 1—Two methods to determine fresh and hardened entrained air content of pervious concrete: (a) AVA and (b) RapidAir 457 device.

the difference in weight between a sample oven dry and submerged under water and using the standard procedure developed at the University of South Carolina [10].

The permeability was determined using a falling head permeability test apparatus. A flexible sealing gum was used around the top perimeter of a sample to prevent water leakage along the sides of a sample. The samples were then confined in a latex membrane and sealed in a rubber sleeve, which was surrounded by adjustable hose clamps. The average coefficient of permeability (k) was determined using falling head permeability measurement, which follows Darcy's law and assumes laminar flow [11].

Freeze-thaw durability was tested using ASTM Standard C666 procedure A [12] in which samples were frozen and thawed in the saturated condition. Two sets of criteria were used to evaluate freeze-thaw durability, relative dynamic modulus, and mass loss. Tests were completed at either 60 % relative dynamic modulus or 15 % mass loss. Samples were tested every 20–30 cycles. The results of other mixtures and more details are summarized in Schaefer et al. [13] and Kevern [14].

Fresh air tests were performed on the concrete using ASTM Standard C231, "Standard Test Method for Air Content of Freshly Mixed Concrete by the Pressure Method," [15] pressure method and ASTM Standard C173, "Standard Test Method for Air Content of Freshly Mixed Concrete by the Volumetric Method," [16] volumetric method. Fresh air was determined on the mortar by the CAI and AVA. Mortar was obtained by vibrating a 4.75 mm sieve basket of fresh pervious concrete until enough mortar was separated from the mixture to create the test samples. CAI was determined using AASHTO T199-00 [17]. AVA testing was performed according to the test method outlined by Taylor et al. [18] (Fig. 1(a))

Values determined from the RapidAir device (Fig. 1(b)) are reported according to ASTM Standard C457 [19]. Five traverse lines per frame were used to distinguish between the black sections (aggregate or mortar) and the white

TABLE 2—Concrete material properties.

Property	Mixture		
	Small RG	Large RG	
7-day comp. str.	17.8 (2578)	16.0 (2322)	MPa (psi)
28-day comp. str.	22.8 (3305)	22.8 (3304)	MPa (psi)
56-day comp. str.	24.3 (3521)	23.4 (3399)	MPa (psi)
28-day spl. tens.	2.6 (380)	2.3 (338)	MPa (psi)
28-day MOR	2.7 (393)	3.5 (509)	MPa (psi)
Voids	23.0	27.8	%
Unit weight	2000 (124.8)	1923 (120.0)	kg/m ³ (pcf)
Permeability—7.6 cm diam.	1260 (496)	1692 (666)	cm/h (in./h)
Permeability—10.2 cm diam.	1764 (695)	2268 (893)	cm/h (in./h)

portions (water-permeable voids or entrained air). The threshold values were 120 for both pea gravel mixtures. Threshold values are not very sensitive to some changes, and ultimately the threshold used for testing is best determined by experience according to specific conditions [20].

Results and Discussion

Standard Material Properties

The material properties for both mixtures are shown in Table 2. The mixture made with larger-sized RG had slightly higher voids and correspondingly lower unit weight than the mixture with smaller-sized RG. Compressive strength and splitting tensile strength values were similar between the mixtures. Due to the lack of standard placing technique, only one MOR beam was placed of each, while all other values represent triplicate testing with coefficient of variation (COV) of less than 15 %. The larger mixture with higher voids also had higher permeability. The 10.2 cm (4 in.) diameter specimens had approximately 25 % higher permeability than the 7.6 cm (3 in.) samples, which is consistent with previous findings [21].

Variability in Porosity

Pervious concrete contains two types of air systems, intentionally designed porosity and entrained air in the mortar surrounding the aggregate particles. Porosity represents the large water-permeable voids, while entrained air does not contribute to the permeability but aids freeze-thaw durability [3]. The current method of pervious concrete placement is a “pile and rake” method where piles of pervious concrete are placed and raked by hand to roughly level with the forms preceding the method of finishing and compaction. Since pervious concrete load carrying capacity and permeability are controlled by the interconnected large voids, the mixture workability, placement technique, and

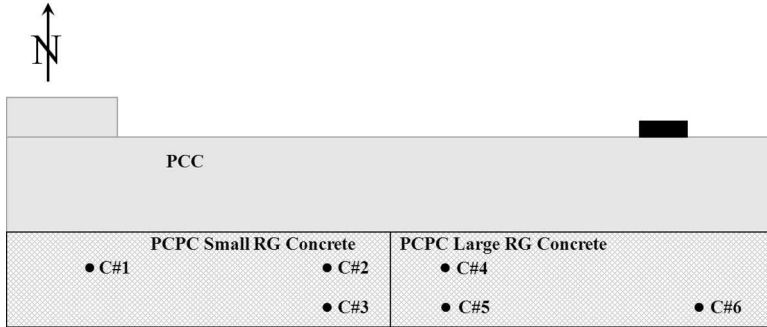


FIG. 2—Lot 122 core sample locations.

compaction/finishing technique are all important to the final in situ density consistency. Figure 2 shows the location of the core samples removed to verify in situ placement consistency. Three cores were tested from each mixture.

Porosity results from the core samples are shown in Table 3. The void content and unit weights were highly variable for both mixtures. The unit weight value was 228 kg/m^3 (14.3 pcf) for the small-sized RG mixture and 278 kg/m^3 (17.4 pcf) for the larger-sized RG mixture, producing 10.4–12.1 % voids, respectively. Permeability values were also highly variable, ranging from almost impermeable (5 cm/h) to extremely permeable (4000 cm/h), corresponding to voids. Although the unit weight values were variable, the COV was relatively low (<10 %). However for the same samples, COV for permeability was much higher. The high variability of results from the core samples suggests that improvements in placing methods are required to produce more consistent pavement.

TABLE 3—Core variability results.

Core (Number)	Mixture	Voids (%)	Unit Weight kg/m^3 (pcf)	Permeability cm/h (in./h)
1	Small RG	29.0	1855 (115.8)	2772 (1091)
2	Small RG	22.4	2010 (125.5)	936 (369)
3	Small RG	18.6	2083 (130.1)	5(2)
4	Large RG	36.9	1695 (105.8)	4104 (1616)
5	Large RG	27.4	1932 (120.6)	2664 (1049)
6	Large RG	24.8	1973 (123.2)	1,440 (567)
Small average		23.3	1983 (123.8)	1331 (524)
Small COV (%)		22.7	5.9	97.9
Large average		31.1	1829 (114.2)	2736 (1077)
Large COV (%)		21.6	8.6	48.5

TABLE 4—*Fresh concrete air testing results reported in percent air.*

Mixture	Pressure	Volumetric	CAI	Air Void Analyzer	
				<2 mm	<0.35 mm
Small RG	8.5	7.5	1.5	1.20	0.73
Large RG	6.0	5.0	1.0	0.40	0.13

Plastic Air Determination

Results from the four test methods used to investigate fresh air properties are shown in Table 4. CAI and the AVA measure air content of the mortar, while the pressure and volumetric methods measure air content of the entire concrete volume. The CAI and AVA values shown in Table 4 have been converted to volume percentage of total concrete. Both the standard pressure and volumetric air tests yielded results typically expected for normal concrete. These methods require placing fresh concrete in a given container and using water to either fill surface voids between the upper chamber and fresh concrete or record air released during agitation. When applied to pervious concrete, both methods fill the water-permeable voids without fully releasing all of the air caught in the large void space. A similar response occurs when using the pressure method on concrete containing high porosity aggregate. Testing voids of hardened pervious concrete requires vigorous tapping of the cylinders under water to fully release the air present in the void structure. Since it was not possible to agitate fresh pervious concrete underwater, without releasing the entrained air, it can be assumed that the higher values reported by the pressure and volumetric test methods contain both air caught in the large voids as well as entrained air in the mortar. Unless modifications are developed, the standard fresh air tests are not appropriate for pervious concrete.

The other two air tests involved testing mortar obtained through a vibrating screed. When properly tested on traditional concrete, only entrained air voids are measured. The CAI indicated that the small-sized RG mixture had slightly more entrained air. Due to the coarseness of the measurements, only 0.5 % precision was possible. Values obtained from the AVA are shown for both total measured air (<2 mm) and entrained air (<0.35 mm). Similar to the CAI results, the AVA indicated that the small-sized RG mixture contained more entrained air.

Results for the three AVA samples tested for each mixture are shown in Tables 5(a) and 5(b). AVA testing had low variability for total air and entrained air for either of the mixtures. The smaller mixture had higher entrained air and correspondingly a higher specific surface area (SSA) and better spacing factor (SpF) than the larger aggregate mixture. The smaller mixture had a SpF less than 0.2 mm suggested for freeze-thaw durability [18], while the larger aggregate mixture had a much higher SpF. Since pervious concrete has a smaller amount of free mortar than traditional concrete, about 40 kg (80 lb) of material was required to produce enough mortar for one sample. The low levels of entrained air (0.73–0.13 %) may indicate a loss of entrained air during the extensive vibrating during the mortar extraction sieving process.

TABLE 5(a)—AVA results for small RG mixture.

Sample	Air (%)		SSA (mm ⁻¹)	SpF (mm)
	<2 mm	<350 μ m		
Small RG #1	1.2	0.80	52.8	0.152
Small RG #2	1.2	0.80	51.9	0.159
Small RG #3	1.2	0.60	43.9	0.186
Average	1.20	0.73	49.53	0.17

Hardened Air Determination

Representative samples prepared for RapidAir testing are shown in Fig. 3 for both mixtures. Figure 3(c) and 3(d) shows the water-permeable voids in white and the aggregate and mortar stained black. These images are lacking a clear third phase typically observed in either air entrained typical or pervious concrete grey regions. The white color from fine entrained air systems combined with the black color produces visually a grey entrained air paste. Previous investigation on air entrainment of pervious concrete has distinguished three clear phases not present in either of the samples, indicating lower entrained air content [3].

Typical sample variability of the RapidAir testing is shown in Table 6 for a sample rotated 90° between trials. COVs for the repeatability of total void content, entrained air content, SpF, and SSAs were all less than 15 %. Entrained air/water-permeable void boundary was considered at 1 mm (Fig. 4). The average testing results and variability of all the samples are shown in Table 7. Total voids measured by the RapidAir include those less than 4 mm. Testing values for both sets of samples were similar. Total air was 10–12 % and entrained air was around 2.5 %. Since the entrained air determination by the RapidAir includes larger bubbles (up to 4 mm), it is expected that RapidAir values should be larger than those determined by the AVA where air is measured only up to 2 mm. SpF values ranged between 0.2 and 0.3 mm, which are slightly above the desired value of 0.2 mm for freeze-thaw durability [18].

The cumulative air content for both samples was similar with a clear increase in the water-permeable voids at greater than 1 mm, shown in Fig. 4. The

TABLE 5(b)—AVA results for large RG mixture.

Sample	Air (%)		SSA (mm ⁻¹)	SpF (mm)
	<2 mm	<350 μ m		
Large RG #1	0.50	0.20	34.00	0.342
Large RG #2	0.40	0.10	19.80	0.656
Large RG #3	0.30	0.10	31.00	0.477
Average	0.40	0.13	28.27	0.49

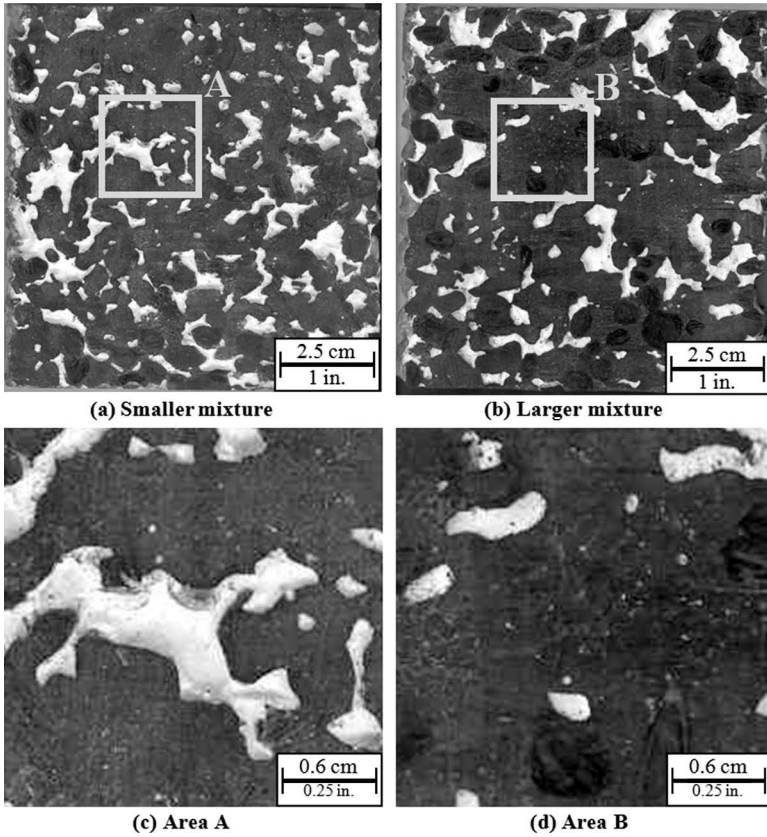


FIG. 3—Samples prepared for RapidAir testing.

TABLE 6—RapidAir variation for a typical sample.

Small RG #1	Total Air (<4 mm)			Entrained Air (<1 mm)		
	Air (%)	SpF (mm)	SSA (mm ⁻¹)	Air (%)	SpF (mm)	SSA (mm ⁻¹)
1 (0°)	11.73	0.331	5.19	1.96	0.290	22.13
2 (9°)	11.26	0.334	5.20	1.88	0.288	22.73
3 (180°)	11.66	0.286	6.04	2.34	0.266	22.32
4 (270°)	10.92	0.283	6.53	1.96	0.227	28.33
Average	11.39	0.309	5.74	2.04	0.268	23.88
Std. dev.	0.38	0.028	0.66	0.21	0.029	2.98
COV (%)	3.31	9.001	11.50	10.16	10.929	12.48

Note: SpF: Spacing factor. SSA: Specific surface area.

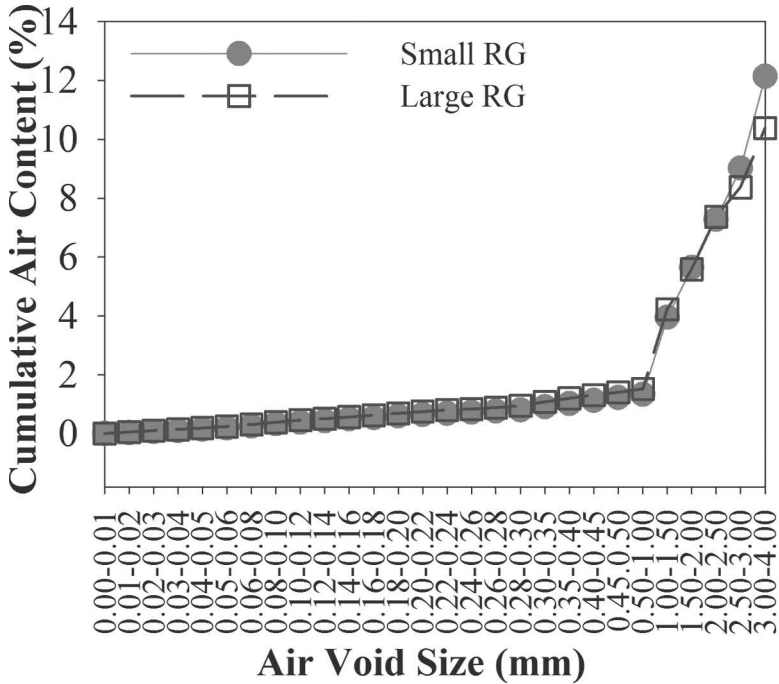


FIG. 4—Cumulative air content from RapidAir device.

air void distribution is shown in Fig. 5. Both mixtures followed a similar trend, with the only difference being double the number of 0.02–0.03 mm sized air bubbles occurring in the large-sized RG mixture.

Freeze-Thaw Durability

Samples tested for freeze-thaw durability were placed on-site and have the properties listed in Table 2. Durability of the concrete was judged using both a 60 % relative dynamic modulus and 85 % mass remaining criteria. Figure 6

TABLE 7—Hardened air results from the RapidAir device.

Mixture	Average of RA Analysis				Average of RA Analysis		
	Voids (%)	Total Air < 4 mm			Entrained Air < 1 mm		
		Air (%)	SpF (mm)	SSA (mm ⁻¹)	Air (%)	SpF (mm)	SSA (mm ⁻¹)
Small RG	23.00	12.13	0.279	6.08	2.41	0.256	23.28
COV (%)		6.4	11.6	12.2	5.7	8.1	11.7
Large RG	27.80	10.43	0.247	8.30	2.66	0.215	26.57
COV (%)		13.1	9.6	8.0	23.4	19.5	14.9

Note: SpF: Spacing factor, SSA: Specific surface area.

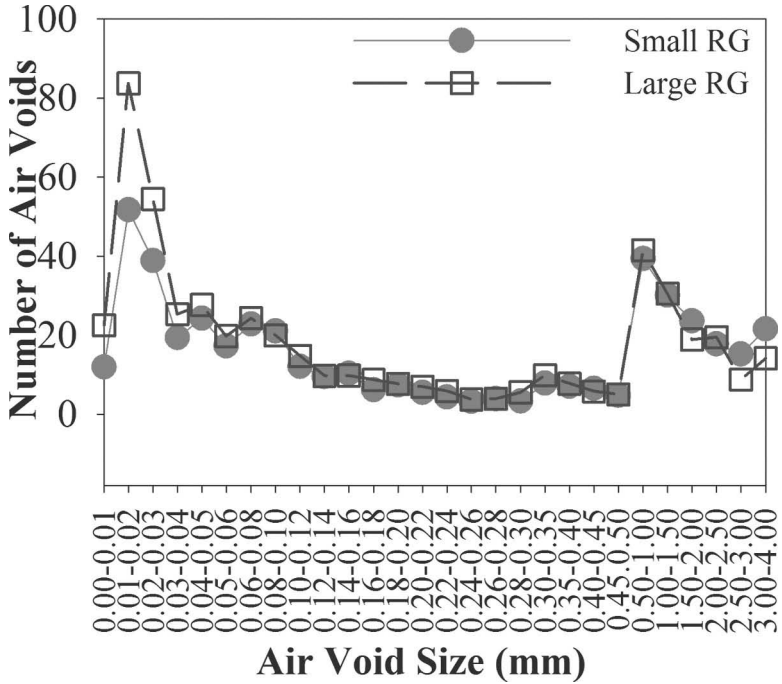


FIG. 5—Air void distribution from RapidAir device.

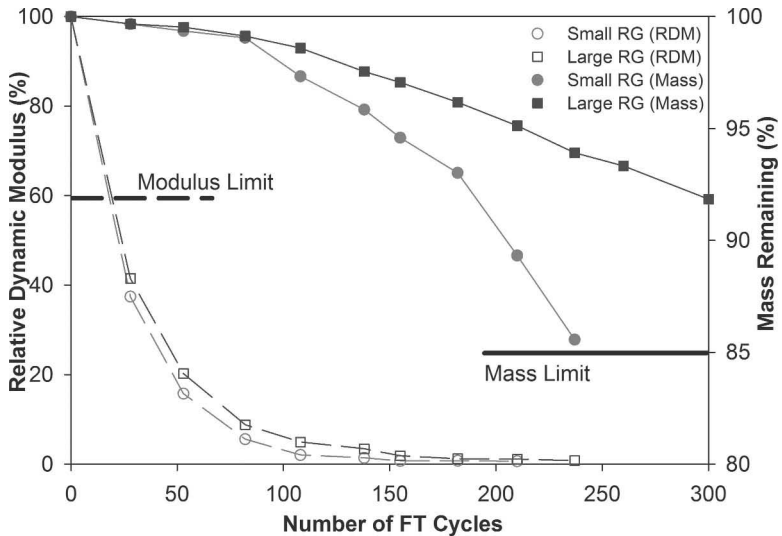


FIG. 6—Freeze-thaw durability results.

shows the freeze-thaw responses of both concrete mixtures. As seen in Fig. 6, freeze-thaw durability using relative dynamic modulus testing was poor with durability factors resulting from 60 % relative dynamic modulus measurements of four for both mixtures studied. When evaluated for durability using mass loss, both mixtures had similar response until 100 cycles. After 100 cycles the larger aggregate mixture had a better performance. Durability factors calculated based on 85 % mass remaining were 92 for the large-sized RG concrete and a 67 for the small-sized RG concrete. Samples before and after testing are shown in Fig. 7. The darker initial samples were saturated prior to testing, while the lighter post testing samples had dried.

It is noted from Table 5(a) and 5(b) that the average SpF measured from AVA was 0.17 mm for the small-sized RG mix and 0.49 mm for the large-sized RG mix, which contradicted to the freeze-thaw durability results. In the AVA test excessive vibration and excessive time required to obtain sufficient mortar samples may have affected the test results by lowering the air content. Differently, the RapidAir test results showed that both samples had SpF values greater than but near the 0.20 mm target value. Of the two, the large-sized RG concrete had a slightly higher number of small bubbles (0.02–0.03 mm; Fig. 5) and had a lower SpF of 0.21 mm.

Although some level of air entrainment was measured in the mortar, the samples generally had poor freeze-thaw durability, even though previous pervious concrete testing has shown air entrainment improves freeze-thaw durability [3]. However the mode of freeze-thaw deterioration was different than others observed in previous laboratory testing. The deterioration first began with mortar flaking from the outside aggregate particles followed by raveling of entire aggregate pieces. This suggests poor aggregate-to-mortar bonding most likely caused by unwanted fine dust on the surface of the relatively smooth RG aggregate. Poor mortar bonding would expedite freeze-thaw deterioration of the concrete, even though both the mortar and aggregate appeared durable.

To date the concrete at the ISU Lot 122 parking area had experienced three winters. Although the ASTM Standard C666 test results indicated that the freeze-thaw durability factors of the pervious concrete studied were very low, no freeze-thaw related durability distresses have been observed and the pavement is performing as designed. It has been well recognized that ASTM Standard C666 is a severe test for evaluating concrete freeze-thaw durability, particularly for pervious concrete, which may be rarely saturated any time. Long-term performance monitoring of the pervious concrete at the ISU Lot 122 is ongoing, and the results will be used to correlate properties obtained in the laboratory with actual future performance.

Conclusions and Recommendations

From this study the following conclusions can be drawn:

- (1) Of all test methods evaluated for characterizing air system of pervious concrete, the SpF determined by the RapidAir test co-related best with the freeze-thaw mass loss behavior.
- (2) Traditional pressure or volumetric air measurements appeared not ap-

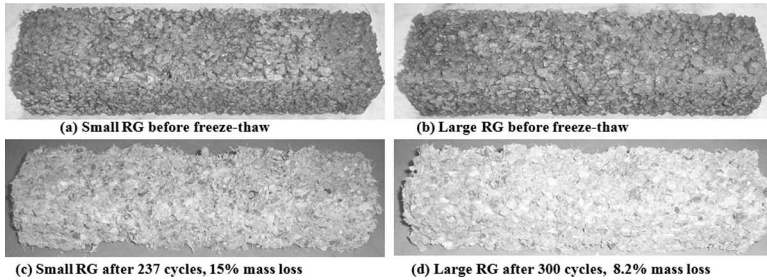


FIG. 7—Freeze-thaw durability samples before and after testing.

appropriate for characterizing air system of pervious concrete. They over predicted the air content due to the inability to remove all of the atmospheric air attached inside the water-permeable voids.

- (3) Excessive vibration and time were required for obtaining sufficient mortar samples for an AVA test. The test procedure seemed to have adverse effect on the test results. More studies are needed to further evaluate this test method.
- (4) Although the ASTM Standard C666 test results indicated that the freeze-thaw durability factors of the pervious concrete studied were very low, no freeze-thaw related durability distresses have been observed after 3 years of service, and the pavement is performing as designed. The ASTM Standard C666 freeze-thaw test method is an overly severe test, a more realistic test may be required to related pervious concrete freeze-thaw durability in the laboratory with that experienced in the field.
- (5) These findings suggest that current criteria and test methods for air content and air void systems do not apply with any reliability to pervious concrete. Some of the conventional test methods may be used with modification; however more research is needed to determine appropriate acceptance criteria for pervious concrete.

Acknowledgments

This study was funded by the Iowa Department of Natural Resources, the Iowa Ready Mixed and Concrete Paving Associations, and the National Concrete Pavement Technology Center at ISU. The assistance provided by Steve Jones installing the sensors and soil testing performed by Heath Gieselmann, Mark Thompson, and Muhannad Suleiman is greatly appreciated. The opinions, findings, and conclusions presented here are those of the writers and do not necessarily reflect those of the research sponsors.

References

- [1] Kosmatka, S. H., Kerkhoff, B., and Panarese, W. C., *Design and Control of Concrete*

- Mixtures, EB001*, Portland Cement Association, Skokie, IL, 2002.
- [2] ASTM Standard C1688, 2008, "Standard Test Method for Density and Void Content of Freshly Mixed Pervious Concrete," *Annual Book of ASTM Standards*, Vol. 04.02, ASTM International, West Conshohocken, PA.
 - [3] Kevern, J. T., Wang, K., and Schaefer, V. R., "A Novel Approach to Characterize Entrained Air Content in Pervious Concrete," *J. ASTM Int.*, Vol. 5, No. 2, 2008, Paper ID JAI101434.
 - [4] ASTM Standard C192, 2003, "Standard Practice for Making and Curing Concrete Test Specimens in the Laboratory," *Annual Book of ASTM Standards*, Vol. 04.02, ASTM International, West Conshohocken, PA.
 - [5] ASTM Standard C617, 2003, "Standard Practice for Capping Cylindrical Concrete Specimens," *Annual Book of ASTM Standards*, Vol. 04.02, ASTM International, West Conshohocken, PA.
 - [6] *User's Manual RapidAir 457* (2002), Concrete Experts International, Vedbæk, Denmark, www.concrete-experts.com (Last accessed date 9 Sept. 2009).
 - [7] ASTM Standard C39, 2003, "Standard Test Method for Compressive Strength of Cylindrical Concrete Specimens," *Annual Book of ASTM Standards*, Vol. 04.02, ASTM International, West Conshohocken, PA.
 - [8] ASTM Standard C496, 2003, "Standard Test Method for Splitting Tensile Strength of Cylindrical Concrete Specimens," *Annual Book of ASTM Standards*, Vol. 04.02, ASTM International, West Conshohocken, PA.
 - [9] ASTM Standard C78, 2003, "Standard Test Method for Flexural Strength of Concrete (Using Simple Beam with Third point Loading)," *Annual Book of ASTM Standards*, Vol. 04.02, ASTM International, West Conshohocken, PA.
 - [10] Montes, F., Valavala, S., and Haselbach, L. M., "A New Test Method for Porosity Measurements of Portland Cement Pervious Concrete," *J. ASTM Int.*, Vol. 2, No. 1, 2005, Paper ID JAI12931.
 - [11] "American Concrete Institute (ACI) Pervious Concrete," *Committee Report ACI 522*, ACI, Farmington Hills, MI, 2006.
 - [12] ASTM Standard C666, 2003, "Standard Test Method for Resistance of Concrete to Rapid Freezing and Thawing," *Annual Book of ASTM Standards*, Vol. 04.02, ASTM International, West Conshohocken, PA.
 - [13] Schaefer, V. R., Wang, K., Sulieman, M. T., and Kevern, J., "Mix Design Development for Pervious Concrete in Cold Weather Climates," *A Report from the National Concrete Pavement Technology Center (CP Tech Center), Report No. 1*, Iowa State University, Ames, IA, 2006, http://www.ctre.iastate.edu/reports/mix_design_pervious.pdf (9 Sept. 2009).
 - [14] Kevern, J. T., 2006, "Mix Design Determination for Freeze-Thaw Resistant Portland Cement Pervious Concrete," M.S. thesis, Iowa State University, Ames, IA.
 - [15] ASTM Standard C231, 2004, "Standard Test Method for Air Content of Freshly Mixed Concrete by the Pressure Method," *Annual Book of ASTM Standards*, Vol. 04.02, ASTM International, West Conshohocken, PA.
 - [16] ASTM Standard C173, 2007, "Standard Test Method for Air Content of Freshly Mixed Concrete by the Volumetric Method," *Annual Book of ASTM Standards*, Vol. 04.02, ASTM International, West Conshohocken, PA.
 - [17] AASHTO T199-00, 2003, "Air Content of Freshly Mixed Concrete by the Chace Indicator—Standard Specifications for Transportation Materials and Methods of Sampling and Testing, V. 2A," American Association of State Highway and Transportation Officials, Washington, D.C.
 - [18] Taylor, P., Kosmatka, S., and Voigt, G., "Integrated Materials and Construction Practices for Concrete Pavement: A State-of-the-Practice Manual," *A Report from*

the National Concrete Pavement Technology Center and Federal Highway Administration (FHWA Publication No. HIF-07-004), Iowa State University, Ames, IA, 2006, www.cptechcenter.org/publications/imcp/ (Last accessed date 9 Sept. 2009).

- [19] ASTM Standard C457, 1998, "Standard Test Method for Microscopical Determination of Parameters of the Air-Void System in Hardened Concrete," *Annual Book of ASTM Standards*, Vol. 04.02, ASTM International, West Conshohocken, PA.
- [20] Jakobsen, U. H., Pade, C., Thaulow, N., Brown, D., Sahu, S., Magnusson, O., De Buck, S., and De Schutter, G., "Automated Air Void Analysis of Hardened Concrete—A Round Robin Study," *Cem. Concr. Res.*, Vol. 36, 2006, pp. 1444–1452.
- [21] Kevern, J. T., Wang, K., and Schaefer, V. R., *The Effect of Coarse Aggregate on the Freeze-Thaw Durability of Pervious Concrete*, SN3063, Portland Cement Association, Skokie, IL, 2008, 41 pages.

Gilson Lomboy¹ and Kejin Wang²

Effects of Strength, Permeability, and Air Void Parameters on Freezing-Thawing Resistance of Concrete with and without Air Entrainment

ABSTRACT: The present research is aimed at investigating effects of concrete properties, particularly concrete rapid chloride permeability, strength, and air void parameters, on freezing-thawing (FT) resistance. In this study, concrete mixtures are made with different types of cement (Types I with 15 % class C fly ash and Type IP cements), different water-to-binder ratios ($w/b = 0.25, 0.35, 0.45, \text{ and } 0.55$), and with or without air entraining agent. The 28-day compressive strength, rapid chloride permeability, and FT durability of the concrete are determined according to ASTM C873, C1202, and C666A, respectively. The air void parameters of the concrete are measured with air void analyzer, Rapid Air, and porosity (ASTM C642) tests. The results indicate that although concrete made with a low w/b (≤ 0.35) has low rapid chloride permeability (≤ 1320 C), it generally still requires proper air entrainment for a desirable FT resistance (with a durability factor of $\geq 85\%$), except for the concrete having very low rapid chloride permeability (520 C) and very high 28-day compressive strength (88 MPa or 12 760 psi). For the non-air-entrained concrete studied, there are clear relationships between FT durability and porosity, w/b , and permeability. However, such relationships do not exist for air-entrained concrete. The FT resistance of air-entrained concrete is largely dependent on the concrete air void characteristics.

KEYWORDS: freeze-thaw durability, permeability, strength, air void, porosity

Manuscript received April 2, 2009; accepted for publication August 28, 2009; published online September 2009.

¹ Dept. of Civil, Construction, and Environmental Engineering, Iowa State Univ., Ames, IA 50011-3232.

² Dept. of Civil, Construction, and Environmental Engineering, Iowa State Univ., Ames, IA 50011-3232 (Corresponding author), e-mail: kejinw@iastate.edu

Cite as: Lomboy, G. and Wang, K., "Effects of Strength, Permeability, and Air Void Parameters on Freezing-Thawing Resistance of Concrete with and without Air Entrainment," *J. ASTM Intl.*, Vol. 6, No. 10. doi:10.1520/JAI102454.

Copyright © 2009 by ASTM International, 100 Barr Harbor Drive, PO Box C700, West Conshohocken, PA 19428-2959.

Introduction

In cold climate regions, many concrete pavement deteriorations are associated with cyclic freezing and thawing (FT) and repeated applications of deicing chemicals. The FT damages generally result from the volume change due to ice formation and water migration, which generate hydraulic and osmotic pressures, in concrete [1,2]. Proper air entrainment is therefore essential for the concrete because well-distributed micro-air bubbles can cut the water paths and provide additional spaces for ice, thus reducing the hydraulic and osmotic pressures [3,4].

Researchers and engineers have noted that a precondition for concrete to have FT damage is the existence of freezable water in the concrete. Generally, concrete becomes vulnerable to FT damage when it reaches a critical saturation condition [5]. This later becomes a base for argument for whether or not very low permeability concrete or high strength concrete (HSC) needs air entrainment.

Modern concrete has much lower permeability than the concrete made a few decades ago due to the increasing use of lower water-to-binder ratios (w/b) and larger amounts of supplementary cementitious materials. Because of its very low permeability, little water can penetrate into the concrete, and the concrete rarely reaches its critical saturation condition. Consequently, no significant FT damage would take place. From the microstructure point of view, HSC contains mostly very fine pores. Due to surface tension, the water in these fine pores is very difficult to freeze, and therefore, HSC is less susceptible to FT damage.

Pigeon et al. [6] tested FT durability of 17 concrete mixtures with low w/b and analyzed effects of various factors (type of cement, aggregate, and curing period). They reported that the w/b limit below which air entraining agent (AEA) would not be required for good FT durability was 0.25 (or 0.30 in certain cases). However, Cohen et al. [7] showed that the strength of HSC reduced with an increase in FT cycles, which indicated that air entrainment might be necessary. Bassuoni and Nehdi [8] also pointed out that non-air-entrained low w/b concrete could be vulnerable to FT, and such vulnerability might not be detected using classical frost durability tests. Currently, in Norway, air entrainment is not required for low w/b concrete, while in Canada, air entrainment is required regardless of w/b [9]. More research is necessary on this subject to provide proper guidelines for designing and constructing durable concrete.

The emphasis of the present research is on the study of effects of concrete properties (such as strength, rapid chloride permeability, porosity, and air void parameters) on the FT resistance of low permeability concrete. It is also to find out whether or not a permeability value exists, below which AEA is not necessary for concrete to have good FT durability.

Experimental Program

The concrete mixtures studied were made with different types of cements (Types I with 15 % class C fly ash and Type IP cements), different w/b (0.25, 0.35, 0.45, and 0.55), and with or without AEA. All concrete mixtures were

TABLE 1—Chemical compositions of cementitious materials.

	Na ₂ O	MgO	Al ₂ O ₃	SiO ₂	SO ₃	K ₂ O	CaO	Fe ₂ O ₃	LOI
Type I	0.15	3.34	4.17	20.20	2.47	0.69	63.20	2.96	2.37
Type IP	0.29	2.87	8.51	30.10	3.38	0.70	48.50	3.17	1.60
C-fly ash	1.64	4.87	17.68	31.92	1.68	0.43	30.92	6.54	0.47

controlled to have a similar slump by using different dosages of high range water reducing (HRWR) agent. The rapid chloride permeability and FT durability of the concrete were determined according to ASTM C1202 [10] and ASTM C666A [11], respectively. The air void parameters of the concrete were studied with the air void analyzer (AVA), Rapid Air, and porosity tests (ASTM C642 [12]).

Materials

The cementitious materials used in the study were types I and IP cements and class C fly ash. The type IP cement contained 25 % class F fly ash. The chemical composition and compounds of these cementitious materials are listed in Table 1.

The FT durable limestone was used as coarse aggregate, and it had a nominal maximum size of 25 mm (1 in.). The fine aggregate was river sand. The gradation and properties of the aggregates are shown in Table 2.

Two groups of concrete mixtures were studied: one was made with 85 % Type I cement and 15 % class C fly ash (referred here as I-FA) and the other was made with 100 % Type IP cement as a binder (referred here as IP). Each group had four mixtures with different *w/b* (*w/b*=0.25, 0.35, 0.45, and 0.55). A polycarboxylate-based HRWR was used for mix slump adjustment. The dosage

TABLE 2—Gradation and properties of aggregates.

Sieve Size	% Passing (By Mass)	
	Limestone, NMSA=25 mm (1 in.)	River Sand (FM=3.16)
25 mm (1 in.)	100.00	...
19 mm (3/4 in.)	85.85	...
12.5 mm (1/2 in.)	45.87	...
9.5 mm (3/8 in.)	26.97	100.00
4.75 mm (No. 4)	3.46	97.96
2.36 mm (No. 8)	1.04	84.84
1.18 mm (No. 16)	...	63.06
600 μm (No. 30)	...	31.04
300 μm (No. 50)	...	6.48
150 μm (No. 100)	...	0.44
Specific gravity	2.66	2.61
Absorption, %	0.72	1.09

of the HRWR used ranged from 365 to 1595 mL per 100 kg of cementitious (5.6–24.5 oz per 100 lbs cementitious); the latter of which doubled the recommended dosage. Table 3 provides the proportions of all concrete mixtures studied.

Sample Preparation and Test Methods

All concrete mixtures were mixed according to ASTM C192 [13]. Nine $100 \times 200 \text{ mm}^2$ ($4 \times 8 \text{ in.}^2$) cylinder samples were prepared from each mixture for compressive strength (three samples), rapid chloride permeability (three samples), porosity (two samples), and Rapid Air (one sample) tests. Three $75 \times 100 \times 400 \text{ mm}^3$ ($3 \times 4 \times 16 \text{ in.}^3$) molded beam samples from each mixture were prepared for FT tests. All samples were moist cured for 28 days before testing.

For fresh concrete, slump, air content, and unit weight of all concrete mixtures were measured according to ASTM C143 [14], C231 [15], and C138 [16], respectively. The air void parameters were determined by AVA. (Two samples were tested per mixture.) The AVA test was performed according to the test method outlined by Taylor et al. [17] In the test, a mortar sample (approximate 20 mL) was extracted from the tested fresh concrete using a vibrating cage and a syringe. The extracted mortar was injected into a cylinder containing a glycerol solution with a given viscosity. To start a test, a motor in the AVA device was turned on and stirred the mortar sample. The air bubbles in the mortar were then released by the stirring condition. Depending on their size, these air bubbles rose at different speeds through the glycerol solution to reach the buoyancy recorder at the top of the cylinder. The buoyancy recorder recorded the change in buoyancy over time. Based on the recorded data, a computer program finally calculated air content, spacing factor (SF), and specific surface (SS) of the tested sample.

For hardened concrete, 28-day compressive strength, rapid chloride permeability, and porosity tests were conducted for all concrete mixtures according to ASTM C39 [18], C1202 [10], and C642 [12], respectively. The FT resistances of the concrete mixtures were evaluated according to ASTM C666A [11]. Air void parameters of the concrete were examined using a Rapid Air test device. The Rapid Air test device automatically analyzes the air void parameters in hardened concrete according to ASTM C457 [19,20]. To measure the air void parameters of the concrete, $100 \times 100 \times 10 \text{ mm}^3$ ($4 \times 4 \times 3/8 \text{ in.}^2$) samples were cut from the center of $100 \times 200 \text{ mm}^2$ ($4 \times 8 \text{ in.}^2$) cylinders. The samples were then polished according to ASTM C457 [20]. After having a flat and smooth sample, it was coated with a thin film of black dye and let dry and heated to about 50°C . Then, a zinc oxide paste (white in color) was rubbed into the concrete to fill all air voids on the sample surface. After the sample cooled down, the extra zinc oxide was scrapped off using a blade, leaving only the zinc oxide in air voids. The aggregate faces were then colored black; as a result, the sample showed a black concrete surface with white air voids. Using a microscope and a computer program, the Rapid Air device identified white spots (air voids) and provided information on the air void content, SF, and SS of the

TABLE 3—Concrete mix proportions.

Binder	Mix ID	Mix Design, kg/m ³ (pcy)							w/c
		Cement	Fly Ash	Water	Fine Aggregate	Coarse Aggregate	AEA, ml/m ³ (oz/cy)	HRWR, ml/m ³ (oz/cy)	
I-FA	I-FA55	296 (498)	52 (88)	191 (322)	836 (1408)	1018 (1714)	222 (5.7)	0	0.55
	I-FA45	306 (516)	54 (91)	162 (273)	866 (1458)	1055 (1776)	230 (6.0)	1316 (34)	0.45
	I-FA35	318 (535)	56 (94)	131 (220)	899 (1513)	1094 (1842)	239 (6.2)	2514 (65)	0.35
	I-FA25	330 (556)	58 (98)	97 (163)	934 (1572)	1137 (1914)	248 (6.4)	6190 (160)	0.25
IP	IP55	348 (585)	0	191 (322)	839 (1412)	1023 (1723)	222 (5.7)	0	0.55
	IP45	360 (607)	0	162 (273)	869 (1463)	1060 (1785)	230 (6.0)	1316 (34)	0.45
mix.	IP35	374 (629)	0	131 (220)	901 (1517)	1100 (1851)	270 (7.0)	2514 (65)	0.35
	IP25	388 (654)	0	97 (163)	936 (1576)	1143 (1923)	330 (8.5)	6190 (160)	0.25

Note: In Mix ID, the letters denote the type of cementitious materials used and the numbers correspond to the w/b used in the given

TABLE 4—Properties of fresh and hardened concrete.

	Fresh Concrete Properties			Hardened Concrete Properties			
	Slump, mm (in.)	Air, % (C231)	Unit Weight, kg/m ³ (pcf)	f_{c28} , MPa (psi)	RCP, C	Porosity, %	DF (%)
Concrete without AEA							
I-FA55	181.2(7.25)	1.5	2284 (142.4)	46.4 (6730)	4300	5.6	5.0
I-FA45	187.5(7.50)	1.8	2262 (141.0)	54.4 (7890)	3220	6.6	8.8
I-FA35	162.5(6.50)	2.2	2306 (143.8)	58.6 (8500)	960	5.5	18.9
I-FA25	150.0(6.00)	2.8	2318 (144.5)	61.0 (8850)	480	4.3	38.9
IP55	175.0(7.00)	1.5	2310 (144.0)	43.6 (6320)	2080	13.0	3.7
IP45	168.8(6.75)	2.5	2278 (142.0)	51.8 (7510)	1720	10.5	10.3
IP35	162.5(6.50)	2.2	2374 (148.0)	54.1 (7840)	1320	8.1	29.6
IP25	200.0(8.00)	1.5	2518 (157.0)	88.0(12760)	520	5.0	94.3
Concrete with AEA							
I-FA55-AEA	193.8(7.75)	7.8	2278 (142.0)	42.4 (6150)	5090	12.7	93.0
I-FA45-AEA	187.5(7.50)	7.0	2270 (141.5)	47.4 (6870)	3920	9.9	95.0
I-FA35-AEA	175.0(7.00)	8.0	2302 (143.5)	52.2 (7570)	1160	11.0	93.7
I-FA25-AEA	175.0(7.00)	8.2	2326 (145.0)	55.5 (8050)	660	10.1	94.7
IP55-AEA	200.0(8.00)	6.0	2276 (141.9)	31.3 (4540)	1290	13.3	92.2
IP45-AEA	200.0(8.00)	8.0	2278 (142.0)	39.3 (5690)	1290	11.9	86.7
IP35-AEA	200.0(8.00)	7.0	2318 (144.5)	49.3 (7150)	1070	11.0	95.8
IP25-AEA	187.5(7.50)	7.5	2400 (149.6)	57.5 (8330)	350	9.4	95.2

tested sample. A threshold setting of 170 was used to achieve the best distinction of the actual air voids in concrete from the black background [19].

Results and Discussions

Fresh Concrete Properties

Table 4 presents slump, unit weight, and air content of all fresh concrete mixtures studied. It can be seen from the table that the slumps of the mixtures with $w/b=0.55$ (with and without AEA) was 175–200 mm (7–8 in.). The slumps of other mixtures ($w/b=0.45$, 0.35, and 0.25) were adjusted to reach 175 ± 25 mm (7 ± 1 in.) by adding different dosages of HRWR. For mixtures made with the same w/b and the same amount of HRWR, the slump of the mixtures made with IP cement was higher than the corresponding mixtures made with I-FA binder.

The air content measured with a pressure meter (ASTM C231 [15]) was 1.5–2.8 % for concrete without AEA, while it was 6.0–8.2 % for concrete with AEA. The same amount of AEA was used for all mixtures made with I-FA binder to achieve the target air content (6–8 %). However, for the concrete made with IP cement, as w/b decreased, an increased AEA amount was required for the concrete to reach the target air content (6–8 %).

The unit weight of concrete mixtures generally ranged from 2260 to 2325 kg/m³ (141–145 pcf), but a few mixtures made with IP cement had higher unit weight. The concrete made with IP cement and w/b of 0.25 had the highest unit weight, 2518 kg/m³ (157 pcf).

Air Void Parameters of Fresh Concrete Measured by Air Void Analyzer

Table 5 summarizes the air content, SF, and SS of the fresh concrete mixtures studied. It should be noted that the AVA device measures only the air voids with a size equal or less than 2 mm. In air-entrained concrete, when the total air is used as a measure of frost resistance, it is assumed that the air is mostly small air bubbles [21]. At 6 ± 1 % total air content, most of the air voids should be 0.3–0.1 mm to achieve a $SF \leq 0.2$ mm and be effective for freeze-thaw resistance [22]. Therefore, both the total air (≤ 2 mm) and small air (≤ 300 μm) content measurements are presented in the tables. As seen in Table 5, the total air content measured by AVA ranged from 0.2 % to 2.4 % for concrete without AEA and ranged from 2.8 % to 9.3 % for concrete with AEA. Since AVA measures only air voids with size equal or less than 2 mm, the total air content measured by AVA is generally less than that measured by the ASTM C231 tests [15,23]. It is not clear at this moment why some mixtures in the present study had higher AVA total air content.

Previous research indicated that concrete would be FT durable if its air void parameters are $SF \leq 0.2$ mm and $SS \geq 24$ mm²/mm³, measured based on the ASTM C457 test method [20,24]. Recent research has suggested that concrete with $SF \leq 0.3$ mm measured from AVA tests is also acceptable [23]. In Table 5, only the concrete mixtures with AEA had AVA $SF \leq 0.3$, and this suggests that the concrete without AEA might not be FT durable. As discussed later, this inference was generally approved by FT test results with only one exception.

Figure 1 illustrates the relationship between SF and the content of small air voids (≤ 300 μm) measured by AVA. It shows that SF decreased with the content of the small air voids. The correlation coefficient of this relationship (R^2) is 0.96. When the total AVA air content is considered, a similar relationship still exists, but its R^2 value reduced to 0.83.

Hardened Concrete Properties

Table 4 presents the hardened concrete properties, including 28-day compressive strength, rapid chloride permeability, and porosity. Figure 2 demonstrates the relationships between these concrete properties. The following observations can be made from Table 4 and Fig. 2.

- (1) The concrete strength decreased, but rapid chloride permeability and porosity increased with increased w/b . When w/b increased higher than 0.35, the concrete permeability and porosity increased more rapidly (Fig. 2(b) and 2(c)).
- (2) Concrete with AEA had slightly lower strength but much higher porosity than that without AEA.
- (3) Concrete with AEA had much higher porosity but not much higher

TABLE 5—Air void parameters from AVA and Rapid Air tests.

	From AVA				From Rapid Air				
	Total Air % (size ≤ 2 mm)	Small Air, % (size ≤ 300 μm)	SS, mm ⁻¹	SF, mm	Total Air % (size ≤ 2 mm)	Small Air, % (size ≤ 300 μm)	SS, mm ⁻¹	SF, mm	DF (%)
Concrete without AEA									
I-FA55	0.3	0.06	16.9	1.07	1.5	0.39	18.4	0.50	5.0
I-FA45	1.8	0.07	6.2	1.36	1.6	0.43	17.7	0.49	8.8
I-FA35	0.8	0.10	10.3	1.11	4.1	0.63	9.6	0.58	18.9
I-FA25	1.0	0.05	9.5	1.02	3.0	1.13	20.9	0.29	38.9
IP55	0.2	0.05	14.0	1.43	0.4	0.16	21.3	0.81	3.7
IP45	0.5	0.00	7.6	1.86	1.3	0.29	13.6	0.76	10.3
IP35	2.4	0.80	18.9	0.37	2.7	0.97	20.7	0.34	29.6
IP25	1.5	0.08	8.1	1.03	1.5	0.24	10.5	0.83	94.3
Concrete with AEA									
I-FA55-AEA	5.9	2.47	21.5	0.24	5.3	3.02	25.8	0.21	93.0
I-FA45-AEA	9.3	4.50	25.4	0.14	8.2	3.63	21.4	0.19	95.0
I-FA35-AEA	8.0	4.43	31.0	0.13	7.0	2.85	22.1	0.20	93.7
I-FA25-AEA	7.7	1.96	17.2	0.20	6.7	2.15	19.0	0.22	94.7
IP55-AEA	2.8	1.44	26.1	0.28	6.7	3.00	22.6	0.22	92.2
IP45-AEA	8.2	4.55	31.0	0.13	9.1	5.26	27.6	0.14	86.7
IP35-AEA	5.6	1.62	17.3	0.28	6.2	3.13	24.2	0.19	95.8
IP25-AEA	9.3	6.54	28.4	0.10	7.1	3.84	28.1	0.14	95.2

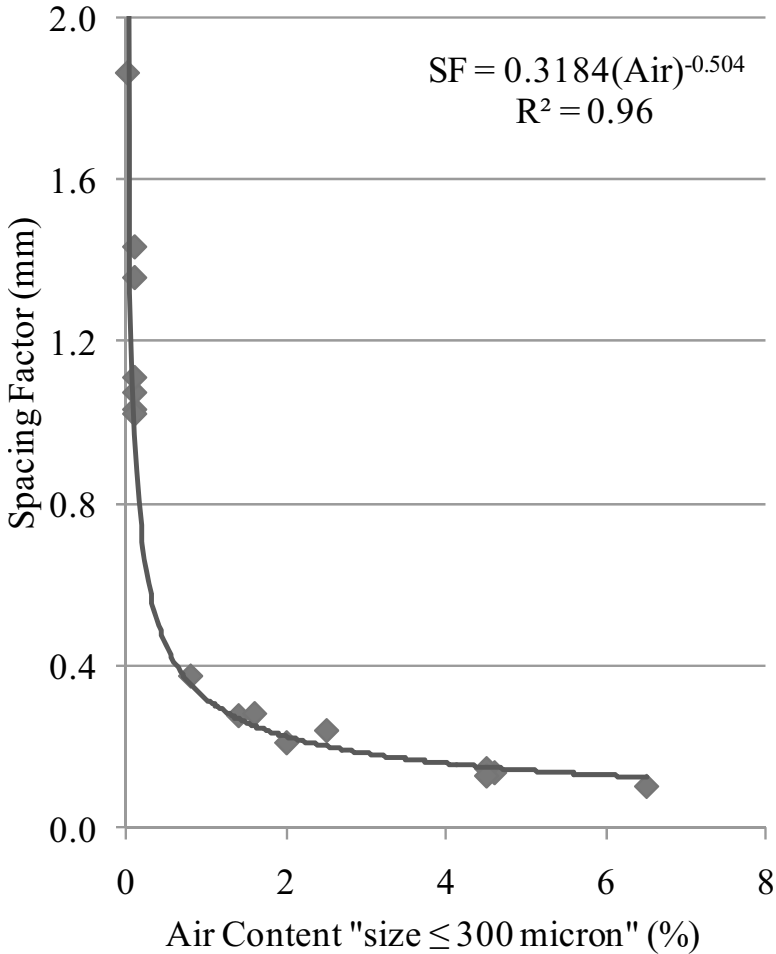


FIG. 1—Relationships between SF and content of small air voids measured by AVA.

rapid chloride permeability than concrete without AEA (Fig. 2(d)). In other words, some concrete had a relative low value of rapid chloride permeability but a relative high value of porosity.

- (4) There was no clear relationship between concrete strength and rapid chloride permeability.
- (5) In addition to having the highest unit weight, concrete made with IP cement, *w/b* of 0.25, without AEA (IP25) had the highest strength (88 MPa or 12 760 psi) and the lowest porosity (5 %) among all mixtures. Such properties significantly influence the concrete FT resistance.

Air Void Parameters of Hardened Concrete Measured by Rapid Air

Table 5 summarizes the air content, SF, and SS of the hardened concrete samples studied. Different from AVA device, the Rapid Air equipment measured

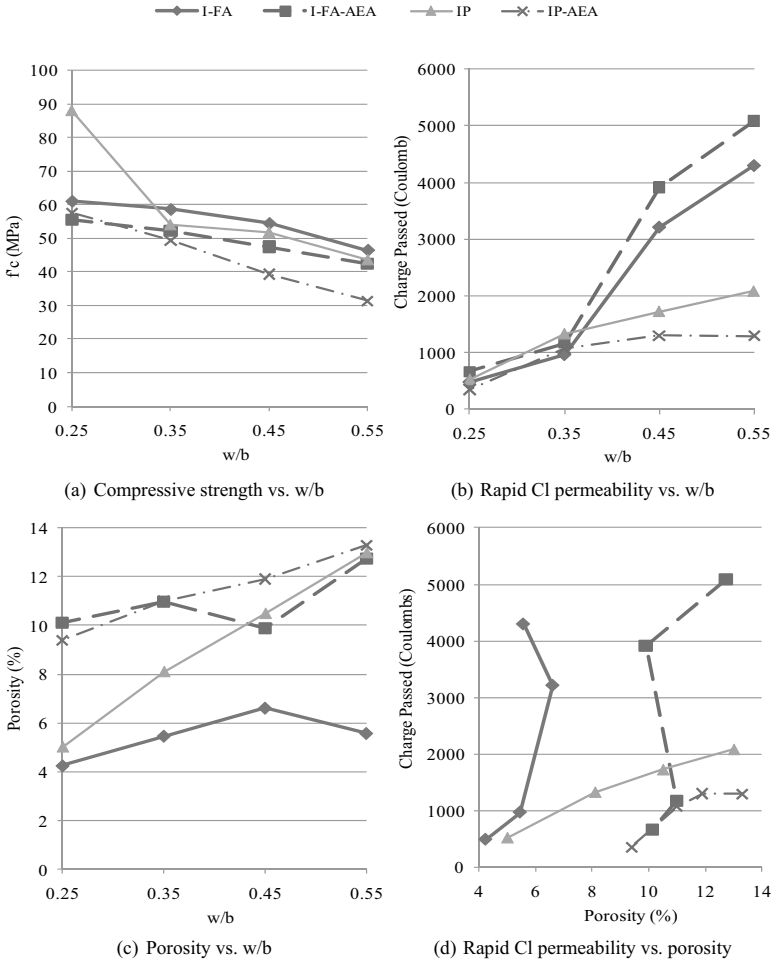


FIG. 2—Relationship between hardened concrete properties.

all voids observed under an optical microscope. The total air content measured by Rapid Air ranged from 0.4 % to 4.1 % for the concrete without AEA, and it ranged from 5.3 % to 9.1 % for the concrete with AEA.

Figure 3 illustrates the relationships between the air void parameters measured by Rapid Air; the trends of which are the same as those in Fig. 1.

Figure 4 shows that certain relationships did exist between Rapid Air and AVA measurements. Based on the present test data, the total air content and SS measured by the Rapid Air test method were noticeably higher than those measured by the AVA test method. The contents of small air voids ($\leq 300 \mu\text{m}$) measured by the both test methods were comparable. The SF measured by the Rapid Air test method was much lower than that measured by the AVA test method.

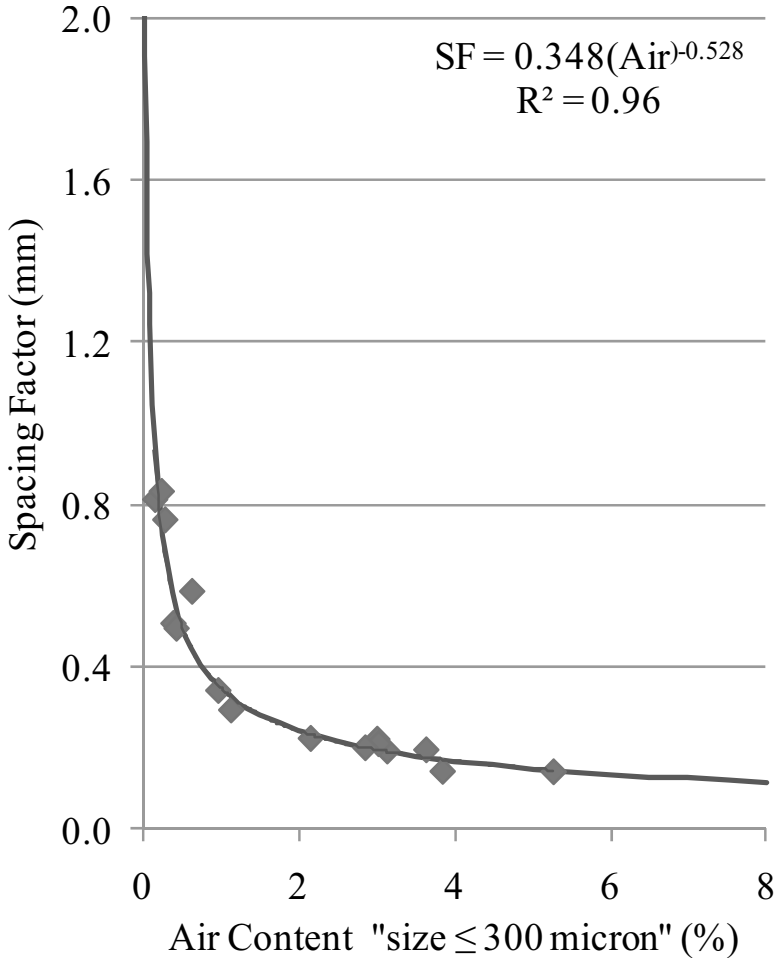


FIG. 3—Relationships between SF and content of small air voids measured by Rapid Air.

FT Durability

Based on ASTM C666A [11], the relative dynamic modulus of elasticity (RDME) and FT durability factor (DF) of tested concrete mixtures are reported in Figs. 5 and 6. A high RDME and DF value indicate a better FT resistance. For concrete without AEA, Fig. 5(a) illustrates that at a given FT cycle, RDME decreased with increased w/b . Generally, the concrete made with IP cement had better FT resistance than the corresponding concrete made with I-FA binder. All concrete mixtures without AEA had a RDME of less than 40 % at 300 FT cycles, except for the mix made with IP cement and with w/b of 0.25 (mix IP25), whose RDME was 94.3 % at 300 FT cycles. In the present study, a RDME of 85 % at 300 cycles was considered to be associated with adequate freeze-thaw resis-

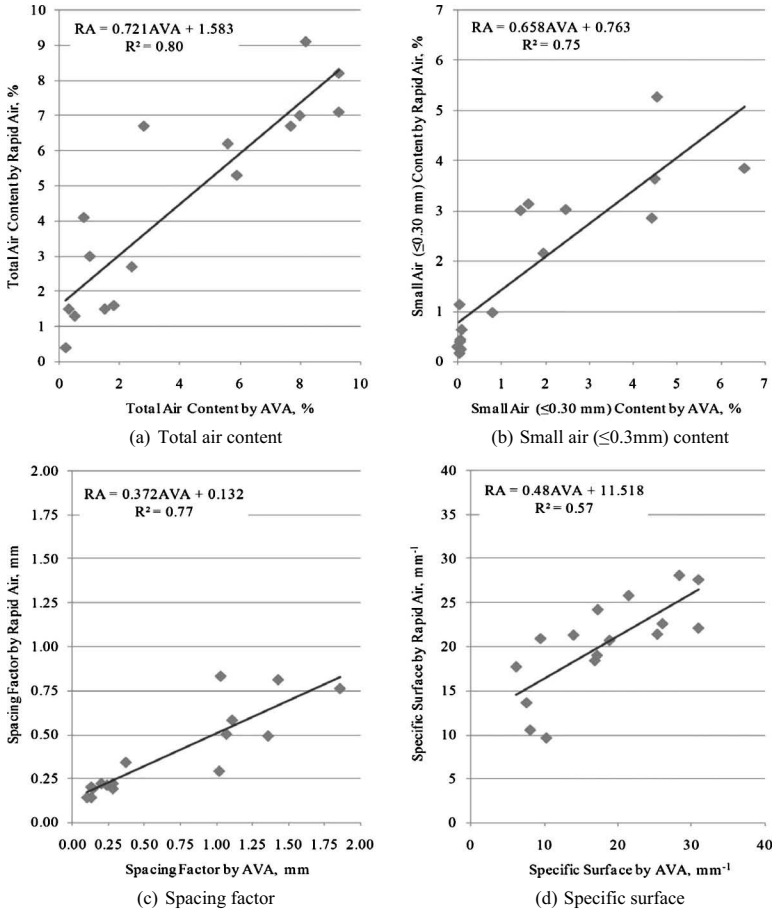


FIG. 4—Relationships between Rapid Air and AVA measurements.

tance [23]. The present FT test results implied that concrete without AEA may not be FT durable even if its rapid chloride permeability value was lower than 1000 C. However, exception could be made for the concrete having very low rapid chloride permeability and very high strength (such as mix IP25, which had a rapid chloride permeability value of 570 C, porosity of 5 %, and 28-day compressive strength of 88 MPa (12 760 psi)). Figures 5(b) and 6 indicate that the DF values of concrete with AEA were all higher than 90 %, except that mix IP45-AEA had a DF value of 86.7 %, and they are all considered as FT durable.

Effects of Concrete Properties on Freezing-Thawing Durability

There are many factors affecting FT durability of concrete, such as the amount and structure of air voids, permeability or porosity of concrete, FT durability of aggregates, concrete strength, and surface condition. In the following sections,

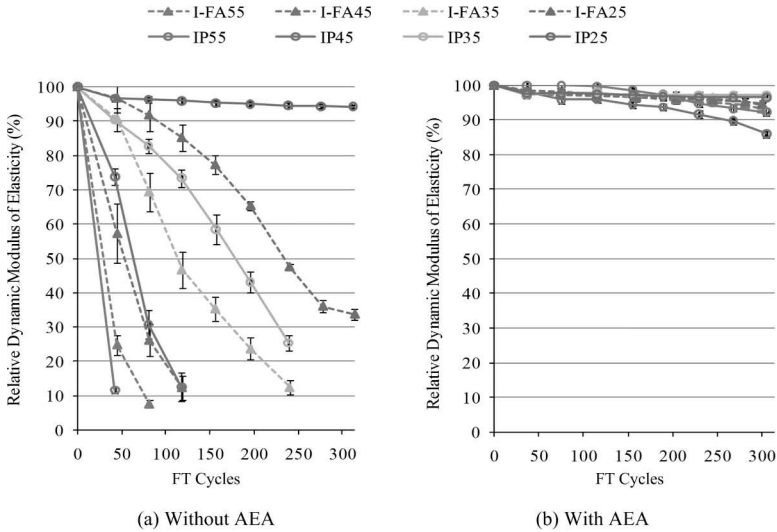


FIG. 5—Relative dynamic modulus of concrete subjected to FT cycles.

the effects of rapid chloride permeability, porosity, strength, and air void parameters on the FT durability of concrete are discussed based on the results from the present study.

Effect of Concrete Permeability and Porosity on Freezing-Thawing Durability

Figure 7 illustrates the relationships between concrete FT durability and rapid chloride permeability/porosity on FT durability. These relationships were clearly shown by the concrete made with given cementitious materials without AEA; however, they did not exist for the concrete with AEA.

As observed in Fig. 7, DF of concrete without AEA decreased with increased rapid chloride permeability and porosity. A simple explanation for this is that a more permeable and porous concrete might permit more freezable water to get into the concrete, have a higher degree of saturation under the FT test condition, and result in more severe FT damage. Based on the present test results, the relationships between DF and rapid chloride permeability or porosity can be expressed by Eqs 1 and 2, respectively

$$DF_{I-FA} = 7531.8k^{-0.86} \quad \text{and} \quad DF_{IP} = 4.0e7k^{-2.06} \tag{1}$$

$$DF_{I-FA} = 5158.9n^{-3.35} \quad \text{and} \quad DF_{IP} = 13120n^{-3.09} \tag{2}$$

where:

- subscripts I-FA and IP denote the cementitious materials (types I cement with 15 % class C fly ash and IP cement, respectively),
- k = rapid chloride permeability, and
- n = porosity of concrete.

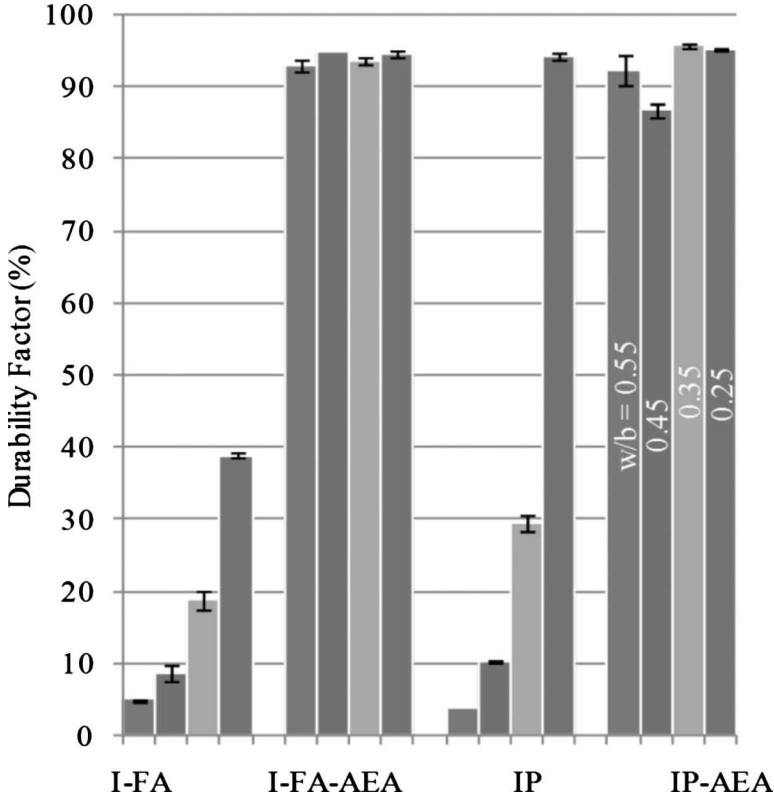


FIG. 6—FT DFs of concrete.

Based on Fig. 7 and Eqs 1 and 2, concrete made with type I cement and class C fly ash appeared less durable than the concrete made with type IP cement. To be FT durable (having $DF \geq 85\%$), concrete made with type I cement and class C fly ash shall have rapid chloride permeability of ≤ 185 C and porosity of $\leq 3.4\%$, while concrete made with IP cement requires a rapid chloride permeability value of ≤ 608 C and porosity of $\leq 5.0\%$.

Effect of Concrete Strength and w/b on Freezing-Thawing Durability

Generally, concrete gets damaged because the stresses developed in the concrete are higher than the concrete strength. Since concrete strength is closely related to w/b (decreasing as w/b increases strength), concrete FT durability usually increases with increased strength and decreased w/b . This concept was once again proven by the performance of the concrete without AEA as shown in Fig. 8. For concrete with AEA, the relationships between concrete FT DF and strength or w/b were not clear, although the relationship between concrete strength and w/b held well.

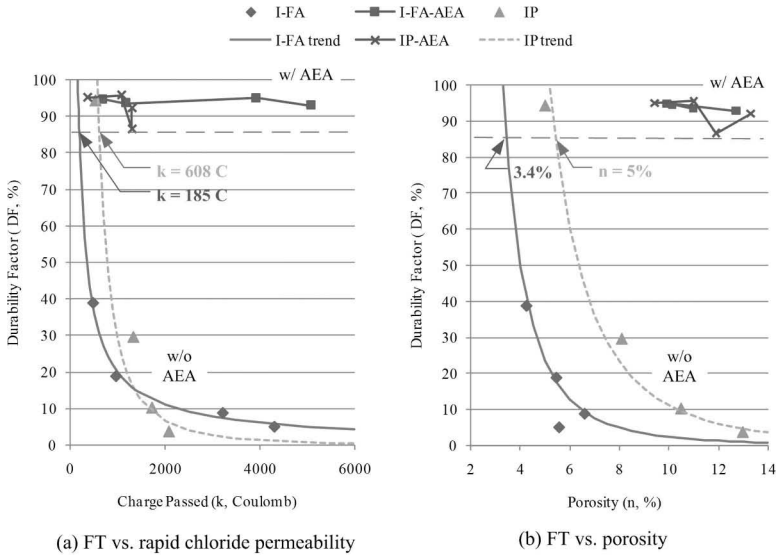


FIG. 7—Effects of concrete permeability and porosity on FT durability.

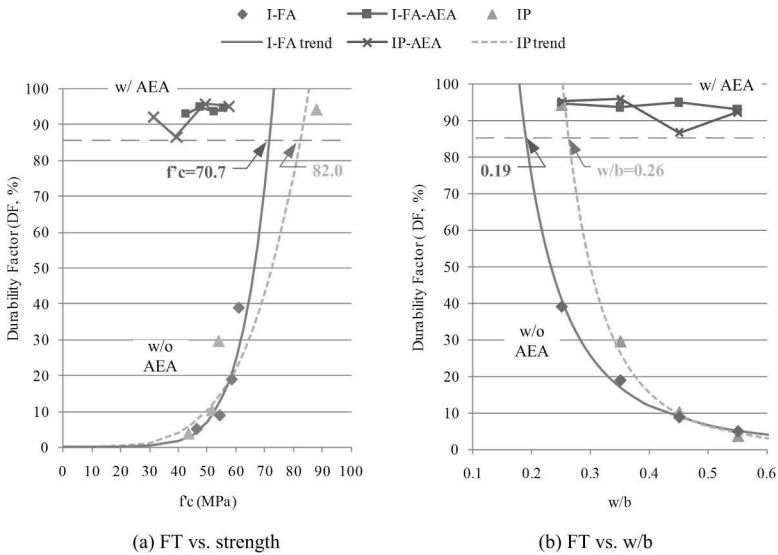


FIG. 8—Effects of concrete strength and w/b on FT durability (with predicted f'_c and w/b).

Based on the present study, the relationships between DF and 28-day compressive strength (f'_c) or w/b of non-air-entrained concrete can be expressed by Eqs 3 and 4, respectively

$$DF_{I-FA} = 1.05e - 11(f'_c)^{6.96} \quad \text{and} \quad DF_{IP} = 5.24e - 7(f'_c)^{4.29} \quad (3)$$

$$DF_{I-FA} = 1.09(w/b)^{-2.62} \quad \text{and} \quad DF_{IP} = 0.48(w/b)^{-3.72} \quad (4)$$

According to Eqs 3 and 4, concrete made with type I cement and class C fly ash requires 28-day compressive strength of 70.7 MPa (10 246 psi) or w/b of 0.19 to be FT durable ($DF \geq 85\%$). Such low w/b concrete is very difficult to be achieved in field, and therefore, air entrainment is recommended. The concrete made with IP cement required 28-day compressive strength of 82 MPa (11 880 psi) or w/b of 0.26.

Effect of Air Void Parameters on the Freezing-Thawing Durability

Figure 9 presents the relationships between FT resistance and air void parameters measured with different test methods. As discussed previously, all concrete mixtures made without AEA had ASTM C231 [15] content equal to or less than 2.8 %, and all mixtures made with AEA had ASTM C231 [15] air content larger than 6 %. Overall, the total air content measured by AVA and Rapid Air was slightly lower than that measured by ASTM C231 [15]. Figure 9(a) again shows that all mixtures made with AEA were FT durable ($DF \geq 85\%$), while all mixtures made without AEA did not meet the criterion of $DF \geq 85\%$, except for the mix made with IP cement and w/b of 0.25 (IP25, $DF = 94.3\%$). It should be noted that although mix IP25 had the highest ASTM C231 [15] air content (2.8 %) among all non-air-entrained mixtures and the highest strength (88 MPa) among all mixtures with and without AEA studied, its rapid chloride permeability and porosity were only 520 C and 5 %, respectively, the third lowest among all concrete mixtures. These results imply that for non-air-entrained concrete, strength, in addition to permeability, of concrete plays a vital role in controlling FT durability of the concrete.

Figure 9(b) and 9(c) indicates that for the air-entrained FT durable concrete, the maximum SF was 0.28 mm from the AVA tests, slightly lower than 0.30 mm as recommended by the previous research [23], and 0.22 mm from the Rapid Air tests, slightly higher than 0.20 mm that recommended for hardened concrete tested with ASTM C457 [20]. Unfortunately, Fig. 9(d) does not show any clear SS criterion for concrete FT durability. The criterion of $SS \geq 24 \text{ mm}^2/\text{mm}^3$ proposed by Tanesi and Meininger [24] for ASTM C457 [20] test method does not apply to the test results shown in Fig. 9 since it rejects some good concrete mixtures.

The results in Fig. 9 also suggest that although having slightly lower strength than non-air-entrained concrete, air-entrained concrete (with the minimum 28-day compressive strength of 31.3 MPa or 4 540 psi in the present study) is FT durable as long as it possesses proper air void parameters. In the other words, a proper air void system plays a vital role in controlling FT durability of normal and high strength (31.3–57.5 MPa) air-entrained concrete.

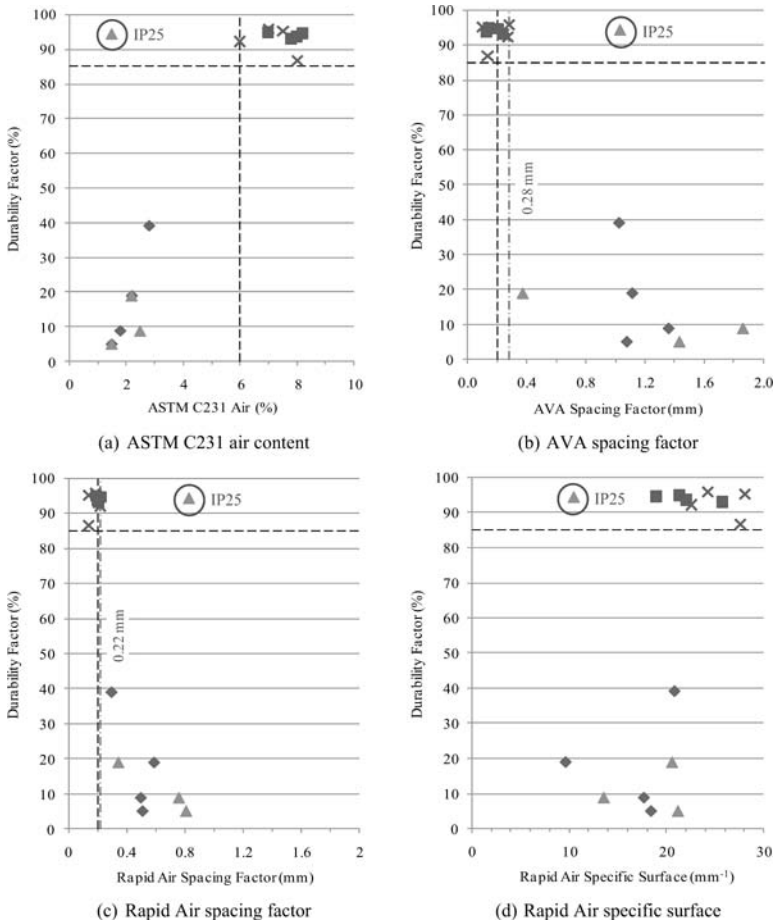


FIG. 9—Relationships between FT resistance and air void parameters.

Pigeon et al. [6] studied FT durability of HSC and suggested that the limiting w/b , below which air entrainment is not required for concrete made of type I cement, 6 % silica fume, and dolomitic limestone, is “probably” of the order 0.25, which is a similar result range in the present study. It is also interesting to note that in their study, the 28-day compressive strength and SF for FT durable concrete were 82.3 MPa (11 930 psi) and 0.69 mm, respectively. In the present study, the only FT durable concrete mix without AEA is mix IP25, which had compressive strength of 88.0 MPa (12 760 psi) and SF of 0.83 mm (measured by Rapid Air).

Whiting [25] studied FT durability of HSC and reported that all moist cured samples without air entrainment failed with a dynamic modulus below 60 % before reaching 300 FT cycles. The concrete he studied had non AEA, w/b ranging from 0.31 to 0.56, and 28-day compressive strength between 6000 and

10 000 psi. The results from the present study are consistent with those from the previous research [25], although different test methods for concrete air void parameters analysis were applied.

Conclusions

The following conclusions can be drawn from the present study.

- (1) Concrete FT durability increased with decreased rapid chloride permeability and increased strength. Low permeability concrete without air entrainment was FT durable when the concrete also had very high strength. In the present study, the concrete mixture made with type IP cement and without AEA had DF of 94.3 %, along with a rapid chloride permeability of 520 C and 28-day compressive strength of 88.0 MPa or 12 760 psi.
- (2) For normal strength concrete (approximately 4500–9000 psi), proper air entrainment is necessary for good FT resistance. Based on the test results from the present study, proper air entrainment may include ≥ 6 % air content measured with ASTM C231 [15] and the SF ≤ 0.28 mm measured using AVA or ≤ 0.22 mm measured using Rapid Air test device.
- (3) The relationships between concrete FT durability and other properties (such as rapid chloride permeability, porosity, and w/b) had been clearly demonstrated by the concrete made with given cementitious materials without AEA. These relationships can be expressed as a power form $DF = a(P)^{-b}$, where a and b are constants and P is the above-mentioned concrete properties. These relationships do not exist for the concrete with AEA.

Acknowledgments

The present study was sponsored by the Iowa Department of Transportation (IADOT) and the National Center for Concrete Pavement Technology (CP Tech Center). Mr. Bob Steffes and Dr. Gang Lu at Iowa State University helped in designing and conducting some of the tests described in this paper. The sponsorship and technical assistances are greatly appreciated.

References

- [1] Powers, T. C., "The Air Requirement of Frost Resistant Concrete," *Proc., Highway Res. Brd.*, Vol. 29, 1949, pp. 184–211.
- [2] Powers, T. C. and Helmuth, R. A., "Theory of Volume Changes in Hardened Cement Paste During Freezing," *Proc., Highway Res. Brd.*, Vol. 32, 1953, pp. 285–297.
- [3] Powers, T. C., "Basic Considerations Pertaining to Freezing and Thawing Tests," *Research Department Bulletin No. RX058*, Portland Cement Association, Skokie, IL, 1955.
- [4] Lerch, W., *Basic Principles of Air-Entrained Concrete, T-101*, Portland Cement As-

sociation, Skokie, IL, 1960.

- [5] Fagerlund, G., "The Critical Degree of Saturation Method of Assessing the Freeze/Thaw Resistance of Concrete," *Mater. Struct.*, Vol. 10, No. 4, 1977, pp. 217–229.
- [6] Pigeon, M., Gagne, R., Aitcin, P. C., and Banthia, N., "Freezing and Thawing Tests of High-Strength Concretes," *Cem. Concr. Res.*, Vol. 21, No. 5, 1991, pp. 844–852.
- [7] Cohen, M. D., Zhou, Y., and Dolch, W. L., "Non-Air-Entrained High-Strength Concrete—Is It Frost Resistant?" *ACI Mater. J.*, Vol. 89, No. 4, 1992, pp. 406–415.
- [8] Bassuoni, M. T. and Nehdi, M. L., "The Case for Air-Entrainment in High-Performance Concrete," *Proc. Inst. Civ. Eng., Struct. Build.*, Vol. 158, No. 5, 2005, pp. 311–319.
- [9] Jacobsen, S., Sellevold, E., and Matala, S., "Frost Durability of High Strength Concrete: Effect of Internal Cracking on Ice Formation," *Cem. Concr. Res.*, Vol. 26, No. 6, 1996, pp. 919–931.
- [10] ASTM Standard C1202, 2005, "Standard Test Method for Electrical Indication of Concrete's Ability to Resist Chloride Ion Penetration," *Annual Book of Standards*, Vol. 4.02, ASTM International, West Conshohocken, PA, pp. 645–650.
- [11] ASTM C666A, 2003, "Standard Test Method for Resistance of Concrete to Rapid Freezing and Thawing" *Annual Book of Standards*, Vol. 4.02, ASTM International, West Conshohocken, PA, pp. 344–349.
- [12] ASTM C642, 1997, "Standard Test Method for Density, Absorption, and Voids in Hardened Concrete," *Annual Book of Standards*, Vol. 4.02, ASTM International, West Conshohocken, PA, pp. 341–343.
- [13] ASTM C192, 2006, "Standard Practice for Making and Curing Concrete Test Specimens in the Laboratory," *Annual Book of Standards*, Vol. 4.02, ASTM International, West Conshohocken, PA, pp. 132–139.
- [14] ASTM C143, 2005, "Standard Test Method for Slump of Hydraulic-Cement Concrete," *Annual Book of Standards*, Vol. 4.02, ASTM International, West Conshohocken, PA, pp. 100–103.
- [15] ASTM C231, 1997, "Standard Test Method for Air Content of Freshly Mixed Concrete by the Pressure Method," *Annual Book of Standards*, Vol. 4.02, ASTM International, West Conshohocken, PA, pp. 152–160.
- [16] ASTM C138, 2001, "Standard Test Method for Density (Unit Weight), Yield, and Air Content (Gravimetric) of Concrete," *Annual Book of Standards*, Vol. 4.02, ASTM International, West Conshohocken, PA, pp. 94–97.
- [17] Taylor, P. C., Kosmatka, S. H., and Voigt, J. F., "Integrated Materials and Construction Practices for Concrete Pavement: A State-of-the-Practice Manual," *FHWA Publication No. HIF-07-004*, A Report from the National Concrete Pavement Technology Center and Federal Highway Administration, Iowa State University, Ames, IA, 2006, www.cptechcenter.org/publications/imcp/ (Last accessed date 21 Sept. 2009).
- [18] ASTM C39, 2005, "Standard Test Method for Compressive Strength of Cylindrical Concrete Specimens," *Annual Book of Standards*, Vol. 4.02, ASTM International, West Conshohocken, PA, pp. 21–27.
- [19] Zhang, S. and Wang, K., "Investigation into the Effects of Materials and Mixing Procedures on Air Void Characteristics of Fresh Concrete Using Air Void Analyzer (AVA)," *J. ASTM Int.*, Vol. 3, No. 10, 2006, pp. 1–15, Paper ID JAI100435.
- [20] ASTM C457, 2006, "Standard Test Method for Microscopical Determination of Parameters of the Air-Void System in Hardened Concrete," *Annual Book of Standards*, Vol. 4.02, ASTM International, West Conshohocken, PA, pp. 248–261.
- [21] Metha, P. K. and Monteiro, P. J. M., *Concrete: Microstructure, Properties, and Materials*, McGraw-Hill, New York, 2006.

- [22] Dransfield, J., "Admixtures for Concrete, Mortar and Grout," *Advanced Concrete Technology: Constituent Material*, J. B. Newman and B. S. Choo, Eds., Elsevier, Ltd., Butterworth-Heinemann, Burlington, MA, 2003.
- [23] Wang, K., Mohamed-Metwally, M., Bektas, F., and Grove, J., "Improving Variability and Precision of Air-Void Analyzer (AVA) Test Results and Developing Rational Specification Limits," *Final Project Report No. DTFH-61-06-H-00011*, National Concrete Pavement Technology Center, Iowa State University, Ames, IA, 2008.
- [24] Tanesi, J. and Meininger, R., "Freeze-Thaw Resistance of Concrete with Marginal Air Content," *Publication No. FHWA-HRT-06-17*, Federal Highway Administration, McLean, VA, 2006.
- [25] Whitting, D., "Durability of High Strength Concrete," *Concrete Durability, Katharine and Bryant Mather International Conference*, Scanlon, J. M., Ed., ACI SP100, Atlanta, GA, 1987, pp. 169-186.

M. Tyler Ley¹

Determining the Air-Entraining Admixture Dosage Response for Concrete with a Single Concrete Mixture

ABSTRACT: Currently there is no standardized test method to determine the interaction of the ingredients of a concrete mixture with a dosage of air-entraining admixtures (AEAs). Typically, to investigate the AEA demand, multiple concrete mixtures are made with varying dosages of AEA, and the resulting air contents are measured. This method is not ideal as it is time consuming, uses large amounts of material, and allows several variables to change that could cause changes in the dosage response of the mixture. A method is presented that is able to measure the AEA dosage response of a mixture through a correlation between the gravimetric (ASTM C138-01a) and pressure method (ASTM C231-03) with only minimal changes to the volume of the mixture. This allows the AEA demand to be determined from a single concrete mixture rather than sequential mixtures. Testing results are also provided for concrete mixtures containing fly ashes with various AEA demands. These mixtures are evaluated for changes in AEA demand with water reducer, mixing temperature, fly ash replacement level, and type of AEA.

KEYWORDS: freeze-thaw, concrete, durability, quality control, admixtures, air entrainment

Introduction

While there are several existing methods available to design a concrete mixture, all of them require making a trial mixture with the actual materials to verify the assumptions of the design method and to make any adjustments to the mixture. One issue that is not able to be easily answered with a single trial mixture is the response of the mixture to admixture dosage.

Manuscript received April 20, 2009; accepted for publication November 20, 2009; published online January 2010.

¹ Oklahoma State Univ., Stillwater, OK 74078, e-mail: tyler.ley@okstate.edu

Cite as: Ley, M. T., "Determining the Air-Entraining Admixture Dosage Response for Concrete with a Single Concrete Mixture," *J. ASTM Intl.*, Vol. 7, No. 2. doi:10.1520/JAI102463.

Copyright © 2010 by ASTM International, 100 Barr Harbor Drive, PO Box C700, West Conshohocken, PA 19428-2959.

One admixture whose dosage is exceptionally difficult to characterize in a concrete mixture is air-entraining admixture (AEA). The addition of AEA during the mixing of concrete is a common method to provide concrete with resistance to salt scaling and freezing and thawing. There are a large number of variables that have the ability to affect the air void system in concrete. Some of these include cement chemistry, mixture water chemistry, aggregate gradation, supplementary cementitious materials (SCMs), and other chemical admixtures [1].

The current method of examining the response of a mixture to AEA is to prepare several trial batches with different dosages of AEA and then examine how the mixtures respond. This method is useful as it allows a direct observation of how these materials perform in concrete. In creating each one of these mixtures, it is difficult to ensure that no unintentional variables have been introduced that can affect the results. Any of the following changes between batches could cause differences in results: moisture content of the aggregates, batch weights, sand gradation, and mixing methods.

Practitioners would benefit considerably if a new method to determine the response of a mixture to AEA demand could be developed from a single batch of material. This would minimize the efforts to create the mixtures while also removing the variability between mixtures. This method must allow the mixture to be evaluated without substantially changing the volume of the mixture in order to keep the mixing action at a constant level, as this could lead to changes in the resulting air content. Furthermore, this method must provide a good correlation to individual mixtures cast at discrete dosages of AEA.

The need for this method is increasing as recent EPA mandated changes to emission standards for coal-fired power plants in the United States has led to an increase in the amount and activity of the remaining carbon in fly ash concrete. This change in the carbon has led to significant increases in the required AEA dosage of the resulting concrete [2–6]. While the increase in dosage has been somewhat of a nuisance, the most significant impact has been in the daily variability in AEA demand of the material. This variability has caused a significant amount of concrete mixtures to be rejected for not meeting the fresh air content specification.

While rapid test methods using simplified systems (such as paste and slurries) have been shown to be useful to predict the changes in AEA demand of fly ashes [3], these simplified systems are not capable of reproducing the impacts of different admixtures or changes in environment. Since the method presented uses concrete instead of a simplified system, then these challenges can be overcome, and additional information about the AEA demand of a concrete mixture can be determined.

Methods of Measuring Air Content in Concrete

To examine the total volume of air content in fresh concrete there are currently three common methods: Gravimetric (ASTM C138-01a [7]), pressure (ASTM C231-03 [8]), and volumetric (ASTM C173-07 [9]).

In the gravimetric method a container of a known volume is filled with the concrete to be investigated and consolidated in a standard manner. This volume

of concrete is then weighed, and from this weight, material properties, and theoretical batch weights, the total volume of air can be calculated for that mixture. Some problems with this method have been pointed out by Roberts [10]. These problems include the need for very accurate batch weights, material properties, and moisture content of aggregates. Because of these limitations it is difficult, in the laboratory or in the field, to get an accurate measure of air content with the gravimetric method. One advantage of this method is that it allows the concrete in the test to be reused after being returned to the mixer and re-mixed as the material was not altered only consolidated.

The pressure and volumetric methods of measuring air content do not rely on an accurate characterization of the mixture materials and instead attempt to directly measure the amount of air in the mixture. However, both of these methods require water to be added to the concrete specimen. This addition of water changes the water content of the mixture and forces the concrete analyzed in the test to be discarded. Because of this when using either of these methods, the resulting volume of the mixture that is being investigated will decrease in size. While this size change is not a concern when a large truck or central batch mixer is used, this volume decrease will be significant for a laboratory mixer. By using either one of these methods to evaluate the air content of a laboratory mixer, it is likely that the mixture volume will change from 10 % to 25 %. Therefore, after investigating the air content of the laboratory mixture, the remaining material would have to be discarded if the dosage did not yield the required air content as the mixing volume, and therefore mixing action of the material in the mixer has significantly changed.

While criticisms have been made of possible inaccuracies of both the pressure and volumetric methods of measuring the air content of concrete, the pressure meter was used for this testing as it is the most widely used to evaluate the air content of fresh concrete. For this reason this test method was used in this research. The methods presented though should work for either meter, but no testing was completed with the volumetric method.

Combining the Gravimetric and Pressure Method

If one were able to accurately measure the air content of a mixture while holding the volume of the mixture constant, then it would be possible to prepare a single concrete mixture and evaluate how the air content of that mixture changes as AEA is added. However, none of the existing methods, at least individually, allow this to happen.

By combining the results of a density measurement from the gravimetric test and total air content from either the pressure or volumetric method, one can correlate the volume of air in a mixture to the measured density. Assuming both tests are performed properly, then a measure of the total air void volume has been tied to the density of the mixture. After this correlation is made, any changes in the air content (density) can be evaluated by only monitoring changes in the gravimetric measurements as long as no other variables are allowed to change.

By using the gravimetric method to monitor the density change and then

TABLE 1—Composition of the Type I/II cement as determined by RQXRD.

Phase	Percentage
C ₃ S	68.0
C ₂ S	15.7
C ₃ A	2.7
C ₄ AF	8.7
Gypsum	1.3
CaCO ₃	2.6

returning the materials to the mixer, it allows successive AEA dosages to be made to a mixture and the resulting changes in the air content to be measured.

Objectives

The objectives of this work are to develop a test method that is able to utilize a single concrete mixture to determine the impact on AEA demand of the ingredients. This test method will then be utilized to investigate the impact of several variables commonly reported to cause an impact on the AEA demand of concrete mixtures.

Experimental Methods

Materials

In all of the mixtures presented in this paper, Type I/II cement (conforming to ASTM C150-02 [11]) was used, with an equivalent alkali content ($\text{Na}_2\text{O}_{\text{eq}}$) of 0.53 and a Blaine fineness of 3630 cm^2/g . The phases of the cement are reported in Table 1 as determined by a Rietveld quantitative X-ray diffraction (RQXRD) [12,13] completed with the Topas Academic Software. The aggregates used in the mixtures were locally available river gravel and sand that are commercially used in concrete. All of the AEAs were obtained from commercial sources and meet ASTM C260 [14]. The water reducer (WR) used in this research met the requirements of ASTM C494/C494M-05 [15] as a types A and D.

In this paper the AEA demand for 19 different fly ashes (all meeting ASTM C618-05 [16]) was investigated. Of these fly ashes a more detailed investigation of AEA demand was completed for three of the ashes. These three fly ashes were chosen as they exhibited different AEA demands in prior laboratory testing. Fly ashes 6 and 7 were obtained from the same source; however, fly ash 6 had been treated with a sacrificial surfactant to improve the AEA demand in concrete [17]. No information was provided by the manufacturer about the amount of sacrificial surfactant that was added to the fly ash. Therefore, all results for fly ash 6 are likely dependent on this concentration. If the concentration is changed, then the results for fly ash 6 would also be expected to

TABLE 2—Oxide analysis and LOI data for three fly ashes.

Fly Ash Name	1	6 ^a	7
Silicon dioxide (SiO ₂), %	56.18	52.07	52.04
Aluminum oxide (Al ₂ O ₃), %	20.37	23.65	23.75
Iron oxide (Fe ₂ O ₃), %	6.77	4.55	4.59
Sum of SiO ₂ , Al ₂ O ₃ , Fe ₂ O ₃ , %	83.32	80.27	80.38
Calcium oxide (CaO), %	9.95	12.76	12.63
Magnesium oxide (MgO), %	2.55	2.02	2.01
Sulfur trioxide (SO ₃), %	0.53	0.78	0.79
Sodium oxide (Na ₂ O), %	0.47	0.31	0.28
Potassium oxide (K ₂ O), %	1.08	0.80	0.81
Total alkalis (as Na ₂ O), %	1.18	0.84	0.81
ASTM C618 classification	F	F	F
LOI (ASTM C311)	0.12	0.79	0.79

^aFly ash 7 that has been treated with a sacrificial surfactant.

change. An oxide analysis completed with X-ray fluorescence spectroscopy and loss-on-ignition (LOI) measurements from ASTM C311-05 [18] are reported in Table 2 for each of the three fly ashes.

Concrete Mixing and Testing

The following methodology was used to investigate the response of a single concrete mixture to increases in AEA dosage. Initially, a 64 L batch of concrete was prepared in an 85 L drum mixer. The mixture used a 0.45 w/cm with 335 kg/m³ (equivalent to six sacks of cement) of total cm, with a 20 % replacement of the fly ash (by mass of cement). Proportions for the mixture can be found in Table 3.

All of the materials for the mixture were stored at 23°C for 24 h prior to mixing to keep the mixing temperature constant. Coarse and fine aggregates were brought in from the stock piles and individually mixed. A moisture correction for each was used to adjust the batch weights. The rock and sand were added to the mixture first and 2/3 of the mixing water. The mixture was agitated for 1 min. Next the cement, fly ash, and the remaining mixing water were added and mixed for 3 min. At this point, the mixer was stopped, and any material gathering on the sides or back of the mixer was removed. During the final 3 min

TABLE 3—Concrete mixture design.

Components	Mass (kg/m ³)
Cement	268
Fly ash	67
Coarse aggregate	1098
Fine aggregate	742
Water	151

mixing period, a normal WR was added to the mixture in either a desired dosage or to bring the mixture to a desired slump (ASTM C143-05a [19]). It was found for the materials used in this study that there was interplay between the efficiency of the AEA and the WR dosage used. In order to compare results between mixtures, it was necessary to have mixtures that had a similar WR dosage and workability. These issues are discussed in detail in later sections.

The following samples were taken after the mixing was completed: a 7 L sample for a gravimetric test, a slump test, and a 1 L rectangular prism for hardened air void analysis. The air content of the gravimetric sample was determined by the pressure method, establishing the relationship between the air content and the density of the mixture. The concrete used for the slump test was returned to the mixer, leaving the volume of the batch equal to 56 L. Next a commercially available AEA was added to the mixture and mixed for three minutes. Slump and gravimetric measurements were taken, and the concrete was returned to the mixer. A 1 L rectangular prism was also taken for hardened air void analysis. These steps were repeated in regular dosage increments with 3 min of mixing time after each AEA dosage, and the gravimetric measurement was taken until the change in the density from the initial sample was approximately 6 %. A minimum of four AEA dosages was investigated for each mixture. A final slump, air content by the pressure meter, and rectangular prism were taken from the mixture. All measurements for a mixture were typically made within an hour of initial mixing.

By using the combination of results from the gravimetric and pressure methods, it was possible to measure the initial density and total air content of a mixture and correlate them. This correlation was then used to monitor the density change in the mixture with increased dosages of AEA and mixing. The percent change between the initial density and the density being investigated for a given AEA dosage was assumed to be equal to the change in air content for the mixture. Since these measurements were able to be made without significantly decreasing the volume of the mixture, additional AEA dosages could be added to the mixture, and the mixture could be re-evaluated. After the unit weight of the concrete mixture had changed by approximately 6 %, a final pressure meter reading was taken from the mixture.

The predicted air content at that AEA dosage from the initial pressure meter reading and the unit weight measurements were compared to the final pressure meter reading. The difference between these values was found, and the measured results were adjusted to correct for this difference. This correction was made by dividing the difference by the number of measurements and making an equal adjustment to each of the measurements. This difference between the air content predicted and measured by the final pressure meter reading was typically less than 0.5 %, and so corrections were small. A linear trend was then fit to the estimated air content versus the AEA dosage. This trend line could then be used to estimate the AEA dosage required for that mixture to estimate the total volume of air in the mixture.

Test Results and Validation

Figure 1 shows a typical set of data from a single concrete mixture (solid points), a linear trend line fitted to these points, as well as the air content from

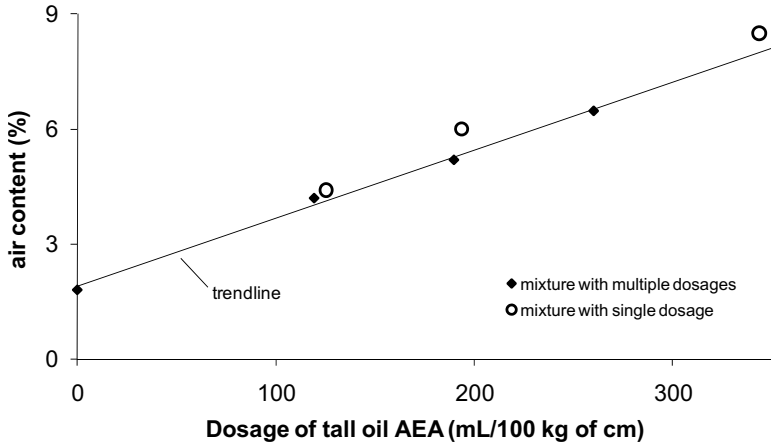


FIG. 1—Air content versus AEA dosage from single mixture method compared to several individual mixtures with a trend line fit to the single mixture method results.

individual concrete mixtures with different dosages of AEA that did not use the multiple dosage method. As can be seen in the figure, the trend line seems to represent the data well and shows a satisfactory estimate of how concrete mixtures performed that used single dosages of AEA and how mixtures performed that used multiple dosages.

The trend line established can now be used to compare the AEA demand between concrete mixtures that have different variables. This comparison could be made by comparing the amounts of AEA required to produce a desired air content, or the slope of the trend line provides information on the change in air content for a given dosage of AEA. In this paper the dosage of AEA required to produce an air content of 6 % was used. A value of 6 % air content was chosen as it is a common value required in specifications for concrete.

It was found for these mixtures that even though the air content changed by 6 % with increased AEA dosage, the slump of the mixtures often did not increase by more than 25 mm. It is possible that different results may be obtained with the same materials if the mixture were prepared with different mixing durations, speeds, or energy per unit volume of mixture. Nevertheless, this method has been used with three drum mixers of three different volumes, and each time allowed a useful comparison for the response of a concrete mixture to AEA dosages.

A correlation coefficient (r^2 value) is a measurement of how accurate the fit of the data is to the regression analysis. In this study for the 96 different mixtures investigated, a correlation coefficient of a linear trend line was found to be consistently close to one for the majority of the data as the average was 0.96, with a standard deviation of 0.07. This suggests that the response of the mixtures investigated to increases in AEA dosage as measured by this method seems to consistently fit a linear trend.

In order to examine how well this method is able to represent the performance of mixtures made with individual dosages of AEA, a comparison was

TABLE 4—Comparison of measured air content in mixtures with single dosages of AEA and that predicted by a mixture using multiple dosages of AEA.

Fly Ash	AEA Product	Slump (mm)	Normal WR (mL/100 kg CM)	AEA (mL/100 kg CM)	Percent Air Content		
					Measured	Predicted	Difference
1	Tall oil	89	170	50	5.7	5.2	0.5
1	Tall oil	89	170	100	7.8	8	-0.2
1	Wood rosin	70	44	27	6	6	0
1	Wood rosin	51	46	47	6.2	6.3	-0.1
6	Synthetic	76	166	36	3.2	3.2	0
6	Synthetic	76	166	89	5.6	5.4	0.2
6	Synthetic	76	166	140	7.3	7.5	-0.2
6	Tall oil	70	169	194	6	5.3	0.7
6	Tall oil	76	169	344	8.5	9.3	-0.8
6	Tall oil	70	169	125	4.4	4.6	-0.2
6	Wood rosin	89	83	30	2	2.6	-0.6
6	Wood rosin	89	83	93	5.4	5.2	0.2
7	Wood rosin	51	108	32	3.2	3.2	0
7	Vinsol resin	95	33	124	4.5	4.5	0
15	Wood rosin	76	72	44	5.3	5.4	-0.1
15	Wood rosin	76	72	69	7.3	7.2	0.1
					Average		0.0
					Standard deviation		0.4

made between the air content measured from a single dosage of AEA and the values predicted by the linear trends from the mixtures of multiple doses. This comparison was made between mixtures that contained different AEAs and fly ashes. The results of a comparison between 32 different mixtures (16 mixtures using individual dosages and 16 using multiple dosages) are shown in Table 4. The largest difference between the air content measured and predicted was found to be 0.8 %, with an average difference of 0.0 % and a standard deviation of 0.4 %. This shows that despite the differences in mixing procedures, there is a good correspondence between the air content measured in several individual mixtures and the air content predicted by correlating the density and air content determined by the pressure method in a single mixture and using multiple dosages of AEA.

These results show that not only are the dosage response of the mixtures linear but that the interpolated results closely match the value obtained from concrete mixtures with a single dosage of AEA.

Evaluation of Air-Entraining Admixture Demand for Various Concrete Mixtures Using the New Test Method

Now that this method has been shown to be able to predict the AEA dosage of a concrete mixture, it was used to investigate concrete mixtures that contained

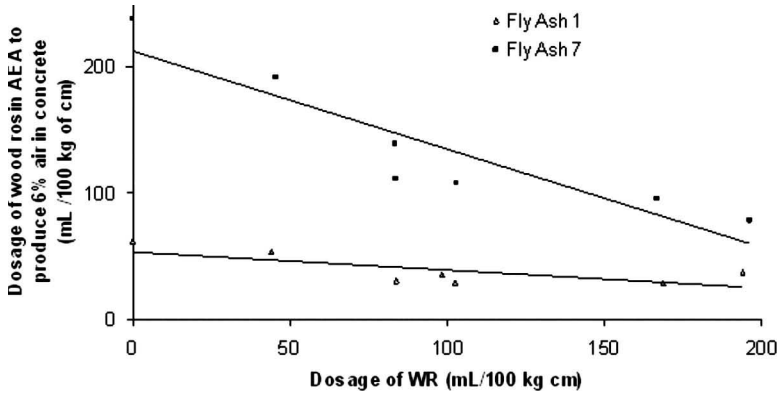


FIG. 2—AEA demand interpolated from single mixture method for two different fly ashes with different dosages of WR.

fly ash of varying AEA requirements. In addition a smaller subset of fly ashes was investigated in combination with other variables such as WR admixtures, changes in temperature, and different AEA types. For each of these mixtures, the WR dosage was held constant where possible in order to investigate the effects of each variable. Care should be taken in extrapolating comparisons beyond what is presented in the table as the WR dosage was not held constant between all variables due to the large differences in water demand between the mixtures.

Effect of Water Reducer Dosage on Air-Entraining Agent Dosage

In order to investigate the affect of the WR dosage on AEA demand for a fly ash concrete mixture with wood rosin AEA, 14 different mixtures were prepared with different dosages of WR. The AEA demand was determined in a single mixture as previously described. The results are shown in Fig. 2. As can be seen it appears that the AEA dosage required in concrete to produce 6 % air content decreased with a good correlation to the increase in the WR dosage. This data should be examined with the realization that the workability of a mixture would also be expected to increase with WR dosage. An increase in workability would be expected to increase the effectiveness of the AEA and therefore decrease the AEA demand of the mixture.

These results suggest that if two mixtures are to be compared to one another, then it is important to have a similar WR dosage in the mixture. However, in preliminary testing it was found that a minimum workability was needed to efficiently entrain air in concrete. Because of this it was decided that the concrete mixtures should have a similar slump and WR dosage to be accurately investigated. Each mixture was prepared with a WR dosage between 45 and 85 mL/100 kg CM and a slump between 50 and 100 mm unless otherwise noted.

TABLE 5—A ranking of several fly ashes commercially used in concrete by the AEA demand from the single mixture method.

Fly Ash	Slump (mm)	WR (mL/100 kg CM)	AEA Demand ^a (mL/100 kg CM)
1	100	83	31
23	95	45	32
19	95	66	34
11	70	81	36
27	64	45	38
10	95	46	39
8	89	64	42
2	76	51	44
9 ^b	57	132	44
25	64	58	48
15	95	68	49
20	70	46	49
5	64	46	50
16	76	72	52
26	89	48	64
4	83	47	83
14	83	50	93
6 ^b	57	111	138
7	83	71	147

^aDosage of wood rosin AEA required to produce 6 % air content in the mixture. The value is interpolated from the dosage response curve.

^bThese mixtures required high dosages of WR to obtain an acceptable slump. This increase in WR could cause a response in the AEA demand of the mixture.

Evaluation of Air-Entraining Admixture Demand of Fly Ash Concrete

Nineteen different fly ashes that were investigated with a single concrete mixture are reported in Table 5. For two of the mixtures the WR dosage had to be adjusted due to insufficient slump of the concrete caused by differences in water demand. Both of these mixtures required dosages of around 110 mL/100 kg CM and have been reported with a footnote in Table 5. These mixtures contained fly ashes that were treated with a sacrificial surfactant to decrease the AEA demand of the fly ash. It is possible but not certain that this treatment contributed to this increase in water demand observed.

Fly Ash Type and Replacement

The amount of wood rosin AEA required to produce 6 % air in concrete for mixtures utilizing fly ashes 1, 6, and 7 at replacement levels of 20 %, 35 %, and 50 % is shown in Table 6. Fly ash 1 shows a reduction in the amount of AEA demand required in the mixture as a higher fly ash replacement is used. For fly ash 6, a complete data set was not obtained as the slump of the mixture at a 20

TABLE 6—Effects of fly ash replacement on AEA demand in concrete for three fly ashes.

Fly Ash Replacement (%)	Fly Ash					
	1		6		7	
	AEA Demand ^a	Ratio to Standard ^b	AEA Demand ^a	Ratio to Standard ^b	AEA Demand ^a	Ratio to Standard ^b
50	44	0.71	203	...	368	1.54
35	40	0.65	196	...	267	1.12
20	63	1.00	239	1.00

^aThe amount of wood rosin AEA (mL/100 kg CM) required to produce 6 % air in concrete. The value is interpolated from the dosage response curve.

^bThe ratio of the AEA demand for the variable being investigated and fly ash compared to a mixture prepared with wood rosin AEA at 23 °C, with a fly ash replacement of 20 % and with a 0.53 Na₂O_{eq} cement.

% replacement level was not comparable to the mixtures at 35 % and 50 % replacement and WR dosage used. However, there was little change in the AEA demand as the amount of fly ash in the mixture increased. This behavior is different than what was observed with mixtures containing fly ash 7 as the AEA demand increased as the amount of fly ash replacement increased. The increase in AEA demand with increasing ash volume replacement was not linear.

Air-Entraining Admixture Type

Four different commercial AEAs (wood rosin, synthetic, tall oil, and Vinsol resin) were used in concrete mixtures with different fly ashes to investigate the AEA demand. The results are shown in Table 7. For all of the AEAs investigated fly ash 1 showed the lowest AEA demand, fly ash 6 showed more AEA demand than fly ash 1, and fly ash 7 showed the highest AEA demand. When comparing the difference in AEA demand between fly ashes 1 and 7, it was determined that

TABLE 7—Effects of AEA type on AEA demand in concrete for three fly ashes.

AEA	Fly Ash					
	1		6		7	
	AEA Demand ^a	Ratio to Standard ^b	AEA Demand ^a	Ratio to Standard ^b	AEA Demand ^a	Ratio to Standard ^b
Synthetic	33	1.00	104	3.12
Tall oil	67	1.00	181	2.72	231	3.47
Vinsol resin	40	1.00	73	1.84	142	3.57
Wood rosin	29	1.00	95	3.32	147	5.14

^aThe amount of wood rosin AEA (mL/100 kg CM) required to produce 6 % air in concrete. The value is interpolated from the dosage response curve.

^bThe ratio of the AEA demand for the variable being investigated and fly ash compared to a mixture prepared with wood rosin AEA at 23 °C, with a fly ash replacement of 20 % and with a 0.53 Na₂O_{eq} cement.

TABLE 8—Effects of mixing temperature on AEA demand in concrete for three fly ashes.

Mixing Temperature (°C)	Fly Ash					
	1		6		7	
	AEA Demand ^a	Ratio to Standard ^b	AEA Demand ^a	Ratio to Standard ^b	AEA Demand ^a	Ratio to Standard ^b
32	32	1.03	187	1.35	224	1.16
23	31	1.00	138	1.00	192	1.00
10	29	0.94	60	0.43	80	0.42

^aThe amount of wood rosin AEA (mL/100 kg CM) required to produce 6 % air in concrete. The value is interpolated from the dosage response curve.

^bThe ratio of the AEA demand for the variable being investigated and fly ash compared to a mixture prepared with wood rosin AEA at 23°C, with a fly ash replacement of 20 % and with a 0.53 Na₂O_{eq} cement.

the largest change was for the wood rosin AEA and the smallest change was for the synthetic AEA. The AEA demand for the tall oil and Vinsol resin fell in between these values but was closer to the values for the synthetic AEA at 3.47 and 3.57 times higher than the AEA demand for fly ash 1. When investigating the change in AEA demand between mixtures containing fly ashes 1 and 6, it was found that the wood rosin still showed the highest change in demand and the Vinsol resin showed the least. It should be noted that a mixture with fly ash 6 and the synthetic AEA was not investigated.

Mixing Temperature

To compare the effects of different mixing temperatures on fly ash concrete with different AEA demands, mixtures were prepared with the constituent materials initially conditioned to 10, 23, and 32°C. For each mixture, the AEA demand was determined by the dosage of AEA required to produce 6 % air content in the mixture. These results are presented in Table 8. In each one of these comparisons a constant WR dosage was used for all of the mixtures containing a given fly ash, and the results of each mixture are compared back to a mixture at 23°C.

It appears that the change in temperature had little effect on the AEA demand for mixtures with fly ash 1. However, the AEA demand decreased for the mixtures with fly ashes 6 and 7 as the mixing temperature increased. Past research suggested that as the mixing temperature increases, the efficiency of the AEA decreases [20].

Discussion of Results

One significant finding from the testing was that fly ash 6 behaved notably different than fly ashes 1 and 7 in the testing. As reported earlier fly ash 6 is a sample from the same source as fly ash 7 but was treated with a sacrificial surfactant of an unknown dosage to reduce the AEA demand of the fly ash. As

can be seen from the results, this treatment does consistently reduce the AEA demand of the concrete mixture over the variables investigated when compared to fly ash 7. Other notable behavior is that fly ash 6 seems to show a greater change in AEA efficiency when the mixing temperature is raised. This difference in behavior is likely attributable to the sacrificial surfactant that was added to fly ash 6.

The mixtures containing fly ash 1 at different replacement levels show a decrease in AEA demand with increasing replacement levels of fly ash. Fly ash 1 was shown to have a very low AEA demand when used at 20 % replacement in concrete. When larger replacements are used in a mixture, then one would expect the workability to increase. This increase in workability appears to have caused a decrease in the AEA demand as it has made it easier to entrain air in the mixture.

Fly ash 7 was found to consistently require a higher AEA dosage than either fly ash 1 or 6 and was found to have the highest of the 19 fly ashes investigated. From the results of the different AEAs used in combination with the different fly ashes, it appears that the change in AEA demand between fly ash 1 and 7 was very similar for all of the AEAs investigated except for the wood rosin AEA. This suggests that the wood rosin AEA may be more sensitive to changes in AEA demand from the fly ash than the other commercial AEAs investigated with the normal WR used in this study.

As a whole, this study shows that the AEA demand of every fly ash is different, and its response to changes in dosage, temperature, and AEA dosage/type can vary considerably from source to source (and possibly from time to time for a given source). This reinforces the need to have readily available test methods that can accurately and efficiently investigate the performance of the materials in actual concrete mixtures such as the methodologies presented in this paper.

Conclusions

This paper has presented a method to produce an AEA dosage response curve for a concrete mixture while only using a single mixture. The method was then compared to the AEA dosage response of several sequential mixtures, and the results were found to be closely comparable for air contents up to 8 %. Next, the method was utilized to build a large data set to compare several variables that affect the AEA demand of concrete that are not easily measurable by using single mixtures for three fly ashes. These include effects of WR dosage on AEA demand, ranking the AEA demand of several fly ashes, mixing temperature, fly ash replacement, and comparison of different commercially available AEAs. This data set provides insight into how these variables impact concrete containing fly ash with a high and low AEA demand as well as with a sacrificial surfactant to reduce the AEA demand in fly ash concrete.

The results of this paper suggest the following.

- The WR used in this paper showed the ability to reduce the wood rosin AEA demand in fly ash concrete with increasing dosages.

- A sacrificial surfactant that is used on fly ash with high AEA demand can decrease the AEA demand of fly ash concrete.
- The mixing temperature had a larger impact on the AEA demand of a fly ash treated with a sacrificial surfactant than the other fly ash mixtures investigated.
- As the percent fly ash replacement increases in a concrete mixture, the AEA demand in fly ash concrete decreased if the AEA demand of the fly ash was low or increased if the AEA demand of the fly ash was high. This increase occurred in a nonlinear fashion.
- A wood rosin AEA is the most sensitive of the AEAs examined to a fly ash with a high AEA demand in concrete.

Acknowledgments

This work was funded by a grant from the Texas Department of Transportation under TxDOT grant #5207-Effects of Texas Fly Ash on Air-Entrainment in Concrete. The Author would like to thank Kevin Folliard, Ken Hover, and Nathan Harris for participating in this research. Thanks should also be given to Maria Juenger for her careful proofreading of the manuscript. This work could not have been completed without the help of Dustin Wilson and Adam Haggerty in completing the mixtures contained in this paper. The author would also like to acknowledge the following suppliers for providing material for this study: Boral Material Technologies, ISG Resources, Alamo Cement, BASF Admixture, Lafarge International, and TXI Aggregate. A special thanks should also be given to Boral Material Technologies for their assistance in performing the chemical analysis of the fly ash for the samples reported in this paper.

References

- [1] Whiting, D. and Stark, D., "Control of Air Content in Concrete," *NCHRP Report No. 258*, Transportation Research Board, National Research Council, Washington, D.C., May 1983.
- [2] Gebler, S. and Klieger, P., "Effect of Fly Ash on the Air-Void Stability of Concrete, Fly Ash Silica Fume, Slag and Other Mineral By-Products in Concrete," SP-79, American Concrete Institute, Detroit, 1983, pp. 103–142.
- [3] Ley, T. Harris, N. J., Folliard, K. J., and Hover, K. C., "Investigation of Required Air Entraining Admixture Dosage in Fly Ash Concrete," *ACI Concr. Mater. J.*, Vol. 105, 5, 2008, pp. 494–498.
- [4] Hill, R. and Folliard, K., "The Impact of Fly Ash on Air-Entrained Concrete," *HPC Bridge Views*, Vol. 43, 2006, pp. 5–6.0002-7820
- [5] Kūlaots, I., Hurt, R., and Suuberg, E., "Size Distribution of Unburned Carbon in Coal Fly Ash and Its Implications," *Fuel*, Vol. 83, 2004, pp. 223–230.
- [6] Freeman, E., Gao, Y., Hurt, R., and Suuberg, E., "Interaction of Carbon-Containing Fly Ash with Commercial Air-Entraining Admixtures for Concrete," *Fuel*, Vol. 76, No. 8, 1997, pp. 761–765.
- [7] ASTM C138-01a, 2001, "Standard Test Method for Density (Unit Weight), Yield,

- and Air Content (Gravimetric) of Concrete,” *Annual Book of ASTM Standards*, ASTM International, West Conshohocken, PA.
- [8] ASTM C231-03, 2003, “Standard Test Method for Air Content of Freshly Mixed Concrete by the Pressure Method,” *Annual Book of ASTM Standards*, ASTM International, West Conshohocken, PA.
- [9] ASTM C173-07, 2007, “Standard Test Method for Air Content of Freshly Mixed Concrete by the Volumetric Method,” *Annual Book of ASTM Standards*, ASTM International, West Conshohocken, PA.
- [10] Roberts, L. R., *Air Content, Temperature, Density (Unit Weight), and Yield, Significance of Tests and Properties of Concrete and Concrete-Making Materials*, ASTM STP 169D, ASTM International, West Conshohocken, PA, 2006, pp. 73–79.
- [11] ASTM C150-02, 2002, “Standard Specification for Portland Cement,” *Annual Book of ASTM Standards*, ASTM International, West Conshohocken, PA.
- [12] Rietveld, H., “A Profile Refinement Method for Nuclear and Magnetic Structures,” *J. Appl. Crystallogr.*, Vol. 2, 1969, pp. 65–71.
- [13] Stutzman, P. E., “Guide for X-Ray Powder Diffraction Analysis of Portland Cement and Clinker,” *Internal Report No. 5755*, National Institute of Standards and Technology, 1996.
- [14] ASTM C260, 2006, “Standard Specification for Air-Entraining Admixtures for Concrete,” *Annual Book of ASTM Standards*, ASTM International, West Conshohocken, PA.
- [15] ASTM C494/C494M-05, 2005, “Standard Specification for Chemical Admixtures for Concrete,” *Annual Book of ASTM Standards*, ASTM International, West Conshohocken, PA.
- [16] ASTM C618-05, 2005, “Standard Specification for Coal Fly Ash and Raw or Calcinated Natural Pozzolan for Use in Concrete,” *Annual Book of ASTM Standards*, ASTM International, West Conshohocken, PA.
- [17] Hill, R., Jolicoeur, C. R., Page, M., Spiratos, I., and To, T. C., “Sacrificial Agents For Fly Ash,” U.S. Patent No. 20,040,206,276 (January 22, 2004).
- [18] ASTM C311-05, 2005, “Standard Test Methods for Sampling and Testing Fly Ash or Natural Pozzolans for Use in Portland-Cement Concrete,” *Annual Book of ASTM Standards*, ASTM International, West Conshohocken, PA.
- [19] ASTM C143-05a, 2005, “Standard Test Method for Slump of Hydraulic-Cement Concrete,” *Annual Book of ASTM Standards*, ASTM International, West Conshohocken, PA.
- [20] Gay, F. T., “The Effect of Mix Temperature on Air Content and Spacing Factors of Hardened Concrete Mixes with Standardized Additions of Air-Entraining Agent,” *Proceedings of the Seventh International Conference on Cement Microscopy*, Fort Worth, TX, International Cement Microscopy Assoc., Duncanville, TX, 1985, pp. 305–315.

Donald J. Janssen¹

Freeze-Thaw Performance of Concrete: Reconciling Laboratory-Based Specifications with Field Experience

ABSTRACT: Specifications relating to frost resistance of concrete are generally based on laboratory tests of laboratory-produced concrete. Quality control for laboratory-produced concrete is usually significantly better than what can be achieved in the field, and laboratory freeze-thaw tests generally produce conditions that are not close to any real field exposure conditions. Field exposure testing is also problematic. Exposure conditions are not the same from one location to the next and may not even be the same from one year to the next at the same location. This paper attempts to provide guidance for interpreting the results of field tests of concrete exposed to natural freezing and thawing conditions. Types of frost damage as well as types of field test sites are discussed, and recommendations are provided for the use of field test results to modify frost-resistance specifications.

KEYWORDS: air-void parameters, concrete, freeze-thaw, internal damage, scaling, spacing factor, w/c , w/cm

Introduction

Frost resistance is necessary for Portland cement concrete exposed to freezing conditions to serve its intended functions. This frost resistance is generally mandated by mixture specifications, which are primarily based on laboratory testing and laboratory pre-qualification tests. With the exception of frost-deterioration associated with the coarse aggregate used in the concrete (D -cracking), the specifications generally focus on the water-cementitious materials ratio (w/cm) and the entrained air-void system. Though the basic frost-resistance specifications [1,2] have remained essentially unchanged for almost half a century, they have almost always resulted in concrete that has shown

Manuscript received May 12, 2009; accepted for publication September 22, 2009; published online November 2009.

¹ Univ. of Washington, Seattle, WA 98195-2700.

Cite as: Janssen, D. J., "Freeze-Thaw Performance of Concrete: Reconciling Laboratory-Based Specifications with Field Experience," *J. ASTM Intl.*, Vol. 7, No. 1. doi:10.1520/JAI102506.

Copyright © 2010 by ASTM International, 100 Barr Harbor Drive, PO Box C700, West Conshohocken, PA 19428-2959.

adequate frost resistance in the field. Newer materials (air-entraining-, water-reducing-, and high-range water-reducing-admixtures as well as supplementary cementitious materials) have come into use since the development of these specifications, and questions have been raised concerning whether the current specifications are too conservative. Also, occasional “failures” of concrete thought to have met the specifications have raised questions concerning their appropriateness. Numerous field tests have been conducted in order to provide improved insight. The purpose of this paper is to provide guidance for interpreting observed field performance in order to possibly revise frost-resistance specifications.

Definition of Damage and Laboratory-Based Specifications

Non-aggregate-related frost damage is generally categorized as either internal damage or surface scaling. These two types of frost damage are quantified differently and therefore must be examined separately.

Internal Damage

Internal damage is the loss of concrete integrity due to the development of microcracks (and eventually macrocracks). The concrete gradually loses strength from continued exposure to freezing and thawing conditions and eventually may not have sufficient strength to serve its intended (structural) purpose.

Internal damage in the laboratory is normally evaluated by comparing the dynamic modulus of elasticity of a specimen, after a specific amount of freeze-thaw exposure, to the dynamic modulus prior to the start of freeze-thaw exposure. This value, expressed as a percentage of the original dynamic modulus of elasticity, is generally referred to as the relative dynamic modulus (RDM). The dynamic modulus of elasticity is usually determined by measuring the fundamental transverse vibrational frequency (ASTM C215 [3]), though some researchers have also used the ultrasonic transit time (ASTM C587 [4]). Failure is defined by various agencies and researchers as the RDM dropping below a specific value after a specified number of cycles. A RDM of 60 % after 300 cycles is typically interpreted as failure for concrete tested in accordance with ASTM C666 [5], Procedure A, while a RDM of 80 % after 56 cycles is the typical failure criteria for the CIF procedure (using ultrasonic transit time for the determination of RDM) [6,7]. There is no direct equivalent procedure for determining failure of in-place field concrete, but since compressive strength would need to be reduced approximately 64 % to produce a modulus of elasticity corresponding to a RDM of 60 (based on ACI 318 modulus of elasticity equation), failure by internal damage in the field would probably be evidenced by significant loss of concrete material from a structure (Fig. 1).

Surface Scaling

Surface scaling is the loss of material from the outside surface of a concrete element with little or no damage to the interior of the concrete. Scaling can be



FIG. 1—Loss of concrete from stairs due to internal freeze-thaw damage.

considered an appearance problem and can contribute to a decrease in surface friction on sidewalks as well as highway pavements and bridge decks when the textured surface has scaled off leaving smoother aggregate pieces exposed. While surface scaling generally stabilizes after the surface layer of mortar has been lost, in extreme cases it can continue as a progressive loss of material that even includes coarse aggregate.

Laboratory characterization of scaling has been done both qualitatively and quantitatively. ASTM C672 [8] uses a qualitative visual evaluation ranging from no scaling (a rating of zero) to severe scaling with coarse aggregate visible across the entire surface (a rating of five). The Swedish slab test (CEN/TS 12390-9 [9]) as well as the CDF test [10] uses the mass of material removed by scaling after a specified number of cycles. The slab test considers failure to be a mass loss of more than 1.0 kg of material per square meter of test surface after 56 cycles of freezing and thawing, while the CDF test sets the limit at 1.5 kg/m² after 28 cycles of freezing and thawing. Both tests use a sodium chloride solution of fixed concentration on the test surface. The large difference in test requirements can be explained by the fact that the Swedish slab test uses a sawn surface, while the CDF test uses a cast surface. A cast surface would be expected to have a greater percentage of paste at the test surface. Figure 2 shows typical acceptable and unacceptable scaling results for concrete made with slag-cement and tested using the CDF procedure.

For normal-weight air-entrained concrete, a scaling of 1.5 kg/m² corresponds to a uniform scaling depth of about 0.7 mm. This would be equivalent to the loss of the finer mortar from a concrete surface similar to a visual rating of about three used for ASTM C672 [8]. Field concrete typically scales from the

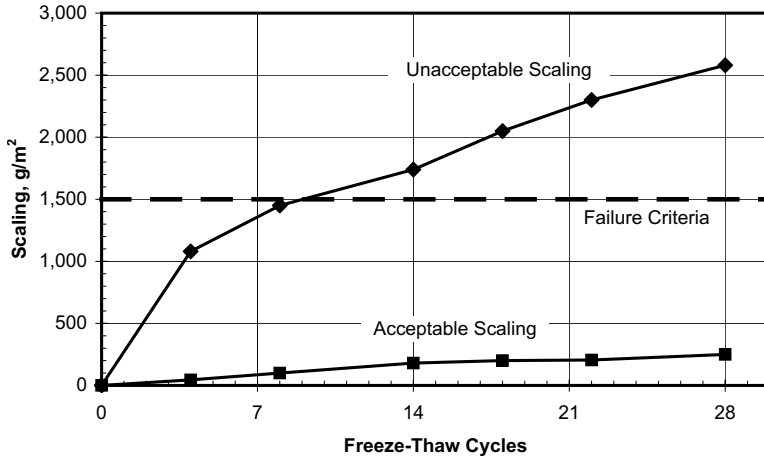


FIG. 2—Typical acceptable and unacceptable scaling results for concrete made with slag-cement and tested using the CDF procedure. [after 7]

finished surface, which has a considerably higher paste/mortar content due to the effects of finishing operations. A scaled layer of 3 mm would expose mostly larger fine aggregate particles, while 5 mm or more would need to be removed to expose significant coarse aggregate. An example of a severely scaled sidewalk is shown in Fig. 3. The actual definition of failure in the field would depend on the use of the concrete. Appearance problems in the field would probably be equivalent to a laboratory scaling depth of 0.5 mm or less, while a scaling depth of 5 mm would be necessary to significantly reduce surface friction. Greater scaling, resulting in the loss of coarse aggregate pieces, could be considered structural failure (significant loss of function) and could also result in significant loss of cover in reinforced concrete structures such as bridge decks.

Types of Field Tests

Before trying to interpret frost exposure results, it is important to understand the type of test the results are from. Field tests can be field exposure tests or field concrete tests, and the way the results can be used depends on the type of test.

Field Exposure Tests

Field exposure tests are tests in which laboratory-fabricated specimens are placed in a specific field location and subjected to natural weathering under the existing field exposure at that location. An example of such a test type is the Treat Island Marine Exposure Station at Treat Island, Maine [11]. Specimens have been placed there since 1936, where they have been exposed to alternating



FIG. 3—*Severely scaled sidewalk.*

wetting in saltwater and drying as well as freezing and thawing (thawing either in air due to daytime temperatures or thawing in water due to submersion during high tide).

The advantages of field exposure tests include the fact that the specimens can be made under controlled conditions in a laboratory so that the properties can be easily determined and that specimens can be subjected to non-destructive testing in a laboratory for better quantification of progressive deterioration. Disadvantages relate to the specimen preparation techniques as well as boundary-condition effects. Whiting and Schmitt [12] concluded that one of the most significant factors affecting the scaling of concrete is changes to the near-surface entrained air voids caused by finishing. The hand finishing of laboratory-scale specimens does not duplicate the typical machine finishing received by large concrete structures placed in the field. Laboratory specimens exposed to freezing in the field also generally experience weathering on all surfaces, while structures usually only have one or two surfaces exposed. This difference in surface exposure or boundary conditions affects heat transfer as well as moisture movement. For example, wetting and drying can be more extreme for small specimens placed in the field (as compared to actual structures), and temperature fluctuations can be more rapid as well. With these examples in mind, it is easy to understand that the primary usefulness of field exposure sites is to determine if specimens evaluated in a laboratory test behave similarly to specimens exposed to weathering in the field. For example, of the ten high-strength concrete mixtures that performed poorly in laboratory

freeze-thaw testing, only two of them showed significant damage after three Winters of field exposure at a test site in Finland [13]. The rest showed steady or improving RDM measurements after the first Winter. This suggests that the laboratory exposure conditions may be more severe than the field exposure. Additional years of field monitoring results would be necessary to make this conclusive.

Field Concrete Sites

Field concrete sites, like the field exposure sites described above, expose the concrete to real weathering conditions. The primary difference, however, is that the concrete is part of a pavement or structure built in the field rather than being small laboratory-produced specimens. The field concrete sites can be either normal construction sites that are later investigated to determine the cause(s) of premature deterioration, or they can be specially constructed field test sites in which specific mixtures are placed in order to monitor their performance when exposed to field weathering conditions. The latter type of field test site often includes the preparation of a number of laboratory-scale test specimens for the determination of both concrete properties and performance of the field mixtures in laboratory durability tests (for example, test sites installed as a part of the Strategic Highway Research Program [14]). In addition, cores are often taken (especially when the field test site is of the first type; a part of normal construction and may have had only minimal quality-control testing) for material property evaluation.

The advantages of field test sites include field-scale (rather than laboratory-scale) consolidation and concrete finishing as well as test conditions that do not have unusual specimen boundary conditions (freezing and moisture exposure from multiple sides as opposed to unidirectional, which is typical for field-scale concrete). The disadvantages include the fact that field variability is often significantly greater than variability in the laboratory. This includes, but is not limited to variations in concrete from the beginning to the end of the truck, variations in consolidation and finishing and variations in curing conditions. These variations can have significant effects, especially when evaluating surface scaling. Figure 4 shows an extreme case of scaling variability possibly caused by the application of water to the concrete surface. (Compare with Fig. 3, which shows uniform severe scaling.)

Understanding Field Tests and Results

Field tests are much more difficult to interpret than laboratory tests, and a number of additional considerations are discussed below.

Effect of Field Weather Conditions

Some advantages and limitations of the main types of field tests have already been discussed, but one additional aspect must be considered. Field tests represent the behavior of the concrete to the specific weathering conditions experienced at the particular field site. Different field sites can have different con-



FIG. 4—*Significant variation in surface scaling.*

ditions, and which set of conditions is the most severe may depend on the characteristics of the concrete mixture itself. Cooling rate, average low temperature experienced, and moisture conditions (both wetting and drying) can all affect field freeze-thaw behavior. Exposure to deicing salt and the type of deicing agent used can also have effects. Even with laboratory testing it can be difficult to anticipate which conditions will be most severe. For example, laboratory testing conducted in conjunction with the field testing program in Finland that has been previously mentioned included freezing to -20°C as well as to -40°C (on separate specimen sets) [13]. Though the initial assumption might be that the -40°C freezing would be more severe, over half of the mixtures prepared at a w/cm of 0.30 (including mixtures at various levels of silica fume replacement of cement) showed lower RDM values for the freezing to -20°C . Interestingly, almost all of the mixtures prepared at a w/cm of 0.42 (including a variety of types and amounts of cement replacements) had lower RDM values for the -40°C testing (than for the -20°C testing). Truly evaluating field severity would require a large number of test sites with identical concretes.

Time Effects and the Effect of Autogenous Healing

Field tests are also slow. Laboratory test procedures, besides providing consistent and reproducible weathering conditions, are almost always accelerated tests. Field tests require many years to provide conclusive results, especially results that would show that concrete meeting a given set of requirements is frost resistant. Internal damage is generally a progressive deterioration with

little or no damage apparent initially. For example, *D*-cracking can require 10–15 years before it is apparent in the field [15]. Autogenous healing [16] or self-healing of microcracks in concrete during warm weather between consecutive Winter periods is one of the factors contributing to the delayed appearance of internal damage [15]. Surface scaling, on the other hand, is generally not amenable to autogenous healing since the scaled material is generally loosened by either gravity (for vertical surfaces) or traffic (for horizontal surfaces such as sidewalks or pavements). Sufficient time is necessary, however, to determine if the surface scaling is stabilizing over time (very little additional scaling in subsequent years after the initial scaling is noticed) or progressing at a regular rate. Since scaling in the field is generally measured by more qualitative methods such as visual surveys, repeated annual measurements are necessary both for repeatability/reliability and in order to determine if the scaling is stabilized or progressing.

Effect of Sample Size and Boundary Conditions

One of the field exposure sites in Finland [13] has already been mentioned. Though it has also already been mentioned that laboratory specimens placed in the field may not actually experience the exact same exposure as true field concrete due to size effects and boundary conditions, the weathering exposure will probably be more severe for the small specimens. At corners and edges the concrete is exposed to moisture intrusion from multiple directions, and the degree of saturation would be expected to be higher at these locations. Deterioration in pavements and structures often occurs at these corners and edges (for example, the joint failures discussed in the following section [17]). Since a larger proportion of the total volume of a small specimen is close to corners and edges than for larger structures, small specimens would be expected to be more susceptible to damage during frost exposure. Thus the failure of small specimens at field exposure sites would not necessarily mean that concrete in larger structures would also fail. However, good performance of small specimens in the field would probably mean that large-scale concrete installations would also perform well in that environment once a sufficient number of years of weathering exposure have been experienced in order to provide confidence in the results.

Effect of Concrete Material Properties

An investigation of a number of failures along joints in Indiana pavements [17] looked at air-void parameters in concrete directly adjacent to the deteriorated areas as well as in non-deteriorated concrete in the same pavements. The deterioration was so severe that in many cases, the concrete near the joints was actually missing. Three different deteriorated pavements as well as two additional similar but not deteriorated pavements were investigated. The researchers found a significant difference in air-void parameters between the deteriorated and non-deteriorated concretes, with all of the deteriorated concrete having spacing factors (\bar{L}) of about 0.45 mm, while all of the non-deteriorated

concrete had average \bar{L} values of 0.32 or less. Similar significant differences were not evident for either total air content or specific surface (α).

Since both the deteriorated and non-deteriorated concrete for each pavement section were originally the same concrete, the authors attributed the changes in \bar{L} (as well as changes in the other measured air-void parameters) to infilling of some of the voids at the pavement joints [17].

This field test site suggests that \bar{L} is the significant parameter with respect to internal damage of pavement concrete. Since the pavements were only 10–15 years old, it may be premature to identify a critical \bar{L} -value based on this study (deterioration could occur in the un-damaged concrete as the pavement ages). However, \bar{L} -values double the ACI 201-recommended 0.2 mm [1] could be considered unacceptable based on this field study, and even values that were 50 % greater could be considered borderline. Of course these values only apply to the climatic exposure in Indiana. Other climates could be more or less severe.

Effect of Sample Surface Condition on Scaling

Whiting and Schmitt [12] examined 12 existing field structures consisting of highway bridge decks, bridge deck overlays, and pavements for the purpose of identifying factors contributing to observed surface scaling on the structures. All were between 4 and 12 years old. They found that less than 4 % of the total area examined showed any scaling, and less than 0.5 % showed scaling severe enough to expose much of the coarse aggregate. They identified the three most important parameters (statistically) that contributed to increased scaling: w/c , loss of entrained air at the surface due to placing and finishing, and \bar{L} of the concrete. They emphasized that the first two factors had a greater influence on scaling resistance than the third. Their model predicts that a 0.45 w/c mixture with an \bar{L} at the recommended 0.2 mm and no surface void removal would have only light scaling (only finer sand particles visible), but if half the near-surface voids were removed due to surface finishing, the coarser sand particles would be visible from scaling. More severe void removal from finishing, higher w/c , or higher initial \bar{L} could all lead to the coarse aggregate being visible. Finishing with water on the surface (bleedwater or water added to aid finishing) could result in complete loss of surface mortar due to both increased w/c and increased loss of near-surface air voids. The authors pointed out that since the observed scaling on the sections that they monitored was mostly isolated, poor finishing practice rather than the initial concrete mixture properties probably contributed to the worst of the observed scaling. They recommended that field finishing operations be kept to the minimum necessary in order to avoid scaling of field concrete. Figure 4 has already been presented and shows an extreme case of differences in surface scaling probably due to changes caused to the concrete surface during finishing.

The above field concrete site summary identifies a very important aspect of using surveys of field condition for evaluating the effectiveness of concrete specifications for resisting scaling: Variability in placing and especially finishing can result in isolated areas of scaling in concrete that otherwise meets

recommended w/c and air-void parameter specifications. In fact the above-referenced authors [12] concluded that "... it is the quality of the thin (<6 mm) near-surface zone that determines the resistance of concrete to scaling." They further went on to explain that traditional testing to ensure compliance to material specifications cannot adequately address the influence of the surface layer in final field performance. This suggests that the next step in improving concrete specifications with respect to scaling resistance should focus on the following:

- (1) Limitations on the finishing operations so as to minimize the loss of near-surface entrained air and
- (2) Changes to the mixture requirements that will result in mixtures that are more robust and better able to resist deleterious modifications due to finishing.

The first approach above would need to focus on a procedural specification. While it is easy to say "avoid over finishing," that is essentially an unenforceable specification. Therefore, revisions to frost-resistance specifications will need to emphasize the second approach. One possible way of accomplishing this would be to pre-approve concrete mixtures for specific (severe) applications by testing the base mixture as well as the same mixture prepared with an increased amount of mix-water (for example, 10 % more water). Though there would be an increase in w/c (for example, from 0.40 to 0.44), the greater change would be to the viscosity of the paste portion of the concrete. If this decreased-viscosity concrete could retain an adequate air-void system for resistance to scaling damage, the base mixture would be more likely to "survive" field placing and finishing.

Since the material of interest (the near-surface concrete) is the very material that is lost due to scaling, the most useful field concrete test sites will be those in which the surface layer can be characterized prior to freeze-thaw exposure. Such sites, especially ones in which concrete expected to fail is placed, are rarely constructed.

Conclusions and Recommendations

Field test sites can provide valuable information relative to the appropriateness of specifications for frost-resistant concrete. However specific considerations must be kept in mind when using the results of field test sites to justify changes to specifications.

- (1) Deterioration may progress slowly in the field, and the data should represent an adequate period of field exposure (probably at least 10 years for internal damage) in order to verify that non-deteriorated concrete is really durable.
- (2) Size and boundary-condition effects must be considered when analyzing results from field exposure sites using laboratory-prepared samples.
- (3) Scaling results may be significantly affected by placing and finishing operations, and it may not be possible to quantify the near-surface concrete properties of the material if the surface has scaled off.
- (4) Severity of weathering exposure varies from field site to field site (and

even from year to year), and the conditions that are the most severe may vary depending on the properties of the concrete mixtures used at the specific sites.

- (5) Data from a considerable number of field test sites representing a wide range of concrete properties may be necessary before specification changes can be justified.

As additional field freeze-thaw performance data becomes available, changes to existing frost-resistance specification may be justified. Instances of unacceptable field performance of concrete meeting existing specifications should be the most important reason for changes. For cases where concrete not meeting specifications still appears to perform adequately, specification changes should only be made with caution and especially with due consideration of items (1), (4), and (5), above.

References

- [1] ACI 201, "Guide to Durable Concrete," reported by ACI Committee 201, *ACI Manual of Concrete Practice* American Concrete Institute, Detroit, MI, 2008.
- [2] ACI 318, "Building Code Requirements for Structural Concrete (ACI 318-08) and Commentary, An ACI Standard," reported by ACI Committee 318, *ACI Manual of Concrete Practice* American Concrete Institute, Detroit, MI, 2008.
- [3] ASTM C215, "Standard Test Method for Fundamental Transverse, Longitudinal, and Torsional Frequencies of Concrete Specimens," *Annual Book of ASTM Standards*, Vol. 4.02, ASTM International, West Conshohocken, PA.
- [4] ASTM C587, *Annual Book of ASTM Standards*, Vol. 4.02, ASTM International, West Conshohocken, PA.
- [5] ASTM C666/C666 M-03, *Annual Book of ASTM Standards*, Vol. 4.02, ASTM International, West Conshohocken, PA.
- [6] Setzer, M. J., "Recommendation of RILEMTC 176-IDC: Test Methods of Frost Resistance of Concrete. CIF-Test—Capillary Suction, Internal Damage and Freeze Thaw Test, Reference Method and Alternative Methods A and B," *Mater. Struct.*, Vol. 37, No. 34, 2001, pp. 515–525.
- [7] Setzer, M. J., "Frost Attack on Concrete: Modeling by the Micro-Ice-Lens Model, Evaluating by RILEM CDF/CIF Test," Lecture Notes, 2008.
- [8] ASTM C672/C672 M-03, *Annual Book of ASTM Standards*, Vol. 4.02, ASTM International, West Conshohocken, PA.
- [9] CEN/TS 12390-9, 2006, "Testing hardened concrete-Part 9: Freeze-thaw resistance—Scaling," *Technical Specifications*, European Committee for Standardization, Brussels, Belgium.
- [10] RILEM, "Draft Recommendation for Test Method for the Freeze-Thaw Resistance of Concrete: Tests with Water (CF) or with Sodium Chloride Solution (CDF)," *Mater. Struct.*, Vol. 28, No. 31995, pp. 175–182.
- [11] Malhotra, V. M. and Bremner, T. W., "Performance of Concrete at Treat Island, USA: CANMET Investigations," *ACI Special Publications*, Vol. SP-163, 1996, pp. 1–52.
- [12] Whiting, D. and Schmitt, J., "Durability of In-Place Concrete Containing High-Range Water-Reducing Admixtures," *National Cooperative Highway Research Program Report No. 296*, Transportation Research Board, Washington, D.C., 1987.
- [13] Kuosa, H., Vesikari, E., Holt, E., and Leivo, M., "Field and Laboratory Testing and

- Service Life Modelling in Finland,” *Proceedings of Nordic Concrete Federation Miniseminar: Nordic Exposure Sites*, Hirtshals, Denmark, November 12–14, 2008, pp. 181–208.
- [14] Janssen, D. J. and Snyder, M. B., “Resistance of Concrete to Freezing and Thawing,” *Report No. SHRP-C-391*, Strategic Highway Research Program, National Research Council, Washington, D.C., 1994.
- [15] Janssen, D. J., DuBose, J. D., Patel, A. J., and Dempsey, B. J., “Predicting the Progression of D-Cracking,” *Transportation Engineering Series No. 44*, Civil Engineering Studies, University of Illinois, Urbana, IL, 1986.
- [16] Munday, J. G., Sangha, C. M., and Dhir, R. K., “Comparative Study of Autogenous Healing of Different Concretes,” *First Australian Conference on Engineering Materials*, University of New South Wales, 1974, University of New South Wales.
- [17] Radlinski, M., Olek, J., del Mar Arribas, M., Rudy, A., Nantung, T., and Byers, M., “Influence of Air-Void System Parameters on Freeze-Thaw Resistance of Pavement Concrete-Lessons Learned from Field and Laboratory Observations,” *Proceedings of the Ninth International Conference on Concrete Pavements*, International Society for Concrete Pavements, Bridgeville, PA, 2008.

www.astm.org

ISBN: 978-0-8031-3419-5

Stock #: STP1511